

JSCSEN 74(11)1155–1333(2009)

Journal of the Serbian Chemical Society

ersion
lectronic

VOLUME 74

No 11

BELGRADE 2009

Available on line at



www.shd.org.rs/JSCS/

The full search of JSCS
is available through

DOAJ DIRECTORY OF
OPEN ACCESS
JOURNALS
www.doaj.org



CONTENTS

D. M. Opsenica and B. A. Šolaja: Antimalarial peroxides (Review)..... 1155

Organic Chemistry

N. D. Divjak, N. R. Banjac, N. V. Valentić and G. S. Ušćumlić: Synthesis, structure and solvatochromism of 5-methyl-5-(3- or 4-substituted phenyl)hydantoins..... 1195

V. I. Mićović, M. D. Ivanović and Lj. Došen-Mićović: Structural requirements for ligands of the δ -opioid receptor..... 1207

V. V. Dabholkar and F. Y. Ansari: Synthesis and characterization of selected fused isoxazole and pyrazole derivatives and their antimicrobial activity (Short communication)..... 1219

Biochemistry and Biotechnology

D. I. Batovska, I. T. Todorova and S. S. Popov: Seasonal variations in the leaf surface composition of field grown grapevine plants..... 1229

P. M. Mishra, A. Sree, M. Acharya and A. P. Das: Fatty acid profile, volatiles and antibacterial screening of lipids of the sponge *Fasciospongia cavernosa* (Schmidt) collected from the Bay of Bengal (Orissa Coast)..... 1241

Inorganic Chemistry

B. B. Zmejovski, G. N. Kaluđerović, S. Gómez-Ruiz and T. J. Sabo: Palladium(II) complexes with R_2 edda derived ligands. Part III. Diisobutyl (*S,S*)-2,2'-(1,2-ethanediyl-diimino)di(4-methylpentanoate) and its palladium(II) complex: synthesis and characterization..... 1249

Ž. K. Jaćimović, G. A. Bogdanović, B. Holló, V. M. Leovac and K. M. Szécsényi: Transition metal complexes with pyrazole-based ligands. Part 29. Reactions of zinc(II) and mercury(II) thiocyanate with 4-acetyl-3-amino-5-methylpyrazole..... 1259

K. Krishnankutty, M. B. Ummathur and P. Ummer: 1-Naphthylazo derivatives of some 1,3-dicarbonyl compounds and their Cu(II), Ni(II) and Zn(II) complexes..... 1273

Physical Chemistry

A. Daković, Ž. Sekulić, G. E. Rottinghaus, A. Stojanović, S. Milićević and M. Kragović: T-2 toxin adsorption by hectorite..... 1283

Electrochemistry

X. Yu, S. Chen and L. Wang: Effect of solution treatment conditions on the sensitization of austenitic stainless steel..... 1293

Thermodynamics

I. R. Radović, M. Lj. Kijevčanin, A. Ž. Tasić, B. D. Djordjević and S. P. Šerbanović: Densities and excess molar volumes of alcohol + cyclohexylamine mixtures..... 1303

Environmental Chemistry

J. D. Joksić, M. Jovašević-Stojanović, A. Bartonova, M. B. Radenković, K.-E. Yttri, S. Matić-Besarabić and Lj. Ignjatović: Validation of an HPLC–UV method for the determination of digoxin residues on the surface of manufacturing equipment..... 1319

Published by the Serbian Chemical Society
Karnegijeva 4/III, 11000 Belgrade, Serbia
Printed by the Faculty of Technology and Metallurgy
Karnegijeva 4, P.O. Box 35-03, 11120 Belgrade, Serbia



J. Serb. Chem. Soc. 74 (11) 1155–1193 (2009)
JSCS–3909

Journal of
the Serbian
Chemical Society

JSCS@tmf.bg.ac.rs • www.shd.org.rs/JSCS

UDC 615.285+541.459:616.936

Review

REVIEW

Antimalarial peroxides

DEJAN M. OPSENICA^{1*#} and BOGDAN A. ŠOLAJA^{2*#}

¹*Institute of Chemistry, Technology and Metallurgy, University of Belgrade, Njegoševa 12, 11000 Belgrade and* ²*Faculty of Chemistry, University of Belgrade, Studentski trg 16, P.O. Box 51, 11158 Belgrade, Serbia*

(Received 19 May 2009)

Abstract: The problem of endemic malaria continues unabated globally. Malaria affects 40 % of the global population, causing an estimated annual mortality of 1.5–2.7 million people. The World Health Organization (WHO) estimates that 90 % of these deaths occur in sub-Saharan Africa among infants under the age of five. While a vaccine against malaria continues to be elusive, chemotherapy remains the most viable alternative towards treatment of the disease. During last years, the situation has become urgent in many ways, but mainly because of the development of chloroquine-resistant (CQR) strains of *Plasmodium falciparum* (Pf). The discovery that artemisinin (ART, **1**), an active principle of *Artemisia annua* L., expresses a significant antimalarial activity, especially against CQR strains, opened new approaches for combating malaria. Since the early 1980s, hundreds of semi-synthetic and synthetic peroxides have been developed and tested for their antimalarial activity, the results of which were extensively reviewed. In addition, in therapeutic practice, there is no reported case of drug resistance to these antimalarial peroxides. This review summarizes recent achievements in the area of peroxide drug development for malaria chemotherapy.

Keywords: antimalarial; peroxides; trioxanes; trioxolanes; tetraoxanes; chimeras.

CONTENTS

1. INTRODUCTION
2. THE LIFE CYCLE OF THE MALARIA PARASITE
3. ARTEMISININ AND ITS DERIVATIVES
 - 3.1. First generation artemisinin derivatives
 - 3.2. Second generation artemisinin derivatives
 - 3.3. New artemisinin derivatives
4. 1,2,4-TRIOXANES

* Corresponding author. E-mail: : *dopsen@chem.bg.ac.rs; **bsolaja@chem.bg.ac.rs

Serbian Chemical Society member.

doi: 10.2298/JSC0911155O

1155

Available online at www.shd.org.rs/JSCS/

2009 Copyright (CC) SCS



5. 1,2,4-TRIOXOLANES
6. 1,2,4,5-TETRAOXANES
7. CHIMERIC PEROXIDE – QUINOLINE COMPOUNDS
8. METABOLISM AND DRUG COMBINATION ASSAYS
9. MECHANISM OF ACTION
10. CONCLUSIONS

1. INTRODUCTION

The problem of endemic malaria continues unabated globally. Malaria affects 40 % of the global population, causing an estimated annual mortality of 1.5–2.7 million people.¹ The World Health Organization (WHO) estimates that 90 % of these deaths occur in sub-Saharan Africa among infants under the age of five.² While a vaccine against malaria continues to be elusive,³ chemotherapy remains the most viable alternative towards treatment of the disease. During the last years, the situation has become urgent in many ways, but mainly because the malaria parasite has developed multiple drug resistance to clinically established drugs (Fig. 1). This resistance is most serious with chloroquine (CQ), the most widely employed and cheapest drug used to treat malaria, and CQ-resistant (CQR) strains of *Plasmodium falciparum* (Pf) – Indochina W2, Brazil IEC-306, FCR3 and K1. The problem of combating malaria is even more complex because of the contemporary development of resistance of the mosquito vector to currently employed insecticides.

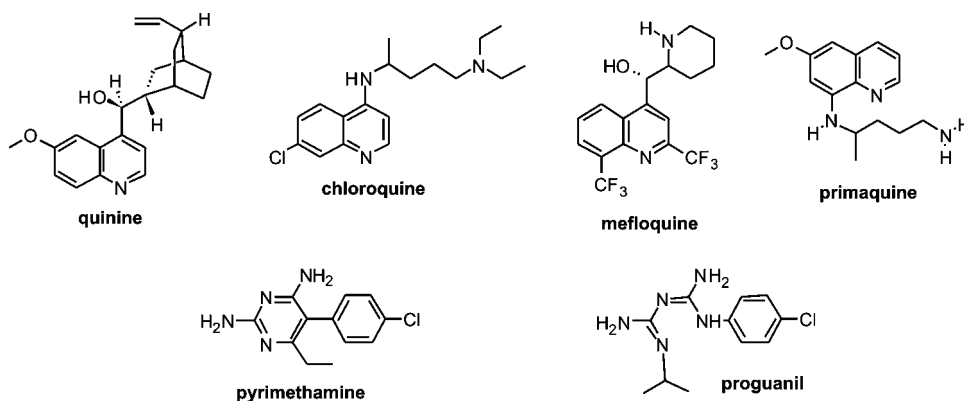


Fig. 1. Antimalarial drugs against which the malaria parasite has developed resistance.

The discovery that artemisinin (ART, **1**), an active principle of *Artemisia annua* L., expresses a significant antimalarial activity, especially against CQ-resistant (CQR) strains,⁴ opened new approaches for combating malaria. Since the early 80s, hundreds of semi-synthetic and synthetic peroxides have been developed and tested for their antimalarial activity, the results of which were exten-

sively reviewed.⁵ In addition, in therapeutic practice, there is no reported case of drug resistance to these antimalarial peroxides. The only evidence for *in vitro* resistance was found in French Guiana where certain ART derivatives were used in uncontrolled and illegal self-medication.⁶

This review summarizes recent achievements in the area of peroxide drug development for malaria chemotherapy.

2. THE LIFE CYCLE OF THE MALARIA PARASITE

Protozoa of the genus *Plasmodium* cause malaria. Four species of *Plasmodium* are responsible for the disease in humans: *P. falciparum*, *P. malaria*, *P. ovale* and *P. vivax*. Of these, *P. falciparum* may cause the condition known as cerebral malaria, which is responsible for the majority of fatal outcomes.

The pathogenesis⁷ and life cycle of the malaria parasite are complex,⁸ consisting of two stages: a sexual stage (sporogony), which occurs within the mosquito, and an asexual stage (schizogony), which occurs in the host.^{5c,9} The illness is started when an infected female mosquito of the genus *Anopheles* feeds on the blood of an uninfected vertebrate host. Mosquitoes inject parasites (sporozoites) into the subcutaneous tissue, less-frequently directly into the bloodstream. In less than 1 hour, the sporozoites travel to the liver, invade the hepatocytes and undergo exoerythrocytic schizogony. After some time, depending on the plasmodium species, the schizonts are transformed into merozoites, which after release into the blood stream invade erythrocytes. After significant reorganization of the membrane proteins of an occupied erythrocyte,^{8e} the merozoites undergo erythrocytic schizogony, which comprises young rings (12 h after erythrocyte infection), mature rings (18 h), early trophozoites (24 h), mature trophozoites (30 h), early schizonts (36 h) and mature schizonts (42 h). At the end of erythrocytic schizogony, the parasites return into the merozoite form but enormously multiplied causing splattering of the erythrocyte. The released merozoites invade new red blood cells and start a new erythrocytic schizogony cycle. Erythrocytic schizogony occurs every 2–3 days, depending on the plasmodium species. Each cycle is accompanied by typical malaria symptoms, such as fever, chills, headache and exhaustion. After several cycles, some of the merozoites undergo sexual development and are transformed into gametocytes.

The gametocytes remain in the erythrocytes and are consumed by an *Anopheles* mosquito. In the mosquito, female and male gametocytes join and form zygote. Within 18 to 24 h, the zygote transforms into a slowly motile ookinete. Between 7 and 15 days, depending on the plasmodium species and the ambient temperature, a single oocyst forms more than 10,000 sporozoites. The motile sporozoites migrate into the salivary glands and accumulate in the acinar cells. When infected, the mosquito bites a susceptible vertebrate host; a new parasite cycle commences. The length of the *P. falciparum* life cycle is presented in Table I.

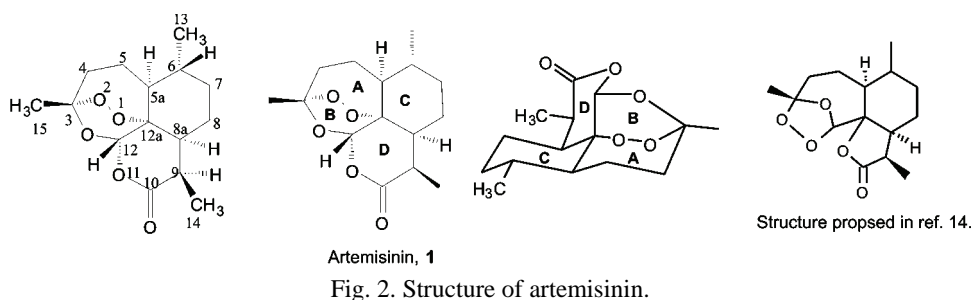
TABLE I. Length of the various stages of the life cycle of *P. falciparum*

Stage	Definition	Duration
1	Ookinete formation	24 to 48 h
2	Oocyst maturation	9 days
Invasion of salivary glands (1+2)		10 days
3	Circulation of sporozoites in the blood stream	1 h max.
4	Hepatic schizogony	6 days
5	Erythrocytic schizogony	48 h
6	Gametocytogony	10 days
Complete cycle (1 to 6)		27 days

The malaria parasite has a limited capacity for *de novo* amino acid synthesis and its survival is dependent on haemoglobin proteolysis. Parasite digests haemoglobin in the food vacuole (FV), supplies itself with amino acids necessary for nutrition and liberates free haem (Fe(II)PPIX), which is subsequently oxidized to haematin (Fe(III)PPIX). Free haematin can damage cellular metabolism by inhibiting enzymes, by peroxidation of membranes, and by producing oxygen radicals in the acidic environment of the FV.¹⁰ In order to protect itself, the parasite eliminates haematin by polymerizing it into hemozoin. Hemozoin is a non-covalent aggregate of several units of haematin linked *via* coordinate bonds formed between Fe(III) of one haematin and the carboxylate side chain of the adjacent one.¹¹ Hemozoin is insoluble, and it is accumulated in the lymphatic tissue, liver, bone marrow and the brain. It was found that haem [Fe(II)PPIX] can not polymerize to hemozoin and is an effective inhibitor of Fe(III)PPIX polymerization, even better than CQ.¹²

3. ARTEMISININ AND ITS DERIVATIVES

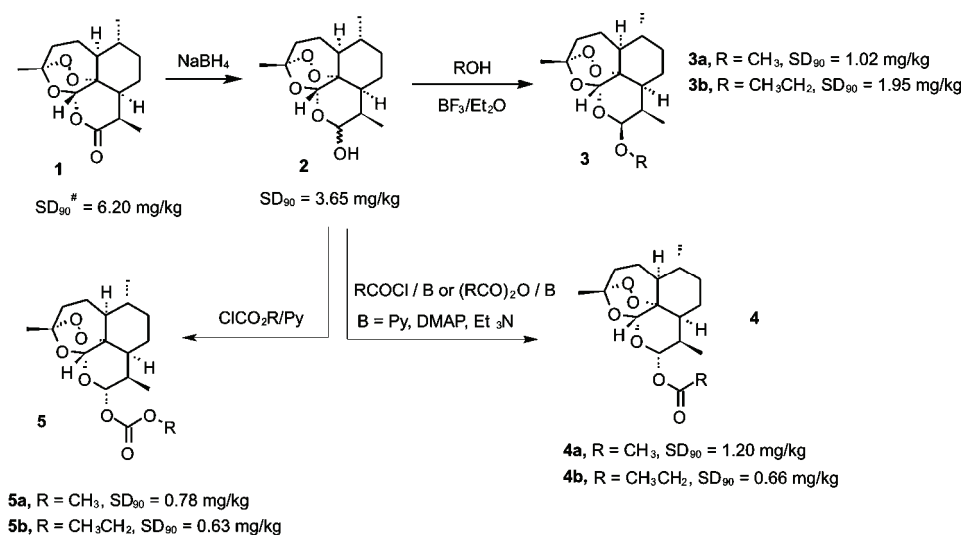
The herb *Artemisia annua* L. has been used in Chinese traditional medicine for centuries. The usage of plants extracts for the treatment of malaria fever is well documented.^{5a} The active ingredient of the potion was identified as artemisinin **1** (ART, qinghaosu – QHS, Fig. 2), a sesquiterpene lactone with an endoperoxide function.⁴ The very same compound was also isolated by the Belgrade group in the early 1970s; however, the wrong structure of **1** was proposed (Fig.



2).¹³ The structure of ART was elucidated in 1979 by X-ray analysis, which was supported by total synthesis.¹⁴ Since then, many total syntheses have been achieved,¹⁵ including the newest one.¹⁶ ART is an erythrocytic schizonticide which exhibits rapid activity against all types of human and most animal malaria. It is effective against both CQ-sensitive (CQS) and CQR strains of *P. falciparum* (IC_{50}) D6 = 9.0 nM, W2 = 6.7 nM, TM91C235 = 13.0 nM)¹⁷ and it has been successfully used for the treatment of severe cerebral malaria.^{5c} ART has poor solubility in water and it is administered as a water or oil suspension. Better results were achieved when it was administered intramuscularly (i.m.) as a suspension in oil, than orally (p.o.) in water. Metabolites isolated after p.o. administration were devoid of peroxide function and had no antimalarial activity, strongly suggesting that the peroxide function is a critical part of the pharmacophore. It was assumed that the good activity of **1** was due, at least partially, to its amphiphilic structure that facilitates cell membrane permeability. The shortcoming of the usage of **1** is the high recrudescence rates related to its pharmacokinetic profile, which is characterized by a short half-life, low oral bioavailability and auto-induction of metabolism.

3.1. First generation of artemisinin derivatives

The first semi-synthetic derivatives of ART were simple ethers (**3**), esters (**4**) and carbonates (**5**) of dihydroartemisinin (DHA, **2**) (Scheme 1).^{4b,5a} DHA is a lactol easily obtained from **1** by $NaBH_4$ reduction. It is twice as active as ART but exhibits a relatively high degree of neurotoxicity. In spite of poor oral bio-



Scheme 1. Transformations of artemisinin into first generation derivatives (SD₉₀ – the dose required for 90% suppression of parasitemia; data taken from ref. 4b. Compounds were administered i.m. as oil suspension to mice infected with *P. berghei*).

availability, high recrudescence and noteworthy reports on its neurotoxicity, DHA is as effective against severe cerebral malaria as ART.

Artemether **3a** and arteether **3b** are β -alkyl ethers of DHA designed to increase lipid solubility, pharmacokinetic profile and antimalarial activity as compared to **1** and **2**. Both derivatives are fast acting blood schizonticides and are especially active against CQR strains. Some studies indicated significant neurotoxicity when the drugs were administered in high doses, probably due to their metabolism to DHA. Later studies showed that neurotoxicity occurred when the compounds were administered at least five times higher doses than is recommended. Today, artemether **3a** is the most widely used derivative and is applied as an oil solution for i.m. injection (Artenam[®] and Artemos[®]), or recently in combination with lumefantrine (Coartem[®]).

Although carbonates **5** exhibited higher *in vivo* activity than **1**, **2** and **3**, there is no reported clinical application, probably because of their low stability under physiological conditions, due to their rapid hydrolysis to **2**.

For treatment of severe forms of malaria, water-soluble derivatives of ART, such as sodium artesunate **4c**^{4b} and artelinic acid **6**,¹⁸ are indispensable. Both compounds can be administered intravenously (i.v.) and thus can be delivered much faster and be more efficacious than less polar ones which are administered i.m. as an oil suspension.

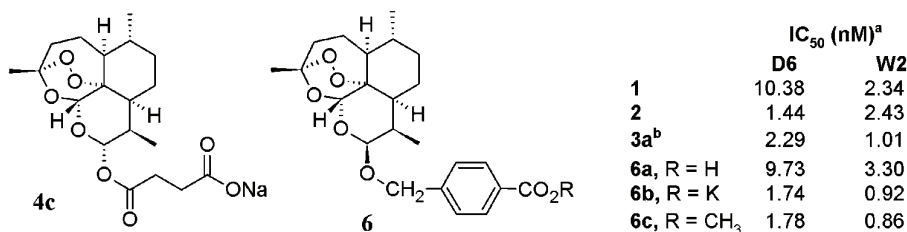
Artesunate **4c** (Fig. 3) rapidly diminishes parasitemia and is very efficacious in the restoration to consciousness of comatose cerebral malaria patients.¹⁹ Its shortcoming is high recrudescence of the disease and **4c** is normally used in combination therapies with mefloquine^{5e} and amodiaquine (Arsucam[®]). Na artesunate is used as a freshly prepared solution in dextrose or saline because of its rapid hydrolysis to **2**.

Artelinic acids **6a** (Fig. 3) possess a C(10) β -ether linkage and are thus hydrolytically more stable than artesunate **4c**. The acid **6a** expresses *in vitro* activity comparable to **1** and **4c** against D6 and W2* strains of *P. falciparum*, but showed superior *in vivo* activities against *P. berghei* as compared to both compounds.¹⁸ Moreover, the acid **6a** has a longer plasma-life,¹⁸ a higher plasma concentration, higher binding capacities and the lower toxicity among the first generation of semi-synthetic derivatives of ART **1**.^{5c} Although the methyl ester **6c** exhibits higher *in vitro* activity, it is less suitable because of its low solubility in water.

The described derivatives suffer from serious disadvantages – short plasma life and CNS toxicity as consequence of their rapid metabolism into dihydroART **2**.²⁰ Ethers **3** are metabolized by cytochrome P-450, forming the C(α)-hydroxyl derivative **7**, which is later transformed into **2** (Scheme 2). Esters **4** simply hyd-

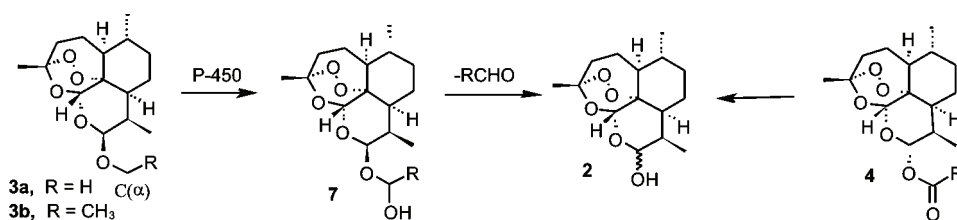
*D6 (Sierra Leone strain) is resistant to mefloquine and susceptible to chloroquine, pyrimethamine and sulfadoxine; W2 (Indochina strain) is resistant to chloroquine, quinine, pyrimethamine and sulfadoxine and susceptible to mefloquine.

rolyze to **2**. In addition, all these derivatives possessing acetal or hemi-acetal group in the D-ring readily hydrolyze under acidic conditions after p.o. administration. The longer plasma half-life of arteminic acid **6a** is probably the result of steric hindrance and poorer accessibility to P-450. The second generation of semi-synthetic derivatives of ART was designed to overcome these disadvantages.



^a Data taken from reference 18; ^b Data taken from ref. 20.

Fig. 3. Structures and antimalarial activities of derivatives **4a** and **6**.



Scheme 2. Metabolic transformations of derivatives **3**, **4** and **7**.

3.2. Second generation of artemisinin derivatives

The first efforts towards metabolically stable compounds included a modification of arteminic acid **6**.²⁰ The new compounds (Fig. 4) exhibited higher activity against the W2 than against the D6 clone. It was found that electronic effects, the

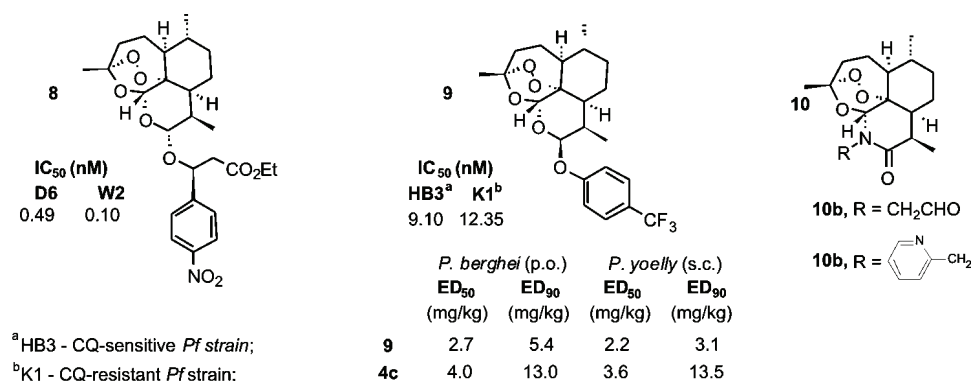


Fig. 4. Structures and antimalarial activities of derivatives **8–10** (ED₅₀ – effective dose, the dose that decreases parasitemia by 50 %).

configuration at C(α) (the (*S*)-isomers were more active than the (*R*) ones), lipophilicity and steric factors have a considerable influence on the antimalarial activity. The most active compound **8** was 10, 20 and 40 times more active than compounds **3b**, **1** and **6a**, respectively.

Replacing the *O*-alkyl group with an *O*-phenyl group should prevent oxidative dealkylation with P-450 and the formation of dihydroartemisinin **2**. Consequently, a series of C(10)-aryloxy derivatives **9** and lactams **10** were synthesized and their antimalarial activity assessed (Fig. 4).²¹ Derivative **9** was *in vitro* as active as artemether but had outstanding *in vivo* antimalarial activity, which was higher than the clinically used sodium artesunate. Moreover, derivative **9** was metabolically more stable than the parent compound (H instead of CF₃).

Many 11-azaartemisinins **10** (Fig. 4) were described as being more stable under physiological conditions.²² In addition, the possibility of changing the substituents on the nitrogen enabled the fine-tuning of the activity. New compounds **10a** and **10b** were, respectively, 26 and 22 times more active than ART.^{22b}

The superior activity of deoxyartemisinin **11**²³ encouraged the synthesis of a series of C(9)-substituted derivatives **12** (Fig. 5).^{24,25} Derivatives **12a–b** were 21–33 times more active than ART against the W2 clone and 50–70 times more active against the D6 clone, clearly demonstrating that the removal of the lactone carbonyl provides excellent potency enhancement.²⁵ These and some new derivatives²⁵ were tested *in vivo* both s.c. and p.o. The activity of derivative **12a** was superior to that of ART, curing all mice at an 8 mg/kg/day s.c. dose.

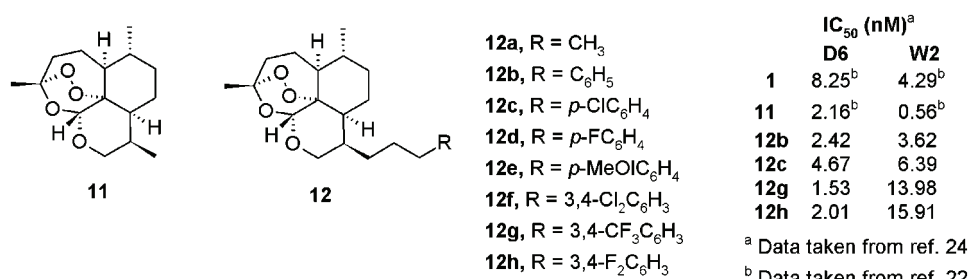


Fig. 5. Structures and antimalarial activities of derivatives **11** and **12**.

A series of C(10) carbon heterocyclic substituted derivatives (Fig. 6) of deoxyartemisinin were synthesized using a short and efficacious synthetic procedure.²⁶ The compounds were tested *in vitro* against the CQ-sensitive (CQS) NF54 *P.f.* strain and demonstrated activity at least that of ART. Derivative **13a** was the most active in the series with IC₅₀ = 1.4 nM. A special group of these derivatives were of dimeric structure. The compounds were more stable under physiological conditions than the parent compound **1** and simultaneously retained

very good to excellent activity.²⁷ Some of these derivatives were significantly more active ($IC_{50} = 1.3\text{--}3.2$ nM) than ART ($IC_{50} = 9.9$ nM) against the CQS NF54 *P.f.* strain.

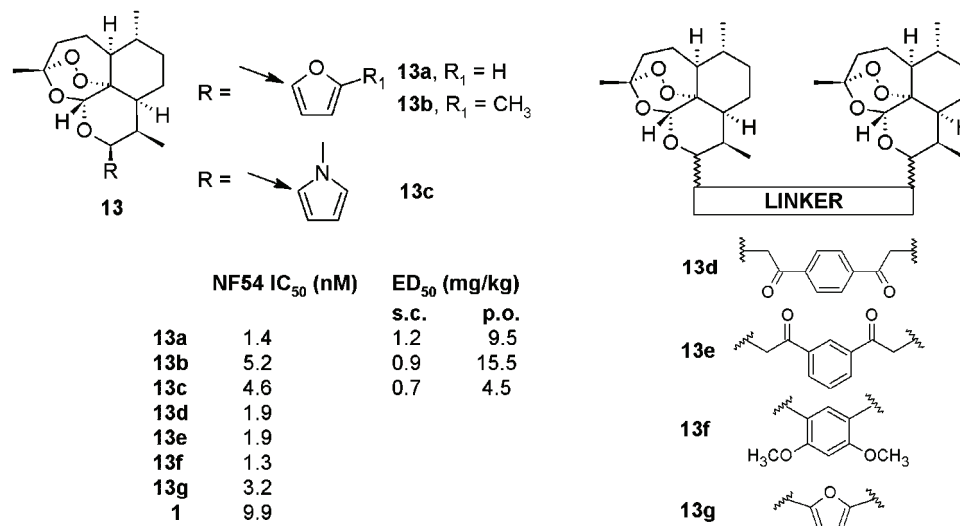


Fig. 6. Structures and antimalarial activities of derivatives **13**.

3.3. New artemisinin derivatives

With the aim of preventing metabolic transformation of artemisins to dihydroartemisinin **2** and thus avoiding neurotoxicity, several 10-(alkylamino)artemisins **14** were designed (Fig. 7).^{28,29} All the tested compounds showed excellent *in vivo* activities against *P. berghei*, with **14c**, as the most active derivative, being almost 25 times (s.c.) and 7 times (p.o.) more active than artesunate **4c**. Unfortunately, **14c** suffers from being seriously neurotoxic even at low doses, thus indicating once again that the more lipophilic compounds are more toxic.²⁹ However, derivative **14e** (artemisone) showed no toxicity and possesses tractable physicochemical properties. *In vivo* experiments revealed that artemisone has a greatly enhanced bioavailability, as reflected in the greater and significantly more sustained activity in plasma as compared to other artemisins. Moreover, in 3-day combinations with mefloquine (5 mg/kg) or amodiaquine (20 mg/kg), a single oral dose of artemisone (10 mg/kg) completely cured infected monkeys.²⁹

A series of C(10)-ether derivatives **15** (Fig. 8) possessing voluminous lipophilic groups were tested p.o. against multi-drug resistant *P. yoelii nigeriensis* and several of them were 2 to 4 times more active than β -arteether.³⁰ Most active were the **15a** and **15b** derivatives that afforded 100 % protection at a 12 mg/kg \times 4 day dose. The least active derivative was the corresponding β -isomer of **15a**.

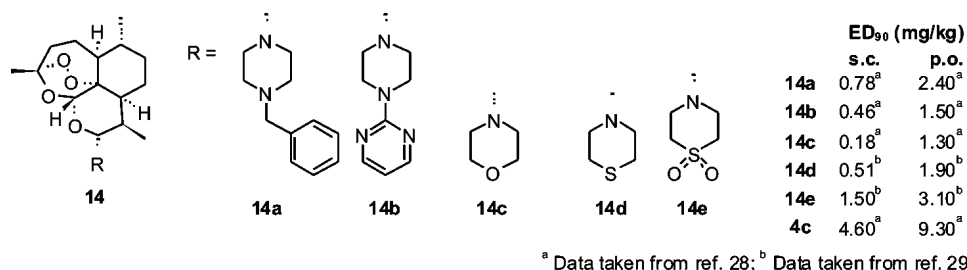


Fig. 7. Structures and antimalarial activities of derivatives **14**.

Similar relative relationships between α - and β -epimers were observed with other derivatives described in this study, which is in sharp contrast to the activity profile of arteether, where the β -isomer showed higher activity than the α -isomer. The corresponding C(10)-esters **16** (Fig. 8) were more active *in vivo* than β -arteether against *P. yoelii nigeriensis*, with **16c** being the most active derivative with 4/5 cured mice at 12 mg/kg \times 4 day p.o. dose.³¹ Comparing the members of the two series, the structurally similar esters were less active than the corresponding ethers (**16a** vs. **15a**, and **16b** vs. **15b**).

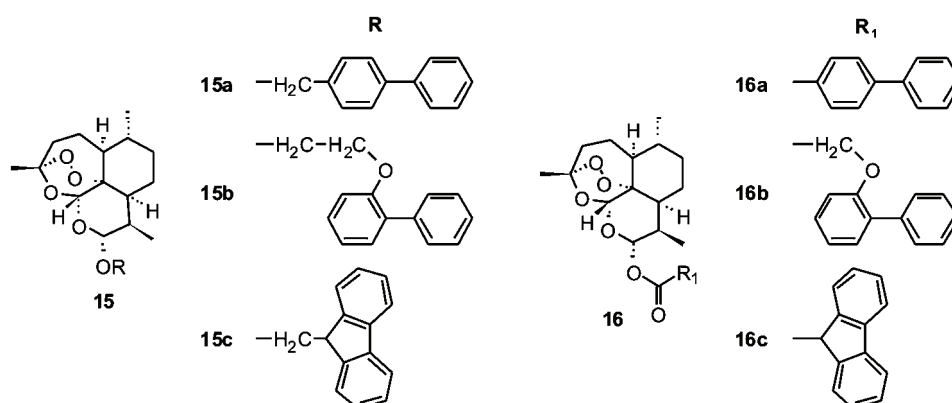


Fig. 8. Structures of derivatives **15** and **16**.

Hydrolytically stable C(10)-nonacetal artemisinin dimers **17** (Fig. 9), which possess phthalate derivatives as linker, showed higher *in vitro* antimalarial activities against the CQS NF54 *P. falciparum* strain than ART **1**, with **17a** and **17b** being the most active.³² These two dimers were, respectively, 3 times and 37 times more efficacious than artesunate **4c** when administered s.c. and **17b** was 1.5 times more efficacious than **4c** (p.o.).

A new generation of ART dimers with excellent *in vivo* activity in *P. berghei* infected mice was developed.^{33,34} Eleven new derivatives **18–24** (Fig. 10) showed curative activity at a 3 \times 30 mg/kg oral dose. At this dose, the average

mouse survival period was ≥ 3 times longer in comparison to artesunate **4c** (> 30 days for derivatives **18–24** vs. 7 days for **4c**).³⁴

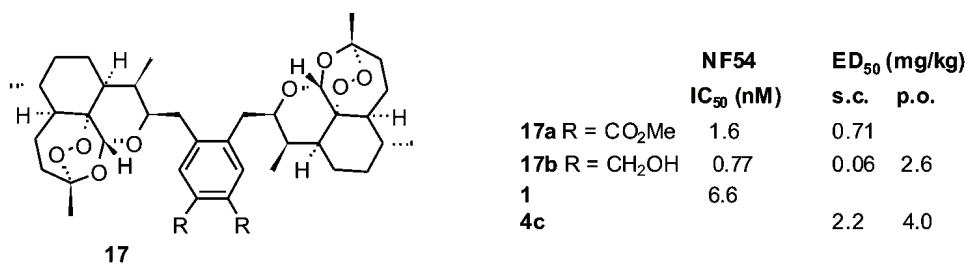


Fig. 9. Structures and antimalarial activities of dimers **17**.

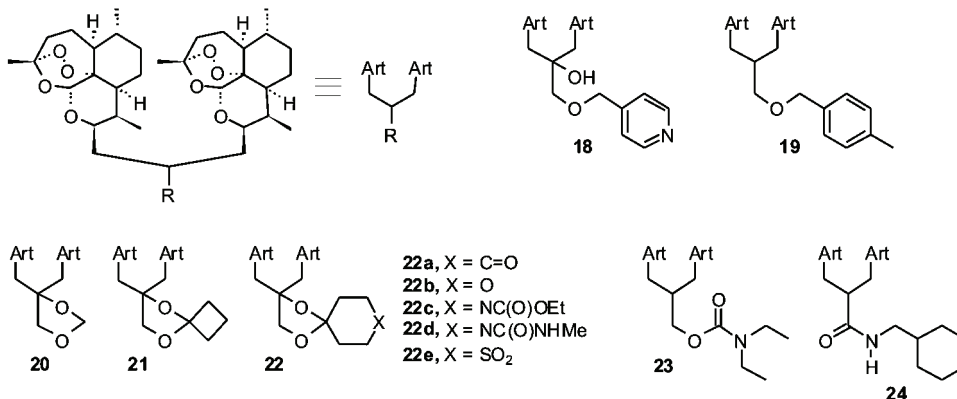


Fig. 10. Structures of derivatives **18–24**.

4. 1,2,4-TRIOXANES

Very important finding was the high antimalarial activity of trioxanes. These compounds have a much simpler structure than the ARTs, *e.g.*, the trioxanes **25–29** (Fig. 11).^{35–38} The activity data significantly contributed to the understanding of the minimum structural requirements for exhibition of good antimalarial activity. The results strongly indicate that ring D and the lactone ring are of no importance for good antimalarial activity, but all derivatives confirmed the importance of the unique 1,2,4-trioxane structure. The results showed that small stereo or structural differences have a significant contribution to the activity, *e.g.*, epimers **25** showed different *in vitro* activity³⁵ (particularly significant against the CQS strain D6), or in the case of derivatives **26**, in which the methyl substituents are replaced with the spirocyclopentyl group (**26a** vs. **26b**).³⁵ Contrary to the observed stereoselectivity, the enantiomers of **27a** and **27c** or **27b** and **27d** showed very similar activities, suggesting that *cis*-fusion significantly contributes to the activity.³⁶ Probably the most interesting example is represented by epimers **28**,

where the change of the configuration at one stereocentre dramatically changed the activity.³⁷ A similar structure-activity relationship, SAR, could be developed for **29** and **30**.³⁸

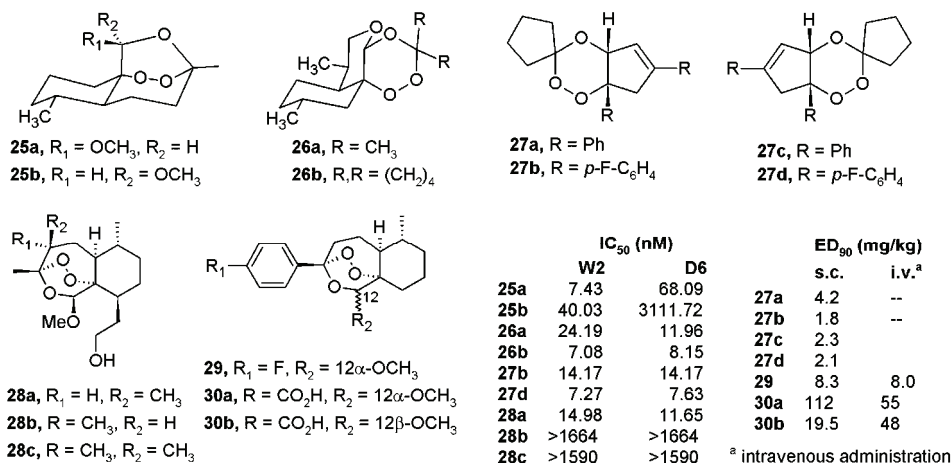


Fig. 11. Structures and antimalarial activities of derivatives **25**–**30**.

Structurally similar to the *cis*-fused trioxanes **27**, the *trans*-fused derivatives **31**–**34** (Fig. 12) also exhibited high activities.³⁹ They caused a 96–100 % suppression of parasitemia on day 4 after a 96 mg/kg/day p.o. dose, with the spirocycloheptane **33** as the most active. Although trioxanes **31**–**34** are somewhat less effective than β -arteether under the same test conditions (100 % of suppression at

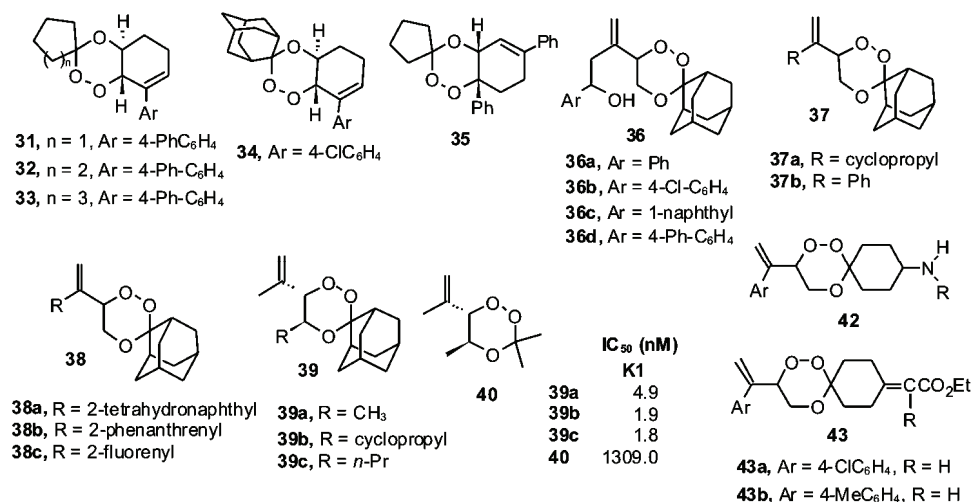
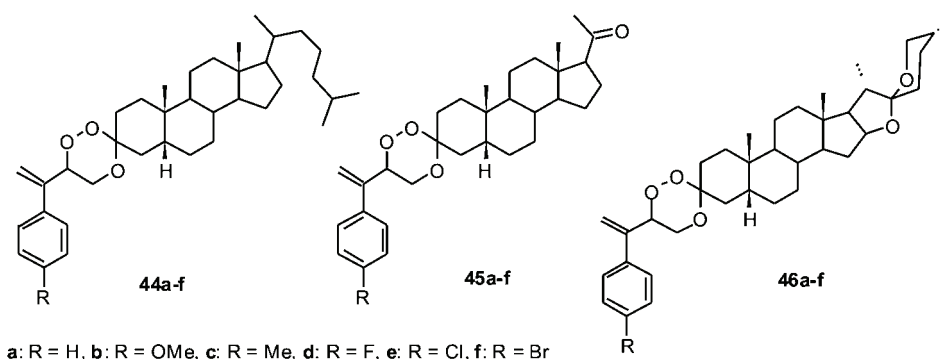


Fig. 12. Structures and antimalarial activities of derivatives **31**–**43**.

48 mg/kg/day), the obtained results suggested that *trans*-fusion may also provide good antimalarial activity and that some other structural aspects should additionally be taken into consideration. Accordingly, the *cis*-fused trioxane **35** (Fig. 10) showed IC_{50} and IC_{90} values of 893 nM and 1845 nM, respectively, against the W2 *P. falciparum* clone, while under the same screening conditions, the *cis*-fused trioxane **27a** showed corresponding values of 15 nM and 36 nM, respectively.⁴⁰

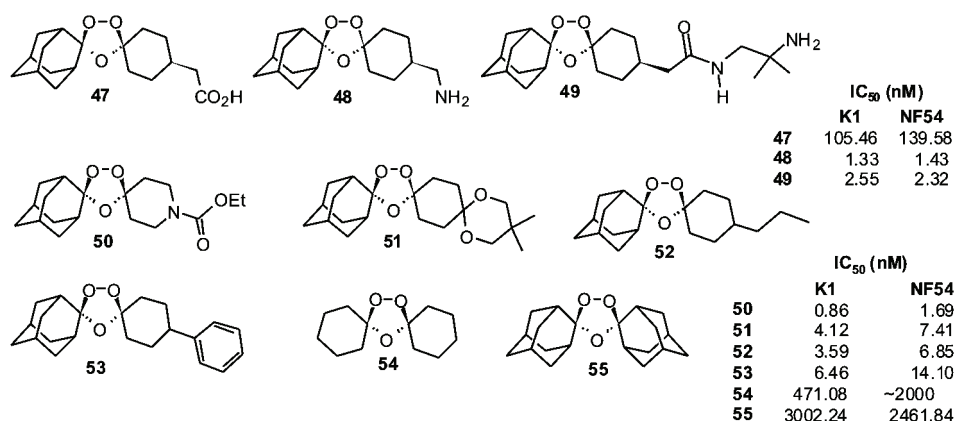
Trioxanes **36–43** (Fig. 12) were obtained due to efforts aimed at creating peroxides with a simpler structure but still sufficiently active for treating malaria. Using different starting materials, such as geranyl acetate⁴¹ (trioxanes **36**), cyclopropyl or cyclohexyl allylic alcohols⁴² (trioxanes **37**), aryl substituted allyl alcohols (trioxanes **38**)⁴³ or methyl substituted allyl alcohols (trioxanes **39** and **40**)⁴⁴ for obtaining β -hydroxyhydroperoxides which were later coupled to different carbonyl compounds, very active trioxanes with diverse structures were obtained.^{45,46} Of all the given examples, the most active were the 2-adamantyl derivatives. Derivatives **36–38** were tested against multidrug resistant *P. yoelli* in mice and exhibited 100 % suppression of parasitemia on day 4 at 96 and 48 mg/kg \times 4 days (Peter's test) doses p.o. The most active 2-fluorenyl derivate **38c** showed 100 % of suppression of parasitemia on day 4 even at 24 mg/kg \times 4 days, which appears to be the half effective dose of arteether.⁴³ Intramuscular injection decreased the activity of these derivatives and thus confirmed, once again, that hydrophobic compounds show better bioavailability on oral administration. Derivatives **39** and **40** with a C(5)-alkyl substituted 1,2,4-trioxane ring were tested against the CQR K1 *P.f.* strain and showed activities which strongly depended on the C(3)-substituent. While the spiroadamantane derivatives **39** were as active as ART **1**, the *gem*-dimethyl derivative **40** was 270 times less active.⁴⁴ Replacing the spiroadamantyl with a spirocyclohexyl group bearing an ionisable arylamino moiety, as in **42**,⁴⁵ or other polar groups, as in **43**,⁴⁶ also resulted in loss of activity. Although some derivatives, such as **43a** and **43b**⁴⁶ that exhibit 100 % suppression of parasitemia on day 4 at 96, 48 and 24 mg/kg \times 4 days doses p.o., were active, in general, these compounds were less potent than the adamantyl derivatives. These results convincingly introduced the adamantyl-spiro-1,2,4-trioxane motif as a significant contributor to good antimalarial activity.

The antimalarial activity of a series of steroids possessing the 1,2,4-trioxane moiety **44–46** (Fig. 13) was also tested.⁴⁷ Only the pregnane-based trioxanes **45a–f** expressed good activity. They showed 100 % suppression of parasitemia on day 4 and 40–100 % protection at a 96 mg/kg \times 4 days dose, with **45b** being the most efficacious. Cholestane- and tigonenin-based derivatives were much less successful with 15–73 % suppression.

Fig. 13. Structures of steroid-based 1,2,4-trioxanes **44–46**.

5. 1,2,4-TRIOXOLANES

1,2,4-Trioxolanes, the ozonides, are a very well known class of organic compounds. They are intermediates in the transformation of olefins into carbonyls during ozonolysis. It was an unexpected and surprising discovery⁴⁸ that ozonides are stable enough and that some of them express excellent activity against the malaria parasite, as do the structurally similar 1,2,4-trioxanes. Moreover, these compounds were more active than artesunate **4c** and artemether **3a**, both *in vivo* and *in vitro*. The compounds **47–49** (Fig. 14) showed superior pharmacokinetic results, such as prolonged half-life and enhanced bioavailability after a single oral dose. The derivative **49** had inferior antimalarial results and a higher recrudescence level compared to **48**, however, it was chosen as the development candidate primarily because of its improved toxicological profile and reduced concentrations in brain tissue after oral dosing.⁴⁸ The other derivatives **50–53** (Fig. 14) afforded further insight into SAR in the context of the physicochemical, biopharmaceutical, and toxicological profile of trioxolanes.⁴⁹ Interestingly, it was

Fig. 14. Structures and antimalarial activities of derivatives **47–55**.

shown that symmetrically substituted derivatives **54** and **55** (Fig. 14) were significantly less active than their non-symmetrical counterparts,⁴⁹ thus confirming an earlier observation of higher activity of non-symmetrical substituted peroxides.⁵⁰

The tolerance of the 1,2,4-trioxolane moiety to diverse synthetic conditions⁵¹ enabled the synthesis of a significant number of derivatives and some of them showed very good *in vitro* and *in vivo* activities, e.g., the derivatives **56**–**60**,⁵² the piperidine derivatives **61**–**63**⁵³ and derivatives containing aliphatic and aromatic amino functional groups or azole heterocycles as substituents (**64**–**70**) (Fig. 15).⁵⁴ The lack of activity of **71** indicates the essential contribution of the spiro-adamantane system to the antimalarial properties of this class of compounds.⁵⁴ As the authors concluded from the obtained results, *in vitro* activities are not always a reliable predictor of *in vivo* potency.^{52, 54} Many of the examined derivatives showed excellent *in vitro* results but failed during *in vivo* tests, toxi-

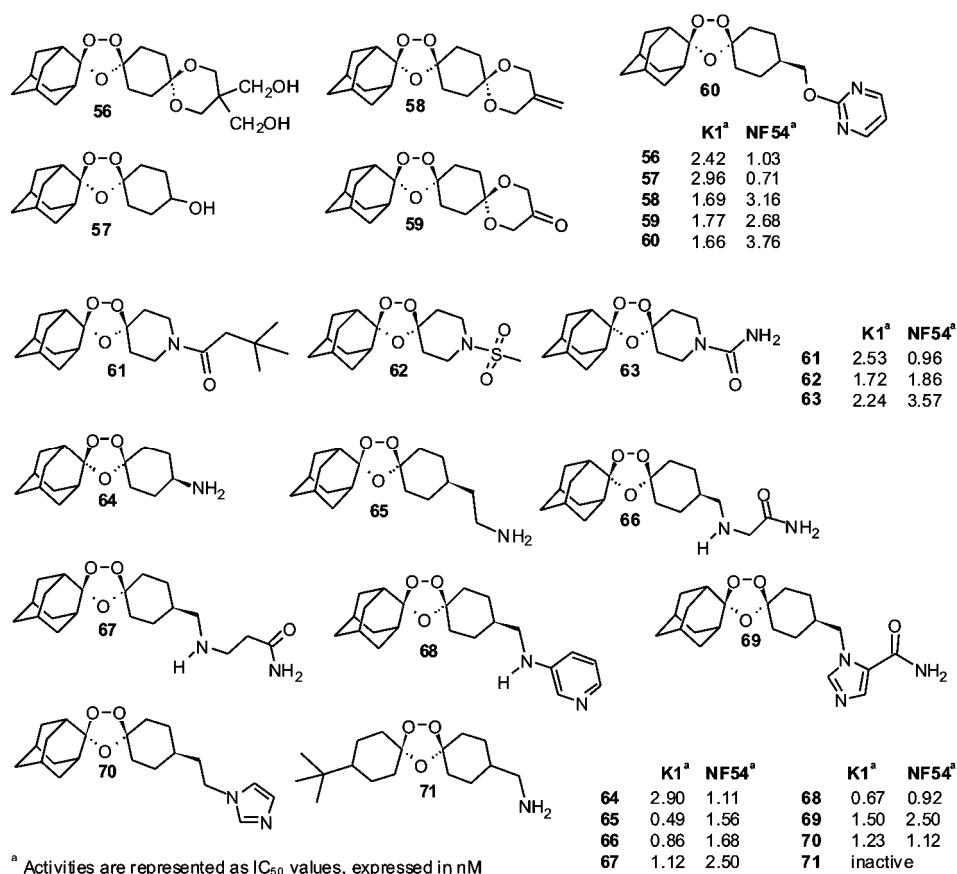


Fig. 15. Structures and antimalarial activities of derivatives **56**–**71**.

city trials or metabolic stability and bioavailability tests. The more lipophilic trioxolanes tend to have better oral activities but are metabolically less stable than their more polar counterparts are. Such behaviour is consistent with results obtained for other classes of synthetic peroxides. Trioxolanes with a wide range of neutral and basic groups had good antimalarial profiles, contrary to derivatives with acidic groups.

6. 1,2,4,5-TETRAOXANES

3,6-Substituted derivatives of 1,2,4,5-tetraoxacyclohexane (1,2,4,5-tetraoxane) have been known for many years and were used for different purposes.⁵⁵ They are readily formed by acid-catalyzed peroxyacetalization of carbonyl compounds with hydrogen peroxide or bis-trimethylsilylperoxide.^{56–58} The discovery that inexpensive 3,6-dicyclohexylidene tetraoxanes exhibited pronounced antimalarial activity opened new possibilities in combating this pestilence.⁵⁹ Since then, many efforts have been made to find better procedures for synthesizing and designing new derivatives with improved activities.^{60,61} Many of them were reviewed and their antimalarial activities analyzed.^{5f,5g,62}

After the first report in which they were described,^{50,63} mixed tetraoxanes* have acquired significant attention.⁶² Since then, some new procedures for their synthesis,^{64,65} or the synthesis of *gem*-dihydroperoxides as key precursors⁶⁶ have been developed with aim of improving the yields of tetraoxane compounds.

A new group of mixed dicyclohexylidene tetraoxanes, bearing polar neutral or basic groups, demonstrated high activities against both CQS and CQR *P.f.* strains (Fig. 16).⁶⁷ The compounds were designed with the aim of obtaining the simplest amphiphilic structures of the kind and to minimize the influence of steric effects on the antimalarial activity. In addition to this, a thorough examination

	Structure	R	IC ₅₀ (nM)		
			D6	W2	TM91C235
72:		R = NHCH ₂ CH ₂ N(CH ₃) ₂	72 ^a	72 ^b	72 ^c
73:		R = OH	73 ^b	73 ^b	73 ^b
74:		R = N ₃	74 ^b	74 ^b	74 ^b
75:		R = NH ₂	75 ^b	75 ^b	75 ^b
76:		R = NHC ₆ H ₁₁	76 ^b	76 ^b	76 ^b
77:		R = NHPr'	77 ^b	77 ^b	77 ^b
78:		R = NHCH ₂ Ph	78 ^b	78 ^b	78 ^b
79:		R = OCH ₃	79 ^c	79 ^c	79 ^c
80:		R = NH ₂	80 ^c	80 ^c	80 ^c
81:		R = NHCH ₂ CH ₂ N(CH ₃) ₂	81 ^c	81 ^c	81 ^c

^a Data from ref. 67a; ^b Data from ref. 67b;

^c Data from ref. 67c. Compounds were tested as mixture of diastereoisomers

Fig. 16. Structures and antimalarial activities of derivatives 72–81.

*The term “mixed tetraoxanes” describes 1,2,4,5-tetraoxacyclohexanes differently substituted at positions 3 and 6.⁵⁰

of the chemical stability under basic and acidic conditions, and under oxidative, reductive and reductive amination conditions revealed a significant stability of the tetraoxane moiety that enabled the synthesis of variety of derivatives.^{67c} Interestingly, the most active compounds within the group of dicyclohexylidene tetraoxanes **72–81** have very similar activities irrespective of the presence of neutral (**74**, **79**), polar protic (**73**) or a basic ionisable group (**72**, **75–78**, **81**). Such behaviour impedes profound SAR analysis. In the present set of derivatives, amines **75** and **76** were the most active *in vivo*. They both cured 5/5 mice at 300 mg kg⁻¹ day⁻¹ doses s.c.* with 150 mg kg⁻¹ day⁻¹ doses s.c., **75** retained the same efficiency but **76** was less active with 4/5 cured mice.

A structurally similar group of cyclohexylidene mixed tetraoxanes was synthesized⁶⁸ using a procedure previously applied to this class of compounds (Fig. 17).^{50,67a} The compounds were screened against CQS *P.f.* strain 3D7 and the most active derivatives **82–88** had activities within the same range as the ones described above. Monospiro tetraoxanes that exhibited a much lower antimalarial potency (**87** and **88**) confirmed the superiority of the 3,6-dispiro-1,2,4,5-tetraoxane structural motif. Adamantyl derivatives **85** and **86** showed 100 % inhibition on p.o. administration at 30 mg kg⁻¹ doses and derivative **86** had better *ED* values against *P. berghei* (ANKA) as compared to artemether: *ED*₅₀ = 3.18 mg kg⁻¹ and *ED*₉₀ = 3.88 mg kg⁻¹ for **86**; *ED*₅₀ = 5.88 mg kg⁻¹ and *ED*₉₀ = 10.57 mg kg⁻¹ for artemether.

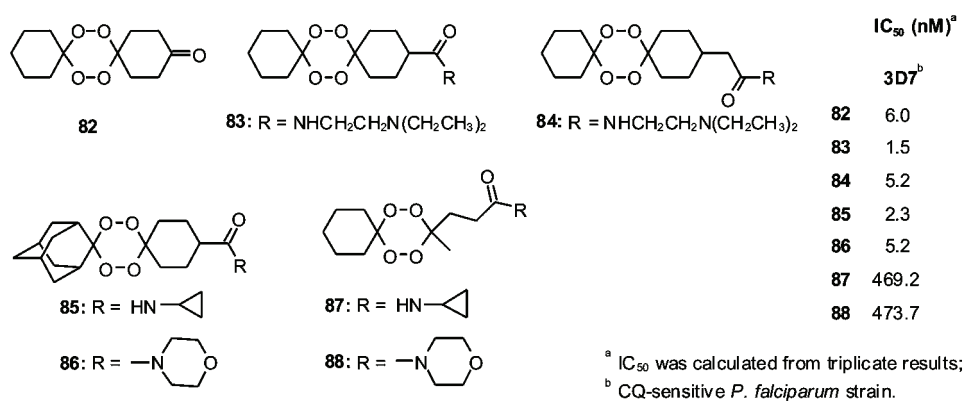


Fig. 17. Structures and antimalarial activities of derivatives **82–88**.

The ability of adamantyl substituent to stabilize the structure and to improve the antimalarial activity was additionally exemplified with a new series of amphiphilic adamantyl-based mixed tetraoxanes (Fig 18).⁶⁹ The derivatives that contain polar sulphonamide groups at one end and a highly lipophilic adamantyl

* Modified Thompson test. "Cure" is defined as a mouse alive at day 31 with no parasitemia.

group at the other end exhibit activity in the 3–30 nM range, with **89–92** as the most active compounds against the 3D7 *P. f.* strain. In addition, derivative **89** was tested *versus* seven additional strains of *P. falciparum* and exhibited activity in the 1.9–3.8 nM range. Compounds **89** and **91** were noticeably active *in vivo* (p.o., *P. berghei* ANKA): $ED_{50} = 6.61 \text{ mg kg}^{-1}$ for **89** and $ED_{50} = 7.93 \text{ mg kg}^{-1}$ for **91**, $ED_{50} = 8.42 \text{ mg kg}^{-1}$ for ART.

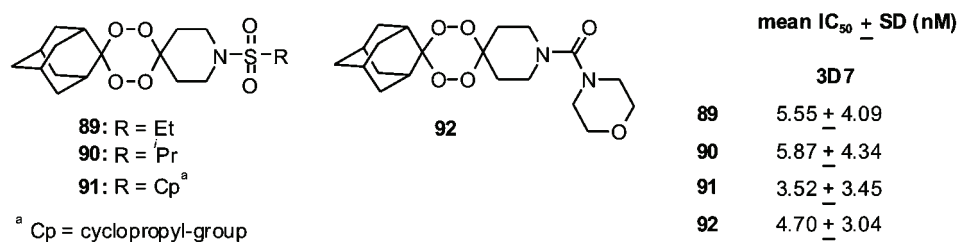


Fig. 18. Structures and antimalarial activities of derivatives **89–92**.

Some other types of tetraoxanes were less successful as antimalarials. Such examples are symmetrically substituted 3,3,6,6-tetraalkyl-1,2,4,5-tetraoxanes derived from acyclic ketones⁷⁰ and symmetric and non-symmetric 1,2,4,5-tetraoxane derivatives of substituted benzaldehydes (Fig. 19).⁷¹ The compounds were tested as mixtures of the corresponding isomers and, in general, exhibited rather poor antimalarial activity against both CQS and CQR *P. falciparum* strains. Within the series of acyclic derivatives, compounds **93–95** were the most active but still they were 1.6–2.2 times less active than the corresponding tetraoxanes **96** derived from cyclohexane, and 40–50 times less active than artemether.⁷⁰ Within the benzaldehyde series, compound **97** was the most active, while the other members were significantly less active with IC_{50} values in the range 1.4–17 μM ,⁷¹ which is far less than the corresponding 1,2,4,5-tetraoxanes or 1,2,4-trioxanes considered as active. Nevertheless, these results offer valuable basic information for the correlation between structure and antimalarial activity of the simple peroxides.

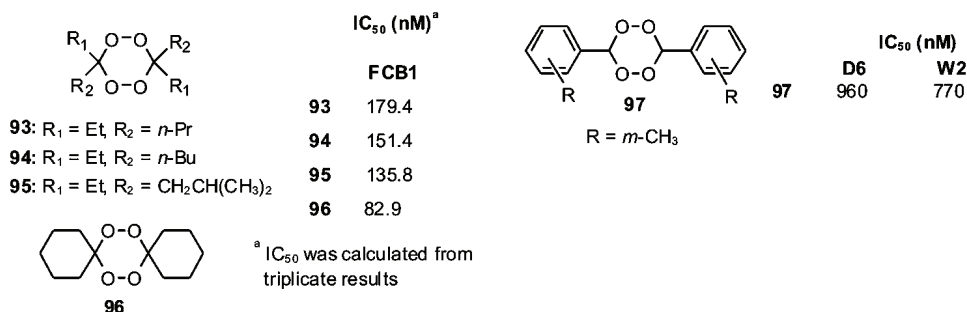


Fig. 19. Structures and antimalarial activities of derivatives **93–97**.

1,2,4,5,7,8-Hexaoxonanes are customary side products of the synthesis of 1,2,4,5-tetraoxacyclohexanes (Fig. 20). Their activities against K1 and NF54 *P. f.* strains showed that hexaoxonanes **98–103** are convincingly less active than the corresponding tetraoxanes, with 3–4 orders of magnitude lower IC_{50} values.⁷² Since peroxide bonds are essential for antimalarial activity, such poor efficiency was attributed to steric hindrance of the peroxide bonds. An analogous behaviour was also noticed with the asymmetric 1,2,4,5,7,8-hexaoxonane **104**.^{67c}

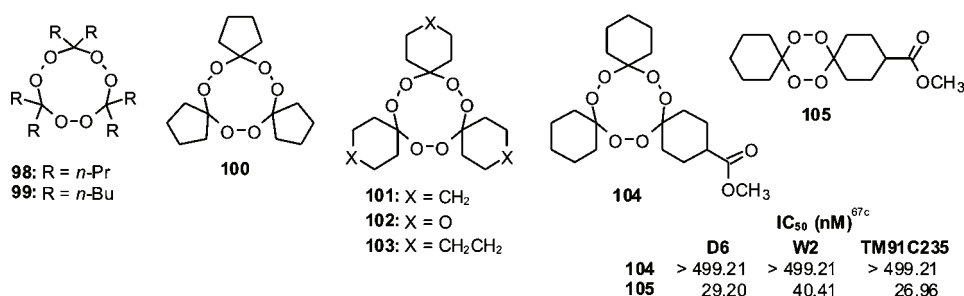


Fig. 20. Structures and antimalarial activities of derivatives **98–105**.

The first described steroidal 1,2,4,5-tetraoxanes **106** and **107** were derivatives from 5 α -cholestane-3-one (Fig. 21).⁵⁸ Although tetraoxane **106** was less active in comparison to ART (IC_{50} (D6) = 155 nM), the results of this pioneering research clearly showed that even complex molecules such as steroids could be good carriers of the tetraoxane pharmacophore. Replacing cholestane with derivatives of cholic acid significantly improved the antimalarial activity (Fig. 21).^{57,73} The compounds obtained as series of diastereomers, named as *cis*-C(2)C(2a) and *trans*-C(2)C(2a), showed moderate to high activity against both CQS and CQR strains. The most active were the primary amide **108** (IC_{50} (W2) = 18.79 nM) and the *n*-propyl amides **109** and **110** (IC_{50} (D6) = 9.29 nM and 20.08 nM, respectively).

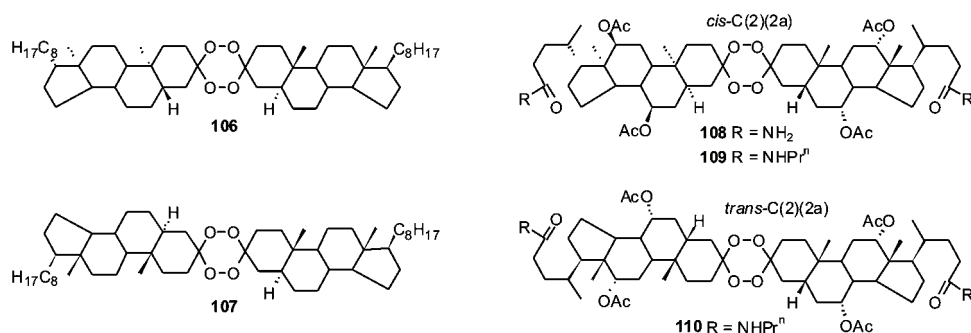


Fig. 21. Structures of derivatives **106–110**.

Replacing one steroid with a simpler alkylidene moiety enabled the synthesis of the second generation of steroidal tetraoxanes based on cholic acid derivatives. Starting from 4-alkyl,^{50,74} 4-aryl,⁷⁵ 4-carboxy substituted cyclohexanones⁷⁶ and the acetone⁷⁷ afforded the synthesis of a numbers of various derivatives (Fig. 22). The stability of the tetraoxane moiety under a range of reaction conditions enabled the synthesis of diverse derivatives.^{67c} Some of the shown mixed steroidal tetraoxanes exhibited impressive *in vitro* and *in vivo* antimalarial activity. The contribution of the cholic acid moiety as carrier is clearly emphasized by the pronounced activity of derivative **118**; bis-isopropylidene tetraoxane was completely inactive.⁷⁸

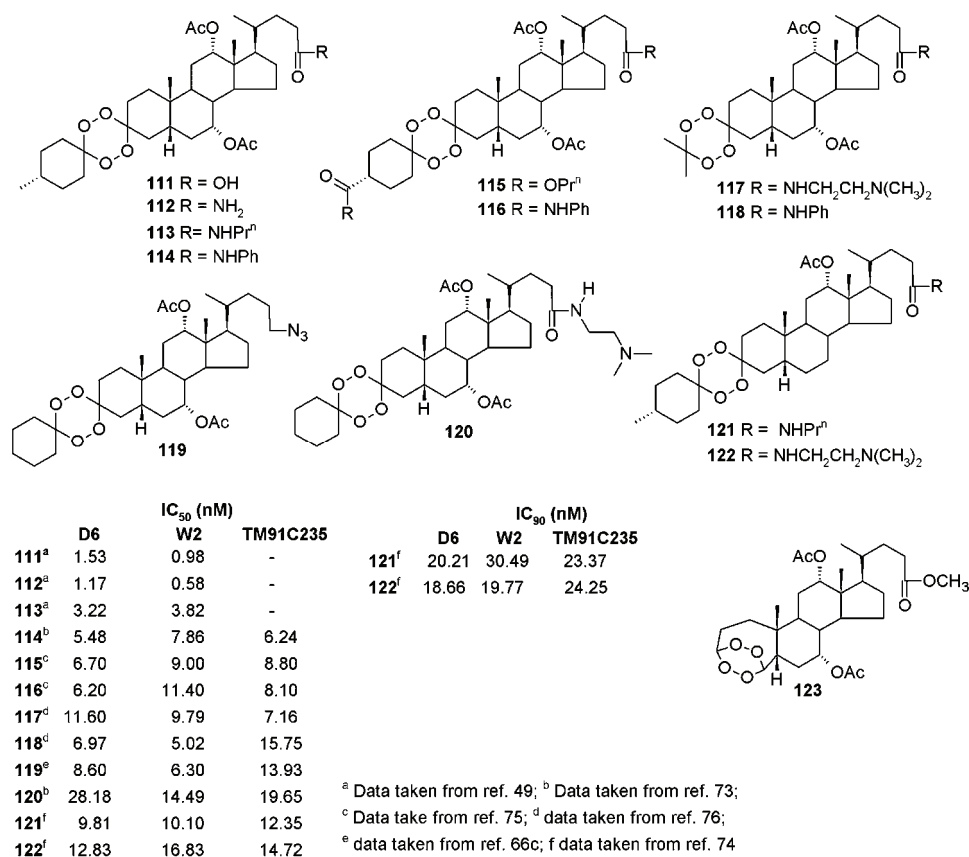


Fig. 22. Structures and antimalarial activities of derivatives **111–123**.

When administered to mice (p.o., *P. berghei* KBG 173 strain), tetraoxane **112** cured 4/5 mice at 200 mg kg⁻¹ day⁻¹ doses,* while being moderately active

* Modified Thompson test. “Cure” is defined as a mouse alive at day 31 with no parasitemia.

when applied at $50 \text{ mg kg}^{-1} \text{ day}^{-1}$ (cured 2/5).⁵⁰ The administration of tetraoxane **117** (p.o.) produced 2/5 cured mice at $320 \text{ mg kg}^{-1} \text{ day}^{-1}$ doses, however, the same compound was more efficient at $160 \text{ mg kg}^{-1} \text{ day}^{-1}$ s.c. doses with 5/5 cured mice.⁷⁷ All the cured mice had negative blood smears during all the test days (6–31). Tetraoxane **120** cured 5/5 mice at $320 \text{ mg kg}^{-1} \text{ day}^{-1}$ and demonstrated moderate activity using lower doses ($80 \text{ mg kg}^{-1} \text{ day}^{-1}$) with 3/5 cured mice.⁷⁴ It should be emphasized that all these compounds showed no toxic effects towards the tested animals at any applied concentration. In addition, they have low activity against the Vero cell line, exhibiting a cytotoxicity/antimalarial potency ratio $1/(1400 - 9500)$.⁵⁰ Furthermore, the *n*-propyl amide **113** revealed no healthy erythrocyte (RBC) membrane lysis,⁷⁹ suggesting that the antimalarial activity of these compounds was the consequence of interaction specific to infected RBC, and was not the result of uncontrolled RBC membrane lysis.

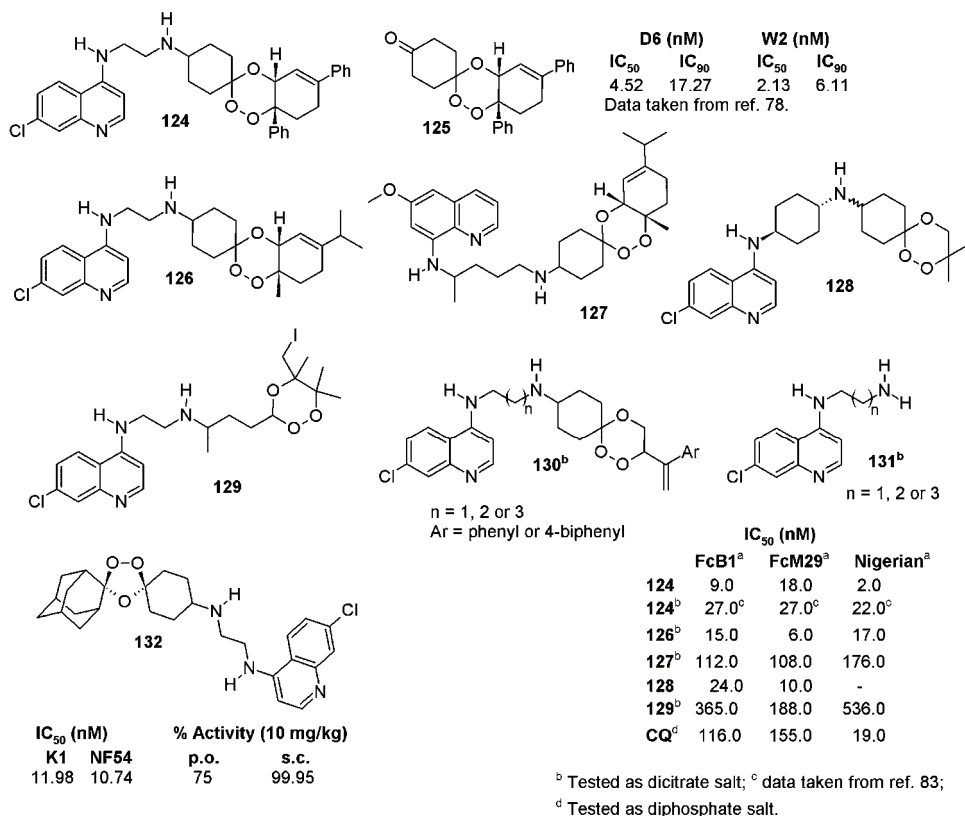
A series of tetraoxanes based on deoxycholic derivatives were prepared with the aim of comparing them to cholic acid-derived tetraoxanes (Fig. 22).⁷⁴ In general, these compounds follow the same trends as the cholic acid derivatives: higher activity of the 4''-methylcyclohexyl derivatives than the non-substituted cyclohexyl ones and higher activity of 4''*R*- over 4''*S*-epimers. However, tetraoxanes with deoxycholic acid-derived carriers are less active than the corresponding cholic acid derivatives suggesting that the C(7) acetyloxy group appreciably contributes to their antimalarial activity. Within this group of tetraoxanes, the derivatives **121** and **122** were the most active exhibiting activities similar to ART and mefloquine. *In vivo*, compound **122** cured 3/5 mice at $160 \text{ mg kg}^{-1} \text{ day}^{-1}$ doses (p.o., *P. berghei* KBG 173 strain), however, at lower doses of $40 \text{ mg kg}^{-1} \text{ day}^{-1}$, the activity declined sharply with no cured mice.

The only intramolecular steroidal 1,2,4,5-tetraoxane **123** (Fig. 22) hitherto tested* exhibited moderate *in vitro* antimalarial activity against *P. falciparum* strains (IC_{50} (D6) = $0.63 \mu\text{M}$; IC_{50} (W2) = $0.52 \mu\text{M}$).^{80a}

7. CHIMERIC PEROXIDE–QUINOLINE COMPOUNDS

A new concept for treating malaria was introduced with the chimeric peroxides, compounds that possess covalently bonded two well-known pharmacophores – the quinoline functionality and an appropriate peroxide moiety. The compounds were designed with the aim of overcoming resistance of the parasite to CQ-based drugs and to take advantage of the pharmacokinetic properties of trioxanes, ozonides and tetraoxanes. The initial set of derivatives were more active than chloroquine against CQR strains, with compound **124** being the most active on both laboratory strains⁸¹ and on human isolates (Fig 23).⁸²

* After submission of the manuscript, the authors became aware of new intramolecular tetraoxanes prepared by the Russian group: Alexander O. Terent'ev, Dmitry A. Borisov, Vladimir V. Chernyshev, Gennady I. Nikishin, *J. Org. Chem.* **74** (2009), doi jo900226b.



^a FcB1 - Colombia CQR strain *P.f.*; ^a FcM29 - Cameroon highly CQR strain *P.f.*; ^a Nigerian - CQS stain *P.f.*

Fig. 23. Structures and antimalarial activities of derivatives **124–132**.

Certain simplifications of structure lead to trioxaquine **126** that was very active against both CQS and CQR strains of *P. falciparum*:⁸³ ED₅₀ = 5 and 18 mg kg⁻¹ day⁻¹ (*P. vinckei*), i.p. and p.o. administration, respectively. Parasitemia clearance, without recrudescence, was achieved after an 18 mg kg⁻¹ day⁻¹ i.p. dose and no toxic effect in mice was observed even at 120 mg kg⁻¹ day⁻¹ p.o. dose over four consecutive days. Coupling of the same trioxane ketone and primaquine produced trioxaquine **127**, which demonstrated significantly lower activity against all three examined strains, and thus limited this concept to only 4-aminoquinolines. Trioxaquine **128** also exhibited high *in vitro* and *in vivo* activity.⁸⁴ The compound completely cured mice infected with CQR strain *P. vinckei* and CQS strain *P. vinckei* at 30 mg kg⁻¹ day⁻¹ p.o. doses.

Other variations in the trioxane structure produced derivatives **129**⁸⁵ and **130**,⁸⁶ which expressed lower activities than the previously described derivatives.

Although some very active trioxaquinines were prepared, the concept of these drugs did not justify itself for several of reasons. First, these compounds did not show the expected synergism since in many cases the parent trioxane ketones^{78,86} were more active than the hybrids, see ketone **125** vs. chimera **124** for comparison. In addition, 4-aminoquinolines **131** are themselves antimalarials. They suppressed parasitemia in mice (i.m., 87–97 %) but, as with trioxaquinines **130**, no treated mice survived.⁸⁶ Even though some authors wish to establish these chimeras as therapeutics with dual activity,^{84,87} all the available evidence on the mechanism of antimalarial activity of trioxanes and 4-aminoquinolines indicate that they have the same target.⁸⁴ Lastly, many of these hybrid molecules were tested as inseparable mixture of diastereomers. These circumstances deprived one of the possibilities to realize the actual scope of the antimalarial capacity of these compounds.

Based on the concept that the compounds have two integrated pharmacophores and enhanced activities of trioxolanes with the basic side chain, chimeric trioxolane **132** was obtained (Fig. 23).⁸⁸ Although it is very active *in vitro* against the K1 and NF54 strains and *in vivo* against the ANKA strain of *P. berghei*, **132** did not achieve a synergic effect of the two pharmacophores, especially when compared to trioxolanes **64** and **68**.

Another variation of trioxane hybrid antimalarials was made with covalently bonded dihydroartemisinin **2** and C(18)-quinine acid **133** (Fig 24).⁸⁹ The two segments were bonded with a hydrolytically labile ester bond and it is possible that under physiological conditions, hybrid **134** actually delivers two active agents.

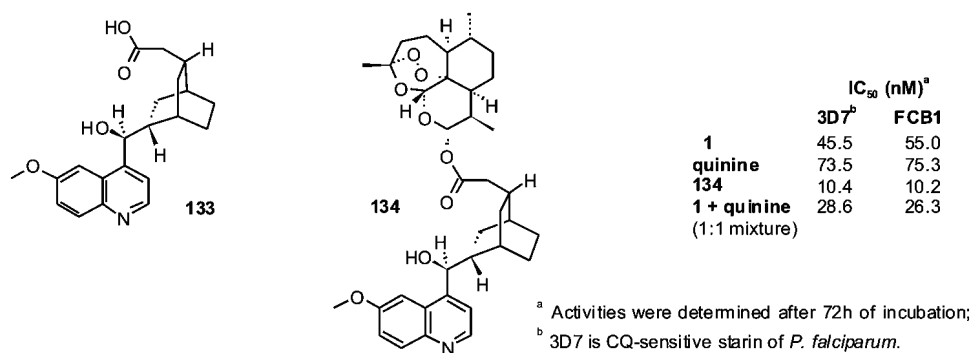


Fig. 24. Structure and antimalarial activity of derivative **134**.

This approach seems to be logical since there is evidence that ARTs and quinine are active in the same stage of the *P. falciparum* life cycle,⁹⁰ but differ in the mechanism of their action.⁸⁹ The obtained results showed that hybrid **134** had a significantly higher antimalarial activity than ART and quinine alone, or when it is compared to an equimolar mixture of ART and quinine. However, the ob-

served results would be more significant if the authors had compared hybrid **134** to dihydroART **2** rather than ART and/or to acid **133**.

Based on data obtained from research into the mechanism of tetraoxane action⁷⁶ (*vide infra*), chimeric tetraoxaquinones were designed with the aim of examining the effects of the presence of two pharmacophores within the same molecule (Fig. 25).⁹¹ Three of them were as active as ART or mefloquine against the tested strains of *P. falciparum* and all of them showed higher activity than chloroquine against CQR strains. Although a synergic effect was not achieved, it could be noted that derivatives exhibited higher activity than the corresponding non-chimeric derivatives (compare **135** to **72**, **136** to **77** and **78**, **137** and **138** to **120**).^{67c} *In vivo* experiments (p.o., *P. berghei* KBG 173 strain) revealed that derivatives **135** and **136** cured all tested mice at 320 mg kg⁻¹ day⁻¹ doses. At the lower dose of 80 mg kg⁻¹ day⁻¹, the derivatives were less effective, however, but still cured 3/5 of the examined mice. Both compounds have a minimum active dose (MAD) of 20 mg kg⁻¹ day⁻¹ with no toxic effects even at the highest applied dose of 960 mg kg⁻¹ day⁻¹.

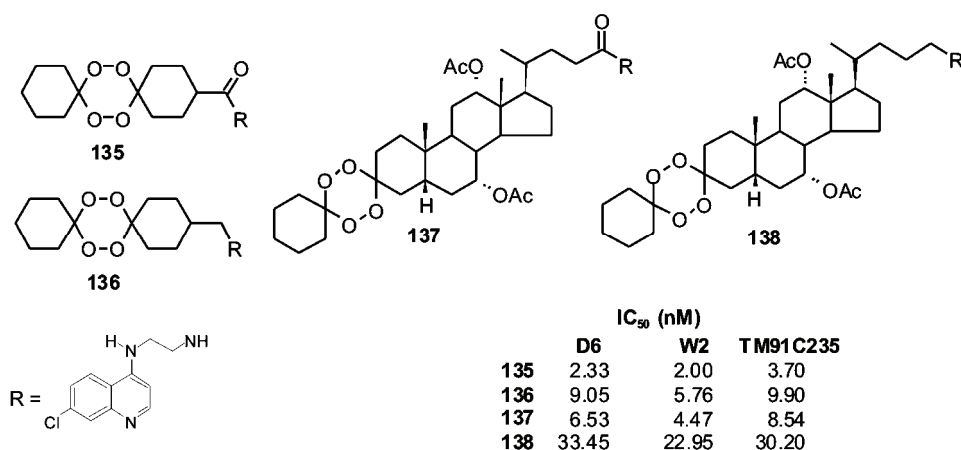


Fig. 25. Structures and antimalarial activities of derivatives **135**–**138**.

8. METABOLISM AND DRUG COMBINATION ASSAYS

Although a significant numbers of 1,2,4,5-tetraoxane antimalarials have been reported and some of them exhibited extraordinary antimalarial activity, their pharmacological properties have been much less explored than those of the 1,2,4-trioxanes. Vennerstrom was the first to give a detailed metabolic and pharmacological profile of the tetraoxanes.⁹² It was shown that compound **139** (Fig. 26) is synergistic with mefloquine and quinine against both CQS D6 and CQR W2 *P. f.* strains. Tetraoxane **139** is also synergistic with chloroquine, unlike ART that shows an additive interaction with chloroquine and synergism only at high con-

centrations.⁹³ In addition, **139** is synergistic with ART in contrast to other semi-synthetic derivatives which have a uniformly additive effect. Derivative **139** is a modest inhibitor of human CYP1A2 activity and has a different metabolic pathway to ART. Artemisinin induces its own metabolism⁹² and is metabolized by CYP2B6, CYP2C19 and, to the less extent, by CYP3A4. Tetraoxane **139** is most likely metabolized by CYP1A2 and, unlike artemisinin, **139**, has prophylactic activity, protecting 4/7 mice against *P. berghei*. These results suggest that tetraoxanes have different metabolic pathways with regard to ART and may have a somewhat different mechanism of action. Šolaja *et al.* reported the results of a metabolic stability assay and metabolic identification for many cyclohexylidene and steroidal mixed tetraoxanes.^{67b,67c,74,76,77,91} Incubation of human, mouse, rat and rhesus monkey liver microsomes with the examined compounds showed dissimilar half-lives and various mono- and dihydroxylated products, as well as the products of dehydration and deacetylation, were also detected. Unfortunately, the results of the metabolic stability assays and proposed metabolite structures could not be correlated with the *in vitro* and *in vivo* antimalarial activities of these derivatives. It is important to note that no products of peroxide bond cleavage were detected. Drug combination assays of tetraoxane **140** (Fig. 26) showed that this derivative is additive with ART **1**, dihydroART **2** and artesunate **4a** against both CQS (D6) and CQR (W2 and TM91C235) *P. falciparum* strains; however, tetraoxane **140** showed synergism with artelinic acid **6a** against all three strains.⁹⁴ Tetraoxane **140** is additive with mefloquine under high concentrations against D6 and TM91C235, but at low concentrations it exhibits an antagonistic effect. With chloroquine, tetraoxane **140** showed antagonism against all three tested strains.

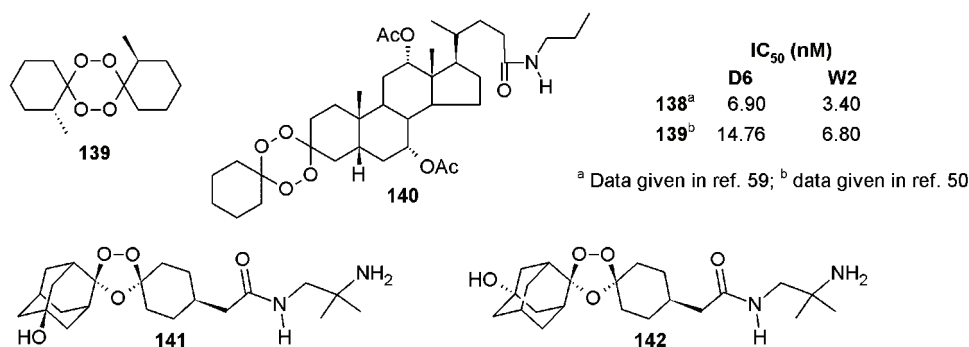
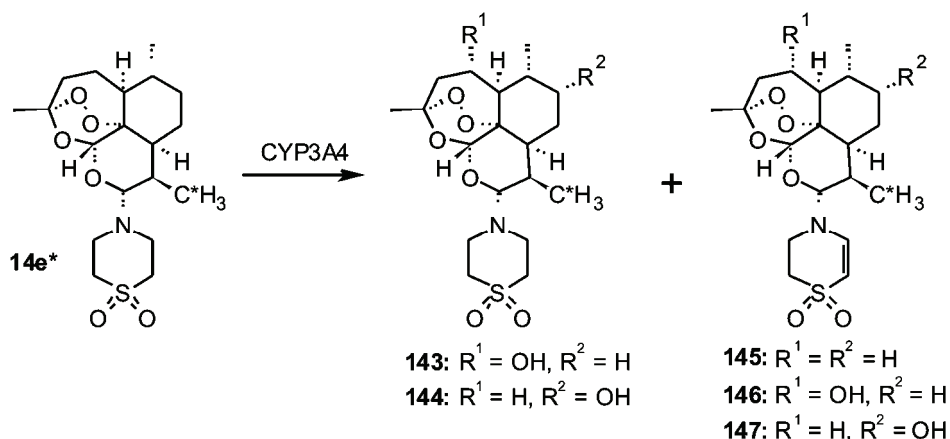


Fig. 26. Structures and antimalarial activities of derivatives **139**–**142**.

After incubation of ozonide **49** with human liver microsomes *in vitro*, three mono-hydroxylated metabolites were detected.⁹⁵ Two major metabolites **141** and **142** (Fig. 26) appeared after hydroxylation of the adamantane substructure. Both

141 and **142** had low antimalarial activity with IC_{50} values > 245 nM against the CQR K1 *P. falciparum* strain.

Incubation of isotopically labelled artemisone **14e*** with human liver microsomes after 30 min gave mono- and di-hydroxylated metabolites **143–147**, with *syn* hydroxyl and peroxide groups (Scheme 3).²⁹ Incubation with microsomes and 14 recombinant CYP isoforms together with selective inhibitors showed that only the recombinant CYP3A4 significantly metabolized artemisone, indicating that artemisone **14e** and ART, in spite of being structurally similar, have different metabolic profiles in *P. falciparum*. The isolated metabolites were tested against the *P. falciparum* K1 strain and the results showed that metabolites **144** and **145** exhibited similar activities to **14e** (**144**: $IC_{50} = 5.51$ nM and **145**: $IC_{50} = 4.26$ nM; **14e**: $IC_{50} = 1.99$ nM), but **143** was less active with $IC_{50} = 61.55$ nM.



Scheme 3. Metabolic transformations of artemisone.

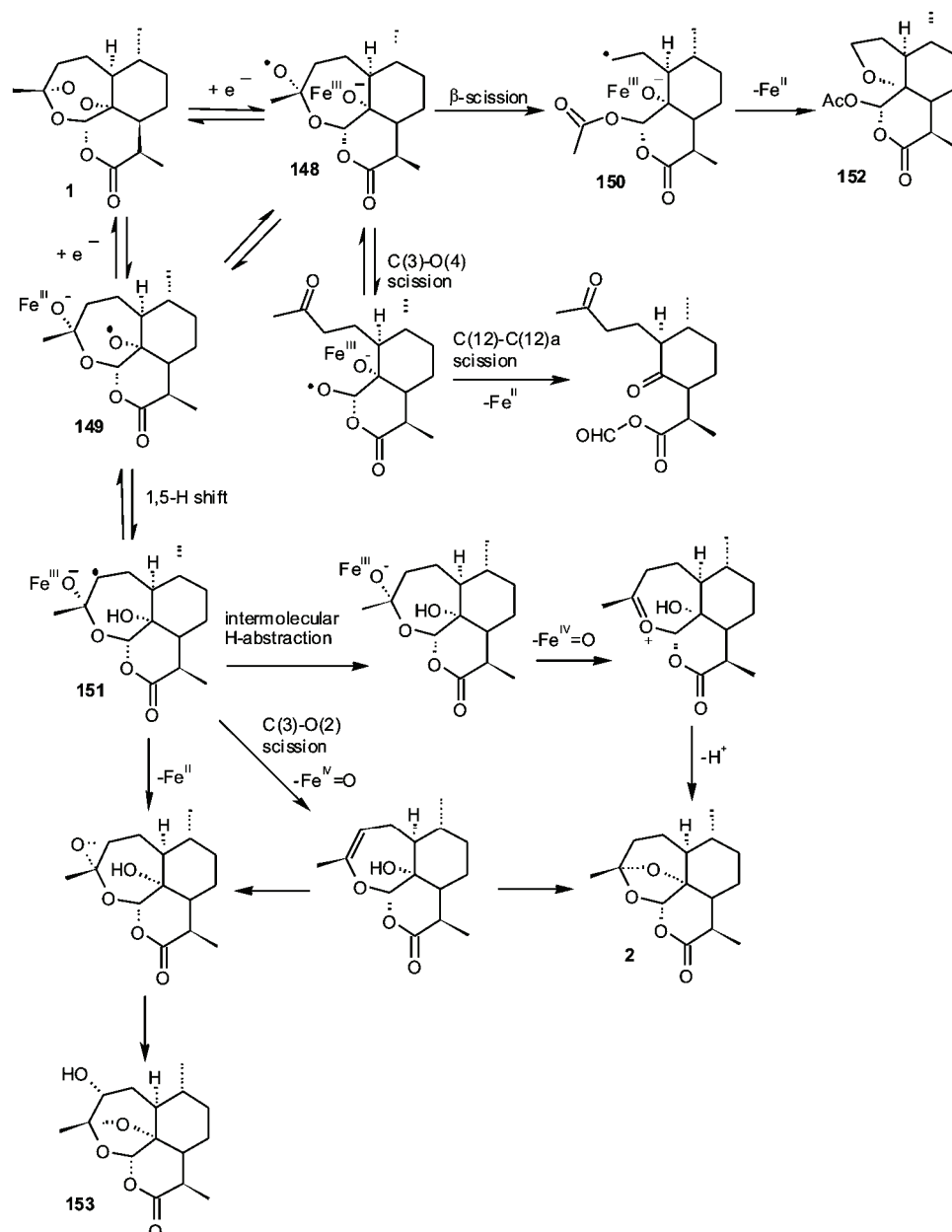
It can be seen that a common denominator is an iron species in the haem prosthetic group, and during interaction of all these structurally diverse compounds with CYP enzymes, scission of the peroxide bond never occurred.

9. MECHANISM OF ACTION

Many research groups were involved in solving the mechanism of action of antimalarial peroxides and many reports can be found on this subject. However, it was realized that the scientific literature is very controversial with many authors disagreeing about the site of action, the putative target and lethal reaction species, the actual killers of the parasite.

Several groups investigated the mechanism of action for more than fifteen years.^{36,37,96–100} In general, it was found that the process commences with the formation of oxygen radicals **148** and **149**, which arise upon homolytic peroxide bond scission in the presence of ferrous ions (Scheme 4). It is assumed that ions

148 and **149** undergo intramolecular rearrangements (1,5-hydrogen shift and β -scission) to form C-radicals **150** and **151**. Both the O- and C-centred radicals



Scheme 4. Proposed mechanism of Fe(II)-induced decomposition of artemisinin and generation of lethal O- and C-radical species.

are highly reactive species and are lethal to the parasite. During these processes, one or more intermediates probably react with vital biomolecules, inhibit their activity and cause the death of the parasite. It was proved that one of the side products is a high-valent iron-oxo species Fe(IV)=O , which could also be toxic to the parasite.^{101,102} In the absence of a suitable target that would be alkylated, the products **152** and **153** were formed.^{100b} The adducts **154–158** (Fig. 27) were found indicative for primary and secondary radicals and the ability of ART and its derivatives to act as alkylating agents.^{96c,99,100} The results obtained with artesunic acid and trioxaquine **126** additionally confirmed the capability of peroxides or chimeras to alkylate haem.¹⁰³

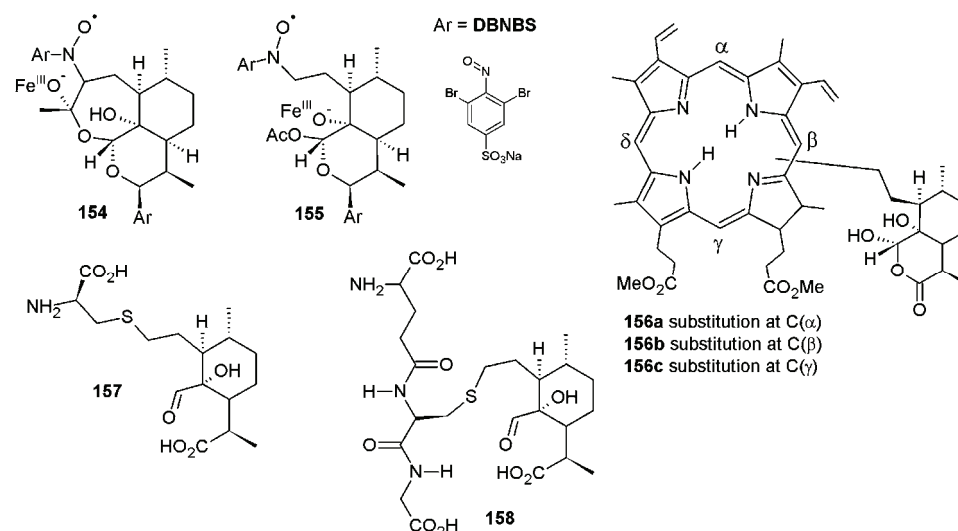


Fig. 27. Structures of covalent adducts **154–158** derived from C-centred radicals.

After incubation of erythrocytes infected with D6 or FCR3 *P.f.* strains and with isotope-labelled $[10\text{-}^3\text{H}]\text{-2}$ or $[15\text{-}^3\text{H}]\text{-3b}$, radioactivity was detected in protein fractions originating from the parasite.¹⁰⁴ After treatment with EtSH or 8 M urea, it was concluded that the proteins and isotopic-labelled fragments of **2** and **3b** were covalently bonded. No radioactivity was detected after incubation with non-infected erythrocytes or with radiolabelled deoxoART. Some of alkylated proteins were *P. falciparum* membrane proteins MSA-1, MSA-2, CRA.5.1, TCTP (translationally controlled tumour protein) and histidine-enriched protein (42 kDa).^{105,106} TCTP possesses bonded haem and to some extent is present in FV membrane. Compound **2** reacted *in vitro* with recombinated TCTP in the presence of *in situ* generated haem and formed a covalent adduct in a 1:1 ratio. The amount of covalent adduct decreased to 60 % when one of the cysteines was chemically blocked.

Results of very important research¹⁰⁷ revealed that ART is a very effective inhibitor of sarco/endoplasmic reticulum calcium-dependent ATPase (SERCA) orthologue (*P. falciparum* ATP6) and that a catalytic amount of Fe(II) enhanced the inhibiting activity of **1**. It was evidenced that a possible site of action of ART could be outside the FV and that the trigger for ART toxicity towards the parasite could be Fe(II) situated in the cytosol and not necessarily the free haem within the FV.

In vitro resistance of 530 *P. falciparum* isolates from three countries (Cambodia, French Guiana and Senegal) towards ART and its closest derivatives was investigated.¹⁰⁸ It was found that the resistance was positively correlated only with a mutation of the SERCA *P. falciparum* ATPase6 genes and that *P. falciparum* ATPase6 is the target of ART antimalarials. All resistant isolates came from areas with uncontrolled use of ART derivatives.

Artemisinin **1** and arteether **3b** effectively inhibit FV proteolytic activity of enzymes that degrade haemoglobin, specifically cysteine-protease.¹⁰⁹ Compound E-64 (for structure see ref. 110) a specific inhibitor of cysteine-protease is both a **1** and **3b** antagonist. These observations were further confirmed by *ex vivo* experiments showing accumulation of haemoglobin in the parasites treated with ART, suggesting the inhibition of haemoglobin degradation. According to the above findings, it is not clear how artemisins and other peroxides would exert their antimalarial activity after reaction with free haem in the FV, when they inhibit the catabolism of haemoglobin and the liberation of haem.

Recently,¹¹¹ it was found that artemisinin, sodium artesunate and dihydro-artemisinin react with haemoglobin (ferrous haem), but not with methaemoglobin (ferric haem) under standard solution conditions (50 mM phosphate buffer, pH 7, 37 °C). The authors claim that the reaction selectively occurs at the haem sites and consists of the progressive, slow decay of the Soret band, as a consequence of haem alkylation and subsequent loss of π -electron delocalization. This finding further complicates the elucidation of the mechanism of action of artemisinins.

Antimalarial activity does not necessarily correlate with chemical reactivity. Amino artemisinins **14a** and **14b** reacted readily with haem giving the expected products but derivatives **159** and **160** did not (Fig. 28).^{28,112} On the contrary, derivative **159** reacted with aqueous Fe(II) but **160**, **14a** and **14b** were inert.^{28,113} Very interesting information came from the discovery that compounds, such as **161–164**, which can generate neither primary nor secondary C-radicals, exhibited pronounced antimalarial activity.⁹⁸ Similarly to the 10-deoxy derivative **159**, artemisone **14e** readily reacted with aqueous Fe(II) affording the corresponding products.¹¹³ Both compounds reacted with Fe(OAc)₂ and in the presence of the radical scavenger 4-oxo-TEMPO gave the corresponding covalent adducts (3 % for **159**, 10 % for **14e** and 73 % for **165**). DFO, an iron chelator, antagonized the antimalarial activity of aqueous Fe(II)-susceptible artesunate and trioxane **159**

but had no observable effect on either the aqueous Fe(II)-resistant derivative **160** or on artemisone **14e**.¹¹³ It was found that **14e** efficiently alkylates haem.¹¹⁴

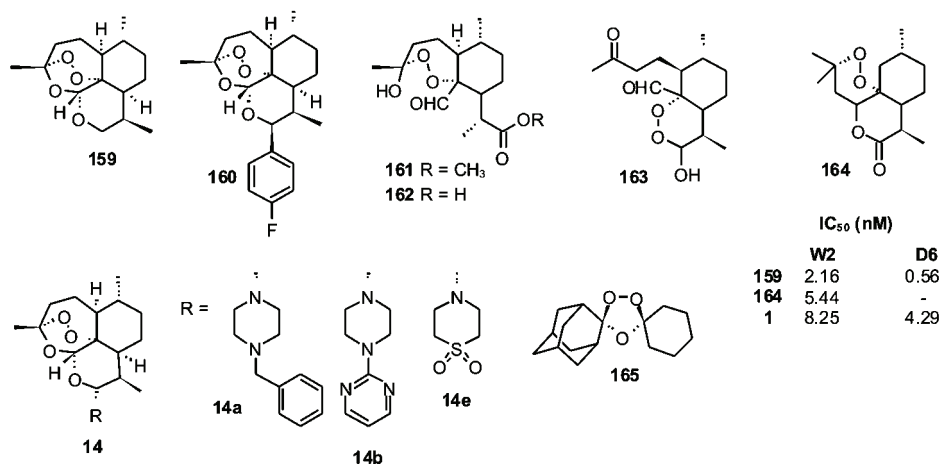
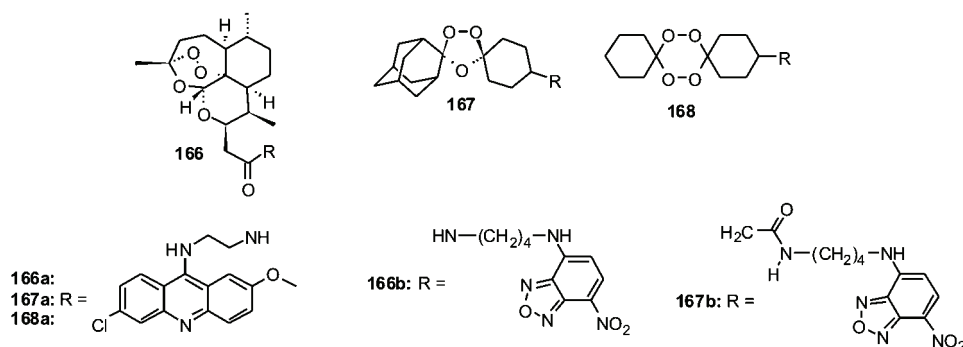


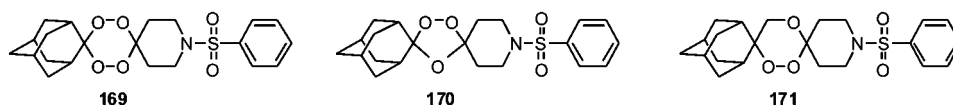
Fig. 28. Structures and antimalarial activities of derivatives **159** – **165** and selected derivatives **14**.

Due to the great specificity of ARTs to malaria parasite SERCA ATPase and inhibition of SERCA orthologues of *P. falciparum* (PfATP6) and *P. vivax* (PvSERCA), it was found that artemisone **14e** is an even better inhibitor having K_i 1.7 ± 0.6 nM for PfATP6 and K_i 0.072 ± 0.012 nM for PvSERCA, in comparison to ART, K_i 169 ± 31 nM for PfATP6 and K_i 7.7 ± 4.9 nM for PvSERCA.²⁹ In contrast to these derivatives, compound **160** has a low inhibitory activity for PfATP6 (K_i 277 ± 39 nM), which is in contrast to its high *in vitro* potency (IC_{50} 3D7 = 1.44).¹¹³

Studies with conjugates **166**–**168** of ART derivatives, ozonides and 1,2,4,5-tetraoxanes with acridine and nitrobenzylidiazole (NBD) fluorochromes (Fig. 29) showed that they accumulate only in infected erythrocytes, both within the cytoplasm and FV of the parasite.^{69,115} The formation of stable adducts of acridine and NBD-tagged peroxides with biomolecules within the parasite was inhibited by co-incubation with the iron chelator DFO. In addition, the investigated peroxides and their conjugates showed marked antagonism in combination with the iron chelators DFO and DFP.¹¹⁵ All the investigated conjugates showed high *in vitro* antimalarial activity in the 5–13 nM range against the 3D7 *P. falciparum* strain. These results suggest that both the cytoplasm and FV of the parasite could be equally the possible site of action of antimalarial peroxides, and that both haem from the FV or chelatable “free” iron from the cytoplasm could trigger the scission of the peroxide bond.

Fig. 29. Structures of conjugates **166–168**.

Adamantyl tetraoxane **169**, ozonide **170** and 1,2,4-trioxane **171** (Fig. 30) were subjected to reaction with different ferrous salts. It was shown that the tetraoxane **169** showed significant stability under the applied reaction conditions,⁶⁹ while the ozonide **170** and the trioxane **171** readily reacted and formed secondary carbon radicals that were scavenged by TEMPO.¹¹⁶

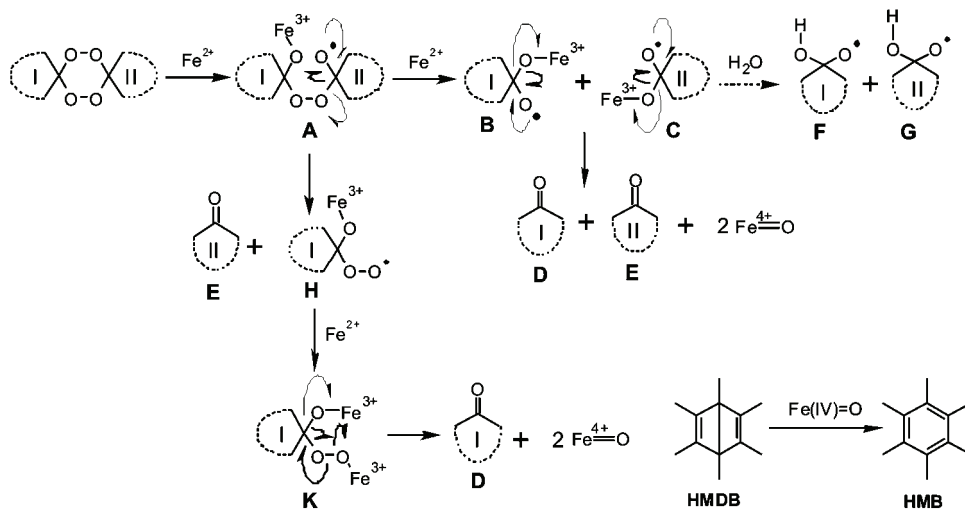
Fig. 30. Structures of peroxides **169–171**.

Ozonide **49** inhibits *Pf*ATP6 with a lower potency in comparison to ART, *i.e.*, K_i (**49**) = 7.7 mM *vs.* K_i (ART) = 79 nM, which thus suggests that these two peroxides may have different mechanisms of action.¹¹⁷ However, the two compounds have certain similarities, such as abrogation of the activity of **49** in the presence of DFO, antagonism in combination with DFO¹¹⁷ and the formation of a C-centred radical during reaction with Fe(II) and the formation of the corresponding adduct with TEMPO.⁴⁸ A fluorescent derivate of **49** was localized in the parasite cytosol in one parasite and in the FV in the other. In the cytosol, it was associated with the parasite endoplasmatic reticulum. In addition, the ozonide **49** showed antagonism in combination with artesunate.

A three-dimensional QSAR pharmacophore model for the antimalarial activity of bis-steroidal and mixed steroidal 1,2,4,5-tetraoxanes was developed.¹¹⁸ The model contains two hydrogen bond acceptors (lipid) and one hydrophobic (aliphatic) feature and maps well onto the potent analogues and many other active peroxide antimalarials, such as ART, arteether, artesunic acid, and simpler tetraoxanes. It appears that the presence of at least one hydrogen bond acceptor in the trioxane or the tetraoxane moiety is a necessity for good activity of this class of compounds. Docking calculations with haem suggest that the proximity of the

Fe(II) and oxygen atom of the trioxane or the tetraoxane moiety favours potent activity of the compounds and that electron transfer from the peroxide oxygen is crucial for the mechanism of action.

Differences between 1,2,4,5-tetraoxanes and the other peroxides were emphasised in studies of the mechanism of action of bis- and mixed steroidal tetraoxanes.⁷⁶ Performing experiments under the same conditions as for other antimalarial active peroxides, unexpectedly the steroidal tetraoxanes generated only oxygen centred radical that did not further rearrange to a carbon centred radical. Using DMPO and DEPMPO, both O- and C-radical traps, EPR experiments revealed only DMPO-•OR and DEPMPO-•OR spin-trapped adducts. As the only organic products, the corresponding starting ketones were isolated from the reaction mixture and no traces of rearranged products that would result from C-radical intermediates were detected. Indirect evidence of the existence of high valent Fe(IV)=O species was obtained from the rearrangement HMDB → HMB. Based on these evidences, two pathways (Scheme 5) were proposed, in which it was suggested that tetraoxane peroxides serve as an RO• radical source, as well as the source of the Fe(IV)=O species. RO• radical species are capable of membrane hydroperoxidation (RBC membrane, parasite membrane, cytosol, or FV) or possibly attack other vital biomolecules.



Scheme 5. Proposed mechanism of action of tetraoxanes.

10. CONCLUSIONS

Synthetic and semi-synthetic peroxides are effective drugs and are employed with success in the treatment of severe malaria. They are especially efficient against CQR strains of *P. falciparum*, the cause of cerebral malaria. Accessi-

bility, relatively inexpensive preparation and the stability of 1,2,4-trioxane and 1,2,4,5-tetraoxane function to a broad spectrum of reaction conditions enables the syntheses of derivatives with diverse structures and makes possible the discovery of even more effective drug(s). All authors emphasized the low toxicity of these compounds with rare cases of unwanted side effects. To date, there are no major examples of the appearance of resistance of Plasmodium species, except in the cases when drugs were used without proper control. These facts, together with the possibility for combination with other non-peroxide drugs, chiefly aminoquinolines, open unrestricted possibilities in combating malaria.

Reported results concerning the mechanism of antimalarial peroxide action are contradictory at a first glance. However, bearing in mind that the compounds differ significantly in their structures that are responsible for different log *P* values, bioavailability, passage through cellular membranes and stereospecific interactions with assumed receptors or trigger species, the observed differences are logical. In our opinion, antimalarial peroxides may themselves have different action pathway and they may have different targets. This said, certain common behaviour, such as the capability of acting as alkylating agents, is not excluded. In addition, this does not exclude the possibility that one compound is simultaneously activated against several different targets. Perhaps it should not be expected that all peroxides could be fitted into a unique mechanism of action. It is more likely that they have a complex, multi-targeted mechanism, including oxidative stress.¹¹³

Acknowledgements. This work was supported by the Ministry of Science and Technological Development of the Republic of Serbia (Grant No. 142022), and the Serbian Academy of Sciences and Arts. The authors are indebted to the Walter Reed Army Institute of Research, Silver Spring, USA, for a decade long cooperation.

ИЗВОД

ПЕРОКСИДНИ АНТИМАЛАРИЦИ

ДЕЈАН М. ОПСЕНИЦА¹ и БОГДАН А. ШОЛАЈА²¹*Институт за хемију, технологију и металургију, Универзитет у Београду, Њевошева 12, Београд и*²*Хемијски факултет, Универзитет у Београду, Студентски брџ 16, б. бр. 51, 11158 Београд*

Ширење маларије је стално присутан проблем на глобалном нивоу. Од маларије годишње оболи 40 % светске популације и око 1,5–2,7 милиона људи умре. Према подацима Светске здравствене организације, 90 % смртних случајева је у земљама подсахарске Африке, међу којима доминирају деца старости до 5 година. Услед немогућности развоја вакцине, хемотерапија остаје као једини поуздан облик лечења од ове болести. Последњих година проблем борбе против маларије постаје ургентан из бројних разлога, међу којима је најзначајнији развој хлорокин-резистентних сојева паразита. Откриће да артемизинин (АРТ, I) и његови деривати показују изузетну ефикасност према хлорокин-резистентним сојевима отворило је велике могућности у борби против маларије. Од тада, посебно током 80-тих година, синтетисан је велики број једињења и резултати њихове активности описани су у многим научним публикацијама. Осим тога, у клиничкој пракси нису забележени примери по-

јаве резистенције паразита према овој класи антималярика. У овом ревијалном раду описани су најновији резултати у развоју пероксидних антималярика.

(Примљено 19. маја 2009)

REFERENCES

1. *Malaria Foundation International*, <http://www.malaria.org/>
2. *World Health Organization*, Global Malaria programme (GMP), www.who.int/malaria/
3. S. L. Hoffman, G. M. Subramanian, F. H. Collins, J. C. Venter, *Nature* **415** (2002) 702
4. a) Qinghaosu Antimalaria Coordinating Research Group, *Trad. Chin. Med. J.* **92** (1982) 811; b) X.-D. Luo, C.-C. Shen, *Med. Res. Rev.* **7** (1987) 29
5. a) D. L. Klayman, *Science* **228** (1985) 1049; b) K. Borstnik, I.-H. Paik, T. A. Shapiro, G. H. Posner, *Int. J. Parasitol.* **32** (2002) 1661; c) K. Borstnik, I.-H. Paik, T. A. Shapiro, G. H. Posner, *Mini Rev. Med. Chem.* **2** (2002) 573; d) Y. Lin, Y.-L. Wu, *Curr. Med. Chem.* **10** (2003) 2197; e) P. M. O'Neill, G. H. Posner, *J. Med. Chem.* **47** (2004) 2945; f) Y. Tang, Y. Dong, J. L. Vennerstrom, *Med. Res. Rev.* **24** (2004) 425; g) A. Masuyama, J.-M. Wu, M. Nojima, H.-S. Kim, Y. Wataya, *Rev. Med. Chem.* **5** (2005) 1035
6. R. Jambou, E. Legrand, M. Niang, N. Khim, P. Lim, B. Volney, M. T. Ekala, C. Bouchier, P. Esterre, T. Fandeur, O. Mercereau-Puijalon, *Lancet* **366** (2005) 1960
7. L. H. Miller, D. I. Baruch, K. Marsh, O. K. Doumbo, *Nature* **415** (2002) 673
8. a) C. E. Chitnis, M. J. Blackman, *Parasitol. Today* **16** (2000) 411; b) L. H. Bannister, J. M. Hopkins, R. E. Fowler, S. Krishna, G. H. Mitchell, *Parasitol. Today* **16** (2000) 427; c) P. Baldacci, R. Ménard, *Mol. Microbiol.* **54** (2004) 298; d) B. M. Cooke, K. Lingelbach, L. H. Bannister, L. Tilley, *Trends Parasitol.* **20** (2004) 581; e) P. D. Parker, L. Tilley, N. Klonis, *Blood* **103** (2004) 2404; f) J. M. Przyborski, M. Lanzer, *Parasitology* **130** (2005) 373
9. M. Frédérick, J.-M. Dogné, L. Angenot, P. De Mol, *Curr. Med. Chem.* **9** (2002) 1435
10. S. E. Francis, D. J. Sullivan Jr., D. E. Goldberg, *Ann. Rev. Microbiol.* **51** (1997) 97
11. a) S. Pagola, P. W. Stephens, D. S. Bohle, A. D. Kosar, S. K. Madsen, *Nature* **404** (2000) 307; b) D. J. Sullivan, *Int. J. Parasitol.* **32** (2002) 1645
12. D. Monti, B. Vodopivec, N. Basilio, P. Olliaro, D. Taramelli, *Biochemistry* **38** (1999) 8858
13. D. Jeremić, A. Jokić, A. Behbud, M. Stefanović, in *Proceedings of 8th International Symposium on The Chemistry of Natural Products*, New Delhi, 1972, C-54, p. 221
14. G. Schmid, W. Hofheinz, *J. Am. Chem. Soc.* **105** (1983) 624
15. Examination of the *Chemical Abstracts* database afforded 35 references related to synthetic efforts towards **1** and structurally close derivatives, including one that enables the synthesis of isotopically labelled artemisinin, M. A. Avery, W. K. M. Chong, C. Jenning-White, *J. Am. Chem. Soc.* **114** (1992) 974
16. J. S. Yadava, R. S. Babu, G. Sabitha, *Tetrahedron Lett.* **44** (2003) 387
17. Average results obtained from more than eight replicates, Internal WRAIR data
18. A. J. Lin, D. L. Klayman, W. K. Milhous, *J. Med. Chem.* **30** (1987) 2147
19. A. J. Lin, M. Lee, D. L. Klayman, *J. Med. Chem.* **32** (1989) 1249
20. A. J. Lin, R. E. Miller, *J. Med. Chem.* **38** (1995) 764
21. P. M. O'Neill, A. Miller, L. P. D. Bishop, S. Hindley, J. L. Maggs, S. A. Ward, S. M. Roberts, F. Scheinmann, A. V. Stachulski, G. H. Posner, B. K. Park, *J. Med. Chem.* **44** (2001) 58

22. a) M. A. Avery, J. D. Bonk, W. K. M. Chong, S. Mehrotra, R. Miller, W. Milhous, D. K. Goins, S. Venkatesan, C. Wyandt, I. Khan, B. A. Avery, *J. Med. Chem.* **38** (1995) 5038; b) D. S. Torok, H. Ziffer, S. R. Meshnick, X.-Q. Pan, A. Ager, *J. Med. Chem.* **38** (1995) 5045; c) B. Mekonnen, E. Weiss, E. Katz, J. Ma, H. Ziffer, D. E. Kyle, *Bioorg. Med. Chem.* **8** (2000) 1111
23. M. Jung, X. Li, D. A. Bustos, H. N. Elsohly, J. D. McChesney, W. K. Milhous, *J. Med. Chem.* **33** (1990) 1516
24. M. A. Avery, S. Mehrotra, T. L. Johnson, J. D. Bonk, J. A. Vroman, R. Miller, *J. Med. Chem.* **39** (1996) 4149
25. M. A. Avery, M. Alvim-Gaston, J. A. Vroman, B. Wu, A. Ager, W. Peters, B. L. Robinson, W. Charman, *J. Med. Chem.* **45** (2002) 4321
26. G. H. Posner, M. H. Parker, J. Northrop, J. S. Elias, P. Ploypradith, S. Xie, T. A. Shapiro, *J. Med. Chem.* **42** (1999) 300
27. G. H. Posner, P. Ploypradith, M. H. Parker, H. O'Dowd, S.-H. Woo, J. Northrop, M. Krasavin, P. Dolan, T. W. Kensler, S. Xie, T. A. Shapiro, *J. Med. Chem.* **42** (1999) 4275
28. R. K. Haynes, W.-Y. Ho, H.-W. Chan, B. Fugmann, J. Stetter, S. L. Croft, L. Vivas, W. Peters, L. Robinson, *Angew. Chem. Int. Ed.* **43** (2004) 1381
29. R. K. Haynes, B. Fugmann, J. Stetter, K. Rieckmann, H.-D. Heilmann, H.-W. Chan, M.-K. Cheung, W.-L. Lam, H.-N. Wong, S. L. Croft, L. Vivas, L. Rattray, L. Stewart, W. Peters, B. L. Robinson, M. D. Edstein, B. Kotecka, D. E. Kyle, B. Beckermann, M. Gerisch, M. Radtke, G. Schmuck, W. Steinke, U. Wollborn, K. Schmeer, A. Römer, *Angew. Chem. Int. Ed.* **45** (2006) 2082
30. C. Singh, S. Chaudhary, S. K. Puri, *J. Med. Chem.* **49** (2006) 7227
31. C. Singh, S. Chaudhary, S. K. Puri, *Bioorg. Med. Chem. Lett.* **18** (2008) 1436
32. I.-H. Paik, S. Xie, T. A. Shapiro, T. Labonte, A. A. N. Sarjeant, A. C. Baeye, G. H. Posner, *J. Med. Chem.* **49** (2006) 2731
33. G. H. Posner, I.-H. Paik, W. Chang, K. Borstnik, S. Sinishtaj, A. S. Rosenthal, T. A. Shapiro, *J. Med. Chem.* **50** (2007) 2516
34. G. H. Posner, W. Chang, L. Hess, L. Woodard, S. Sinishtaj, A. R. Usera, W. Maio, A. S. Rosenthal, A. S. Kalinda, J. G. D'Angelo, K. S. Petersen, R. Stohler, J. Chollet, J. Santos-Tomas, C. Snyder, M. Rottmann, S. Wittlin, R. Brun, T. A. Shapiro, *J. Med. Chem.* **51** (2008) 1035
35. C. W. Jefford, J. A. Velarde, G. Bernardinelli, D. H. Bray, D. C. Warhurst, W. K. Milhous, *Helv. Chim. Acta* **76** (1993) 2775
36. C. W. Jefford, S. Kohmoto, D. Jaggi, G. Timari, J.-C. Rossier, M. Rudaz, O. Barbuzzi, D. Gerard, U. Burger, P. Kamalaprija, J. Mareda, G. Bernardinelli, *Helv. Chim. Acta* **78** (1995) 647
37. G. H. Posner, C. H. Oh, D. Wang, L. Gerena, W. K. Milhous, S. R. Meshnick, W. Asawamasadka, *J. Med. Chem.* **37** (1994) 1256
38. G. H. Posner, H. B. Jeon, M. H. Parker, M. Krasavin, I.-H. Paik, T. A. Shapiro, *J. Med. Chem.* **44** (2001) 3054
39. C. Singh, N. Gupta, S. K. Puri, *Tetrahedron Lett.* **46** (2005) 205
40. C. W. Jefford, *Drug Discovery Today* **12** (2007) 487
41. C. Singh, N. Gupta, S. K. Puri, *Bioorg. Med. Chem. Lett.* **13** (2003) 3447
42. C. Singh, N. C. Srivastav, S. K. Puri, *Bioorg. Med. Chem.* **12** (2004) 5745
43. C. Singh, R. Kanchan, U. Sharma, S. K. Puri, *J. Med. Chem.* **50** (2007) 521

44. A. G. Griesbeck, T. T. El-Idreesy, L.-O. Höinck, J. Lex, R. Brun, *Bioorg. Med. Chem. Lett.* **15** (2005) 595
45. C. Singh, H. Malik, S. K. Puri, *Bioorg. Med. Chem. Lett.* **14** (2004) 459
46. C. Singh, H. Malik, S. K. Puri, *J. Med. Chem.* **49** (2006) 2794
47. C. Singh, U. Sharma, G. Saxena, S. K. Puri, *Bioorg. Med. Chem. Lett.* **17** (2007) 4097
48. J. L. Vennerstrom, S. Arbe-Barnes, R. Brun, S. A. Charman, F. C. K. Chiu, J. Chollet, Y. Dong, A. Dorn, D. Hunziker, H. Matile, K. McIntosh, M. Padmanilayam, J. S. Tomas, C. Scheurer, B. Scorneaux, Y. Tang, H. Urwyler, S. Wittlin, W. N. Charman, *Nature* **430** (2004) 900
49. Y. Dong, J. Chollet, H. Matile, S. A. Charman, F. C. K. Chiu, W. N. Charman, B. Scorneaux, H. Urwyler, J. S. Tomas, C. Scheurer, C. Snyder, A. Dorn, X. Wang, J. M. Karle, Y. Tang, S. Wittlin, R. Brun, J. L. Vennerstrom, *J. Med. Chem.* **48** (2005) 4953
50. B. A. Šolaja, N. Terzić, G. Pocsfalvi, L. Gerena, B. Tinant, D. Opsenica, W. K. Milhous, *J. Med. Chem.* **45** (2002) 3331
51. Y. Tang, Y. Dong, J. M. Karle, C. A. DiTusa, J. L. Vennerstrom, *J. Org. Chem.* **69** (2004) 6470
52. Y. Dong, Y. Tang, J. Chollet, H. Matile, S. Wittlin, S. A. Charman, W. N. Charman, J. S. Tomas, C. Scheurer, C. Snyder, B. Scorneaux, S. Bajpai, S. A. Alexander, X. Wang, M. Padmanilayam, S. R. Cheruku, R. Brun, J. L. Vennerstrom, *Bioorg. Med. Chem.* **14** (2006) 6368
53. M. Padmanilayam, B. Scorneaux, Y. Dong, J. Chollet, H. Matile, S. A. Charman, D. J. Creek, William N. Charman, J. S. Tomas, C. Scheurer, S. Wittlin, R. Brun, J. L. Vennerstrom, *Bioorg. Med. Chem. Lett.* **16** (2006) 5542
54. Y. Tang, Y. Dong, S. Wittlin, S. A. Charman, J. Chollet, F. C. K. Chiu, W. N. Charman, H. Matile, H. Urwyler, A. Dorn, S. Bajpai, X. Wang, M. Padmanilayam, J. M. Karle, R. Brun, J. L. Vennerstrom, *Bioorg. Med. Chem. Lett.* **17** (2007) 1260
55. a) T. Ledaal, *Acta Chem. Scand.* **21** (1967) 1656; b) P. R. Story, B. Lee, C. E. Bishop, D. D. Denson, P. Busch, *J. Org. Chem.* **35** (1970) 3059; c) J. R. Sanderson, K. Paul, P. R. Story, D. D. Denson, J. A. Alford, *Synthesis* (1975) 159; d) J. R. Sanderson, A. G. Zeiler, *Synthesis* (1975) 125; e) J. H. Sanderson, A. G. Zeile, R. J. Wilterdink, *J. Org. Chem.* **40** (1975) 2239; f) J. R. Sanderson, R. J. Wilterdink, A. G. Zeler, *Synthesis* (1976) 479
56. C. W. Jefford, A. Jaber, J. Boukouvalas, *Synthesis* (1988) 391
57. D. Opsenica, G. Pocsfalvi, Z. Juranić, B. Tinant, J.-P. Declercq, D. E. Kyle, W. K. Milhous, B. A. Šolaja, *J. Med. Chem.* **43** (2000) 3274
58. N. M. Todorović, M. Stefanović, B. Tinant, J.-P. Declercq, M. T. Makler and B. A. Šolaja, *Steroids*, **61** (1996) 688
59. J. L. Vennerstrom, H.-N. Fu, W. Y. Ellis, A. L. Ager Jr., J. K. Wood, S. L. Andersen, L. Gerena, W. K. Milhous, *J. Med. Chem.* **35** (1992) 3023
60. a) Y. Dong, J. L. Vennerstrom, *J. Org. Chem.* **63** (1998) 8582; b) Y. Dong, H. Matile, J. Chollet, R. Kaminsky, J. K. Wood, J. L. Vennerstrom, *J. Med. Chem.* **42** (1999) 1477; c) H.-S. Kim, Y. Shibata, Y. Wataya, K. Tsuchiya, A. Masuyama, M. Nojima, *J. Med. Chem.* **42** (1999) 2604; d) P. H. Dussault, J. M. Raible, *Org. Lett.* **2** (2000) 3377
61. K. Žmitek, S. Stavber, M. Zupan, D. Bonnet-Delpon, J. Iskra, *Tetrahedron* **62** (2006) 1479
62. Y. Dong, *Mini Rev. Med. Chem.* **2** (2002) 113

63. H. S. Kim, K. Tsuchiya, Y. Shibata, Y. Wataya, Y. Ushigoe, A. Masuyama, M. Nojima, K. J. McCullough, *J. Chem. Soc., Perkin Trans. I* (1999) 1867
64. J. Iskra, D. Bonnet-Delponb, J.-P. Bégué, *Tetrahedron Lett.* **44** (2003) 6309
65. A. O. Terent'ev, A. V. Kutkin, Z. A. Starikova, M. Yu. Antipin, Yu. N. Ogibin, G. I. Nikishin, *Synthesis* (2004) 2356
66. a) K. Žmitek, M. Zupan, S. Stavber, J. Iskra, *Org. Lett.* **8** (2006) 2491; b) K. Žmitek, M. Zupan, S. Stavber, J. Iskra, *J. Org. Chem.* **72** (2007) 6534; c) K. Žmitek, M. Zupan, J. Iskra, *Org. Biomol. Chem.* **5** (2007) 3895; d) B. Das, M. Krishnaiah, B. Veeranjanyulu, B. Ravikanth, *Tetrahedron Lett.* **48** (2007) 6286; e) B. Das, B. Veeranjanyulu, M. Krishnaiah, P. Balasubramanyam, *J. Mol. Catal. A: Chem.* **284** (2008) 116
67. a) I. Opsenica, N. Terzić, D. Opsenica, W. K. Milhous, B. Šolaja, *J. Serb. Chem. Soc.* **69** (2004) 919; b) I. Opsenica, D. Opsenica, M. Jadranin, K. Smith, W. K. Milhous, M. Stratakis, B. Šolaja, *J. Serb. Chem. Soc.* **72** (2007) 1181; c) I. Opsenica, D. Opsenica, K. S. Smith, W. K. Milhous, B. A. Šolaja, *J. Med. Chem.* **51** (2008) 2261
68. R. Amewu, A. V. Stachulski, S. A. Ward, N. G. Berry, P. G. Bray, J. Davies, G. Labat, L. Vivas, P. M. O'Neill, *Org. Biomol. Chem.* **4** (2006) 4431
69. G. L. Ellis, R. Amewu, S. Sabbani, P. A. Stocks, A. Shone, D. Stanford, P. Gibbons, J. Davies, L. Vivas, S. Charnaud, E. Bongard, C. Hall, K. Rimmer, S. Lozanom, M. Jesús, D. Gargallo, S. A. Ward, P. M. O'Neill, *J. Med. Chem.* **51** (2008) 2170
70. K. Žmitek, S. Stavber, M. Zupan, D. Bonnet-Delpon, S. Charneau, P. Grellier, J. Iskra, *Bioorg. Med. Chem.* **14** (2006) 7790
71. H. Atheaya, S. I. Khan, R. Mamgaina, D. S. Rawata, *Bioorg. Med. Chem. Lett.* **18** (2008) 1446
72. Y. Dong, D. Creek, J. Chollet, H. Matile, S. A. Charman, S. Wittlin, J. K. Wood, J. L. Vennerstrom, *Antimicrob. Agents Ch.* **51** (2007) 3003
73. D. Opsenica, G. Angelovski, G. Pocsfalvi, Z. Juranić, Ž. Žižak, D. Kyle, W. K. Milhous, B. A. Šolaja, *Bioorg. Med. Chem.* **11** (2003) 2761
74. N. Terzić, D. Opsenica, D. Milić, B. Tinant, K. S. Smith, W. K. Milhous, B. A. Šolaja, *J. Med. Chem.* **50** (2007) 5118
75. D. Opsenica, D. E. Kyle, W. K. Milhous, B. A. Šolaja, *J. Serb. Chem. Soc.* **68** (2003) 291
76. I. Opsenica, N. Terzić, D. Opsenica, G. Angelovski, M. Lehnig, P. Eilbracht, B. Tinant, Z. Juranić, K. S. Smith, Y. S. Yang, D. S. Diaz, P. L. Smith, W. K. Milhous, D. Đoković, B. A. Šolaja, *J. Med. Chem.* **49** (2006) 3790
77. D. M. Opsenica, N. Terzić, P. L. Smith, Y. Yang, L. Anova, K. S. Smith, B. A. Šolaja, *Bioorg. Med. Chem.* **16** (2008) 7039
78. C. W. Jefford, J.-C. Rossier, W. K. Milhous, *Heterocycles* **52** (2000) 1345
79. D. Opsenica, Z. Juranić, B. A. Šolaja, unpublished results. In brief, the whole blood from a healthy person, with K EDTA added as an anticoagulant, was incubated for 48 h at 37 °C with test compound **6** within the concentration range 60 μM–6 nM. No increase of haemoglobin level in the plasma was detected, as compared to a blank probe. Blood diluted with physiological solution was used as the blank, while blood diluted with deionized water was used as the positive control probe.
80. D. Opsenica, G. Pocsfalvi, W. K. Milhous, B. A. Šolaja, *J. Serb. Chem. Soc.* **67** (2002) 465
81. O. Dechey-Cabaret, F. Benoit-Vical, A. Robert, B. Meunier, *ChemBioChem* **1** (2000) 281

82. L. K. Basco, O. Dechy-Cabaret, M. Ndounga, F. S. Meche, A. Robert, B. Meunier, *Antimicrob. Agents Chemother.* **45** (2001) 1886
83. O. Dechy-Cabaret, F. Benoit-Vical, C. Loup, A. Robert, H. Gornitzka, A. Bonhoure, H. Vial, J.-F. Magnaval, J.-P. Séguéla, B. Meunier, *Chem. Eur. J.* **10** (2004) 1625
84. F. Coslédan, L. Fraisse, A. Pellet, F. Guillou, B. Mordmüller, P. G. Kremsner, A. Moreno, D. Mazier, J.-P. Maffrand, B. Meunier, *Proc. Natl. Acad. Sci. USA* **105** (2008) 17579
85. O. Dechy-Cabaret, F. Benoit-Vical, A. Robert, J.-F. Magnaval, J.-P. Séguéla, B. Meunier, *C. R. Chim.* **6** (2003) 153
86. C. Singh, H. Malik, S. K. Puri, *Bioorg. Med. Chem.* **12** (2004) 1177
87. B. Meunier, *Acc. Chem. Res.* **41** (2008) 69
88. J. L. Vennerstrom, Y. Dong, J. Chollet, H. Matile, M. Padmanilayam, Y. Tang, W. N. Charman, US 20040039008 A1
89. J. J. Walsh, D. Coughlan, N. Heneghan, C. Gaynora, A. Bellb, *Bioorg. Med. Chem. Lett.* **17** (2007) 3599
90. T. S. Skinner, L. S. Manning, W. A. Johnston, T. M. E. Davis, *Int. J. Parasitol.* **26** (1996) 519
91. I. Opsenica, D. Opsenica, C. A. Lanteri, L. Anova, W. K. Milhous, K. S. Smith, B. A. Šolaja, *J. Med. Chem.* **51** (2008) 6216
92. J. L. Vennerstrom, A. L. Ager, S. L. Andersen, J. M. Grace, V. Wongpanich, C. K. Angerhofer, J. K. Hu, D. L. Wesche, *Am. J. Trop. Med. Hyg.* **62** (2000) 573
93. S. Gupta, M. M. Thapar, S. T. Mariga, W. H. Wernsdorfer, A. Björkman, *Exp. Parasitol.* **100** (2002) 28
94. W. K. Milhous, L. Gerena, D. Opsenica, B. A. Šolaja, unpublished results.
95. L. Zhou, A. Alker, A. Ruf, X. Wang, F. C. K. Chiu, J. Morizzi, S. A. Charman, W. N. Charman, C. Scheurer, S. Wittlin, Y. Dong, D. Hunziker, J. L. Vennerstrom, *Bioorg. Med. Chem. Lett.* **18** (2008) 1555
96. a) G. H. Posner, C. H. Oh, *J. Am. Chem. Soc.* **114** (1992) 8328; b) G. H. Posner, S. B. Park, L. Gonzalez, D. Wang, J. N. Cumming, D. Klindedinst, T. A. Shapiro, M. D. Bachi, *J. Am. Chem. Soc.* **118** (1996) 3537
97. a) C. W. Jefford, F. Favarger, M. G. H. Vicente, Y. Jacquier, *Helv. Chim. Acta* **78** (1995) 452; b) C. W. Jefford, M. G. H. Vicente, Y. Jacquier, F. Favarger, J. Mareda, P. Millason-Schmidt, G. Brunner, U. Burger, *Helv. Chim. Acta.* **79** (1996) 1475; c) C. W. Jefford, U. Burger, P. Millason-Schmidt, G. Bernardinelli, B. L. Robinson, W. Peters, *Helv. Chim. Acta* **83** (2000) 1239
98. a) R. K. Haynes, S. C. Vonwiller, *Tetrahedron Lett.* **37** (1996) 253; b) R. K. Hynes, S. C. Vonwiller, *Tetrahedron Lett.* **37** (1996) 257
99. a) A. Robert, B. Meunier, *J. Am. Chem. Soc.* **119** (1997) 5968; b) A. Robert, B. Meunier, *Chem. Eur. J.* **4** (1998) 1287; c) J. A. Robert, J. Cazelles, B. Meunier, *Angew. Chem. Int. Ed.* **40** (2001) 1954; d) J. Cazelles, J. A. Robert, B. Meunier, *J. Org. Chem.* **67** (2002) 609
100. a) W.-M. Wu, Z.-J. Yao, Y.-L. Wu, K. Jiang, Y.-F. Wang, H.-B. Chen, F. Shan, Y. Li, *Chem. Commun.* (1996) 2213; b) W.-M. Wu, Y. Wu, Y.-L. Wu, Z.-J. Yao, C.-M. Zhou, Y. Li, F. Shan, *J. Am. Chem. Soc.* **120** (1998) 3316; c) Y. Wu, Z.-Y. Yue, Y.-L. Wu, *Angew. Chem. Int. Ed.* **38** (1999) 2580; d) D.-Y. Wang, Y.-L. Wu, *Chem. Commun.* (2000) 2193

101. a) G. H. Posner, J. N. Cumming, P. Ploypradith, C.-H. Oh, *J. Am. Chem. Soc.* **117** (1995) 5885; b) T. G. Traylor, A. R. Miksztal, *J. Am. Chem. Soc.* **109** (1987) 2770
102. a) S. Kapetanaki, C. Varotsis, *FEBS Lett.* **474** (2000) 238; b) S. Kapetanaki, C. Varotsis, *J. Med. Chem.* **44** (2001) 3150
103. S. A.-L. Laurent, C. Loup, S. Mourgues, A. Robert, B. Meunier, *ChemBioChem* **6** (2005) 653
104. W. Asawamahasakda, I. Ittarat, Y.-M. Pu, H. Ziffer, S. R. Meshnick, *Antimicrob. Agents Chemother.* **38** (1993) 1854
105. J. Bhisutthibhan, X.-Q. Pan, P. A. Hossler, D. J. Walker, C. A. Yowell, J. Carlton, J. B. Dame, S. R. Meshnick, *J. Biol. Chem.* **273** (1998) 16192
106. S. R. Meshnick, *Int. J. Parasitol.* **32** (2002) 1655
107. U. Eckstein-Ludwig, R. J. Webb, I. D. A. A. Van Goethem, J. M. East, A. G. Lee, M. Kimura, P. M. O'Neill, P. G. Bray, S. A. Ward, S. Krishna, *Nature* **424** (2003) 957
108. R. Jambou, E. Legrand, M. Niang, N. Khim, P. Lim, B. Volney, M. T. Ekala, C. Bouchier, P. Esterre, T. Fandeur, O. Mercereau-Puijalon, *Lancet* **366** (2005) 1960
109. A. V. Pandey, B. L. Tekwani, R. L. Singh, V. S. Chauhan, *J. Biochem.* **274** (1999) 19383
110. a) A. Coppi, C. Pinzon-Ortiz, C. Hutter, P. Sinnis, *J. Exp. Med.* **201** (2005) 27; b) F. Sarabia, A. Sánchez-Ruiz, S. Chammaa, *Bioorg. Med. Chem.* **13** (2005) 1691
111. L. Messori, C. Gabbiani, A. Casini, M. Siragusa, F. F. Vincieri, A. R. Bilia, *Bioorg. Med. Chem.* **14** (2006) 2972
112. R. K. Hynes, D. Monti, D. Taramelli, N. Basilico, S. Parapini, P. Olliaro, *Antimicrob. Agents Chemother.* **47** (2003) 1175
113. R. K. Haynes, W. C. Chan, C.-M. Lung, A.-C. Uhlemann, U. Eckstein, D. Taramelli, S. Parapini, D. Monti, S. Krishna, *ChemMedChem* **2** (2007) 1480
114. F. Bousejra-El Garah, B. Meunier, A. Robert, *Eur. J. Inorg. Chem.* **2008**, 2133
115. P. A. Stocks, P. G. Bray, V. E. Barton, M. Al-Helal, M. Jones, N. C. Araujo, P. Gibbons, S. A. Ward, R. H. Hughes, G. A. Biagini, J. Davies, R. Amewu, A. E. Mercer, G. Ellis, P. M. O'Neill, *Angew. Chem. Int. Ed.* **46** (2007) 6278
116. S. Sabbani, P. A. Stocks, G. L. Ellis, J. Davies, E. Hedenstrom, S. A. Ward, P. M. O'Neill, *Bioorg. Med. Chem. Lett.* **18** (2008) 5804
117. A.-C. Uhlemann, S. Wittlin, H. Matile, L. Y. Bustamante, S. Krishna, *Antimicrob. Agents Chemother.* **51** (2007) 667
118. A. K. Bhattacharjee, K. A. Carvalho, D. Opsenica, B. A. Šolaja, *J. Serb. Chem. Soc.* **70** (2005) 329.



J. Serb. Chem. Soc. 74 (11) 1195–1205 (2009)
JSCS–3910

Synthesis, structure and solvatochromism of 5-methyl-5-(3- or 4-substituted phenyl)hydantoins

NATALIJA D. DIVJAK, NEBOJŠA R. BANJAC, NATAŠA V. VALENTIĆ[#]
and GORDANA S. UŠĆUMLIĆ^{*#}

Department of Organic Chemistry, Faculty of Technology and Metallurgy, University of Belgrade, Karnegijeva 4, P.O. Box 3505, 11120 Belgrade, Serbia

(Received 1 July 2008, revised 8 July 2009)

Abstract: Several 5-methyl-5-(3- or 4-substituted phenyl)hydantoins were prepared and their ultraviolet absorption spectra were recorded in the region 200–400 nm in twelve solvents of different polarity. The effect of solvent dipolarity/polarizability and solvent/solute hydrogen bonding interactions were analyzed by means of the linear solvation energy relationship (LSER) concept proposed by Kamlet and Taft. The lipophilic activity of the investigated hydantoins was estimated by calculation of log *P* values with Advanced Chemistry Development Software. The calculated values of log *P* were correlated with the contribution of hydrogen bond donor–solvent interactions. By employing the thus obtained linear dependence, the pharmacological activity of the studied hydantoin derivatives is discussed.

Keywords: hydantoins; absorption frequencies; LSER; lipophilicity parameter; specific solvent interactions; pharmacological activity.

INTRODUCTION

Hydantoins (imidazolidine-2,4-diones) are important anticonvulsant drugs.^{1,2} The anticonvulsant activity of hydantoins has been known since 1938 when Merrit and Putman³ found that 5,5-diphenylhydantoin (phenitoin) showed anti-epileptic activity. In addition, a number of other pharmacological activities of hydantoin derivatives are known, such as in their use as anti-arrhythmic,⁴ anti-inflammatory⁵ and antitumor compounds.⁶

Both the electron distribution and the stereochemistry of hydantoins are important for their pharmacological activity. Following this idea, a pharmacophore model was proposed based on a hydrogen bonding acceptor, a hydrogen bonding donor and an electronegative group with a large hydrophobic part of the molecule

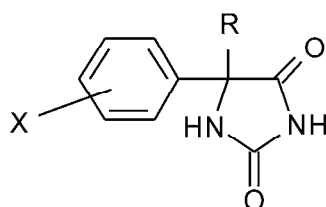
* Corresponding author. E-mail: goca@tmf.bg.ac.rs

[#] Serbian Chemical Society member.

doi: 10.2298/JSC0911195D

in a defined spatial arrangement.⁷ The position of the hydrogen donor in combination with an aromatic ring in a specific orientation was found to be crucial.^{7,8} Previously reported results⁹ clearly confirmed the hypothesis that hydrogen bonding is an essential factor in the anticonvulsant action of these compounds. In order to define the impact of a hydrogen bond forming ability on the anti-epileptic activity, Poupaert *et al.*⁹ tested some phenitoin-related compounds in the maximal electroshock seizure (MES test). A net stepwise decrease of the anticonvulsant activity was observed when the hydantoin ring structure was altered into succinimide and pyrrolidinone and when these rings were N-methylated. The pharmacological data analyzed in terms of structure-activity relationships (SAR) indicate the importance of the capability of forming hydrogen bonds.

Our research on the pharmacological activity of hydantoin derivatives has



Compound	R	X
1	CH ₃	4-NH ₂
2	CH ₃	4-OH
3	CH ₃	4-OCH ₃
4	CH ₃	4-CH ₃
5	CH ₃	H
6	CH ₃	4-Cl
7	CH ₃	4-Br
8	CH ₃	4-NO ₂
9	CH ₃	4-CN
10	C ₆ H ₅	H
11	CH ₃	3-NO ₂
12	CH ₃	3-OCH ₃
13	CH ₃	3-CH ₃
14	CH ₃	3-Cl

Fig. 1. Structure of the investigated 5-methyl-5-(3- or 4-substituted phenyl)hydantoins.

been focused on the determination of the structural and chemical behavior of compounds in different solvents using UV–Vis spectroscopic methods.¹⁰ To the best of our knowledge, the influence of the solvent on the UV absorption frequencies of hydantoin has not been systematically presented before. In this work, fourteen 5-methyl-5-(3- or 4-substituted phenyl)hydantoin (Fig. 1) were synthesized and their ultraviolet absorption spectra were recorded in the region 200–400 nm in twelve solvents of different polarity. The effect of solvent dipolarity/polarizability and hydrogen bonding on the absorption spectra were interpreted by means of the linear solvation energy relationship (LSER) using a Kamlet–Taft equation¹¹ of the form:

$$\nu = \nu_0 + s\pi^* + b\beta + a\alpha \quad (1)$$

where π^* is a measure of the solvent dipolarity/polarizability,¹² β is the scale of the solvent hydrogen bond acceptor (HBA) basicity,¹³ α is the scale of the solvent hydrogen bond donor (HBD) acidity¹⁴ and ν_0 is the regression value of the solute property in cyclohexane as the reference solvent. The regression coefficients s , b , and a in Eq. (1) measure the relative sensitivities of the solvent dependent solute property (absorption frequencies) to the indicated solvent parameters.

Linear free-energy relationships (LFER) are widely used to characterize chemical and biochemical processes. A particular type of LFER is the linear solvation energy relationship (LSER) proposed by Kamlet *et al.*¹⁵ for physico-chemical and biochemical processes that depend on solute–solvent interactions. The LSER have been widely applied to different partition processes, mainly liquid–liquid extraction, such as octanol–water partitioning, and chromatographic processes.¹⁶ The LSER developed by Kamlet and Taft is one of the most ambitious and successful quantitative treatments of solvent effects by means of a multi-parametar equation.^{17–19}

The importance of lipophilicity in a structure-activity relationship has been known for a long time. Thus, transport phenomena *in vivo* and through membranes proved to be dependent on lipophilic contributions. The lipophilic activity of the hydantoin investigated in this work was estimated by calculation of $\log P$ values with Advanced Development (ACD) Software Solaris, version 4.67. The calculated values of $\log P$ were correlated with the contributions of hydrogen bond donor specific solvent interactions as calculated from Eq. (1). Based on a so obtained linear dependence, the pharmacological activity of the studied hydantoin derivatives is discussed.

RESULTS AND DISCUSSION

The chemical structures and the purities of the synthesized hydantoin were confirmed by melting point measurements as well as ¹H-NMR, FT-IR and UV spectroscopy. For the hydantoin **1–11** the obtained results were in agreement

with literature data (Table I). For the newly synthesized compounds **12–14** (3-OCH₃, 3-CH₃, 3-Cl) which, to the best of our knowledge, have not been registered in the literature, full characterization is presented below.

TABLE I. Physical and spectroscopic data for 5-methyl-5-(3- or 4-substituted phenyl)hydantoin

Compound No.	M.p. ^a °C	Lit. m.p. ^a °C	¹ H-NMR (200 MHz, DMSO- <i>d</i> ₆ , δ / ppm)	
			(N-1)H	R, X, (N-3)H
1	181–184	182–184 ²⁰	<i>s</i> , 8.30	(N-3)H (<i>s</i> , 10.30), Ph (<i>d</i> , 7.02), Ph (<i>d</i> , 6.45), NH ₂ (<i>s</i> , 5.00), 5-Me (<i>s</i> , 1.50)
2	240–243	244 ²¹	<i>s</i> , 8.47	(N-3)H (<i>s</i> , 9.53), Ph (<i>d</i> , 7.28), Ph (<i>d</i> , 6.78), 5-Me (<i>s</i> , 1.63)
3	208–210	210–212 ²²	<i>s</i> , 8.40	Ph (<i>d</i> , 7.35), Ph (<i>d</i> , 6.92), OMe (<i>s</i> , 3.73), 5-Me (<i>s</i> , 1.63)
4	200–204	203–204 ²³	<i>s</i> , 8.57	Ph (<i>m</i> , 7.56–7.13), Me (<i>s</i> , 2.30), 5-Me (<i>s</i> , 1.67)
5	194–196	195–196 ²⁴	<i>s</i> , 8.50	Ph (<i>s</i> , 7.37), 5-Me (<i>s</i> , 1.63)
6	258–260	260–261 ²³	<i>s</i> , 8.57	Ph (<i>m</i> , 7.48–7.22), 5-Me (<i>s</i> , 1.67)
7	274–276	276–277 ²⁵	<i>s</i> , 8.63	Ph (<i>m</i> , 7.73–7.33), 5-Me (<i>s</i> , 1.67)
8	228–230	227–229 ²⁶	<i>s</i> , 8.70	Ph (<i>d</i> , 8.22), Ph (<i>d</i> , 7.72), 5-Me (<i>s</i> , 1.70)
9	203–205	206 ²⁷	<i>s</i> , 8.70	Ph (<i>m</i> , 8.00–7.40), 5-Me (<i>s</i> , 1.70)
10	293–295	293–295 ^b	<i>s</i> , 9.17	Ph (<i>s</i> , 7.30)
11	184–191	185–193 ²⁶	<i>s</i> , 8.87	Ph (<i>m</i> , 8.33–7.50), 5-Me (<i>s</i> , 1.73)

^aMelting point; ^bcommercially available (Fluka)

5-(3-Methoxyphenyl)-5-methylhydantoin (12). M.p. 125–130 °C; white crystals. IR (KBr, cm⁻¹): 3277, 3201, 1772, 1721, 1610, 1511, 1459, 1397, 1257, 803. ¹H-NMR (200 MHz, 25 °C, DMSO-*d*₆, δ / ppm): 10.74 (1H, *s*, N-3), 8.83 (1H, *s*, N-1), 7.22–6.74 (4H, *m*, Ph), 3.75 (3H, *s*, OMe), 1.62 (3H, *s*, 5-Me). ¹³C-NMR (50 MHz, 25 °C, DMSO-*d*₆, δ / ppm): 177.1, 159.6, 156.5, 141.9, 130.0, 117.9, 113.2, 111.8, 64.2, 55.5, 25.5.

5-Methyl-5-(3-methylphenyl)hydantoin (13). M.p. 175–180 °C; white crystals. IR (KBr, cm⁻¹): 3267, 3200, 1779, 1719, 1608, 1508, 1424, 1378, 1239, 769. ¹H-NMR (200 MHz, 25 °C, DMSO-*d*₆, δ / ppm): 10.76 (1H, *s*, N-3), 8.47 (1H, *s*, N-1), 7.33–6.93 (4H, *m*, Ph), 2.33 (3H, *s*, Me), 1.67 (3H, *s*, 5-Me). ¹³C-NMR (50 MHz, 25 °C, DMSO-*d*₆, δ / ppm): 176.7, 158.5, 155.8, 139.6, 138.4, 116.2, 111.4, 108.6, 63.6, 54.2, 25.7.

5-(3-Chlorophenyl)-5-methylhydantoin (14). M.p. 180–182 °C; white crystals. IR (KBr, cm⁻¹): 3281, 3204, 1772, 1713, 1606, 1491, 1401, 1299, 1241, 801. ¹H-NMR (200 MHz, 25 °C, DMSO-*d*₆, δ / ppm): 10.88 (1H, *s*, N-3), 8.62 (1H, *s*, N-1), 7.60–7.20 (4H, *m*, Ph), 1.67 (3H, *s*, 5-Me). ¹³C-NMR (50 MHz, 25 °C, DMSO-*d*₆, δ / ppm): 176.4, 158.2, 156.3, 139.0, 132.8, 128.5, 127.4, 126.2, 63.7, 25.1.

The infrared spectra of all the synthesized hydantoin s showed two carbonyl bands at about 1702 and 1778 cm^{-1} and intense N–H bands in the region 3174–3292 cm^{-1} .

The ultraviolet absorption frequencies of the 5-methyl-5-(3- or 4-substituted phenyl)hydantoin s in twelve solvents in the range 200–400 nm are given in Table II.

The effects of the solvent dipolarity/polarizability (nonspecific solvent interactions) and hydrogen bonding (specific solvent interactions) on the investigated hydantoin s were interpreted using the general solvation equation, Eq. (1). Correlation of the spectroscopic data with solvent parameters²⁸ was performed by means of multiple linear regression analysis. It was found that the absorption frequencies for the hydantoin derivatives in twelve selected solvents showed a satisfactory correlation with the π^* , β and α parameters. The results of the multiple regressions are presented in Tables III and IV. The values of the coefficient ν_0 , s and b , and the fit at the 95 % confidence level are given in Table III.

A plot of the ν_{max} values calculated using Eq. (1) *versus* the ν_{max} values observed in different solvents is presented in Fig. 2. The negative sign of the coefficient s in the total solvatochromic equation (Table III) indicates a bathochromic shift with increasing solvent dipolarity/polarizability. The positive signs of the coefficients a and b (excluding the negative sign of the coefficient b for the 4-OH, 4-NO₂ and 3-NO₂ substituents) indicate a hypsochromic shift with increasing solvent hydrogen bond donor acidity and acceptor basicity and imply stabilization of the ground state relative to the electronic excited state. The percentage contributions of the solvatochromic parameters (Table III) for the investigated hydantoin s show that most of the solvatochromism (except for the 4-NO₂ and 3-NO₂ substituents) is due to solvent acidity and basicity (specific solute–solvent interactions) rather than to the solvent dipolarity/polarizability (nonspecific solute–solvent interactions). The solvent acidity effect is predominant in all the investigated molecules, except for 5-methyl-5-(3- or 4-nitrosubstituted phenyl)hydantoin s. These results are in accordance with the preferred existence of hydantoin s in the lactam tautomeric form,³ and the previously reported hypothesis of Poupaert *et al.*⁹ that hydrogen bonding is an essential factor in the anticonvulsant action of 5,5-diphenylhydantoin derivatives.

The evidence for the solvent effects on the structure–activity relationship of hydantoin derivatives was obtained by correlation of the calculated lipophilic log P values with the contributions of hydrogen-bond donor solvent interactions, a . Both parameters depend on the structure of the hydantoin s. The results of the correlation are shown in Fig. 3. The plot of the log P values *versus* a gives a satisfactory linear correlation for moderate electron-donating and electron-accepting substituents.

TABLE II. UV-Vis spectral data ($\nu_{\max} \times 10^{-3} / \text{cm}^{-1}$) of 5-methyl-5-(3- or 4-substituted phenyl)hydantoins

Solvent	Compound													
	1	2	3	4	5	6	7	8	9	10	11	12	13	14
Methanol	40.45	44.72	44.56	44.68	44.48	45.33	45.29	37.48	43.86	45.29	38.49	44.96	44.64	44.80
Ethanol	40.58	44.68	44.13	44.44	44.72	45.13	45.09	37.40	43.59	45.21	38.43	45.09	44.80	44.64
Propan-1-ol	40.39	44.64	44.21	44.60	44.88	44.88	44.08	37.37	44.25	45.25	38.64	44.84	44.92	44.80
Propan-2-ol	40.39	44.76	44.37	44.52	44.56	45.83	45.75	37.43	43.52	45.05	38.55	44.88	44.68	44.48
Methyl acetate	33.94	37.51	36.58	37.88	39.31	37.76	37.74	37.37	36.79	39.06	38.31	38.11	39.06	37.59
Ethyl acetate	34.04	37.26	36.58	38.08	39.59	37.62	37.59	37.23	36.82	38.49	38.34	37.91	38.76	37.54
<i>N,N</i> -Dimethylacetamide	33.56	36.02	35.59	36.82	38.46	37.62	37.57	36.34	36.71	38.91	36.00	37.31	37.59	37.31
Ethylene glycol	40.62	44.96	43.67	44.05	44.05	43.90	43.48	37.01	43.67	44.31	37.99	44.52	44.25	44.52
Tetrahydrofuran	33.76	37.34	36.76	37.74	38.91	37.76	37.71	37.37	37.82	38.76	38.40	37.85	38.17	38.11
Dioxane	33.67	37.37	35.77	37.45	38.85	37.23	37.17	37.37	37.62	38.61	38.37	37.54	37.88	38.05
Dimethyl sulfoxide	33.50	36.10	36.39	36.66	38.02	37.65	37.62	36.18	36.68	37.79	36.87	37.29	37.48	37.01
2-Methylpropan-2-ol	40.98	41.42	42.99	44.25	44.33	43.86	43.82	37.57	43.74	45.70	38.88	44.37	44.44	44.44

TABLE III. Regression fits to the solvatochromic parameters (Eq. (1))

Compound	ν_0	s	b	a	R^a	S^b	F^c	n^d
1	34.09	-1.92 (± 0.71)	1.83 (± 0.71)	7.54 (± 0.35)	0.995	0.43	247	12
2	39.02	-1.56 (± 1.37)	-1.82 (± 1.36)	9.23 (± 0.68)	0.986	0.78	91	12
3	36.81	-1.92 (± 0.72)	1.46 (± 0.72)	8.79 (± 0.35)	0.996	0.44	303	12
4	39.15	-3.21 (± 0.53)	0.94 (± 0.53)	7.84 (± 0.26)	0.998	0.29	597	12
5	40.46	-2.96 (± 0.80)	0.82 (± 0.50)	6.26 (± 0.39)	0.995	0.34	284	12
6	37.61	-2.02 (± 0.74)	2.52 (± 0.74)	7.89 (± 0.36)	0.995	0.45	264	12
7	37.66	-2.33 (± 0.68)	2.74 (± 0.68)	7.70 (± 0.35)	0.994	0.47	229	12
8	38.85	-2.05 (± 0.17)	-0.82 (± 0.17)	0.43 (± 0.08)	0.981	0.10	66	12
9	37.89	-2.24 (± 0.23)	1.37 (± 0.60)	7.49 (± 0.32)	0.993	0.48	198	12
10	39.41	-2.99 (± 0.63)	2.32 (± 0.62)	6.92 (± 0.31)	0.996	0.38	299	12
11	40.85	-3.40 (± 0.64)	-1.40 (± 0.63)	0.85 (± 0.32)	0.918	0.39	14	12
12	38.52	-2.29 (± 0.66)	1.34 (± 0.61)	8.01 (± 0.36)	0.998	0.27	712	12
13	39.66	-2.92 (± 0.56)	0.98 (± 0.51)	7.22 (± 0.28)	0.994	0.45	208	12
14	38.65	-2.40 (± 0.25)	1.14 (± 0.58)	7.93 (± 0.33)	0.997	0.32	496	12

^aCorrelation coefficient; ^bstandard error of the estimate; ^cFisher's test; ^dnumber of solvents used in the calculations

TABLE IV. Percentage contributions of the nonspecific ($P\pi^*$) and specific ($P\alpha$ and $P\beta$) solvent interaction and the log P values

Compound	$P\pi^* / \%$	$P\alpha / \%$	$P\beta / \%$	Log P
1	16.98	66.82	16.20	-0.283
2	12.38	73.22	14.40	0.263
3	15.80	72.22	11.98	0.914
4	26.77	65.37	7.86	1.459
5	29.45	62.35	8.20	0.999
6	16.25	63.51	20.24	1.594
7	18.24	60.31	21.45	1.771
8	62.11	13.05	24.85	0.729
9	20.19	67.46	12.36	0.436
10	24.47	56.58	18.95	2.524
11	60.19	15.10	24.71	0.729
12	19.67	68.79	11.53	0.914
13	26.28	64.89	8.82	1.459
14	20.96	69.12	9.92	1.594

The existence of this correlation (Fig. 3) is strong evidence for the proportionality between the lipophilic parameters and the specific solvatochromic effect of the investigated 5-methyl-5-(4-substituted phenyl)hydantoin and 5,5-diphenylhydantoin that show good anticonvulsant activity as reported previously.^{2,29} The data for hydantoin with substituents in the *meta* positions in the benzene ring did not follow this correlation (Fig. 3). These results are in accordance with their previously reported²⁵ non-anticonvulsant activity.

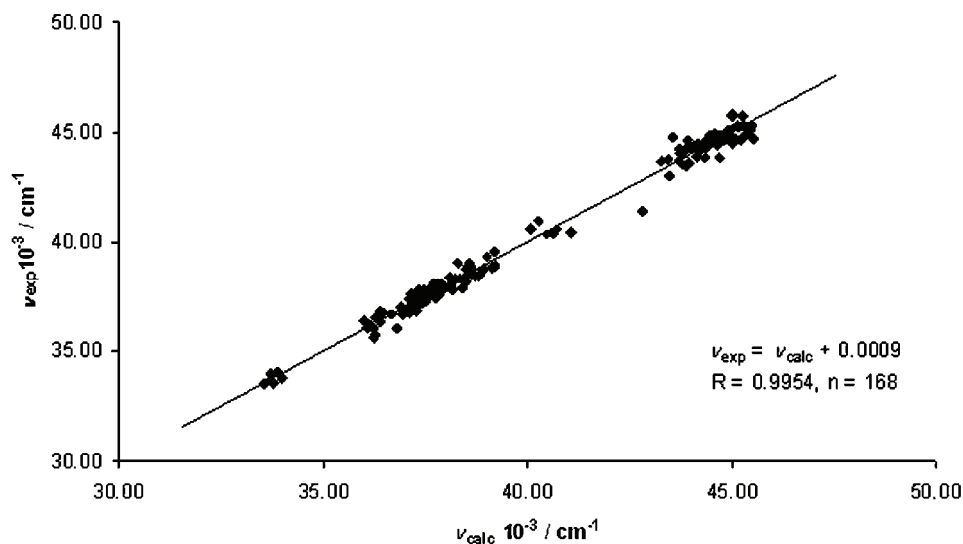


Fig. 2. Plot of ν_{\max} observed against ν_{\max} calculated from Eq. (1) for 5-methyl-5-(3- or 4-substituted phenyl)hydantoin.

Strong electron-donors and acceptors decrease the lipophilic activity of the investigated hydantoin. These compounds also did not follow correlation presented in Fig. 3.

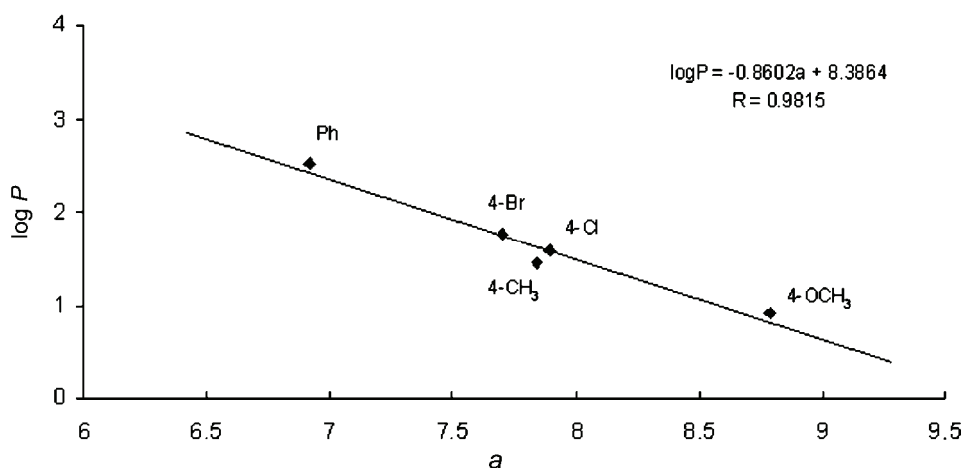


Fig. 3. Correlation of the $\log P$ values with the contribution of hydrogen bond solvent interaction, a , for 5-methyl-5-(4-substituted phenyl)hydantoin.

The satisfactory correlation of the ultraviolet absorption frequencies of the investigated 5-methyl-5-(3- or 4-substituted phenyl)hydantoin with Kamlet–Taft general solvatochromic equation indicates that the selected models give a correct

interpretation of the linear solvation energy relationships of the complex hydantoin system in the solvents used. This demonstrates that an equation with three solvatochromic parameters π^* , β and α can be used to evaluate the effects on both types of hydrogen bonding and the solvent dipolarity/polarizability effects for pharmacologically active hydantoin. For these reasons, it is considered that the results presented in this work may be utilized to quantitatively separate the overall solvent effect into specific and nonspecific contributions using a LSER method. The satisfactory correlation of the lipophilic parameters $\log P$ of the investigated pharmacologically active hydantoin^{2,29} with the contribution of the hydrogen bond donor solvent interactions supports the previously reported⁷ pharmacophore model based on a hydrogen-bond acceptor, a hydrogen-bond donor, and an electronegative group with a large hydrophilic part of the molecule. Following the model proposed in this work, the pharmacological activity of some hydantoin derivatives can be explained and the corresponding potential activity/non-activity of the studied hydantoin, not yet pharmacologically tested, may be predicted.

EXPERIMENTAL

All of the investigated 5-methyl-5-(3- or 4-substituted phenyl)hydantoin were synthesized by a modification of the method of Bucherer.³⁰ Following this procedure, 0.020 mol of ketone was dissolved in 50 ml of 50 % ethanol and 0.080 mol of ammonium carbonate plus 0.040 mol of potassium cyanide were added. This mixture was warmed under a condenser at a temperature of 58–60 °C for 15 h, after which the solution was concentrated to approximately two-thirds of the initial volume and chilled in an ice-bath. The mass was filtered on a Büchner funnel. The product was dissolved in 5 % sodium hydroxide solution, filtered from unreacted ketone and reprecipitated by acidification with hydrochloric acid. Recrystallization of the white solid from 60 % ethanol yielded a crystalline product. The ketones used in these preparations were commercially available (Fluka). The chemical structures and the purities of the synthesized hydantoin 1–14 were confirmed by their melting points, as well as ¹H-NMR, FT-IR and UV spectroscopy.

The FT-IR spectra were recorded on a Bomem MB 100 spectrophotometer. The ¹H- and ¹³C-NMR spectra of DMSO-*d*₆ solutions (TMS as the internal standard) were measured with a Varian-Gemini 200 MHz spectrometer. The UV absorption spectra were measured with a Shimadzu 1700 spectrophotometer. The UV spectra were taken in spectroquality solvents (Fluka) at 10⁻⁵ mol dm⁻³ concentration.

The correlation analysis was performed using Microsoft Excel computer software, which considers the 95 % confidence level. The goodness of fit was discussed using the correlation coefficient *R*, standard error of the estimate, *S* and the Fisher's significance test, *F*.

Acknowledgements. The authors acknowledge the financial support of the Ministry of Science and Technical Development of the Republic of Serbia (Project 142063).

ИЗВОД

СИНТЕЗА, СТРУКТУРА И СОЛВАТОХРОМИЗАМ 5-МЕТИЛ-5-(3- ИЛИ 4-СУПСТИТУИСАНИХ ФЕНИЛ)-ХИДАНТОИНА

НАТАЛИЈА Д. ДИВЈАК, НЕБОЈША Р. БАЊАЦ, НАТАША В. ВАЛЕНТИЋ И ГОРДАНА С. УШЋУМЛИЋ

Технолошко–металуршки факултет Универзитета у Београду, Карнегијева 4, 11120 Београд

У оквиру проучавања утицаја структуре на фармаколошку активност хидантоина, у овом раду синтетизовано је четрнаест једињења и одређени су њихови UV апсорпциони максимуми у дванаест растварача различите поларности. Апсорпциони максимуми су корелисани Камлет–Тафтовом (*Kamlet–Taft*) солватахромном једначином и извршена је квантитативна процена протон-донорских и протон-акцепторских карактеристика проучаваних једињења, које су од великог значаја за њихову физиолошку активност. Израчунате вредности $\log P$ корелисане су са уделом протон-донорских карактеристика растварача и на основу добијених линеарних зависности за молекуле са умереним електрон-донорским и електрон-акцепторским супституентима, дискутована је веза између фармаколошке активности хидантоина и интеракција са молекулима растварача.

(Примљено 1. јула 2008, ревидирано 8. јула 2009)

REFERENCES

1. A. C. Lopez, C. G. Trigo, in *The Chemistry of Hydantoins. Advances in Heterocycles Chemistry*, A. R. Katrizky, Ed., Academic Press, New York, 1985
2. S. Scholl, A. Koch, D. Henning, G. Kemter, E. Kleinpeter, *Struct. Chem.* **10** (1999) 355
3. E. Kleinpeter, *Struct. Chem.* **8** (1997) 161
4. J. Knabe, J. Baldauf, A. Aklhem, *Pharmacie* **52** (1997) 912
5. K. E. Schuite, W. V. von Eur, *J. Med. Chem.* **13** (1978) 25
6. T. R. Rodgers, M. P. LaMontage, A. Markovac, A. B. Ach, *J. Med. Chem.* **20** (1977) 591
7. K. Unverferth, J. Engel, N. Höfgen, A. Rostock, R. Günther, H. J. Lankom, M. Menzer, A. Rolfs, J. Liebscher, B. Müller, H. J. Hofmann, *J. Med. Chem.* **41** (1998) 63
8. G. L. Jones, D. M. Woodbury, *Drug Dev. Res.* **2** (1982) 333
9. J. H. Poupaert, D. Vandervarst, P. Guiot, M. M. Moustata, P. Dumont, *J. Med. Chem.* **27** (1984) 76
10. N. Banjac, G. Ušćumlić, N. Valentić, D. Mijin, *J. Solution Chem.* **36** (2007) 869
11. M. J. Kamlet, J. L. M. Abboud, R. W. Taft, *Prog. Phys. Org. Chem.* **13** (1981) 485
12. J. L. M. Abboud, M. J. Kamlet, R. W. Taft, *J. Am. Chem. Soc.* **99** (1977) 8325
13. M. J. Kamlet, R. W. Taft, *J. Am. Chem. Soc.* **98** (1976) 377
14. M. J. Kamlet, R. W. Taft, *J. Chem. Soc., Perkin Trans. 2* (1979) 349
15. M. J. Kamlet, R. M. Doherty, J. L. M. Abboud, M. H. Abraham, R. W. Taft, *Chemtech* **16** (1986) 566
16. P. W. Carr, R. M. Doherty, M. J. Kamlet, R. W. Taft, W. Melander, C. Horvath, *Anal. Chem.* **58** (1986) 2674
17. D. Ž. Mijin, G. S. Ušćumlić, N. U. Perišić Janjić, N. V. Valentić, *Chem. Phys. Lett.* **418** (2006) 223
18. J. Nikolić, G. Ušćumlić, *J. Serb. Chem. Soc.* **72** (2007) 1217
19. S. Spange, R. Sevs, K. Zimmermann, A. Seifert, I. Roth, S. Anders, K. Hofmann, *New J. Chem.* **27** (2003) 520
20. H. R. Henze, L. M. Long, R. J. Speer, T. R. Thompson, *J. Am. Chem. Soc.* **65** (1943) 323

21. P. C. Wang, C. S. Wang, S. P. Crain, U.S. No. 4,672,101 (1987)
22. M. C. E. Carron, C. L. C. Carron, B. P. Bucher, Fr. No. 5,677 M (1968)
23. R. E. Nitz, W. Persch, A. Schmidt, *Arzneim.-Forsch.* **5** (1955) 357
24. A. S. Endler, E. I. Becker, *J. Am. Chem. Soc.* **77** (1955) 6608
25. H. R. Henze, A. F. Isabell, *J. Am. Chem. Soc.* **76** (1954) 4152
26. T. A. Connors, W. C. J. Ross, J. G. Wilson, *J. Am. Chem. Soc.* (1960) 2294
27. W. Holla, G. Beck, B. Kammermeier, B. Kulitzscher, J. Michalowsky, U.S. No. 6,018,053 (2000)
28. J. A. Vida, C. M. Samour, J. F. Reinhard, *J. Med. Chem.* **14** (1971) 187
29. C. E. Maurice, L. C. Claude, P. B. Bernard, Fr. No. 5677 (1968)
30. H. Bucherer, W. Steiner, *J. Pract. Chem.* **140** (1934) 291.



J. Serb. Chem. Soc. 74 (11) 1207–1217 (2009)
JSCS–3911

Structural requirements for ligands of the δ -opioid receptor

VUK I. MIĆOVIĆ¹, MILOVAN D. IVANOVIĆ^{2,3#} and LJILJANA DOŠEN-MIĆOVIĆ^{2,3**}

¹Institute for General and Physical Chemistry, Belgrade, ²Faculty of Chemistry, University of Belgrade, Studentski trg 12–16, 11158 Belgrade and ³ICTM, Center for Chemistry, University of Belgrade, Njegoševa 12, Belgrade, Serbia

(Received 22 October 2008, revised 28 May 2009)

Abstract: The δ -opioid receptor is sensitive to ligand geometry. In order to assist the synthesis of new δ -selective opioid ligands, the structure elements of δ -selective opioid ligands necessary for their effective binding were investigated. The automated docking procedure with a flexible ligand was used to simulate the binding of 17 δ -selective ligands to the δ -receptor. It was found that voluminous N-alkyl groups reduce the binding potency of naltrindole derivatives by preventing the ligands from adopting the preferred conformation in the receptor. This was confirmed by enantiospecific binding of chiral compounds where only one enantiomer adopts the naltrindole-like preferred conformation in the binding pocket. Voluminous groups replacing the hydroxyl group in the 3-hydroxybenzyl fragment of naltrindole analogs reduce the binding potency due to unfavorable steric interactions with the receptor. The two diastereoisomers of the potent δ -opioid ligand SNC80 confirmed the preferred binding conformation and the major receptor–ligand interactions.

Keywords: molecular modeling; δ -opioid receptor; ligand–receptor interactions; docking simulation.

INTRODUCTION

The δ -opioid receptor is an especially attractive target for the development of new drugs for the control of pain. Compared to other opioid or opioid-like receptors, δ -opioid selective drugs have some advantages, including: greater relief of neuropathic pain, reduced respiratory depression and constipation, and reduced potential for the development of physical dependence.¹ Only one δ receptor has been cloned to date;^{1,2} but several models of this receptor are available in the literature.³ These models are consistent with a vast sample of published biophysical and other experimental data³ but experimental data on the structure of any of the opioid receptors are unavailable. Considering the possible effects of

* Corresponding author. E-mail: lmicovic@chem.bg.ac.rs

Serbian Chemical Society member.

doi: 10.2298/JSC0911207M

different media (the difference in the rhodopsin structure determined in the crystal state⁴ and in solution⁵) and the obvious importance of the exact position of the amino acid residues⁶ which are different in different proteins, the available models may be considered reliable opioid receptor representatives if they are capable of reproducing point mutation studies and other experimental data.

There is experimental evidence that interaction of peptidic ligands with receptors are different from that of small ligands.⁷ Since small organic molecules as possible ligands of the δ -opioid receptor were our target, this study is limited to non-peptidic ligands of the δ -receptor, Table I.

The region of a δ -opioid receptor involved in ligand binding and mediation of receptor function were identified by: a) construction of chimeric receptors containing sequences from μ - or κ -opioid receptors,⁸ b) site-directed mutagenesis of specific amino acid residues⁹ and c) construction of truncated mutant receptors.¹⁰

The site-directed mutagenesis experiments^{9a} showed that Asp128 does not participate in the formation of a salt bridge between a ligand and the receptor, but it does contribute to the stabilization of the binding pocket. Some highly selective non-peptidic δ -ligands were moderately affected^{9b} by mutations of the amino acids: Tyr129Phe, Trp274Ala and Tyr308Phe, indicating that these aromatic residues might be a part of the opioid binding domain. Chimeric receptors and the alanine scan method were used^{8b} to show that Val296 and Val297 of the EC3 loop are important for the binding of the δ -selective ligand SNC80. Leu295 and Ala298 of EC3 were important for the binding of naltrindole. The amino acids Trp284 (TM6 – transmembrane helix 6) and Ser312 (TM7 – trans membrane helix 7) were important for both compounds, although to a lesser degree. Point mutations performed on a mutant receptor emphasized the importance of Leu300, Ala298, Ala299 amino acids. Val281 had a moderate effect on ligand binding.^{8d} It was found^{9c} that Tyr308Phe mutation increased the binding. This amino acid, together with His278 (TM6) was suggested^{9c} to participate in interactions [Asp128 (TM3)–Tyr308 (TM7) and Tyr129 (TM3)–His278 (TM6)] that maintain the δ -receptor in an inactive conformation. The model of the δ -opioid receptor showing important amino acids is presented in Fig. 1.

In this study, the docking of a series of δ -opioid-selective ligands to a model of the human δ -receptor available in literature^{3a} is reported. It is the model of an active form of the receptor, although the entire concept of active and inactive receptors has recently been questioned. Contrary to some earlier findings,¹¹ recent X-ray studies¹² on rhodopsin demonstrated that the transformation from the ground state to the photoactivated intermediate state involved minor changes in the receptor structure. It was suggested¹² that the rigid inactive conformation of the receptor becomes more relaxed upon activation. It was also suggested¹² that one receptor model may be used in docking calculations of both agonists and antagonists.

TABLE I. Names and structures of the compounds 1–17

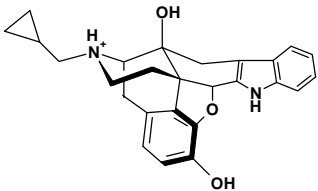
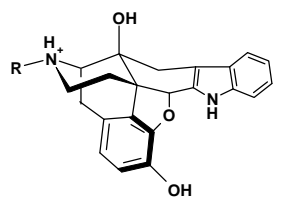
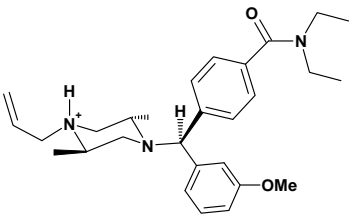
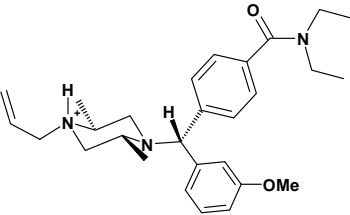
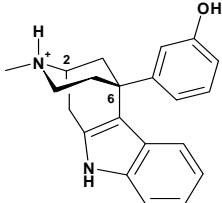
Compound	Name	Structure
1	Naltrindole, NTI	
2	Naltrindole derivatives	
3	Oxymorphindole, R: CH ₃	
4	R: 	
5	R: 	
6	R:  ; R ₁ : CH ₃ ; R ₂ : H	
7	R:  ; R ₁ : CH ₃ ; R ₂ : CH ₃	
8	R:  ; R ₁ : H; R ₂ : CH ₃	
9	R: CH ₃ ; R ₁ : CH ₃ ; R ₂ : H	
10	R: CH ₃ ; R ₁ : CH ₃ ; R ₂ : CH ₃	
11	R: CH ₃ ; R ₁ : H; R ₂ : CH ₃	
12	(+)-4-[(αS)- α -((2 <i>S</i> ,5 <i>R</i>)-4-Allyl-2,5-dimethyl-1-piperazinyl)-3-methoxybenzyl]- <i>N,N</i> -diethylbenzamide	
13	(-)-4-[(αR)- α -((2 <i>R</i> ,5 <i>S</i>)-4-Allyl-2,5-dimethyl-1-piperazinyl)-3-methoxybenzyl]- <i>N,N</i> -diethylbenzamide	
14	(+)-3-[(2 <i>S</i> ,6 <i>R</i>)-1,2,3,4,5,11-Hexahydro-3-methyl-2,6-methano-6 <i>H</i> -azocino[4,5- <i>b</i>]indol-6-yl]phenol	

TABLE I. Continued

Compound	Name	Structure
15	(-)-3-[(2 <i>R</i> ,6 <i>S</i>)-1,2,3,4,5,11-Hexahydro-3-methyl-2,6-methano-6 <i>H</i> -azocino[4,5- <i>b</i>]-indol-6-yl]phenol	
16	(+)-3-[(2 <i>S</i> ,6 <i>R</i>)-1,2,3,4,5,11-Hexahydro-3-(2-phenylethyl)-2,6-methano-6 <i>H</i> -azocino[4,5- <i>b</i>]-indol-6-yl]phenol	
17	(-)-3-[(2 <i>R</i> ,6 <i>S</i>)-1,2,3,4,5,11-Hexahydro-3-(2-phenylethyl)-2,6-methano-6 <i>H</i> -azocino[4,5- <i>b</i>]-indol-6-yl]phenol	

The goal of the present work was to find and compare the binding conformations of δ -selective ligands and to identify the structural fragments the modifications of which may increase the binding and perhaps activation of a δ -receptor.

COMPUTATIONAL METHODS

All computations were performed using a P4/Celeron at 1.5 GHz. The employed δ -receptor model was taken from the literature.^{3a} The receptor model was treated as rigid. The automated flexible ligand docking experiments were realized with the AutoDock 3.0.5. program.¹³ The starting geometries, with a protonated ring nitrogen,¹⁴ were built using the HyperChem program¹⁵ and subsequently optimized using the semi-empirical AM1 method of the same program. The 60×60×60 grid was centered on one of the Asp128 oxygen atoms. The Lamarckian genetic algorithm (LGA) was used in all docking calculations. The docking process was performed in 250 LGA runs; the initial position of the ligand was random. The population was 50, the maximum number of generations was 27000 and the maximum number of energy evaluations was 2.5×10⁶. The resultant ligand orientations and conformations were scored based on the binding energies (the cutoff value for the energies was 16.8 kJ/mol), and they were further evaluated based on the vicinity to important amino acids, found experimentally to be located in the binding site of the δ -selective non peptidic ligands. The clusters were ranked in order of increasing binding energy. The lowest binding energy conformations of all the selected clusters were analyzed in terms of their distances to the important amino acids. The

lowest binding energy conformation with the maximal number of close contacts to the important amino acids is referred to as the preferred conformation.

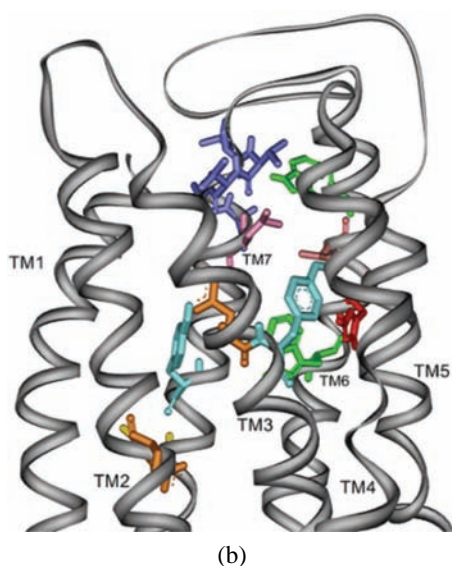
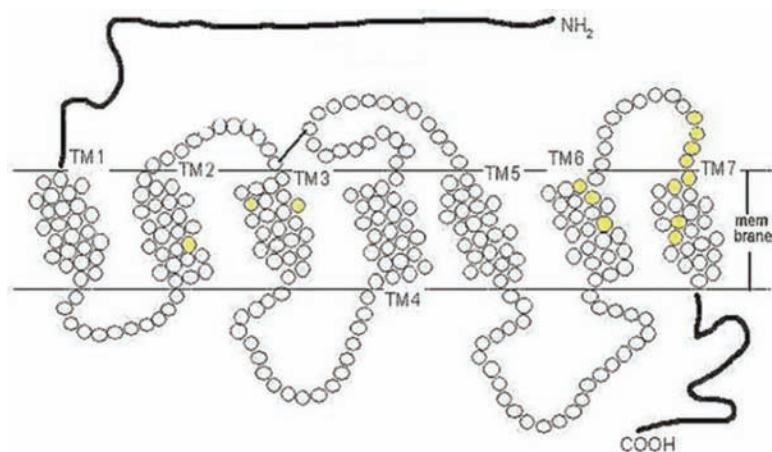


Fig. 1. a) Serpentine model of the δ -opioid receptor. Important amino acids are in yellow (mutagenesis experiments); b) 3D model of the δ -opioid receptor with important amino acids.

RESULTS AND DISCUSSION

Despite apparent structural differences, all the studied δ -selective compounds have similar 3D geometries (Table I), consisting of a protonated piperidine (or piperazine) ring and two aromatic rings. These three structural elements may adopt similar spatial positions in different ligand-receptor complexes, but may, as well, occupy different positions and orientations within the receptor.

Automated docking of compound **1** to the δ -opioid receptor model resulted in several plausible docking orientations and conformations for the ligand. The resulting ligand orientations and conformations were scored based on the values of the binding energies and by the number of close contacts to the receptor amino acids known to form the binding pocket within the δ -receptor, Fig. 1. Based on these criteria, the preferred conformation of compound **1** in the binding pocket of the δ -receptor model has a binding energy ($E_b = -40.3$ kJ/mol) 6.3 kJ/mol above the global minimum conformation. Its orientation is very similar to the one proposed earlier, and follows the “message–address concept”,¹⁶ Figs. 2 and 3.

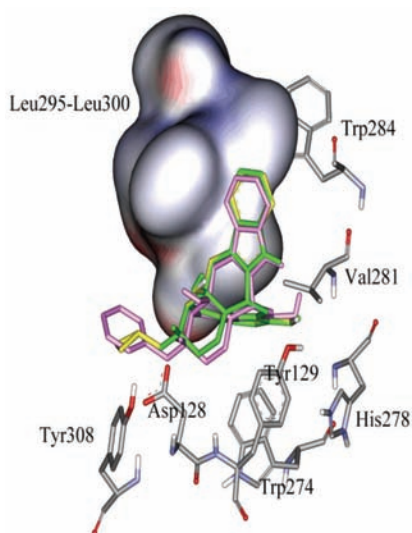


Fig. 2. Ligands: **1** (yellow), **2** (green) and **3** (pink) in the binding pocket.

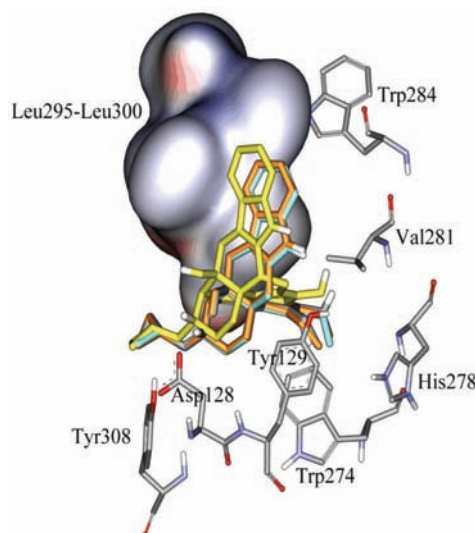


Fig. 3. Ligands: **1** (yellow), **6** (gray), **7** (orange) and **8** (blue) in the binding pocket.

The protonated piperidine and the phenolic component form the “message” moiety related to ligand binding and the indolic component represents the “address” moiety and determines ligand selectivity besides binding. According to the docking results, the “message” moiety interacts (within 0.4 nm) with Asp128, through salt bridge formation ($+NH\cdots O^-$ distance 0.27 nm), with Tyr129 of TM3 and Tyr308 of TM7 (all known from point mutation studied^{9b}), and with Gln105 and Leu102 of TM2. The major interaction with Gln105 is hydrogen bond formation to the 14-hydroxy group of **1** ($NH\cdots O$ distance is 0.22 nm). It was found earlier^{17a} that the 14-hydroxy group plays an important role in δ -selectivity and the binding potency of some δ -selective ligands. On the other hand, it is generally believed¹⁶ that the residues at the top of TM6 and TM7 form a hydrophobic pocket to accommodate the indolic moiety of **1**. According to the docking results

presented here, this hydrophobic pocket is formed by Val297, Val296 (EC3) and Leu300 (TM7) (known from point-mutation studies) and by the Ala195 and Val196 of EC2.

The four derivatives of **1**, ligands **2–5**, differ in their experimentally determined binding constants, Table II. While the *N*-methyl derivative, **2**, has a binding affinity towards the δ -receptor comparable to that of **1**, the *N*-benzyl, *N*-cyclohexylmethyl and *N*-cyclohexylethyl derivatives (**3**, **4** and **5**, respectively) are far less efficient. The docking results are in agreement with the experimental findings. The preferred conformations of **2** and **3** overlap in the binding pocket with the preferred conformation of **1**, Fig. 2, but their binding energies (–38.4 and –35.4 kJ/mol, respectively) are high relative to that of **1**. The other two derivatives, **4** and **5**, cannot even adopt the preferred conformation characteristic for naltrindoles. It seems that the size of the pocket, surrounded by the amino-acid residues Leu102 and Gln105 of TM2 and Ile304 and Tyr308 of TM7 is too small to accommodate voluminous alkyl groups. Therefore any modification of the *N*-alkyl part of the ligand will be limited by the size of the modified group.

TABLE II. Experimental binding constants, K_i and IC_{50}

Compound	δ -Receptor	
	K_i / nM	IC_{50} / nM
1	0.22±0.13 ^a , 0.04 ^b	–
2	0.9±0.2 ^a	–
3	115±32 ^b	–
4	94.5±13.6 ^b	–
5	181±35 ^b	–
6	0.40±0.3 ^a	–
7	19.0±2.0 ^a	–
8	21.8±7.0 ^a	–
9	4.5±0.5 ^a	–
10	41.0±4.0 ^a	–
11	218±33 ^a	–
12	15.2 ^c	56.5±3.10 ^d
13	4.12 ^c	3.50±0.39 ^d
14	–	660.1±160.2 ^e
15	–	5.6±1.5 ^e
16	–	>1000 ^e
17	–	6.2±0.6 ^e

^aRef.17; ^bRef.18; ^cRef.19; ^dRef.20; ^eRef.21

The other group of studied compounds was the ligands obtained by the opening of the 4,5-bridge in either **1** or **2**. The in this way created 3-hydroxy-4-methoxyindomorphinans (**6** and **9**), 3,4-dimethoxyindomorphinans (**7** and **10**) and 3-methoxy-4-hydroxyindomorphinans (**8** and **11**) show reduced binding potency towards the δ -receptor compared to **1** and **2**. This reduction in binding po-

tency is small for **6** and **9** but increased in the case of the 3-methoxy compounds. Differences in affinity at a δ -receptor were earlier assigned^{17b} to a shift in the relative position of the indole. The present docking study showed that this shift is small, less than 0.15 nm, Fig. 3. The reduced binding affinity may also be due to the presence of the 4-hydroxyl and the lack of a 3-hydroxyl group.^{17b} However, the preferred conformations of compounds **6–11** do not allow a 3-hydroxy group to form any hydrogen bond or other important electrostatic interaction. When the 3-hydroxyl group is replaced by a methoxy group, a steric clash occurs with Ile215 of TM5. Therefore, the reduced affinity of the ligands **7**, **8**, **10** and **11** for the δ -receptor may be due to steric interactions. This suggests that voluminous groups at the position 3 are unlikely to improve binding properties of indolomorphinans.

The study of stereoisomers and their interactions with a particular receptor may be very useful. Two pairs of enantiomers were studied: the (+) and (–) forms of 3-[(2*S*,6*R*)-1,2,3,4,5,11-hexahydro-3-methyl-2,6-methano-6*H*-azocino[4,5-*b*]indol-6-yl]phenol (compounds **14** and **15**), and their 2-phenylethyl analogs **16** and **17**. The two enantiomers in both compounds have noticeably different binding affinities towards the δ -receptor.²¹ The (–) form (**15** and **17**) in both compounds binds better to the receptor. According to docking studies, this is the consequence of different preferred conformations of the (+) and (–) ligands in the binding pocket of the receptor. Compound **15** overlaps **1**, Fig. 4, and has most of the major interactions with the receptor: the protonated nitrogen forms a salt bridge with Asp128, the phenolic group interacts with the amino acids at the beginning of the EC3 loop, while the aromatic (indolic) group interacts with Tyr129 of TM3 and with Thr211 and Ile215 of TM5. Compound **14** cannot adopt this preferred conformation. The picture is less clear for compounds **16** and **17**, where the flexible molecule can adopt a number of different conformations. The only explanation for the higher binding potency of **17** over **16** is the conformation of **17** which partially overlaps the preferred conformation of compound **13**, known to have high binding potency, Fig. 5, Table II. Compound **16** cannot adopt a similar conformation. The noticeable difference in binding affinity towards the opioid δ -receptor of SNC80, (+)-4-[(*αR*)-*α*-((2*S*,5*R*)-4-allyl-2,5-dimethyl-1-piperazinyl)-3-methoxybenzyl]-*N,N*-diethylbenzamide and its enantiomer¹⁹ was explained earlier²² by the inability of the enantiomer to achieve the three important interactions with the receptor. SNC80 ($K_i = 0.181$ nM) has a higher affinity for the cloned human δ -receptor than its enantiomer ($K_i = 218$ nM).¹⁹ On the contrary, the *αS*,2*S*,5*R* diastereoisomer of SNC80, compound **12**, has lower affinity for the cloned human δ -receptor than the enantiomer, **13**. According to the docking results, this may also be explained by the classic “three point theory”. Compound **13** in its preferred conformation has a protonated nitrogen close to Asp128 (TM3) and forms a salt bridge. The NEt₂ groups are located close in

the hydrophobic pocket at the beginning of EC3. The 3-methoxybenzyl group points toward Trp274 and His278 of TM6, Fig. 5. These ligand interactions with TM6 may be the major difference between antagonists and agonists and the key process in receptor activation. It was suggested earlier that movement of helices TM3, TM6 and TM7 is essential for activation of rhodopsin²³ and the human δ -receptor.^{3b} It was also suggested²⁴ that the 3-methoxy group was metabolized to a 3-hydroxyl group and that the analgesic activity was performed partially through this hydroxyl group.²⁴ Compound **12**, on the contrary, cannot adopt this favorable conformation and has only weak interactions with the receptor, about 100 times weaker than SNC80.

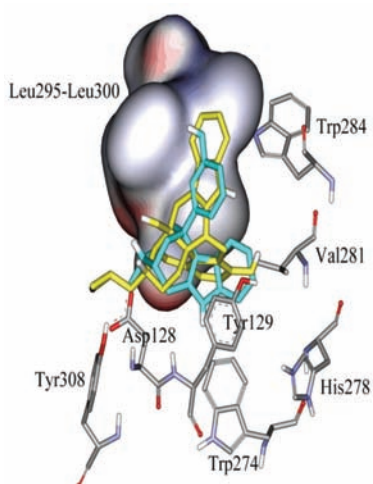


Fig. 4. Ligands **1** (yellow) and **15** (blue) in the binding pocket.

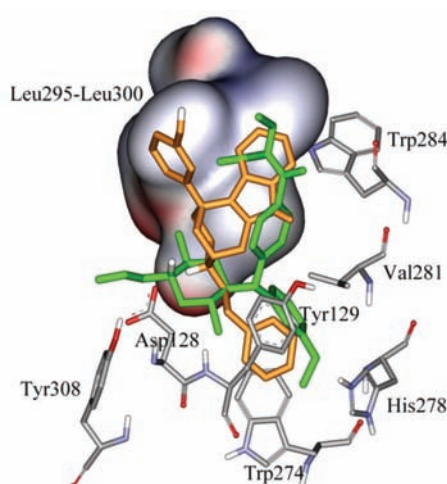


Fig. 5. Ligands **13** (green) and **17** (orange) in the binding pocket.

CONCLUSIONS

An automated docking procedure was applied in order to determine the preferred conformations of a series of δ -opioid receptor selective ligands in the binding pocket of the receptor. The quality of the receptor-ligand complexes was estimated based on their binding energies and the ability to reproduce point mutation experimental data. The following results are believed to assist in synthesis of new δ -selective ligands with a high binding potency. The preferred naltrindole conformation was found to be similar to the one suggested earlier,¹⁶ Fig. 2. The voluminous N-alkyl groups in compounds **1–5** are expected to reduce the binding potency by preventing the ligand from adopting the preferred conformation in the binding pocket. Voluminous groups replacing the hydroxyl group in the 3-hydroxybenzyl fragment of naltrindole analogs, **6–11**, reduce the binding potency due to unfavorable steric interactions with the receptor. Ligand interactions with

the amino acids at the beginning of EC3 are essential for ligand binding. The docking of two diastereoisomers, **12** and **13**, of the potent δ -opioid ligand SNC80 confirmed the preferred binding conformation of this compound proposed earlier,²² and the major ligand–receptor interactions: protonated nitrogen interacting with Asp128 of TM3, hydrophobic groups interacting with EC3 and the phenolic group interacting with TM6 and TM5.

Acknowledgments. This work was supported by the Ministry of Science and Technological Development of the Republic of Serbia.

ИЗВОД

НЕОПОХОДНИ ЕЛЕМЕНТИ СТРУКТУРЕ ЗА ЛИГАНДЕ δ -ОПИОИДНОГ РЕЦЕПТОРА

ВУК И. МИЋОВИЋ¹, МИЛОВАН Д. ИВАНОВИЋ^{2,3} и ЉИЉАНА ДОШЕН-МИЋОВИЋ^{2,3}

¹Институт за општи и физичку хемију, Београд, ²Хемијски факултет, Универзитет у Београду, Студентски брџ 12–16, Београд и ³ИХТМ, Центар за хемију, Универзитет у Београду, Њевошева 12, Београд

δ -Опиоидни рецептор је осетљив на геометрију лиганата. Да би се олакшала синтеза нових δ -селективних опиоидних лиганата, у раду су испитивани елементи њихове структуре који су неопходни за ефикасно везивање. Коришћен је аутоматизовани докинг поступак са флексибилним лигандом да би се симулирало везивање 17 δ -селективних једињења за δ -рецептор. Нађено је да волуминозне N-алкил групе смањују ефикасност везивања деривата налтриндола тако што спречавају ова једињења да заузму конформацију погодну за везивање. Ово је потврђено енантоспецифичним везивањем хиралних једињења код којих само један енантиомер има оријентацију сличну налтриндолу у везујућем месту. Волуминозне групе које замењују 3-хидрокси групу код аналога налтриндола смањују ефикасност везивања због неповољних стерних интеракција са рецептором. Начин везивања два дијастереоизомера ефикасног δ -опиоидног лиганата SNC80, потврђује најбољу конформацију за везивање и најважније рецептор–лиганд интеракције.

(Примљено 22. октобра 2008, ревидирано 28. маја 2009)

REFERENCES

1. R. M. Quock, T. H. Burkey, E. Verga, Y. Hosohata, K. Hosohata, S. Cowell, C. Slate, F. J. Ehlert, W. R. Roeske, H. I. Yamamura, *Pharmacol. Rev.* **51** (1999) 503
2. K. Yasuda, K. Raynor, H. Kong, C. D. Breder, J. Takeda, T. Reisine, G. I. Bell, *Proc. Natl. Acad. Sci. USA* **90** (1993) 6736
3. a) I. D. Pogozheva, A. L. Lomize, H. I. Mosberg, *Biophys. J.* **75** (1998) 612 (www.personal.umich.edu/~him/modeling.htm); b) F. M. Decaillot, K. Befort, D. Filliol, S. Y. Yue, P. Walker, B. L. Kieffer, *Nat. Struct. Biol.* **10** (2003) 629 (www.pdb.org); c) B. L. Podlogar, G. I. Poda, D. A. Demeter, S. P. Zhang, J. R. Carson, L. A. Nielson, A. B. Reitz, D. M. Ferguson, *Drug Des. Discov.* **17** (2000) 34 (www.opioid.umn.edu/strumod.html)
4. K. Palczewski, T. Kumasaka, T. Hori, C. A. Behnke, H. Motoshima, B. A. Fox, I. Le Trong, D. C. Teller, T. Okada, R. E. Stenkamp, M. Yamamoto, M. Miyano, *Science* **289** (2000) 739
5. a) P. L. Yeagle, C. Denis, G. Choi, J. L. Alderfer, A. D. Albert, *Mol. Vis.* **6** (2000) 125; b) P. L. Yeagle, G. Choi, A. D. Albert, *Biochemistry* **40** (2001) 11932

6. a) M. A. Hanson, V. Cherezov, M. T. Griffith, C. B. Roth, V. P. Jaakola, E. Y. Chien, J. Velasquez, P. Kuhn, R. C. Stevens, *Structure* **16** (2008) 897; b) V. Cherezov, D. M. Rosenbaum, M. A. Hanson, S. G. Rasmussen, F. S. Thian, T. S. Kobilka, H. J. Choi, P. Kuhn, W. I. Weis, B. K. Kobilka, R. C. Stevens, *Science* **318** (2007) 1258
7. a) F. Meng, M. T. Hoversten, R. C. Thompson, L. Taylor, S. J. Watson, H. Akil, *J. Biol. Chem.* **270** (1995) 12730; b) E. M. Jutkiewicz, N. P. Walker, J. E. Folk, K. C. Rice, P. S. Portoghese, J. H. Woods, J. R. Traynor, *J. Pharmacol. Exp. Ther.* **312** (2005) 1314
8. a) M.-C. Pepin, S. Y. Yue, E. Roberts, C. Wahlestedt, P. Walker, *J. Biol. Chem.* **272** (1997) 9260; b) M. Valiquette, K. H. Vu, S. Y. Yue, C. Wahlestedt, P. Walker, *J. Biol. Chem.* **271** (1996) 18789; c) X. Li, E. V. Varga, D. Stropova, T. Zalewski, E. Malatynska, R. J. Knapp, W. R. Roeske, H. I. Yamamura, *Eur. J. Pharmacol.* **300** (1996) R1; d) F. Meng, Y. Ueda, M. T. Hoversten, R. C. Thompson, L. Taylor, S. J. Watson, H. Akil, *Eur. J. Pharmacol.* **311** (1996) 285; e) J. Zhu, J. Yin, P.-Y. Law, P. A. Claude, K. C. Rice, C. J. Evans, C. Chen, L. Yu, L.-Y. Liu-Chen, *J. Biol. Chem.* **271** (1996) 1430
9. a) K. Befort, L. Tabbara, S. Bausch, C. Chavkin, C. Evans, B. Keiffer, *Mol. Pharmacol.* **49** (1996) 216; b) K. Befort, L. Tabbara, D. Kling, B. Maigret, B. L. Kieffer, *J. Biol. Chem.* **271** (1996) 10161; c) K. Befort, C. Zilliox, D. Filliol, S. Y. Yue, B. L. Keiffer, *J. Biol. Chem.* **274** (1999) 18574
10. a) X. Zhu, W. Chunhe, Z. Cheng, Y. Wu, D. Zhou, G. Pei, *Biochem. Biophys. Res. Commun.* **232** (1997) 513; b) S. Cvejic, N. Trapaidze, C. Cyr, V. A. Devi, *J. Biol. Chem.* **271** (1996) 4073; c) C. H. Wang, D. H. Zhou, J. Chen, G. E. Li, G. Pei, Z. Q. Chi, *Acta Pharmacol. Sin.* **18** (1997) 337; d) C. Wang, Z. Cheng, Q. Wei, J. Chen, G. Li, G. Pei, Z. Chi, *Biochem. Biophys. Res. Commun.* **249** (1998) 321; e) R. A. Hirst, D. Smart, L. A. Devi, D. G. Lambert, *J. Neurochem.* **70** (1998) 2273
11. Z. Salamon, V. J. Hruby, G. Tollin, S. Cowell, *J. Pept. Res.* **60** (2002) 322
12. D. Salom, D. T. Lodowski, R. E. Stenkamp, I. Le Trong, M. Golczak, B. Jastrzebska, T. Harris, J. A. Ballesteros, K. Palczewski, *Proc. Natl. Acad. Sci. USA* **103** (2006) 16123
13. G. M. Morris, D. S. Goodsell, R. S. Halliday, R. Huey, W. E. Hart, R. K. Belew, A. J. Olson, *J. Comput. Chem.* **19** (1998) 1639
14. Y. Peng, S. M. Keenan, Q. Zhang, W. J. Welsh, *J. Mol. Graphics Modell.* **24** (2005) 25
15. Hypercube, Inc., 419 Phillip St., Waterloo, ON, Canada
16. B. E. Kane, B. Svensson, D. M. Ferguson, *AAPS J.* **8** (2006) E126
17. a) T. A. Kshirsagar, X. Fang, P. S. Portoghese, *J. Med. Chem.* **41** (1998) 2657; b) T. A. Smith, L. N. Thatcher, A. Coop, *Bioorg. Med. Chem. Lett.* **17** (2007) 5175
18. A. Coop, A. E. Jacobson, M. D. Aceto, L. S. Harris, R. J. Traynor, J. H. Woods, K. C. Rice, *Bioorg. Med. Chem. Lett.* **10** (2000) 2449
19. R. J. Knapp, G. Santoro, I. A. DeLeon, K. B. Lee, S. A. Edsall, S. Eaitte, E. Malatynska, E. Varga, S. N. Calderon, K. C. Rice, R. B. Rothman, F. Porreca, W. R. Roeske, H. I. Yamamura, *J. Pharmacol. Exp. Ther.* **277** (1996) 1284
20. S. N. Calderon, R. B. Rothman, F. Porreca, J. L. Flippen-Anderson, R. W. McNutt, H. Xu, L. E. Smith, E. J. Bilsky, P. Davis, K. C. Rice, *J. Med. Chem.* **37** (1994) 212521
21. C. M. Bertha, J. L. Flippen-Anderson, R. B. Rothman, F. Porreca, P. Davis, H. Xu, K. Berckett, X.-Y. Cha, K. C. Rice, *J. Med. Chem.* **38** (1995) 1523
22. V. Mićović, M. D. Ivanović, L. Došen-Mićović, *J. Mol. Modell.* **15** (2009) 267
23. D. L. Farreus, C. Altenbach, K. Yang, W. L. Habbell, H. G. Khorana, *Science* **274** (1996) 768
24. E. M. Jutkiewicz, E. B. Eller, J. E. Folk, K. C. Rice, J. R. Traynor, J. H. Woods, *J. Pharm. Exp. Ther.* **309** (2004) 173.



J. Serb. Chem. Soc. 74 (11) 1219–1228 (2009)
JSCS–3912

SHORT COMMUNICATION

Synthesis and characterization of selected fused isoxazole and pyrazole derivatives and their antimicrobial activity

VIJAY V. DABHOLKAR* and FAISAL Y. ANSARI

*Organic Research Laboratory, Department of Chemistry, K.C. College,
Dinshaw Wachha Road, Churchgate, Mumbai-400 020, India*

(Received 4 July 2008, revised 28 May 2009)

Abstract: New potent antibacterials, fused isoxazole and pyrazole derivatives, were synthesized using 5,5-dimethylcyclohexane-1,3-dione (**1**) and 3-[(4-chlorobenzylidene)amino]-2-thioxoimidazolidin-4-one (**2**) as synthons. Aromatic aldehydes on condensation with **1** and **2** gave 2-arylidene-5,5-dimethylcyclohexane-1,3-dione (**3**) and 5-arylidene-3-[(4-chlorobenzylidene)amino]-2-thioxoimidazolidin-4-one (**4**), respectively. Compounds **3** and **4** were forced to undergo heterocyclization reaction with nucleophilic reagents to give the title compounds. The newly synthesized heterocycles (**5–8**) were characterized based on their chemical properties and spectroscopic data, and were found to inhibit *Staphylococcus aureus* and *Corynebacterium diphtheriae*.

Keywords: isoxazole; pyrazole; thiohydantoin; dimedone; antibacterial activity.

INTRODUCTION

Bacteria are becoming resistant to ever more antimicrobial agents. Currently, bacterial resistance is combated by the discovery of new drugs. However, microorganisms are becoming resistant more quickly than new drugs are being found, thus, future research in antimicrobial therapy may focus on finding ways to overcome resistance to antimicrobials, or methods to treat infections with alternative means. Thiohydantoins have been proven to have anticonvulsant activity.¹ Compounds that comprise the hydantoin moiety exhibit pharmacological properties.^{2–5} Similarly many natural and synthetic products containing heterocyclic rings, such as isoxazoles^{6–8} and pyrazoles,⁹ were reported to possess various pharmacological activities. These were attributed to the presence of the N-bridge heterocyclic nuclei of isoxazole¹⁰ and pyrazole,¹¹ which are described to have herbicide¹⁰ and antibacterial¹² activities.

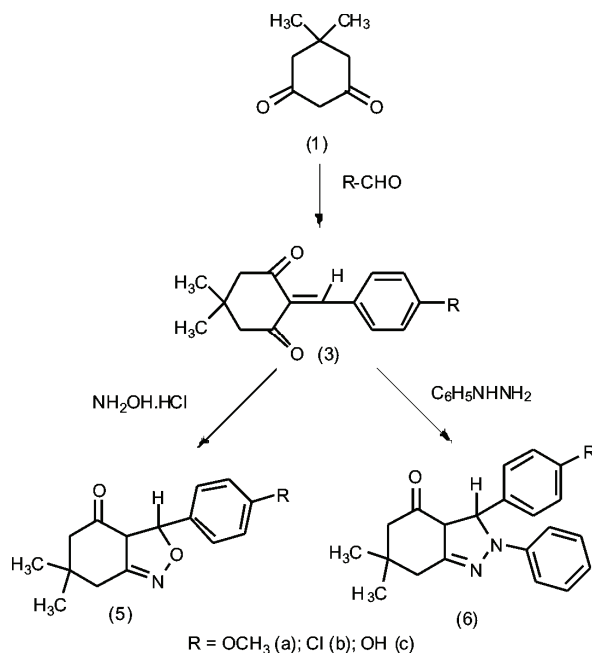
* Corresponding author. E-mail: ansarifaisal_55@yahoo.co.in
doi: 10.2298/JSC0911219D

Dimedone and thiohydantoin constitute a unique group of compounds due to the presence of characteristic keto group, which acts as a starting material for more complex compounds. The thiohydantoin/dimedone system possesses reactive sites which can be suitably modified by the introduction of different heterocyclic moieties to yield the potent COX-1/COX-2 inhibitors.¹³ Bearing this in mind, twelve new fused compounds containing isoxazole and pyrazole moieties were synthesized in order to act as active pharmaceutical. The structures of synthesized compounds were confirmed by spectral data and elemental analysis.

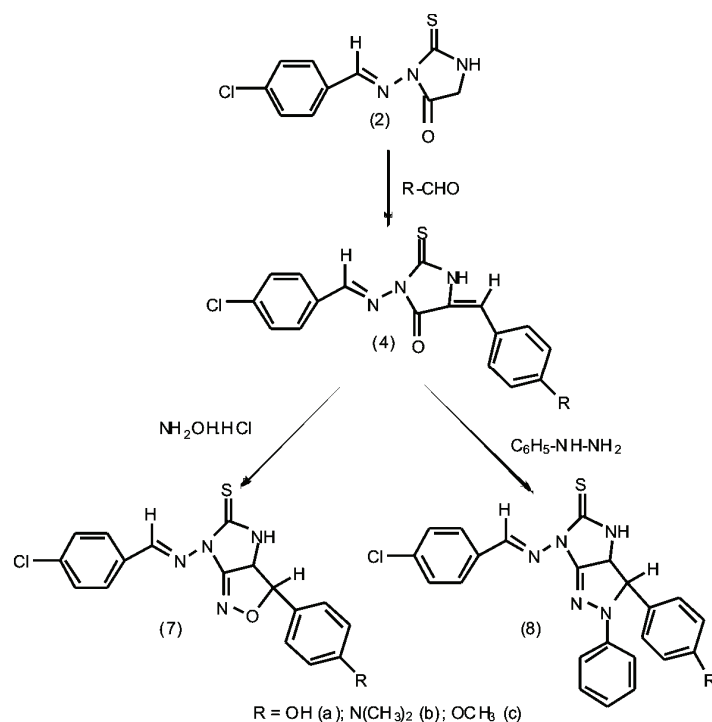
RESULT AND DISCUSSION

Chemistry

The starting material, 5,5-dimethylcyclohexane-1,3-dione (**1**), was obtained by a reported procedure¹⁴ and 3-[(4-chlorobenzylidene)amino]-2-thioxoimidazolidin-4-one (**2**)¹⁵ and derivatives thereof were prepared from the reaction of aromatic aldehydes and thiosemicarbazide to give arylthiosemicarbazone. This was followed by cyclization with ethyl chloroacetate in the presence of fused sodium acetate. Both **1** and **2** (Schemes 1 and 2, respectively) were condensed with appropriate aromatic aldehydes in presence of bases such as piperidine or potassium hydroxide to give 2-arylidene-5,5-dimethylcyclohexane-1,3-dione (**3**) and 5-arylidene-3-[(4-chlorobenzylidene)amino]-2-thioxoimidazolidin-4-one (**4**),¹⁵ respectively. The structures were confirmed based on their chemical and spectral data.



Scheme 1. Reaction pathway for the preparation of compounds **5** and **6**.

Scheme 2. Reaction pathway for the preparation of compounds **7** and **8**.

Cyclocondensation of **3** and **4** with hydroxylamine hydrochloride in the presence of glacial acetic acid yielded 6,6-dimethyl-3-(substitutedphenyl)-3,3a,6,7-tetrahydro-5*H*-2,1-benz-isoxazol-4-one (**5**) and 6-[(4-chlorobenzylidene)amino]-3-(substitutedphenyl)-3a,4-dihydro-3*H*,6*H*-imidazo[4,5-*c*]isoxazole-5-thione (**7**), respectively. Their IR spectra exhibited a band corresponding to -C-O-N (1230 cm^{-1}), which confirmed the presence of the isoxazole ring. The appearance of a peak due to C=N and disappearance of the peak due to C=O in the $^{13}\text{C-NMR}$ spectra further supported the formation of isoxazole.

Compounds **3** and **4** on treatment with phenylhydrazine were transformed into a 3-(substitutedphenyl)-6,6-dimethyl-2-phenyl-2,3,3a,5,6,7-hexahydro-4*H*-indazol-4-one (**6**),¹⁶⁻¹⁸ and 6-[(4-chlorobenzylidene)amino]-2-phenyl-3-(substitutedphenyl)-2,3,3a,4-tetrahydro-6*H*-imidazo[4,5-*c*]pyrazole-5-thione (**8**), in an appreciable yield using potassium hydroxide. Their IR spectra exhibited a band at (1490 cm^{-1}) of N-N and an increased area under the peak in aromatic region, as compared to **3/4**, confirms the formation of **6/8**. This was also supported by $^{13}\text{C-NMR}$ spectrum, as it revealed a peak of C=N and the disappearance of a peak of C=O . The structures assigned to the compounds were supported by the IR, $^1\text{H-NMR}$, $^{13}\text{C-NMR}$ and mass spectral data and elemental analysis, the results of which are given below.

2-(4-Methoxybenzylidene)-5,5-dimethylcyclohexane-1,3-dione (3a). Yield: 62 %; m.p. 130 °C. Anal. Calcd. for C₁₆H₁₈O₃ (FW 258.25): C, 74.41; H, 6.97 %. Found: C, 74.32; H, 7.12 %. IR (KBr, cm⁻¹): 1670 (C=O), 1472 (C=C). ¹H-NMR (CDCl₃, δ / ppm): 0.98 (6H, s, 2×CH₃), 2.46 (4H, s, 2×CH₂), 3.92 (3H, s, OCH₃), 6.99–7.24 (5H, m, ArH and C–H). ¹³C-NMR: 27.32 (2×CH₃), 31.38 (2×CH₂), 40.23 (OCH₃), 115.283, 128–142.64 (C=C and ArC), 162.42 (2×C=O).

2-(4'-Chlorobenzylidene)-5,5-dimethylcyclohexane-1,3-dione (3b). Yield: 60 %; m.p. 116 °C. Anal. Calcd. for C₁₅H₁₅O₂Cl (FW 262.66): C, 68.57; H, 5.71 %. Found: C, 68.32; H, 5.89 %. IR (KBr, cm⁻¹): 1665 (C=O), 1498 (C=C), 627 (C–Cl). ¹H-NMR (CDCl₃, δ / ppm): 0.98 (6H, s, 2×CH₃), 2.46 (4H, s, 2×CH₂), 7.00–7.24 (5H, m, ArH and C–H). ¹³C-NMR: 27.68 (2×CH₃), 31.65 (2×CH₂), 113.28, 129.5–143.25 (C=C and ArC), 164.56 (2×C=O).

2-(4-Hydroxybenzylidene)-5,5-dimethylcyclohexane-1,3-dione (3c). Yield: 57 %; m.p. 122 °C. Anal. Calcd. for C₁₅H₁₆O₃ (FW 244.23): C, 73.77; H, 6.14 %. Found: C, 73.62; H, 6.28 %. IR (KBr, cm⁻¹): 3378 (OH), 1625 (C=O), 1456 (C=C). ¹H-NMR (CDCl₃, δ / ppm): 0.90 (6H, s, 2×CH₃), 2.43 (4H, s, 2×CH₂), 4.60 (1H, s, OH), 6.40–7.24 (5H, m, ArH and C–H). ¹³C-NMR: 28.76 (2×CH₃), 32.16 (2×CH₂), 112.45, 131.53–141.47 (C=C and ArC), 162.52 (2×C=O).

3-(4-Methoxyphenyl)-6,6-dimethyl-3,3a,6,7-tetrahydro-5H-2,1-benzisoxazol-4-one (5a). Yield: 71 %; m.p. 110 °C. Anal. Calcd. for C₁₆H₁₉NO₃ (FW 273.38): C, 70.32; H, 6.95; N, 5.12 %. Found: C, 70.09; H, 6.74; N, 5.22 %. IR (KBr, cm⁻¹): 1670 (C=O), 1562 (C=N), 1230 (–C–O–N–). ¹H-NMR (CDCl₃, δ / ppm): 1.01 (6H, s, 2×CH₃), 2.09 (2H, s, CH₂), 2.46 (2H, s, CH₂), 3.63 (1H, d, J = 7.5 Hz, CH), 3.92 (3H, s, OCH₃), 4.58 (1H, d, J = 6.2 Hz, CH), 6.85–7.89 (4H, dd, J = 7.2 Hz, ArH). ¹³C-NMR: 27.32 (2×CH₃), 29.32 (CH₂), 31.38 (CH₂), 40.23 (OCH₃), 62.21 (CH), 72.34 (CH), 128–142.64 (ArC), 154.25 (C=N), 168.25 (C=O). MS (m/z): 273 (M⁺).

3-(4-Chlorophenyl)-6,6-dimethyl-3,3a,6,7-tetrahydro-5H-benzisoxazol-4-one (5b). Yield: 69 %; m.p. 100 °C. Anal. Calcd. for C₁₅H₁₆NO₂Cl (FW 277.67): C, 64.86; H, 5.76; N, 5.04 %. Found: C, 64.99; H, 5.62; N, 5.12 %. IR (KBr, cm⁻¹): 1670 (C=O), 1534 (C=N), 1226 (–C–O–N–), 627 (C–Cl). ¹H-NMR (CDCl₃, δ / ppm): 1.014 (6H, s, 2×CH₃), 2.09 (2H, s, CH₂), 2.46 (2H, s, CH₂), 3.64 (1H, d, J = 7.1 Hz, C–H), 4.32 (1H, d, J = 6.4 Hz, C–H), 6.65–7.72 (4H, dd, J = 7.1 Hz, ArH). ¹³C-NMR: 27.68 (2×CH₃), 29.87 (CH₂), 31.65 (CH₂), 61.78 (CH), 72.88 (CH), 129.5–143.25 (ArC), 154.53 (C=N), 164.56 (C=O). MS (m/z): 278 (M⁺).

3-(4-Hydroxyphenyl)-6,6-dimethyl-3,3a,6,7-tetrahydro-5H-benzisoxazol-4-one (5c). Yield: 72 %; m.p. 102 °C. Anal. Calcd. for C₁₅H₁₇NO₃ (FW 259.23): C, 69.49; H, 6.53; N, 5.40 %. Found: C, 69.22; H, 6.62; N, 5.56 %. IR (KBr, cm⁻¹): 3378 (OH), 1670 (C=O), 1574 (C=N), 1223 (–C–O–N–). ¹H-NMR (CDCl₃, δ / ppm): 0.97 (6H, s, 2×CH₃), 2.18 (2H, s, CH₂), 2.43 (2H, s, CH₂), 3.72 (1H, d, J = 7.2 Hz, C–H), 4.43 (1H, d, J = 6.3 Hz, C–H), 4.75 (1H, s, OH), 6.62–7.24

(4H, *dd*, $J = 7.2$ Hz, ArH). ^{13}C -NMR: 28.76 ($2\times\text{CH}_3$), 29.55 (CH_2), 32.16 (CH_2), 62.34 (CH), 71.67 (CH), 131.53–141.47 (ArC), 153.51 (C=N), 162.52 (C=O).

3-(4-Methoxyphenyl)-6,6-dimethyl-2-phenyl-2,3,3a,5,6,7-hexahydro-4H-indazol-4-one (6a). Yield: 70 %; m.p. 172 °C. Anal. Calcd. for $\text{C}_{22}\text{H}_{24}\text{N}_2\text{O}_2$ (FW 364.42): C, 72.52; H, 6.59; N, 7.69 %. Found: C, 72.12; H, 6.08; N, 7.34%. IR (KBr, cm^{-1}): 1670 (C=O), 1585 (C=N), 1490 (N–N). ^1H -NMR (CDCl_3 , δ / ppm): 0.96 (6H, *s*, $2\times\text{CH}_3$), 2.19 (2H, *s*, CH_2), 2.46 (2H, *s*, CH_2), 3.64 (1H, *d*, $J = 7.3$ Hz, CH), 4.43 (1H, *d*, $J = 6.2$ Hz, CH), 6.86–8.00 (9H, *m*, ArH); ^{13}C -NMR: 27.32 ($2\times\text{CH}_3$), 29.55 (CH_2), 31.38 (CH_2), 40.23 (OCH_3), 63.21 (CH), 71.23 (CH), 128–139.64 (ArC), 152.35 (C=N), 168.25 (C=O). MS (m/z): 348 (M^+).

3-(4-Chlorophenyl)-6,6-dimethyl-2-phenyl-2,3,3a,5,6,7-hexahydro-H-indazol-4-one (6b). Yield: 79 %; m.p. 152 °C. Anal. Calcd. for $\text{C}_{21}\text{H}_{21}\text{N}_2\text{OCl}$ (FW 352.77): C, 71.38; H, 5.94; N, 7.93 %. Found: C, 71.02; H, 6.23; N, 7.45 %. IR (KBr, cm^{-1}): 1670 (C=O), 1562 (C=N), 1454 (N–N), 627 (C–Cl). ^1H -NMR (CDCl_3 , δ / ppm): 0.96 (6H, *s*, $2\times\text{CH}_3$), 2.19 (2H, *s*, CH_2), 2.46 (2H, *s*, CH_2), 3.72 (1H, *d*, $J = 7$ Hz, C–H), 4.43 (1H, *d*, $J = 6.3$ Hz, C–H), 6.86–8.00 (9H, *m*, ArH). ^{13}C -NMR: 27.68 ($2\times\text{CH}_3$), 29.23 (CH_2), 31.65 (CH_2), 61.45 (CH), 70.23 (CH), 129.5–139.25 (ArC), 155.35 (C=N), 164.56 (C=O). MS (m/z): 353 (M^+).

3-(4-Hydroxyphenyl)-6,6-dimethyl-2-phenyl-2,3,3a,5,6,7-hexahydro-H-indazol-4-one (6c). Yield: 74 %; m.p. 158 °C. Anal. Calcd. for $\text{C}_{21}\text{H}_{22}\text{N}_2\text{O}_2$ (FW 334.43): C, 75.44; H, 6.58; N, 8.38 %. Found: C, 74.87; H, 6.24; N, 8.12 %. IR (KBr, cm^{-1}): 3378 (OH), 1670 (C=O), 1538 (C=N), 1486 (N–N). ^1H -NMR (CDCl_3 , δ / ppm): 0.91 (6H, *s*, $2\times\text{CH}_3$), 2.12 (2H, *s*, CH_2), 2.39 (2H, *s*, CH_2), 3.45 (1H, *d*, $J = 7.1$ Hz, C–H), 4.21 (1H, *d*, $J = 6.1$ Hz, C–H), 4.58 (1H, *s*, OH), 6.52–7.193 (9H, *m*, ArH). ^{13}C -NMR: 28.76 ($2\times\text{CH}_3$), 29.21 (CH_2), 32.16 (CH_2), 63.21 (CH), 72.87 (CH), 128.53–138.47 (ArC), 154.48 (C=N), 162.52 (C=O).

3-[(4-Chlorobenzylidene)amino]-5-(4-hydroxybenzylidene)-2-thioxoimidazolidin-4-one (4a). Yield: 72 %; m.p. 304 °C. Anal. Calcd. for $\text{C}_{17}\text{H}_{12}\text{N}_3\text{O}_2\text{SCl}$ (FW 357.72): C, 57.00; H, 3.35; N, 11.75; S, 8.95 %. Found: C, 56.55; H, 3.62; N, 11.35; S, 8.85 %. IR (KBr, cm^{-1}): 3480 (OH), 3348 (NH), 1705 (C=N), 1311 (C=S), 610 (C–Cl). ^1H -NMR ($\text{DMSO}-d_6$, δ / ppm): 4.62 (1H, *s*, OH), 6.90–7.21 (9H, *m*, ArH and C–H), 8.25 (1H, *s*, CH=N), 10.21 (1H, *s*, NH). ^{13}C -NMR: 129.34–135.34 (ArC and C–H), 155.09 (C=N), 163.24 (C=O), 178.23 (C=S). MS (m/z): 358 (M^+).

3-[(4-Chlorobenzylidene)amino]-5-(4-hydroxybenzylidene)-2-thioxoimidazolidin-4-one (4b). Yield: 79 %; m.p. 320 °C. Anal. Calcd. for $\text{C}_{19}\text{H}_{17}\text{N}_4\text{OSCl}$ (FW 384.78): C, 59.29; H, 4.42; N, 14.56; S, 8.32 %. Found: C, 59.32; H, 4.52; N, 14.22; S, 8.48 %. IR (KBr, cm^{-1}): 3322 (NH), 1735 (C=N), 1348 (C=S), 628 (C–Cl). ^1H -NMR ($\text{DMSO}-d_6$, δ / ppm): 2.95 (6H, *s*, $\text{N}(\text{CH}_3)_2$), 7.12–7.77 (9H, *m*, ArH and C–H), 8.45 (1H, *s*, CH=N), 11.80 (1H, *s*, NH). ^{13}C -NMR: 32.34 ($\text{N}(\text{CH}_3)_2$),

128–135.48 (ArC and C–H), 155.55 (C=N), 166.28 (C=O), 178.87 (C=S). MS (m/z): 385 (M^+).

3-[(4-Chlorobenzylidene)amino]-5-(4-methoxybenzylidene)-2-thioxoimidazolidin-4-one (4c). Yield: 74 %; m.p. 300 °C. Anal. Calcd. for $C_{18}H_{14}N_3O_2SCl$ (FW 371.74): C, 58.14; H, 3.76; N, 11.3; S, 8.60 %. Found: C, 58.24; H, 3.52; N, 11.52; S, 8.52 %. IR (KBr, cm^{-1}): 3295 (NH), 1680 (C=N), 1286 (C=S), 638 (C–Cl). 1H -NMR (DMSO- d_6 , δ /ppm): 3.98 (3H, s, OCH₃), 6.79–7.58 (9H, m, ArH and C–H), 8.25 (1H, s, CH=N), 9.84 (1H, s, NH). ^{13}C -NMR: 34.43 (OCH₃), 128–135.5 (ArC and C–H), 156.25 (C=N), 163.24 (C=O), 179.34 (C=S).

6-[(4-Chlorobenzylidene)amino]-3-(4-hydroxyphenyl)-3a,4-dihydro-3H,6H-imidazo[4,5-c]isoxazole-5-thione (7a). Yield: 56 %; m.p. 258 °C. Anal. Calcd. for $C_{17}H_{13}N_4O_2SCl$ (FW 372.73): C, 54.76; H, 3.42; N, 15.03; S, 8.52 %. Found: C, 54.35; H, 3.52; N, 14.85; S, 8.38 %. IR (KBr, cm^{-1}): 3442 (OH), 3337 (NH), 1715 (C=N), 1220 (–C–O–N–), 1341 (C=S), 620 (C–Cl). 1H -NMR (DMSO- d_6 , δ /ppm): 3.70 (1H, d, $J = 6.3$ Hz, CH), 4.23 (1H, d, $J = 6.8$ Hz, C₄–H of isoxazole), 4.34 (1H, s, OH), 6.90–7.75 (8H, m, ArH), 8.25 (1H, s, CH=N), 10.13 (1H, s, NH). ^{13}C -NMR: 62.23 (CH), 72.23 (CH), 129–136 (ArC), 155.09 and 158.23 (2×C=N), 179.43 (C=S). MS (m/z): 373 (M^+).

6-[(4-Chlorobenzylidene)amino]-3-[4-(dimethylamino)phenyl]-3a,4-dihydro-3H,6H-imidazo[4,5-c]isoxazole-5-thione (7b). Yield: 59 %; m.p. 275 °C. Anal. Calcd. for $C_{19}H_{18}N_5OSCl$ (FW 399.79): C, 59.45; H, 4.69; N, 18.25; S, 8.34 %. Found: C, 59.32; H, 4.74; N, 18.42; S, 8.38 %. IR (KBr, cm^{-1}): 3242 (NH), 1675 (C=N), 1321 (C=S), 1240 (–C–O–N–), 620 (C–Cl). 1H -NMR (DMSO- d_6 , δ /ppm): 2.90 (6H, s, N(CH₃)₂), 3.92 (1H, d, $J = 6.0$ Hz, CH), 4.32 (1H, d, $J = 6.6$ Hz, C₄–H of isoxazole), 6.91–7.98 (8H, m, ArH), 8.22 (1H, s, CH=N), 11.92 (1H, s, NH). ^{13}C -NMR: 30.23 (N(CH₃)₂), 61.23 (CH), 71.45 (CH), 129–136 (ArC), 155.09 and 157.65 (2×C=N), 181.11 (C=S). MS (m/z): 400 (M^+).

6-[(4-Chlorobenzylidene)amino]-3-(4-methoxyphenyl)-3a,4-dihydro-3H,6H-imidazo[4,5-c]isoxazole-5-thione (7c). Yield: 62 %; m.p. 276 °C. Anal. Calcd. for $C_{18}H_{15}N_4O_2SCl$ (FW 386.44): C, 55.74; H, 3.88; N, 14.48; S, 8.27 %. Found: C, 55.83; H, 3.68; N, 14.52; S, 8.63 %. IR (KBr, cm^{-1}): 3322 (NH), 1662 (C=N), 1342 (C=S), 1263 (–C–O–N–), 626 (C–Cl). 1H -NMR (DMSO- d_6 , δ /ppm): 3.73 (1H, d, $J = 6.3$ Hz, CH), 3.96 (3H, s, OCH₃), 4.32 (1H, d, $J = 7.0$ Hz, C₄–H of isoxazole), 6.79–7.58 (8H, m, ArH), 8.00 (1H, s, CH=N), 10.22 (1H, s, NH). ^{13}C -NMR: 31.54 (OCH₃), 63.43 (CH), 72.45 (CH), 127.67–135.56 (ArC), 153.21 and 156.08 (2×C=N), 184.76 (C=S).

6-[(4-Chlorobenzylidene)amino]-3-(4-hydroxyphenyl)-2-phenyl-2,3,3a,4-tetrahydro-6H-imidazo[4,5-c]pyrazole-5-thione (8a). Yield: 64 %; m.p. 156 °C. Anal. Calcd. for $C_{23}H_{18}N_5OSCl$ (FW 447.68): C, 61.60; H, 4.02; N, 15.62; S, 7.14 %. Found: C, 61.25; H, 4.21; N, 15.24; S, 6.89 %. IR (KBr, cm^{-1}): 3456

(OH), 3127 (NH), 1584 (C=N), 1442 (N–N), 1344 (C=S) 624 (C–Cl). ¹H-NMR (DMSO-*d*₆, δ / ppm): 3.59 (1H, *d*, *J* = 6.3 Hz, CH), 4.34 (1H, *d*, *J* = 7.0 Hz, C₄-H of pyrazole), 5.75 (1H, *s*, OH), 6.90–7.42 (13H, *m*, ArH), 8.35 (1H, *s*, CH=N), 10.3 (1H, *s*, NH). ¹³C-NMR: 63.23 (CH), 72.54 (CH), 128.23–136.43 (ArC), 155.09 and 153.12 (2×C=N), 182.54 (C=S). MS (*m/z*): 448 (M⁺).

6-[(4-Chlorobenzylidene)amino]-3-(4-dimethylamino)phenyl]-2-phenyl-2,3,3a,4-tetrahydro-6H-imidazo[4,5-*c*]pyrazole-5-thione (**8b**). Yield: 64 %; m.p. 142 °C. Anal. Calcd. for C₂₅H₂₃N₆SCl (FW 474.92): C, 63.22; H, 4.84; N, 17.70; S, 6.74 %. Found: C, 63.11; H, 4.64; N, 17.54; S, 6.34 %. IR (KBr, cm⁻¹): 3124 (NH), 1564 (C=N), 1452 (N=N), 1422 (N–N), 1324 (C=S), 638 (C–Cl). ¹H-NMR (DMSO-*d*₆, δ / ppm): 2.84 (6H, *s*, N(CH₃)₂), 3.54 (1H, *d*, *J* = 6.2 Hz, CH), 4.34 (1H, *d*, *J* = 7.3 Hz, C₄-H of pyrazole), 6.90–7.42 (13H, *m*, ArH), 8.25 (1H, *s*, CH=N), 10.42 (1H, *s*, NH). ¹³C-NMR: 31.23 (N(CH₃)₂), 62.43 (CH), 73.34 (CH), 128.32–135.65 (ArC), 152.45 and 156.11 (2×C=N), 180.23 (C=S). MS (*m/z*): 475 (M⁺).

6-[(4-Chlorobenzylidene)amino]-3-(4-methoxyphenyl)-2-phenyl-2,3,3a,4-tetrahydro-6H-imidazo[4,5-*c*]pyrazole-5-thione (**8c**). Yield: 68 %; m.p. 164 °C. Anal. Calcd. for C₂₄H₂₀N₅OSCl (FW 451.86): C, 66.4; H, 4.33; N, 15.16; S, 6.93 %. Found: C, 66.24; H, 4.53; N, 15.23; S, 6.63 %; IR (KBr, cm⁻¹): 3193 (NH), 1538 (C=N), 1444 (N=N), 1417 (N–N), 1351 (C=S), 623 (C–Cl). ¹H-NMR (DMSO-*d*₆, δ / ppm): 3.76 (1H, *d*, *J* = 6.8 Hz, CH), 3.90 (3H, *s*, OCH₃), 4.43 (1H, *d*, *J* = 7.3 Hz, C₄-H of pyrazole), 6.8–7.7 (13H, *m*, ArH), 8.23 (1H, *s*, CH=N), 10.72 (1H, *s*, NH). ¹³C-NMR: 34.23 (OCH₃), 63.23 (CH), 72.56 (CH), 129–136 (ArC), 152.21 and 155.23 (2×C=N), 179.57 (C=S).

Antibacterial activity

The newly synthesized compounds (**5–8**) were screened for their antibacterial activity against *Escherichia coli* (ATCC-25922), *Staphylococcus aureus* (ATCC-27853), *Corynebacterium diphtheriae* and *Proteus aeruginosa* (recultured) bacterial strains by the disc diffusion method.¹⁹ The activity of the tested compounds and that of the standard drug, ampicillin, are reported in Table I together with their estimated partition coefficients (log *P*).²⁰

EXPERIMENTAL

Chemistry

All chemicals were supplied by E. Merck (Germany) and S. D. Fine Chemicals (India). The melting points of the synthesized compounds were determined in open capillary tubes using a Veego VMP-1 melting point apparatus and are expressed in °C and uncorrected. The purity of the compounds was monitored by thin layer chromatography on silica gel coated aluminum plates (Merck) as adsorbent and UV light as the visualizing agent. The IR spectra in KBr pellets were recorded on a Perkin–Elmer spectrophotometer in the range of 4000–400 cm⁻¹. The ¹H-NMR spectra were recorded on a Bruker Avance 500 MHz NMR spectrometer from International Equipment Trading Ltd., using CDCl₃ or DMSO-*d*₆ as the solvent and

TABLE I. Antibacterial activity of compounds 5–8

Compound	Zone of inhibition / mm				log <i>P</i>
	Gram-positive		Gram-negative		
	<i>S. aureus</i>	<i>C. diphtheriae</i>	<i>E. coli</i>	<i>P. aeruginosa</i>	
5a	16	10	8	8	3.20
5b	13	12	9	9	3.96
5c	12	11	10	10	3.06
6a	21	10	9	9	4.77
6b	17	12	10	10	5.53
6c	12	18	9	9	4.62
7a	10	14	8	8	4.09
7b	21	17	11	11	4.50
7c	14	20	10	10	4.28
8a	13	16	9	9	5.66
8b	20	18	9	9	6.07
8c	16	15	10	10	5.81
DMSO	–	–	–	–	–
Ampicillin	26	23	32	32	–

TMS as the internal standard. The mass spectra were taken on a Jeol SX-102/PA-6000 (EI) spectrometer. C,H,N estimation was realized on a Carlo Erba 1108 (CHN) elemental analyser.

Preparation of 2-arylidene-5,5-dimethylcyclohexane-1,3-dione (3a–c)

A mixture of 5,5-dimethylcyclohexane-1,3-dione (**1**) (1.41 mg, 0.010 mol), a substituted aromatic aldehyde (0.010 mol) and KOH (0.0050 mol) in ethanol (8.0 mL) was refluxed for 3 h. After monitoring the reaction by TLC, the reaction mixture was cooled to room temperature, poured onto ice, filtered and recrystallized from ethanol.

General procedure for the synthesis of 5-arylidene-3-[(4-chlorobenzylidene)amino]-2-thioxoimidazolidin-4-one (4a–c)

A mixture of 3-[(4-chlorobenzylidene)amino]-2-thioxoimidazolidin-4-one (**2**) (0.010 mol), an aromatic aldehyde (0.010 mol) and piperidine (0.0050 mol) was fused at 120–130 °C for 2 h. The reaction mixture was cooled and acidified with 2 M hydrochloride acid. The crude product was filtered off, washed with water, dried and purified by recrystallization from acetic acid.

General procedure for the synthesis of 6,6-dimethyl-3-(substituted phenyl)-3,3a,6,7-tetrahydro-5H-2,1-benzisoxazol-4-one (5a–c)

An equimolar mixture of **3** (0.010 mol) and hydroxylamine hydrochloride (0.010 mol) in (8.0 mL) glacial acetic acid was refluxed for 8 h after which the reaction mixture was concentrated and cooled. The formed crystals were filtered, washed with petroleum ether and recrystallized from ethanol.

General procedure for the synthesis of 3-(substituted phenyl)-6,6-dimethyl-2-phenyl-2,3,3a,5,6,7-hexahydro-4H-indazol-4-one (6a–c)

A mixture of compound **3** (0.010 mol), phenylhydrazine (0.010 mol) and KOH (0.010 mol) in (8.0 mL) ethanol was refluxed for 3 h. The concentrated reaction mixture was poured onto ice and acidified with 2 M HCl. The resultant solid was filtered, dried and recrystallized from ethanol.

General procedure for the synthesis of 6-[(4-chlorobenzylidene)amino]-3-(substituted phenyl)-3a,4-dihydro-3H,6H-imidazo[4,5-c]isoxazole-5-thione (7a-c)

A mixture of compound **4** (0.010 mol) and hydroxylamine hydrochloride (0.030 mol) in (8.0 mL) glacial acetic acid was refluxed for 9 h after which the reaction mixture was concentrated and cooled. The formed crystals were filtered, washed with petroleum ether and ethyl acetate.

General procedure for the synthesis of 6-[(4-chlorobenzylidene)amino]-2-phenyl-3-substitutedphenyl)2,3,3a,4-tetrahydro-6H-imidazo[4,5-c]pyrazole-5-thione (8a-c)

A mixture of compound **4** (0.010 mol), phenylhydrazine (0.030 mol) and KOH (0.0050 mol) in (8.0 mL) ethanol was refluxed for 5 h. The concentrated reaction mixture was poured onto ice and acidified with 2 M HCl. The resultant solid was filtered, dried and recrystallized from glacial acetic acid.

Antibacterial testing

The newly synthesized compounds (**5(a-c)**–**8(a-c)**) were screened for their antibacterial activity against *Escherichia coli* (ATCC-25922), *Staphylococcus aureus* (ATCC-27853), *Corynebacterium diphtheriae* and *Proteus aeruginosa* (recultured) bacterial strains by the disc diffusion method.¹⁹ The discs (6 mm) were prepared from Whatman filter paper and used after autoclaving at 121 psi for 15 min and drying in a hot air oven. Bacterial inocula equivalent to the 0.5 McFarland turbidity standard were prepared in normal saline and subsequently diluted. The compounds were dissolved in DMSO and tested at a concentration of 250 µg/ml. The zone of inhibition after 16–18 h incubation was measured in mm and the potency was compared with the standard drug ampicillin trihydrate.

CONCLUSIONS

A number of isoxazole and pyrazole derivatives (**5–8**) were prepared and evaluated for their *in vitro* antibacterial activity.¹⁹ The partition coefficients²⁰ of the compounds were estimated. All the tested compounds were found to be ideal drug candidates, except for a few which had log *P* value above the requirement, which specifies that an ideal drug candidate should have a log *P* value in the range –0.5 to +5.0,²¹ or should be less than 4.5 as calculated by Moriguchi method.²² Although the compound **6a**, **7b**, **8b** and **8c** showed good inhibition activity towards Gram-positive bacteria, *i.e.* *S. aureus* and *C. diphtheriae*, their inhibition potency was not in linear correlation with their log *P* values. Thus, it may be concluded that besides lipophilicity, electronic and steric effects may be influencing the activity. The compounds **8a–c**, having high log *P* values, may cause absorption and distribution problems. Hence, for further development, compounds having lower estimated log *P* values should be prepared.

Acknowledgement. The authors are grateful to the Principal Ms. Manju J. Nichani and Management of K. C. College, Mumbai for providing the necessary facilities and to the Head, Department of Microbiology for the antimicrobial studies. The authors are also thankful to the Director, Institute of Science, Mumbai (India), for providing the spectral analyses.

ИЗВОД

СИНТЕЗА И КАРАКТЕРИЗАЦИЈА ОДАБРАНИХ КОНДЕНЗОВАНИХ ИЗОКСАЗОЛСКИХ И ПИРАЗОЛСКИХ ДЕРИВАТА И ЊИХОВА АНТИМИКРОБНА АКТИВНОСТ

VIJAY V. DABHOLKAR и FAISAL Y. ANSARI

Organic Research Laboratory, Department of Chemistry, K.C. College, Dinshaw Wachha Road, Churchgate, Mumbai-400 020, India

Нови потентни антибактерициди, кондензовани изоксазолски и пиразолски деривати, добијени су из 5,5-диметилциклохексан-1,3-диона (**1**) и 3-[(4-хлоробензилиден)амино]-2-тиоксоимидазолидин-4-она (**2**) као синтона. Кондензацијом ароматичних алдехида са **1** или **2** граде се 2-арилиден-5,5-диметилциклохексан-1,3-дион (**3**), односно 5-арилиден-3-[(4-хлоробензилиден)амино]-2-тиоксоимидазолидин-4-он (**4**). Хетероциклизацијом једињења **3** и **4** у присуству нуклеофилних реагенаса добијају се поменута једињења (**5–8**). Новосинтетисани хетероцикли су окарактерисани на основу хемијских особина и спектроскопских података. Једињења **5–8** инхибирају *S. aureus* и *C. diphtheriae*.

(Примљено 4. јула 2008, ревидирано 28. маја 2009)

REFERENCES

1. S. Ramachandran, C. N. Nalini, C. R. Girija, N. S. Begum, *Malays. J. Sci.* **26** (2007) 81
2. E. V. Vladimirskaia, O. T. Novikevich, O. G. Demchuk, *Farm. Zh. (Kiev)* **6** (1991) 67 (in Russian)
3. R. Lakhan, R. L. Singh, *J. Agric. Food Chem.* **39** (1991) 580
4. S. A. H. El-Feky, Z. K. Abd El-Samii, *Arch. Pharm. (Weinheim)* **324** (1991) 381
5. S. A. H. El-Feky, *Pharmazie* **48** (1993) 894
6. A. Farghaly, A. Bekhit, *Arch. Pharm. (Weinheim)* **53** (2000) 333
7. A. M. Farghaly, F. S. G. Soliman, M. M. A. El Smeary, A. F. Rostom, *Pharmazie* **56** (2001) 28
8. J. M. Fevig, J. J. Buriakh, P. F. Stouten, M. R. Robert, N. G. Lam, C. P. Wong, R. R. Wexler, *Bioorg. Med. Chem. Lett.* **9** (1999) 1195
9. B. Barnes, R. Izydore, I. Hall, *Anticancer Res.* **21** (2001) 1857
10. Y. H. Zhou, W. R. Miao, L. B. Chen, *Chin. Chem. Lett.* **14** (2003) 897
11. A. Tantawy, F. Goda, A. Abdel, *Chin. Pharm. J.* **47** (1995) 37
12. J. L. Kane, B. H. Hirth, O. Laing, B. B. Gourlie, S. Nahill, G. Barsomiam, *Bioorg. Med. Chem. Lett.* **13** (2003) 4463
13. G. Dannhardt, W. Kiefer, G. Kramer, S. Maehrlein, U. Nowe, B. Fiebich, *Eur. J. Med. Chem.* **35** (2000) 499
14. R. L. Shriner, H. R. Todd, in *Org. Synth. Coll. Vol. II*, Wiley, New York, 1943, p. 200
15. S. S. Meher, S. Naik, R. K. Behera, A. Nayak, *J. Indian Chem. Soc.* **58** (1981) 274
16. I. Strakova, A. Strakovs, M. Petrova, *Chem. Heterocycl. Compd.* **41** (2005) 1507
17. G. V. Boyd, S. R. Dando, *J. Chem. Soc. C* (1971) 225
18. J. H. Teuber, E. Worbs, D. Cornelius, *Chem. Ber.* **101** (1968) 3918
19. B. A. Arthington-Skaggs, M. Motley, D.W. Warnock, C. J. Morrison, *J. Clin. Microbiol.* **38** (2000) 2254
20. *ChemAxon*, <http://www.chemaxon.com/products.html> (accessed October, 2009)
21. C A Linpinski, F Lombardo, B. W. Dominy, P. J. Feeney, *Adv. Drug Delivery Rev.* **23** (1997) 3
22. I. Moriguchi, S. Hirono, Q. Liu, Y. Nakagome, Y. Matsushita. *Chem. Pharm. Bull.* **40** (1992) 127.



J. Serb. Chem. Soc. 74 (11) 1229–1240 (2009)
JSCS–3913

Seasonal variations in the leaf surface composition of field grown grapevine plants

DANIELA I. BATOVSKA*, IVA T. TODOROVA and SIMEON S. POPOV

*Institute of Organic Chemistry, Centre of Phytochemistry, Bulgarian Academy of Sciences,
Acad. G. Bonchev Str. Bl. 9, Sofia, 1113, Bulgaria*

(Received 12 March, revised 22 April 2009)

Abstract: The leaf surface is the first barrier of grapevine plants towards various environmental stressors causing damage in vineyards. For this reason, identification of leaf surface metabolites in grapevine and their putative role in plant–environment interactions is important for viticulture. In this study, the leaf surface components of 16 grapevine plants (*Vitis vinifera*) growing in an experimental vineyard were analyzed in two consecutive seasons – the summer and the autumn of 2007. Forty-eight individual metabolites typical of the cuticular plant wax were identified by gas chromatography–mass spectrometry (GC–MS). They belonged to the following groups of compounds: hydrocarbons, sterols, terpenes, free and esterified fatty acids, alcohols, aldehydes and ketones. The metabolic profiles of the summer and the autumn samples were statistically different ($P < 0.05$), which was mainly attributed to the specific insects present in the two seasons and to the adaptation of the grapevine to lower temperatures.

Keywords: GC–MS; leaf surface metabolites; seasonal variations; *Vitis vinifera*.

INTRODUCTION

The leaf surface of grapevine (*Vitis vinifera* L.) is rich in metabolites and constitutes the first line of defense towards various biotic and abiotic stressors. The individual components identified to date belong to the classes of terpenoids, steroids, free and esterified fatty acids and heterocyclic compounds.¹ Their qualitative and quantitative composition varies from one grapevine to another depending on age, breeding conditions, season, *etc.*^{2,3} The study of these variations is an important task because it can have implications for a better understanding and manipulation of the biochemical processes related to the adaptability of grapevines. Furthermore, there is an increasing demand for the development of grapevine varieties with increased disease resistance and stress tolerance.⁴

* Corresponding author. E-mail: danibat@orgchm.bas.bg
doi: 10.2298/JSC0911229B

Recently, the first, to the best of our knowledge, investigation of the seasonal variations of the leaf surface composition of grapevine seedlings was conducted.³ The obtained metabolic profiles of summer samples included terpenes, sterols, fatty acids and heterocyclic compounds. Most of the components underwent alteration in autumn. For example, the sterol and fatty acid contents decreased, mono- and diterpenoids and the heterocyclic compounds were missing, while hydrocarbons and alcohols appeared. The observed variations proceeded under conditions of reduced environmental impact because the plants were grown in a greenhouse. Extending such an investigation to grapevines growing in open fields could provide interesting data for their adaptability to various environmental factors.

In this study, attention was focused on 16 grapevine plants growing in an experimental field. Their acetone extracted leaf surface components were readily obtained and analyzed by GC–MS in the summer and in the autumn of 2007. The GC–MS analysis did not give exact quantitative data because the ion current generated depended on the characteristics of the investigated compounds and hence was not a true quantification. However, this method provides valuable data that can be used for comparison between the same compounds as well as for determination of structural diversity. Using this approach statistically significant seasonal differences were observed for the leaf surface compositions of the investigated grapevine plants. The results are discussed in the light of the possible biological functions of the respective components on the grapevine leaf surface.

EXPERIMENTAL

Plant material

Fresh and apparently healthy leaves were collected once from 16 grapevine plants, in a totally randomized design, in the summer (June) and the autumn (September) of 2007. The samples were stored at $-20\text{ }^{\circ}\text{C}$ until extraction. The plants were two-year-old seedlings originating from the self-pollination of the Bulgarian wine-making variety Storgozia. They were grown in an experimental vineyard of the Institute for Agriculture and Seed Science, located near the town of Rousse, Bulgaria. The studied grapevine seedlings were spaced 1.20 m between plants and 3.5 m between rows with dripper irrigation. The original plant material is deposited in the grapevine collection of the institute.

Sample preparation

On the day of their collection, the leaves were transported in a cooler bag to the Institute of Organic Chemistry in Sofia and immediately elaborated as previously described.¹ Briefly, the fresh leaves of each seedling (around 1.0 g) were dipped one by one into acetone (40 mL) for not more than one minute. The resulting extracts were filtrated, evaporated to dryness and analyzed by GC–MS. The yields in % of fresh weight were as follows: 0.1–3.4 %, mean value $0.6\pm 0.8\%$, for the summer samples and 0.2–0.8 %, mean value $0.4\pm 0.2\%$, for the autumn samples.

GC–MS analysis of the leaf surface components

The analysis was performed using a Hewlett Packard 6890 GC System Plus MS 5973 (Hewlett Packard, Palo Alto, CA, USA) equipped with a capillary column HP5-MS (30 cm, 0.25 mm, 0.25 μm film thickness, Agilent Technology, USA). The carrier gas was helium at a flow rate of 0.8 mL/min. The temperature program was 100–300 °C (10 min isotherm) at 5°/min. The method of electron-impact ionization was applied. The ion source was set at 230 °C and the ionization voltage was 70 eV.

Identification of compounds

The GC–MS identification was based on the interpretation of the mass spectral fragmentation, followed by comparisons of the spectra obtained with those of authentic samples. Computer searches in a HP Mass Spectral Library NIST98 (Hewlett Packard, Palo Alto, CA, USA) were also applied. When the spectra of some isomers were similar and they could not be identified unambiguously, comparisons of the GC retention times obtained under the same conditions were used. When there were no suitable authentic samples and/or spectra for comparison, no identification was proposed.

Statistical analysis

The statistical differences between the chemical compositions of the summer and the autumn samples were calculated using the nonparametric, Wilcoxon matched pairs test. Statistically significant values of $P < 0.05$ were accepted.

RESULTS AND DISCUSSION

Surface layers of fresh leaves collected from 16 grapevine plants were obtained in the summer and in the autumn of 2007 and analyzed by GC–MS (see Experimental).

In total, 48 individual metabolites were identified (Tables I and II). Together, they outlined a typical profile of leaf cuticular wax of higher plants, which is a mixture of mainly long-chain aliphatic hydrocarbons, fatty acids, alcohols, ketones and aldehydes.⁵ These are hydrophobic compounds that form a protective layer on the interface between the leaves and environment. The grapevine plants were grown in an open field and were exposed to the effects of various environmental factors. For this reason, their acetone extracted leaf surface metabolites were totally different from those obtained from a previous investigation of greenhouse grown grapevines.³

The summer and the autumn samples showed statistically significant differences in the total hydrocarbons, sterols, terpenoids, free fatty acids, alcohols, aldehydes and ketones present (Table III). This was also true for 36 of the identified individual compounds, which is evidence for presence of substantial seasonal variations. The seasonal ratios and possible functions of the compounds showing statistically significant variation are also presented in Table III and are discussed below.

Hydrocarbons were present predominantly in the summer samples. They were entirely *n*-alkanes with chains ranging in length from 18 to 31 carbons. Long chain hydrocarbons normally occur over areas of plants exposed to the air.

TABLE I. GC-MS data for the surface components of grapevine leaves collected in the summer of 2007 (% of the total ion current)

Surface metabolic components	Plant															
	1	2	3	4	5	6	7	8	9	10	11	12	13	14	15	16
<i>Hydrocarbons</i>	19.8	29.0	48.1	13.4	28.5	10.8	20.9	16.1	16.1	19.0	10.4	19.7	34.4	15.5	17.8	12.8
Octadecane	-	-	-	-	-	-	<0.1	<0.1	<0.1	<0.1	<0.1	0.2	-	0.1	<0.1	-
Nonadecane	-	-	-	-	-	-	<0.1	0.3	<0.1	<0.1	<0.1	0.2	<0.1	0.2	<0.1	-
Eicosane	1.1	0.5	0.4	0.8	0.8	0.7	1.0	1.3	0.9	0.6	1.3	0.8	0.7	0.6	1.3	0.6
Heiteicosane	0.5	<0.1	<0.1	0.4	<0.1	0.3	0.4	0.6	0.4	0.3	<0.1	0.4	<0.1	0.4	0.5	<0.1
Docosane	<0.1	<0.1	0.2	0.3	<0.1	0.3	<0.1	0.5	0.3	0.4	<0.1	0.4	0.3	0.3	0.5	0.3
Tricosane	0.6	<0.1	0.9	0.5	0.7	0.4	0.6	0.9	0.5	0.5	1.1	0.5	0.7	0.7	0.6	0.4
Tetracosane	0.8	<0.1	0.5	0.3	0.8	0.3	0.7	1.0	0.3	0.4	0.7	0.6	0.8	0.6	0.8	0.4
Pentacosane	1.1	1.1	2.0	1.6	1.7	1.3	1.9	0.9	1.7	1.2	2.1	1.1	1.8	3.5	1.8	1.9
Heptacosane	6.2	10.5	9.3	3.4	6.2	2.1	4.8	3.2	4.5	5.3	3.2	4.1	7.2	2.9	3.3	9.2
Nonacosane	8.2	16.9	30.8	6.1	16.0	4.7	10.1	6.6	6.6	9.1	2.0	9.6	19.9	5.8	7.8	-
hentriacontane	1.3	<0.1	4.0	<0.1	2.3	0.7	1.4	0.8	0.9	1.2	-	1.8	3.0	0.4	1.2	-
<i>Terpenes</i>	8.1	16.3	11.8	15.2	10.5	22.8	17.3	7.3	8.0	6.8	9.3	7.9	5.5	116.6	8	8.4
δ -Tocopherol	-	1.2	-	-	2.7	1.7	<0.1	-	-	-	-	-	-	-	-	-
β -Amyrine	1.9	1.2	5.2	<0.1	<0.1	1.6	11.7	1.1	4.4	2.0	<0.1	2.4	1.9	2.5	<0.1	-
Lupcol	5.0	13.9	6.3	15.2	5.9	19.3	5.6	5.5	2.5	4.8	9.3	5.3	2.6	13.7	7.4	-
6,10,14-Trimethyl-pentadecan-2-one	0.5	-	0.3	-	-	-	-	0.7	0.6	-	<0.1	<0.1	0.5	0.2	0.7	-
4,8,12,16-Tetramethylheptadecan-4-olide	0.7	-	<0.1	-	1.9	0.2	-	<0.1	0.5	-	<0.1	0.2	0.5	0.2	0.3	-

TABLE I. Continued

Surface metabolic components	Plant															
	1	2	3	4	5	6	7	8	9	10	11	12	13	14	15	16
<i>Fatty acids</i>	1.1	0.8	1.5	1.1	0.8	2.2	0.7	3.5	0.9	3.1	2.6	2.1	1.8	1.5	1.4	0.6
Tetradecanoic acid	-	-	-	-	-	0.5	<0.1	0.6	<0.1	0.5	<0.1	0.6	0.5	0.4	<0.1	-
Hexadecanoic acid	1.1	0.8	1.5	1.1	0.8	1.7	0.7	1.5	0.9	2.2	1.6	1.5	1.3	1.1	1.4	0.6
Octadecanoic acid	-	-	-	-	-	<0.1	-	1.4	-	0.4	1.0	<0.1	-	-	-	-
<i>Esters</i>	0.8	2.3	0.5	0.6	1.7	1.4	2.1	0.9	1.7	1.8	<0.1	1.0	0.6	1.1	2.2	13.8
Methyl tetradecanoate	-	2.3	-	-	1.7	0.8	1.5	<0.1	1.1	1.1	-	0.5	-	0.7	1.2	13.8
Decyl isobutyrate	0.8	<0.1	0.5	0.6	<0.1	0.6	0.6	0.9	0.6	0.7	<0.1	0.5	0.6	0.4	1.0	<0.1
<i>Alcohols</i>	-	<0.1	-	<0.1	<0.1	0.3	<0.1	0.5	0.3	0.3	<0.1	0.8	<0.1	0.5	0.4	<0.1
Tetradecanol	-	<0.1	-	<0.1	<0.1	0.3	<0.1	0.5	0.3	0.3	<0.1	0.5	<0.1	0.3	0.4	<0.1
Hexadecanol	-	-	-	-	-	-	<0.1	<0.1	<0.1	<0.1	<0.1	0.3	-	0.2	<0.1	-
<i>Ketones</i>	1.7	1.4	<0.1	<0.1	3.2	1.3	2.4	2.3	1.2	1.8	<0.1	0.5	0.5	0.6	0.5	0.8
4-Methyl-3-penten-2-one	<0.1	<0.1	<0.1	<0.1	<0.1	<0.1	<0.1	<0.1	<0.1	0.6	<0.1	0.5	0.5	0.6	0.5	0.8
14,16-Hentriacontanedione	1.7	1.4	<0.1	<0.1	3.2	1.3	2.4	2.3	1.2	1.2	<0.1	<0.1	<0.1	<0.1	<0.1	-

TABLE II. GC-MS data for the surface components of grapevine leaves collected in the autumn of 2007 (% of the total ion current)

components	Plant															
	1	2	3	4	5	6	7	8	9	10	11	12	13	14	15	16
<i>Hydrocarbons</i>	8.7	9.4	15.0	4.9	13.0	3.3	10.0	7.9	25.9	16.9	15.0	3.3	16.4	13.7	5.7	12.5
Nonadecane	-	0.1	-	-	-	-	0.5	-	-	-	-	-	-	-	-	-
Eicosane	-	0.2	0.3	-	-	-	-	<0.1	0.3	0.2	-	-	<0.1	-	-	-
Heneicosane	-	0.2	<0.1	0.1	-	-	-	0.2	<0.1	0.4	-	-	<0.1	0.1	<0.1	-
Docosane	0.3	0.2	0.2	0.1	-	0.1	0.2	0.2	0.3	0.5	-	0.1	0.5	0.1	<0.1	-
Tricosane	1.1	1.0	0.6	0.3	0.4	0.3	0.7	0.6	1.8	1.8	1.2	0.5	0.8	0.3	0.3	0.7
Tetracosane	1.2	0.9	1.4	0.5	0.4	0.4	1.0	0.6	2.4	2.0	1.7	0.1	1.4	0.4	0.5	0.9
Pentacosane	0.8	1.8	1.5	1.3	0.8	0.7	1.9	1.6	7.7	4.7	4.2	1.0	1.6	2.5	1.1	2.9
Heptacosane	1.2	1.6	2.3	0.9	1.4	0.6	2.1	1.3	9.1	3.1	4.7	0.8	2.0	2.3	1.8	3.2
Octacosane	1.9	0.3	1.3	0.3	<0.1	-	0.4	0.4	1.9	1.1	1.3	-	1.0	6.8	0.5	-
Nonacosane	0.8	1.4	1.4	0.7	1.3	0.6	0.8	0.9	2.4	2.1	1.9	0.5	1.2	0.8	1.0	1.1
Triacotane	0.6	0.6	0.9	-	1.2	-	-	0.4	-	-	-	0.3	-	0.4	-	-
hentriacontane	0.8	1.1	5.1	0.7	7.5	0.6	2.4	1.7	-	1.0	-	-	7.9	-	0.5	3.7
<i>Sterols</i>	0.6	0.8	1.4	0.3	<0.1	1.0	2.0	1.3	2.1	-	-	1.7	1.7	0.3	0.2	0.7
Sitosterol	0.6	0.8	1.4	0.3	<0.1	1.0	2.0	1.3	2.1	-	-	1.7	1.7	0.3	0.2	0.7
<i>Terpenes</i>	5.4	50.9	70.3	87.9	76.4	89.8	60.1	60.3	54.5	62.3	62.4	84.1	50.4	76.2	87.8	61.5
γ -Terpinene	-	-	-	0.1	0.3	0.3	0.5	0.4	-	0.2	-	-	-	-	-	1.1
Neophytadiene	-	0.3	0.2	0.2	1.3	0.6	0.5	0.4	0.4	0.6	-	0.3	0.2	-	0.1	1.1
Neophytadiene (isomer)	-	0.5	0.7	0.2	0.6	0.5	0.3	0.4	0.6	1.2	-	0.1	-	-	<0.1	0.6
α -Tocopherol	0.5	1.1	0.8	0.4	1.0	0.7	-	1.0	-	-	-	0.3	2.0	0.1	0.2	2.2
β -Amyrine	0.9	2.6	43.3	2.0	2.0	2.9	33.7	4.3	35.4	12.9	10.5	14.5	14.0	7.6	1.8	30.5
Lupeol	2.9	45.0	25.3	84.4	71.2	84.5	24.5	53.2	16.7	46.5	51.9	68.5	34.2	68.5	85.7	25.3
4,8,12,16-Tetramethylheptadecan-4-olide	1.1	1.4	-	0.6	-	0.3	0.6	0.6	1.4	0.9	-	0.4	-	-	-	0.7

TABLE II. Continued

Surface metabolic components	Plant															
	1	2	3	4	5	6	7	8	9	10	11	12	13	14	15	16
<i>Esters</i>	-	6.8	1.3	0.8	0.4	-	0.6	0.3	2.6	0.7	-	0.1	0.7	0.3	<0.1	<0.1
Methyl hexadecanoate	-	3.7	-	0.5	0.4	-	0.2	<0.1	0.5	-	-	0.1	-	-	<0.1	<0.1
Ethyl linoleate	-	0.8	0.4	-	-	-	-	-	-	-	-	-	-	-	-	-
Methyl eicosanoate	-	1.7	-	0.2	-	-	-	-	-	-	-	-	-	-	-	-
Methyl tetracosanoate	-	0.6	0.9	0.1	-	-	0.4	0.3	2.1	0.7	-	-	0.7	0.3	-	<0.1
<i>Aldehydes</i>	0.2	0.6	0.3	0.6	0.8	0.4	3.0	0.4	1.2	1.9	0.9	1.7	0.5	0.1	0.6	4.5
2-Pentenal	-	-	-	-	-	-	0.4	-	-	<0.1	-	0.2	-	-	0.2	-
Nonanal	<0.1	0.1	<0.1	<0.1	<0.1	<0.1	0.4	<0.1	<0.1	<0.1	-	0.1	<0.1	-	<0.1	1.2
Decanal	0.1	0.1	-	0.4	0.8	0.3	1.3	0.4	0.6	0.7	0.9	0.5	-	-	0.2	1.2
2-Decenal	-	0.2	-	0.1	-	-	0.4	-	<0.1	<0.1	-	0.3	-	-	-	0.5
2-Undecenal	0.1	0.2	0.3	0.1	-	0.1	0.5	-	0.6	1.2	-	0.6	0.5	0.1	0.2	1.6
<i>Ketones</i>	0.4	9.6	1.0	3.0	4.2	1.7	7.1	5.9	5.2	4.5	<0.1	2.4	2.4	0.9	2.2	8.0
4-Methylacetophenone	<0.1	0.2	-	0.6	0.8	0.3	1.5	<0.1	1.0	0.7	-	0.5	-	-	0.4	1.4
4-(3-Cyclohexen-1-yl)-3-buten-2-one	-	-	-	0.1	0.8	0.5	1.0	2.2	-	0.9	-	0.2	-	-	-	4.5
4-(3-Cyclohexen-1-yl) 3-buten-2-one (isomer)	-	-	-	-	-	0.2	0.4	1.2	-	0.3	-	-	-	-	-	1.5
Pentadecanone	-	8.3	0.3	0.3	0.6	0.2	1.4	0.6	0.7	0.4	-	0.3	0.2	-	0.1	0.6
Nonadecanone	-	0.4	0.7	-	-	-	0.7	0.4	1.7	0.2	<0.1	-	0.4	0.2	0.2	<0.1
Pentacosanone	-	0.4	-	0.2	-	-	0.6	0.3	1.8	0.7	-	0.2	-	0.1	0.3	<0.1
14,16-Hentriacontandione	0.4	0.3	<0.1	1.8	2.0	0.5	1.5	1.5	<0.1	1.3	<0.1	1.2	1.8	0.6	1.2	<0.1

TABLE III. Statistically significant seasonal variations in the leaf surface composition of 16 field grown grapevine plants, observed in the summer and the autumn of 2007

Main groups of leaf surface components	Individual components showing statistically significant seasonal variations	Statistical significance, <i>P</i>	Seasonal appearance of the leaf surface components		Possible biological function on the grapevine leaf surface
			Summer	Autumn	
Hydrocarbons	Octadecane	0.0040	++ ^a	+	Prevention of desiccation, displaying of specific pheromone functions
	Eicosane	0.0100	+	-	
	Heptacosane	0.0004	+++++	+	
	Heptacosane	0.0060	++++	+	
	Heptacosane	0.0050	++	+	
	Octacosane	0.0010	-	+	
	Nonacosane	0.0006	+	+++++	
	Triacotane	0.0200	-	+	
	Sitosterol	0.0010	-	+	
	Terpenes	γ -Terpinene	0.0005	+	
Neophytadiene		0.0200	-	+	
Neophytadiene (isomer)		0.0010	-	+	
α -Tocopherol		0.0020	-	+	
β -Amyrine		0.0020	-	+	
Lupeol		0.0300	+	+++++	
		0.0005	+	+++++	
6,10,14-Trimethylpentadecane-2-one		0.0080	+	-	
		0.0004	+	-	
Fatty acids		Tetradecanoic acid	0.0050	+	-
	Hexadecanoic acid	0.0004	+	-	
	Octadecanoic acid	0.0400	+	-	

TABLE III. Continued

Main groups of leaf surface components	Individual components showing statistically significant seasonal variations	Statistical significance, <i>P</i>	Seasonal appearance of the leaf surface components		Possible biological function on the grapevine leaf surface
			Summer	Autumn	
Esters		>0.05 ^b	++	+	Interaction with specific insects
	Decyl isobutyrate	0.0004	+	-	
	Methyl tetradecanoate	0.0030	+	-	
	Methyl hexadecanoate	0.0080	-	+	
Alcohols	Methyl tetracosanoate	0.0050	-	+	Displaying of specific pheromone functions
		0.0010	+	-	
	Tetradecanol	0.0010	+	-	
	Hexadecanol	0.0100	+	-	
Aldehydes		0.0004	-	+	Defense against plant pathogens, signal function, displaying of specific pheromone functions
	Nonanal	0.0010	-	+	
	Decanal	0.0010	-	+	
	2-Decenal	0.0050	-	+	
	Undecenal	0.0010	-	+	
		0.0020	+	+++	
Ketones	4-Methyl-3-penten-2-one	0.0004	+	-	Displaying of specific pheromone functions
	Methylacetophenone	0.0020	-	+	
	4-(3-Cyclohexen-1-yl)-3-buten-2-one	0.0120	-	+	
	4-(3-Cyclohexen-1-yl)-3-buten-2-one (isomer)	0.0400	-	+	
	Pentadecanone	0.0010	-	+	
	Nonadecanone	0.0030	-	+	
	Pentacosanone	0.0050	-	+	

^aThe symbols “+” and “-” show the presence and absence of the metabolite in the samples, respectively; one symbol “+” refers to one unit of available metabolite; ^bthe only main group of surface compounds without statistically significant seasonal variation

They are efficient in maintaining the internal water balance in leaves by preventing desiccation and also affect the absorption of chemicals and microbes. All of the identified hydrocarbons are known semiochemicals and most probably are involved in plant–insects relationships.⁶ However, they affect the behavior of different insects and most probably, the qualitative difference in the hydrocarbon composition between the summer and the autumn samples was due to the presence of different pests in the experimental field during these two seasons.

The terpenoid level in the grapevine leaf surface increased significantly in the autumn, which was mainly due to the accumulation of compounds with triterpenoid biosynthesis, such as β -amyrine, lupeol, and sitosterol. The pentacyclic triterpenes, β -amyrine and lupeol, are supposed to be toxic to insects, due to their ability to inhibit acyl chain packing in the lipid bilayers of the insect membranes.⁷ Hence, their function on the leaf surface in grapevines is most probably connected to the repulsion of some insects appearing in the field in the autumn. Sitosterol, which is the commonest plant sterol, is able to regulate membrane fluidity and plays a role in the adaptation of membranes to temperature.⁸ Its level in plant leaves increased significantly due to acclimation to the lower temperatures in autumn.⁹ Moreover, the terpenoid profiles of the summer and autumn samples were significantly different. Some of the individual components were present solely either in the summer or in the autumn samples, which is related to their possible specific functions in the grapevine leaf surface. Thus, 6,10,14-trimethylpentadecan-2-one (hexahydrofarnesyl acetone), which is connected to the biogenesis of chlorophyll, appeared only in the summer while the chlorophyll breakdown products neophytadienes (2 isomers) were present only in the autumn. The senescing leaves also contained the antioxidants α -tocopherol and γ -terpinene, which were absent in the summer. α -Tocopherol is the major vitamin E compound in leaf chloroplasts, where it deactivates photosynthesis-derived reactive oxygen species and scavenges lipid peroxy radicals in the thylakoid membranes.¹⁰ It is generally assumed that increases in α -tocopherol contribute to plant oxidative stress tolerance and most probably this compound aids the adaptation of the grapevine to the autumn conditions. γ -Terpinene exerts synergistic effects with other plant antioxidants and may also be involved in specific plant–pests interactions.^{6,11}

Fatty acids were observed only in the summer samples. The three identified acids, tetradecanoic (myristic), hexadecanoic (palmitic) and octadecanoic (stearic) acids are known to strengthen cell membranes in higher plants.¹² In this way, they prevent plants from desiccation, leakage of important minerals and volatiles, and also hamper the infiltration of pathogens into the leaves. Their absence in the autumn undoubtedly increases the permeability of the cell membrane, which is one of the common features accompanying senescence.¹³

Esterified fatty acids did not show statistically significant seasonal alterations. However, this was not valid for four of their individual representatives. Decyl isobutyrate and methyl tetradecanoate were found only in the summer samples while methyl hexadecanoate and methyl tetracosanoate were present only in the autumn samples. These compounds probably interact with specific insects, present in the two seasons.⁶ The same probably holds for the long chain alcohols tetradecanol and hexadecanol, which were identified only in the summer samples.

Most carbonyl compounds possess allelochemical functions in plants. Such compounds predominated in the autumn samples. Amongst them, fatty aldehydes appeared only in the autumn. These compounds are emitted by plants as a response to insect attacks.¹⁴ With regards to their possible role on the leaf surface, it should be mentioned that the unsaturated aldehydes, 2-decenal and 2-undecenal, play role in the pathogen defense of some plants and also perform important signal functions in plants.^{15,16} Amongst the ketones, 4-methyl-3-penten-2-one, also known as mesityl oxide, was identified only in the summer samples. In grapes, this compound is a precursor of 4-mercapto-4-methylpentan-2-one, which has an impact on the odor of wines and a lot of grape varieties.¹⁷ The function of 4-methyl-3-penten-2-one in the grapevine leaf surface is not clear. The other identified ketones were found only in the autumn samples.

CONCLUSIONS

Collectively, the present data show that the leaf surface layers of 16 grapevine plants (*Vitis vinifera*) are the source of metabolites typical of cuticular plant wax, which indicate certain interactions between the plant and the environment. Differences in their composition during two consecutive seasons, the summer and the autumn of 2007, were statistically significant. It is suggested that these differences were mainly due to the specific insects available in the two seasons and to the adaptation of grapevine to lower temperatures.

Acknowledgements. This work was supported by the Bulgarian National Foundation for Scientific Research (Contract G-4-03/2004). The authors are thankful to Galya Djakova from the Institute for Agriculture and Seed Science, Rousse, Bulgaria, for providing the grapevine leaves.

ИЗВОД

СЕЗОНСКЕ ПРОМЕНЕ У САСТАВУ ПОВРШИНЕ ЛИСТА ВИНОВЕ ЛОЗЕ КОЈА РАСТЕ У ПОЉУ

DANIELA I. BATOVSKA, IVA T. TODOROVA и SIMEON S. POPOV

*Institute of Organic Chemistry, Centre of Phytochemistry, Bulgarian Academy of Sciences,
Acad. G. Bonchev Str. Bl. 9, Sofia, 1113, Bulgaria*

Површина листа винове лозе је прва заштита од утицаја околине који изазивају оштећење винограда. За гајење винове лозе је, према томе, важно идентификовати метаболите повр-

шине листа и њихову улогу у интеракцији биљка–околина. У овој студији је анализиран састав површине листа 16 врста винове лозе (*Vitis vinifera*), током две узастопне сезоне – лета и јесени 2007. Идентификовано је 48 метаболита типичних за восак кутикуле методом гасно–масене спектрометрије (GC–MS). Ова једињења припадају следећим групама: угљоводоници, стероли, терпени, слободне и естерификоване масне киселине, алкохоли, алдехиди и кетони. Метаболички профили летњих и јесењих узорака су статистички значајно различити ($P < 0,05$), што се може објаснити присуством специфичних инсеката у ове две сезоне и прилагођавањем винове лозе на ниже температуре.

(Примљено 12. марта, ревидирано 22. априла 2009)

REFERENCES

1. D. Batovska, I. Todorova, D. Nedelcheva, S. Parushev, A. Atanassov, T. Hvarleva, G. Djakova, V. Bankova, S. Popov, *J. Plant Physiol.* **165** (2008) 791
2. A. Petrova, M. Popova, S. Parushev, D. Batovska, V. Bankova, S. Popov, *Compt. Rend. Acad. Bulg. Sci.* **59** (2006) 617
3. D. Batovska, I. Todorova, V. Bankova, S. Parushev, A. Atanassov, T. Hvarleva, G. Djakova, S. Popov, *Nat. Prod. Res.* **22** (2008) 1237
4. M. Vivier, I. Pretorius, *Trends Biotechnol.* **20** (2002) 472
5. E. A. Baker, *The Plant Cuticle*, Academic Press, London, 1982, p. 139
6. A. M. El-Sayed, *The Pherobase: Database of Insect Pheromones and Semiochemicals*, 2009 (<http://www.pherobase.org/database/compound/compounds-index.php>)
7. S. Rodriguez, H. Garda, H. Heinzen, P. Moyna, *Chem. Phys. Lipids* **89** (1997) 119
8. R. Moreau, B. Whitakerb, K. Hicks, *Prog. Lipid Res.* **41** (2002) 457
9. D. Lynch, P. Steponkus, *Plant Physiol.* **83** (1987) 761
10. S. Munne-Bosch, *J. Plant Physiol.* **162** (2005) 743
11. J. Grassmann, *Vitam. Horm.* **72** (2005) 505
12. S. Trenkamp, W. Martin, K. Tietjen, *Proc. Nat. Acad. Sci. USA* **101** (2004) 11903
13. M. Antunes, E. Sfakiotakis, *Food Chem.* **110** (2008) 891
14. B. Pophof, G. Stange, L. Abrell, *Chem. Senses* **30** (2005) 51
15. D. Trombetta, A. Saija, G. Bisignano, S. Arena, S. Caruso, G. Mazzanti, N. Uccella, F. Castelli, *Lett. Appl. Microbiol.* **35** (2002) 285
16. D. Abanda-Nkpwatt, U. Krimm, H. Coiner, L. Schreiber, W. Schwab, *Environ. Exp. Bot.* **56** (2006) 108
17. R. Schneider, F. Charrier, A. Razungles, R. Baumes, *Anal. Chim. Acta* **563** (2006) 58.



J. Serb. Chem. Soc. 74 (11) 1241–1248 (2009)
JSCS–3914

Journal of
the Serbian
Chemical Society

JSCS@tmf.bg.ac.rs • www.shd.org.rs/JSCS

UDC 639.61:665.12:577.115:615.281

Original scientific paper

Fatty acid profile, volatiles and antibacterial screening of lipids of the sponge *Fasciospongia cavernosa* (Schmidt) collected from the Bay of Bengal (Orissa Coast)

PRAVAT MANJARI MISHRA, AYINAMPUDI SREE*, MADHUSMITA ACHARYA
and ANURAG PRATAP DAS

*Natural Product Department, Institute of Minerals and Materials Technology
(Formerly RRL), Bhubaneswar-751013, Orissa, India*

(Received 23 March, revised 15 May 2009)

Abstract: The fatty acid composition as well as the volatiles of a lipophilic extract from the marine sponge *Fasciospongia cavernosa* (Schmidt) was analysed. The fatty acids (FA) were characterized by linear saturated fatty acids (33.05 %), branched saturated fatty acids (9.30 %) and mono-unsaturated fatty acids (18.07 %). A significant amount of polyunsaturated fatty acids (PUFA) (30.79 %) was found in the total lipid, which included linoleic acid (18:2 n–6, 11.14 %), 9,12,15-octadecatrienoic acid/ α -linolenic acid (18:3 n–3, 1.99 %), di-homo- γ -linolenic acid (20:3 n–6, 2.03 %) and arachidonic acid (20:4 n–3, 0.51 %). An antibacterial assay of the lipid extract of *F. cavernosa* showed broad-spectrum activity against different human and fish pathogens.

Keywords: sponge; *Fasciospongia cavernosa*; fatty acid; volatiles; antibacterial.

INTRODUCTION

Marine sponges are the most primitive multicellular sedentary animals that produce bioactive metabolites. Among the aquatic animals, sponges are specified by the greatest diversity of fatty acids (FA), which have unusual and sometimes unique structures. This generated the idea that there was something unusual in the structure and/or in the way of functioning of sponge membranes.^{1,2} Some lipids of sponges are characterized as biologically active.^{3–5}

The sterol composition of the sponge *Fasciospongia cavernosa* was previously studied.⁶ Literature evidenced that *F. cavernosa* is a rich source of a new class of sesterterpenoids, named cacospongionolides. Cacospongionolide was the first sesterterpene isolated from the Adriatic Sea sponge *F. cavernosa*, which possesses antimicrobial and antitumor activities.⁷ This class of marine metabolites are the inhibitors of phospholipase A2 with a potent topical anti-inflamma-

* Corresponding author. E-mail: dr_asree@yahoo.co.in

doi: 10.2298/JSC0911241M



tory profile and they show high antimicrobial activity against the Gram-positive bacteria *Bacillus subtilis* and *Micrococcus luteus*.^{1,8} Cacospongionolide B isolated from this sponge collected in the Northern Adriatic was reported to have anti-inflammatory activity.^{9,10} 25-Deoxycacospongionolide B, a bioactive sesterterpene, was also identified as a minor component from this species.¹¹ Three new derivatives of cacospongionolide which exhibited biological activity were also isolated from this sponge.¹² Two new luffarin derivatives which showed strong anti-inflammatory activity were isolated from the Adriatic Sea sponge *F. cavernosa*.¹³ Cavernolide, a novel C₂₁ terpene lactone isolated from the sponge *F. cavernosa*, inhibited human synovial sPLA₂ in a concentration-dependent manner with an IC₅₀ value of 8.8 μM.¹⁴ However, there has been no report on a study of the FA profile and volatiles of the lipid composition of *F. cavernosa*. This is the first report on the analysis of the antibacterial activity, FA and volatile composition of the sponge *F. cavernosa* collected from the Bay of Bengal region of the Orissa Coast.

In this investigation, antibacterial screening of the lipid extract of the sponge *F. cavernosa* was performed against five fish pathogens and two human pathogens, including three MDR (multidrug resistant) strains. The investigation of the FA and volatiles of the lipophilic extract of *F. cavernosa* could give valuable information about its chemotaxonomy. Thus, these minor components appear as biomarkers for such organisms.

EXPERIMENTAL

Sponge material

The sponge *F. cavernosa* (class Demospongiae Sollas, order Dictyoceratida, family Thorectidae Berquist) collected during February–March 2006 from the Bay of Bengal region of the Orissa coast at a depth of 13 m were stored in ethanol and transported to the laboratory. The sample was identified up to genus level by Dr. P. A. Thomas, Ex-Emeritus Scientist (ICAR), Trivandrum, Kerala.

Extraction

The sponge sample was thoroughly washed with distilled water and air-dried in the shade. Ten grams of the sponge sample were homogenised and successively extracted three times with chloroform–methanol (2:1, v/v) to isolate the lipids.¹⁵ The crude lipid extracts were purified by “Folch wash”¹⁶ to remove non-lipid contaminants. The chloroform phase was separated from the combined extract, dried over anhydrous sodium sulphate and concentrated under a nitrogen atmosphere.

Preparation of fatty acid methyl esters

The lipophilic extract (100 mg) was dissolved in 4 mL of 5 % hydrochloric acid in methanol and 0.5 mL benzene and then the mixture was refluxed in a silicone bath at 80–100 °C for 2 h. After cooling, the methyl esters were extracted with petroleum ether, simultaneously neutralised and dried over a sodium sulphate–sodium bicarbonate mixture. The solvent was evaporated to dryness under reduced pressure at 40 °C on a rotary evaporator (Heidolph, Laborota 4000). These fatty acid methyl esters (FAME) were then analysed by GC–MS.

FAME analysis

The FAME analyses were performed on a Shimadzu QP-5000 GC-MS equipped with FID and a 25 m×0.25 mm, 0.25 µm film thickness WCOT column coated with 5 % diphenyl siloxane, supplied by J & W (DB-5). Helium was used as the carrier gas at a flow rate of 1.2 ml/min, at a column pressure of 42 KPa. The column temperature was programmed for fatty acid methyl esters (FAME) from 120–300 °C at a rate of 2 °C/min and held at 300 °C for 10 min, with a total run time of 100 min. The EI ionization voltage was 70 eV. Peak identification was performed by comparison of the obtained mass spectra with those available in the Wiley and NIST libraries (Shimadzu–Wiley Registry™, 8th Edition Mass Spectral Library, Shimadzu and the NIST 08 Mass Spectral Library (NIST/EPA/NIH) – new 2008 version).

Isolation and analysis of the volatile compounds

The lipophilic extract (100 mg) was subjected to a 4 h distillation–extraction in a Lickens–Nickerson apparatus.¹⁷ The volatiles were extracted from the distillate with diethyl ether (yield: 3 mg) and investigated using a Shimadzu QP-5000 GC-MS operating under the same conditions as above except the column temperature was programmed from 40 to 280 °C at a rate of 4 °C/min.

Antibacterial assay

The antibacterial assay of the lipid extract of *F. cavernosa* (200, 100, 50 and 25 µg, all per 6 mm disc) was performed against five fish pathogens (*Edwardsiella tarda*, *Staphylococcus aureus*, *Micrococcus* sp., *Pseudomonas aeruginosa* and *Escherichia coli*) and two human pathogens (*Staphylococcus aureus* and *Salmonella typhi*) including three MDR (multidrug resistant) strains (*Staphylococcus pyogenes*, *Acinetobacter* sp. and *Salmonella typhi*) by the disc-assay method.¹⁸

The test bacterial fish pathogen cultures were obtained from the stock cultures maintained in the Pathology Laboratory of the Central Institute of Fresh Water Aquaculture, ICAR, Bhubaneswar.¹⁹

The human pathogens (MDR) were obtained from the National Institute of Oceanography, Goa.

Briefly, the lipid extract (200 µg/50µL) in an appropriate solvent was applied to sterile paper discs (6 mm in diameter, Whatman No. 1). After solvent evaporation the discs were placed on nutrient agar (Himedia, India) test plates inoculated with an overnight culture of the test pathogen (10⁶ CFU/mL) in Brain Heart Infusion (BHI) broth. The plates were incubated for 48 h at 37 °C. Discs loaded with the respective solvent (50 µL) used for dissolution were taken as controls after evaporation of the solvent. The zone of inhibition around the disc (average of three experiments) was measured. The determination of the minimum inhibitory concentration (MIC) of the lipid extract was performed by the same method as above.

RESULTS AND DISCUSSION

Total lipid extract

GC-MS analysis (Table I) showed the presence of 29 components in the mixture of total lipids of *F. cavernosa* with C₁₀ to C₂₇ FA. The saturated linear FA corresponded to more than 30 % of the total FA content. All of the acids from 10:0 to 24:0 were found, except 21:0. The acids 12:0, 14:0, 18:0 were dominant.

The total content of saturated branched FA was 9.30 %, br-16:0 and br-14:0 being the major among them. The other branched FAs were 3,7,11,15-tetramethylhexadecanoic acid (16:0 br) and br-tetracosanoic acid.

TABLE I. GC–MS analysis of FAME of total lipid of *Fasciospongia cavernosa* (13 m depth)

Retention time, min	Compound	Content, %
2.699	Decanoic acid (10:0)	0.71
3.723	Dodecanoic acid (12:0)	5.77
5.377	Tetradecanoic acid (14:0)	4.40
5.965	Tetradecenoic acid (14:1)	4.86
6.146	12-Methyltetradecanoic acid (14:0 br)	2.04
6.503	Pentadecanoic acid (15:0)	1.52
7.271	Pentadecenoic acid (15:1)	1.22
7.999	Hexadecanoic acid (16:0)	7.86
8.401	<i>cis</i> -9-Hexadecenoic acid (16:1)	2.15
8.544	14-Methylhexadecanoic acid (16:0 br)	4.93
8.860	3,7,11,15-Tetramethylhexadecanoic acid (16:0 br)	1.18
9.246	Octadecanoic acid (18:0)	3.46
11.361	8-Octadecenoic acid (18:1)	3.66
11.701	9-Octadecenoic acid (18:1)	1.24
11.933	9,12-Octadecadienoic acid (18:2, n–6)	11.14
13.589	Nonadecanoic acid (19:0)	1.57
14.838	Eicosanoic acid (20:0)	0.43
15.345	11-Eicosenoic acid (20:1)	2.27
15.635	Eicosadienoic acid (20:2)	1.35
16.257	Eicosatrienoic acid (20:3, n–6)	2.03
17.445	5,8,11,14-Eicosatetraenoic acid (20:4, n–3)	0.51
18.221	Docosanoic acid (22:0)	0.51
18.780	Tricosanoic acid (23:0)	5.80
20.389	9,12,15-Octadecatrienoic acid (18:3, n–3)	1.99
22.151	Tetracosanoic acid (24:0)	1.02
22.598	15-Tetracosenoic acid (24:1)	2.67
22.857	br-Tetracosanoic acid (24:0 br)	1.15
23.520	5,9 Hexacosadienoic acid (26:2)	10.69
29.713	5,9-Heptacosadienoic acid (27:2)	3.08

The mass spectrum of the methyl esters of all the saturated FA exhibited the presence of the corresponding $[M]^+$, $[M-31]^+$ and $[M-43]^+$, as well as intensive peaks at m/z 74, 87 and 143, characteristics of saturated FA methyl esters.²⁰

The total content of mono-enoic FA of linear structure was 18.07 %, including the basic 14:1, 16:1(Δ 9), 18:1(Δ 9) and 20:1(Δ 11). It contains a branched mono-enoic FA, *i.e.*, 15-tetracosenoic acid (24:1 br). The mass spectra of the methyl esters of the mono-enoic FA exhibited the corresponding $[M]^+$, $[M-32]^+$ and $[M-72]^+$.

A significant amount (30.79 %) of polyunsaturated fatty acids (PUFA) was found in the total lipid extract of *F. cavernosa*, whereby linoleic acid (18:2 n–6,

11.14 %) was the major component. The other important PUFA present in *F. cavernosa* were 9,12,15-octadecatrienoic acid/ α -linolenic acid (18:3 n-3, 1.99 %), dihomogamma-linolenic acid (20:3 n-6, 2.03 %) and arachidonic acid (20:4, n-3, 0.51 %). A di-enoic acid 20:2 (Δ 5,11) was also present in a reasonable amount (1.35 %). The mass spectra of the di-enoic and tri-enoic FA methyl esters exhibited the corresponding $[M]^+$ and $[M-31]^+$, as well as ions with m/z values of 141 and 150. The residues of specific super long-chain fatty acids (demospongiic FA) with 24–30 carbon atoms occur in the lipids of sponge cell membranes.²¹ Polyenoic FA of *F. cavernosa* were mainly represented by demospongiic acids, the major part of which has a characteristic 5,9-di-enoic structural fragment of the carbon chain.²² The obtained results showed that 26:2 (5,9) 10.69 % and 27:2 (5,9) 3.08 % acids were dominant.

The FA composition of *F. cavernosa*, including the polyenoic acids, is characteristic of marine sponges.²³

Volatile compounds

The volatile components of the sponge were isolated by distillation–extraction and investigated by GC–MS. The obtained results are presented in Table II.

TABLE II. Composition of the volatile compounds in *Fasciospongia cavernosa*

Volatile compounds	Content, %
3,5-Dimethyloctane	2.23
Isooctyl vinyl ether	5.68
Decane	8.36
2,7-Dimethyl-1-octanol	2.73
2-Nonenal	13.50
3- <i>n</i> -Hexyl-delta-9-tetrahydrocannabinol	2.90
2-Decene-1-ol	2.41
1-Chlorooctane	56.04
1,1-Heptanediol diacetate	3.24
Heptanal	2.29

Volatile compounds often possess valuable biological activities. They serve as allelochemicals defending the organism from bacteria, fungi and viruses. Analogous to other investigated sponges,^{24,25} the volatiles in *F. cavernosa* appeared to be relatively simple. Hydrocarbons, alcohols, aldehydes, ketones, esters, ethers, carboxylic acids *etc.* are generally identified in the volatile profile of sponges.^{26,27} In the present investigation, the volatile profile of *F. cavernosa* is also characterized by hydrocarbons, ester, aldehydes, alcohols and ether. The content of hydrocarbons, including the halogenated ones, was the highest in the volatiles of *F. cavernosa* (66.63 %). 1-Chlorooctane predominated (56.04 % from the total volatile compounds). 3,5-Dimethyloctane (2.23 %) was also found in the volatiles of *F. cavernosa*. Only one *n*-saturated hydrocarbon, decane, was identified

that was also present in a reasonable amount (8.36 %). 2,7-Dimethyl-1-octanol, 2-decene-1-ol and 3-*n*-hexyl-delta-9-tetrahydrocannabinol were identified in the volatiles (2.73, 2.41 and 2.90 %, respectively). Two aldehydes, 2-nonenal and heptanal, were also found in the volatiles of *F. cavernosa* (13.50 and 2.29 %, respectively). Isooctyl vinyl ether and 1,1-heptanediol diacetate were identified in the volatiles of *F. cavernosa* (5.68 and 3.24 %, respectively). Contrary to most other marine organisms, the investigated sponge contained no esters of fatty acids.

Antimicrobial screening

The results of the antimicrobial screening of *F. cavernosa* are presented in Table III. The lipids exhibited broad-spectrum activity against three fish pathogens (*Edwardsiella tarda*, *Micrococcus* sp. and *Pseudomonas aeruginosa*), three MDR (multi drug resistant) strains (*Staphylococcus pyrogenes*, *Acinetobacter* sp. and *Salmonella typhi*) and one human pathogen (*Salmonella typhi*). The MIC values of 50/25 µg showed the significant activity of these lipids. The response of the pathogens to standard antibiotics is provided in Table IV.

TABLE III. Antibiotic activity testing of *F. cavernosa*; the antibacterial assay of the lipid extract (µg/ 6 mm disc) was performed against different fish and human pathogens by the disc-assay method (zone of inhibition in mm, including the 6 mm disc)

Pathogens	Lipid extract, µg			
	200	100	50	25
<i>Staphylococcus aureus</i> ^a	10	Trace	Trace	– ^b
<i>Edwardsiella tarda</i> ^c	10	8.5	–	–
<i>Staphylococcus aureus</i> ^c	8	–	–	–
<i>Salmonella typhi</i> ^a	11	10	9	Trace
<i>Staphylococcus pyrogenes</i> (MDR)	10.5	10	7.5	Trace
<i>Acinetobacter</i> sp. (MDR)	11	10	–	–
<i>Salmonella typhi</i> (MDR)	10	9.5	7	–
<i>Micrococcus</i> sp. ^c	11.5	Trace	–	–
<i>Pseudomonas aeruginosa</i> ^c	11	10	Trace	–
<i>Escherichia coli</i> ^c	7.5	Trace	–	–

^aHuman pathogen; ^bno zone; ^cFish pathogen

Antimicrobial activity is exhibited by many lipids of sponges,^{3–5,28} including fatty acids.^{29,30} *cis*-9-Octadecenoic and *cis*-9,12-octadecadienoic acids,^{28,31} have the maximum antimicrobial activity. The lipid extract of the sponge *F. cavernosa* showed strong activity against all pathogens. This lipid extract contains important polyunsaturated fatty acids, such as linoleic acid (18:2, 11.4 %), α -linolenic acid (18:3, 1.99 %), dihomogamma-linolenic acid (20:3, 2.03 %) and arachidonic acid (20:4, 0.51 %). It was reported that the bactericidal activity of long chain fatty acids against *Staphylococcus aureus* increases with the degree of unsaturation.^{32–34} The antimicrobial activity of arachidonic acid compared to linoleic (18:2) and linolenic (18:3) was found to be higher. The inhibitory activity

was in the following order: arachidonic acid (20:4) > linolenic acid (18:3) > linoleic acid (18:2). Thus, the presence of a good number of PUFA in the lipid content of *F. cavernosa* may be the reason for its strong bioactivity.

TABLE IV. Activity of standard antibiotics against pathogens

Pathogens	Standard antibiotics		
	Gentamycin (10 µg)	Streptomycin (10 µg)	Polymyxin-B (300 U)
<i>Edwardsiella tarda</i>	S ^a	I ^b	R ^c
<i>Pseudomonas aeruginosa</i>	S	I	R
<i>Escherichia coli</i>	S	S	S
<i>Staphylococcus aureus</i>	S	R	R
<i>Micrococcus</i> sp.	S	S	Not done
<i>Salmonella typhi</i>	S	S	Not done

^aSensitive (≥ 12 mm); ^bIntermediate (9 mm to 11 mm); ^cResistant (no zone)

CONCLUSIONS

This study was mainly focused on the lipids of the sponge in the search for new FA structures, evaluation of new sources of major PUFA of biological interest and development of trophic and/or chemotaxonomic biomarkers in the ecosystem. Important essential polyunsaturated fatty acids, such as linoleic acid, α -linolenic acid, dihomo- γ -linolenic acid and arachidonic acid were identified in the lipid composition of *F. cavernosa*. The antibacterial screening of the lipid showed a broad-spectrum activity against different human and fish pathogens. Thus, the study of the lipid composition of *F. cavernosa* is worthwhile.

Acknowledgements. The authors thank the Director, IMMT, Bhubaneswar, for providing the facilities, the Department of Ocean Development (DOD) for financial support and the Indian Navy for diving assistance in the collection of the marine organisms.

ИЗВОД

МАСНЕ КИСЕЛИНЕ, ИСПАРЉИВЕ СУПСТАНЦЕ И АНТИБАКТЕРИЈСКА АКТИВНОСТ ЛИПИДА СУНЂЕРА *Fasciospongia cavernosa* (SCHMIDT) ИЗ БЕНГАЛСКОГ ЗАЛИВА (ОБАЛА ОРИСЕ)

PRAVAT MANJARI MISHRA, AYINAMPUDI SREE, MADHUSMITA ACHARYA и ANURAG PRATAP DAS

Natural Product Department, Institute of Minerals and Materials Technology (Formerly RRL), Bhubaneswar-751013, Orissa, India

Анализиран је садржај масних киселина и испарљивих супстанци из липофилног екстракта морског сунђера *Fasciospongia cavernosa* (Schmidt). Нађене су линеарне засићене масне киселине (33,05 %), разгранате засићене масне киселине (9,30 %) и мононезасићене масне киселине (18,07 %). Такође је нађена значајна количина полинезасићених масних киселина (PUFA, 30,79 %), укључујући линолну киселину (18:2, n-6, 11,14 %), 9,12,15-октадека триенску киселину/ α -линоленску (18:3, n-3, 1,99 %), диомо- γ -линоленску киселину (20:3, n-6, 2,03 %) и арахидонску киселину (20:4, n-3, 0,51 %). Липидни екстракт *F. cavernosa* је показао антибактеријску активност спрам широког спектра хуманих и рибљих патогена.

(Примљено 23. марта, ревидирано 15. маја 2009)

REFERENCES

1. R. W. Morales, C. Litchfield, *Lipids* **12** (1977) 576
2. C. Djerassi, W. K. Lam, *Acc. Chem. Res.* **24** (1991) 69
3. N. M. Carballeira, J. E. Betancourt, E. A. Orellano, F. A. Gonzalez, *J. Nat. Prod.* **65** (2002) 1715
4. M. O. Fatope, O. A. Adoum, Y. Takeda, *J. Agric. Food Chem.* **48** (2000) 1872
5. M. Meyer, M. Guyot, *Lipids* **37** (2002) 1109
6. S. De Rosa, A. Milone, S. Popov, *Comp. Biochem. Physiol. B* **123** (1999) 235
7. S. De Rosa, S. De Stefano, N. Zavodnik, *J. Org. Chem.* **53** (1988) 5020
8. S. De Rosa, M. Mitova, in *Studies in Natural Products Chemistry*, Vol. 32, Atta-ur-Rahman, Ed., Elsevier, Amsterdam, 2005, p. 109
9. S. De Rosa, A. Crispino, A. De Giulio, C. Iodice, R. Pronzato, N. Zavodnik, *J. Nat. Prod.* **58** (1995) 1776
10. P. G. Pastor, S. De Rosa, A. De Giulio, M. Paya, M. J. Alcaraz, *Br. J. Pharmacol.* **126** (1999) 301
11. S. De Rosa, R. Puliti, A. Crispino, A. De Giulio, C. De Sena, C. Iodice, C. A. Mattia, *Tetrahedron* **51** (1995) 10731
12. S. De Rosa, S. Carbonelli, C. Iodice, *Tetrahedron* **63** (2007) 1959
13. S. De Rosa, S. Carbonelli, *Tetrahedron* **62** (2006) 2845
14. I. Posadas, M. C. Terencio, S. De Rosa, M. Payá, *Life Sci.* **67** (2000) 3007
15. W. W. Christie, in *Lipid analysis*, 2nd ed., Pergamon Press, Oxford, 1982, p. 22
16. J. Folch, M. Lees, G. H. S. Stanely, *J. Biol. Chem.* **226** (1957) 497
17. H. Hendriks, J. Geerts, T. Malingre, *Pharm. Weekblad Sci.* **116** (1981) 1316
18. J. F. Acar, in *Antibiotic in Laboratory Medicine*, V. Lorian, Ed., Williams and Wilkins, London, 1980, p. 24
19. A. Vimala, S. Mishra, A. Sree, M. Bapuji, P. Pattnaik, S. C. Mukherjee, C. C. Rath, *J. Aquacult.* **8** (2000) 61
20. B. A. Anderson, *Prog. Chem. Fats Lipids* **16** (1978) 279
21. T. Rezanka, *Prog. Lipids Res.* **28** (1989) 147
22. Y. Ando, Y. Kawabata, K. Narukawa, T. Ota, *Jpn. Fisheries Sci.* **64** (1998) 136
23. P. R. Bergquist, M. P. Lawson, A. Lavis, R. C. Cambie, *Biochem. Syst. Ecol.* **12** (1984) 63
24. S. De Rosa, C. Iodice, J. Nechev, K. Stefanov, S. Popov, *J. Serb. Chem. Soc.* **68** (2003) 249
25. S. De Rosa, S. De Caro, G. Tommonaro, K. Slantchev, K. Stefanov, S. Popov, *Mar. Biol.* **140** (2002) 465
26. V. Roussis, B. E. Mazomenos, K. Vayas, C. Harvala, *J. Essent. Oil Res.* **7** (1995) 393
27. C. Duque, A. Bonilla, E. Bautista, *Biochem. Syst. Ecol.* **29** (2001) 459
28. O. T. Avery, G. E. McCullen, *J. Exp. Med.* **38** (1923) 199
29. H. Galbraith, T. B. Miller, *J. Appl. Bacteriol.* **36** (1973) 635
30. J. Kabara, R. Vrabla, M. S. F. L. K. Jie, *Lipids* **12** (1977) 753
31. D. D. Carson, L. Daneo-Moore, *J. Bacteriol.* **141** (1980) 1122
32. G. W. Butcher, G. King, K. G. H. Dyke, *J. Gen. Microbiol.* **94** (1976) 290
33. D. L. A. Greenway, K. G. H. Dyke, *J. Gen. Microbiol.* **115** (1979) 233
34. E. Kodicek, *Biochemical problems of lipid*, Butterworths, London, 1956.



J. Serb. Chem. Soc. 74 (11) 1249–1258 (2009)
JSCS–3915

Journal of
the Serbian
Chemical Society

JSCS@tmf.bg.ac.rs • www.shd.org.rs/JSCS

UDC 546.982-386+547.171'26:542.913

Original scientific paper

Palladium(II) complexes with R₂edda derived ligands. Part III. Diisobutyl (*S,S*)-2,2'-(1,2-ethanediyldiimino)di(4-methyl- pentanoate) and its palladium(II) complex: synthesis and characterization

BOJANA B. ZMEJKOVSKI¹, GORAN N. KALUĐEROVIĆ^{1*#},
SANTIAGO GÓMEZ-RUIZ² and TIBOR J. SABO^{3#}

¹Department of Chemistry, Institute of Chemistry, Technology and Metallurgy, University of Belgrade, Studentski Trg 12–16, 11000 Belgrade, Serbia, ²Departamento de Química Inorgánica y Analítica, E.S.C.E.T., Universidad Rey Juan Carlos, 28933 Móstoles, Madrid, Spain and ³Faculty of Chemistry, University of Belgrade, P.O. Box 158, 11001 Belgrade, Serbia

(Received 3 April, revised 8 June 2009)

Abstract: A new R₂edda-type ester, diisobutyl (*S,S*)-2,2'-(1,2-ethane-diyldiimino)di(4-methylpentanoate) dihydrochloride, [(*S,S*)-H₂*i*Bu₂eddl]Cl₂, **1**, and its palladium(II) complex, dichloro(diisobutyl (*S,S*)-2,2'-(1,2-ethanediyldiimino)di(4-methylpentanoate))palladium(II), [PdCl₂{(*S,S*)-*i*Bu₂eddl}], **2**, were synthesized and characterized by elemental analysis, as well as IR and NMR spectroscopy. It was found that complex **2** was obtained as mixture of two diastereoisomers, observed in NMR spectra. The crystal structure of compound **1** was determined by X-ray diffraction studies and is described. The isolated crystals consisted of one dicationic species [(*S,S*)-H₂*i*Bu₂eddl]²⁺ and two Cl⁻. The crystal system was tetragonal with the space group *P*4₂. Hydrogen bonds significant for the manner of packing are N–H1N···Cl, 3.049(3) Å, 159(3)° and N–H2N···Cl, 3.100(3) Å, 164(3)°. An infinite chain was formed building a one layer structure, usual for these types of compounds. The C₂ symmetry axis of the compound passes through the C1–C1'ⁱ bond vector and lies perpendicular to the plane N₂Cl₂.

Keywords: palladium complexes; crystal structure; EDDP ligands; characterization.

INTRODUCTION

The area of present research is of consequence to studies on Pt(II/IV) and Pd(II) complexes with bis(carboxyalkylamino)ethane and -propane ligands and their derivatives. Earlier, structural and antiproliferative investigations were per-

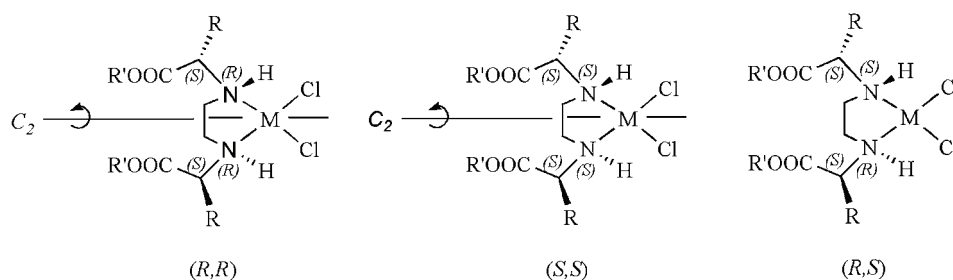
* Corresponding author. E-mail: goran@chem.bg.ac.rs

Serbian Chemical Society member.

doi: 10.2298/JSC0911249Z



¹³C-NMR spectroscopy and supported by DFT calculations.^{18–20} In a recent study, a palladium(II) complex with a partially hydrolyzed isopropyl ester of (S,S)-ethylenediamine-*N,N'*-di-2-propanoic acid (Fig. 1, C) was isolated and determined by X-ray structure analysis, and the (R,R)-*N,N'* configured isomer with the κ²*N,N'*,κ*O* coordination mode was found.¹⁹ All the other complexes mentioned herein had the κ²*N,N'* coordination mode of the ligand.



M = Pt(II), Pd(II); R = Me, *i*Bu; R' = *i*Pr, *i*Bu, Cpe, Cy

Fig. 2. Possible diastereoisomers of the investigated platinum(II) and palladium(II) complexes.

In this study, a new R₂edda-type ester di-isobutyl-(S,S)-2,2'-(1,2-ethane-diyl-diimine)di(4-methylpentanoate) dihydrochloride, [(S,S)-H₂iBu₂eddl]Cl₂, **1**, and its palladium(II) complex, diisobutyl-(S,S) 2,2'-(1,2-ethanediyldiimine)di(4-methylpentanoate))palladium(II), [PdCl₂{(S,S)-iBu₂eddl}], **2** (Fig. 1, D) were synthesized and characterized by elemental analysis, as well as IR and NMR spectroscopy. The crystal structure of **1** is also described.

EXPERIMENTAL

Materials and methods

(S,S)-2,2'-(1,2-ethanediyldiimine)di(4-methyl-pentanoic acid) dihydrochloride, [(S,S)-H₄eddl]Cl₂, was prepared using a similar method to that described in the literature.²¹ K₂[PdCl₄] was purchased from Merck and used without further purification. The infrared spectra were recorded on a Nicolet 6700 FT-IR spectrophotometer using the ATR technique (4000–400 cm⁻¹). ¹H- and ¹³C-NMR spectra were recorded on a Varian “Gemini 2000” (200 MHz) spectrometer in DMSO-*d*₆ using tetramethylsilane as the internal standard. Elemental analyses for C, H and N were realized on a Vario EL III C, H, N, S Elemental Analyzer.

Synthesis of [(S,S)-H₂iBu₂eddl]Cl₂, **1**

[(S,S)-H₂iBu₂eddl]Cl₂, **1**, was prepared using a previously described esterification reaction.^{22,23} Thionyl chloride (4.0 cm³, 55 mmol) was introduced into a flask containing 50 ml of ice-cooled isobutanol (2-methyl-1-propanol) (anhydrous conditions) during 1 h. Subsequently, 2.0 g (5.5 mmol) of (S,S)-2,2'-(1,2-ethanediyldiimine)di(4-methyl-pentanoic acid) dihydrochloride, [(S,S)-H₄eddl]Cl₂, was added into the flask and the suspension was refluxed for 16 h. The mixture was filtered and the filtrate was stored for a few days at 4 °C. A white crystalline

solid was obtained. The ester, contaminated with acid, was recrystallized from methanol. Crystals suitable for X-ray diffraction studies were obtained from the mother liquor which was stored at room temperature for several days.

Synthesis of [PdCl₂{(S,S)-iBu₂eddl}], 2

K₂[PdCl₄] (0.200 g, 0.613 mmol) was dissolved in water (20 ml) and 0.290 g (0.613 mmol) of [(S,S)-H₂iBu₂eddl]Cl₂, **1**, was added. After 2 h of stirring, 10.2 ml of a 0.12 M solution of LiOH was added in small portions to the reaction mixture. A pale yellow precipitate was obtained, which was filtered off, dissolved in 5 ml of CHCl₃ and filtered. A crystalline solid of the pure complex was obtained from the mother liquor.

X-ray crystal structure determination

Data of **1** were collected with a CCD Oxford Xcalibur S ($\lambda(\text{MoK}\alpha) = 0.71073 \text{ \AA}$) using the ω and ϕ scans mode. Semi-empirical corrections for absorption were performed with SCALE3 ABSPACK.²⁴ The structure was solved by direct methods.²⁵ Structure refinement was realized with SHELXL-97.²⁶ All non-hydrogen atoms were refined anisotropically. The crystallographic details are listed in Table I. Hydrogen atoms were refined isotropically. They were placed in the calculated positions with fixed displacement parameters $U_{\text{iso}}(\text{H}) = 1.2 U_{\text{eq}}(\text{C})$ and $U_{\text{iso}}(\text{H}) = 1.5 U_{\text{eq}}(\text{C})$ (riding model), except for the hydrogen atoms attached to the nitrogen atoms which were found in the difference Fourier map and refined freely. The ORTEP-3 program was used for the presentation of the structure.²⁷

The Cambridge Crystallographic Data Center, CCDC No. 723867, contains the supplementary crystallographic data for this paper. These data can be obtained free of charge *via* www.ccdc.cam.ac.uk/conts/retrieving.html (or from the CCDC, 12 Union Road, Cambridge CB2 1EZ, UK; fax: +44 1223 336033; e-mail: deposit@ccdc.cam.ac.uk).

TABLE I. Crystallographic data for **1**

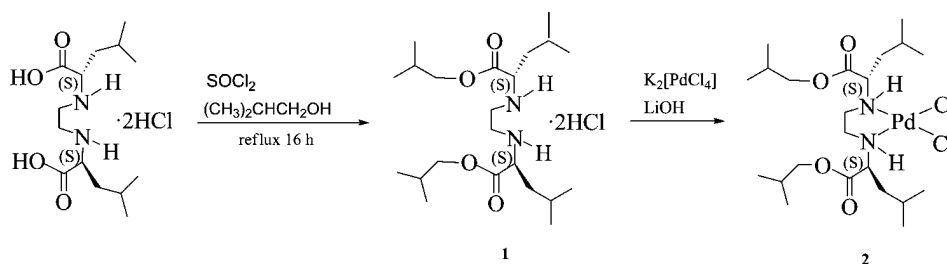
Empirical formula	C ₂₂ H ₄₆ Cl ₂ N ₂ O ₄
M_r	473.51
Crystal system	Tetragonal
Space group	$P4_2$
$a / \text{\AA}$	15.9708(2)
$c / \text{\AA}$	5.2426(1)
$V / \text{\AA}^3$	1337.21(3)
Z	2
$D_{\text{calc}} / \text{g cm}^{-3}$	1.176
$\mu(\text{Mo-K}\alpha) / \text{mm}^{-1}$	0.27
$F(000)$	516
θ Range / °	2.85–25.68
Refln. collected	14178
Refln. Observed ($I > 2\sigma(I)$)	2469
Refln. independent	2002
Data/restraints/parameters	14178/3/106
Goodness-of-fit on F^2	1.349
$R1, wR2$ ($I > 2\sigma(I)$)	0.0588, 0.1414
$R1, wR2$ (all data)	0.0725, 0.1446
Flack parameter, x	–0.17(13)
Largest diff. peak and hole / e \AA^{-3}	1.152/–1.018

RESULTS AND DISCUSSION

Synthesis and characterization

The ester, [(*S,S*)-H₂*i*Bu₂eddl]Cl₂, was synthesized using a previously described esterification reaction^{17,18}. This compound is not soluble in chloroform and is poorly soluble in water. However, it is soluble in methanol and dimethyl sulfoxide.

The complex, [PdCl₂{(*S,S*)-*i*Bu₂eddl}], was synthesized by combining aqueous solutions of K₂[PdCl₄] and the ester. Under stirring, an aqueous solution of lithium hydroxide was added. The obtained complex is soluble in chloroform and dimethyl sulfoxide, but not soluble in water. The preparation routes of the ester and complex are shown in Scheme 1.



Scheme 1. Synthesis of the ester, **1** and the palladium complex **2**.

The analytic and spectral data for **1** and **2** are as follows (numbering as in Fig. 3):

[(*S,S*)-H₂*i*Bu₂eddl]Cl₂ (**1**). Yield: 1.09 g (41.6 %). Anal. Calcd. for C₂₂H₄₆Cl₂N₂O₄: C, 55.80; H, 9.79; N, 5.92 %. Found: C, 55.84; H, 9.41; N, 5.77 %. IR (cm⁻¹): 2965, 2592, 2523, 2398, 1735, 1535, 1468, 1206, 1063, 973, 802. ¹H-NMR (200 MHz, DMSO-*d*₆, δ / ppm): 0.90–1.00 (24H, *m*, C5H₃, C6H₃, C10H₃, C11H₃), 1.77 (6H, *m*, C3H₂, C4H), 1.94 (2H, *m*, C9H), 3.42 (4H, *m*, C1H₂), 3.98 (4H, *d*, C8H₂), 4.13 (2H, *t*, C2H), 9.90–10.40 (4H, *br*, NH₂⁺). ¹³C-NMR (50 MHz, DMSO-*d*₆, δ / ppm): 18.9 (C5,6), 21.4 (C10,11), 23.2 (C4), 24.5 (C9), 27.3 (C3), 41.7 (C1), 57.9 (C2), 71.8 (C8), 169.2 (C7).

[PdCl₂{(*S,S*)-*i*Bu₂eddl}] (**2**). Yield: 313 mg (88.4 %). Anal. Calcd. for C₂₂H₄₄Cl₂N₂O₄Pd: C, 45.72; H, 7.67; N, 4.85. Found: C, 45.94; H, 7.36; N, 4.97 %. IR (cm⁻¹): 3130, 2959, 2873, 1735, 1467, 1370, 1237, 1194, 1141, 976, 737. Isomer A: ¹H-NMR (200 MHz, DMSO-*d*₆, δ / ppm): 0.90–1.10 (24H, *m*, C5H₃, C6H₃, C10H₃, C11H₃), 1.68 (6H, *m*, C3H₂, C4H), 1.90 (2H, *m*, C9H), 2.23 and 2.61 (4H, *m*, C1H₂), 3.88 (4H, *m*, C8H₂), 4.14 (2H, *m*, C2H), 6.50–6.80 (2H, *br*, NH). ¹³C-NMR (50 MHz, DMSO-*d*₆, δ / ppm): 19.0 (C5,6), 21.9 (C10,11), 23.8 (C4), 25.4 (C9), 27.3 (C3), 47.0 (C1), 58.4 (C2), 70.9 (C8), 170.1 (C7). Isomer B: ¹H-NMR (200 MHz, DMSO-*d*₆, δ / ppm): 0.90–1.10 (24H, *m*, C5H₃, C6H₃,

C10H₃, C11H₃), 1.68 (6H, *m*, C3H₂, C4H), 1.90 (2H, *m*, C9H), 2.40 and 2.85 (4H, *m*, C1H₂), 3.88 (4H, *m*, C4H₂), 4.14 (2H, *m*, C2H), 5.85–6.25 (2H, *br*, NH). ¹³C-NMR (50 MHz, DMSO-*d*₆, δ / ppm): 19.0 (C5,6), 21.5 (C10,11), 22.9 (C4), 25.0 (C9), 27.3 (C3), 47.0 (C1), 59.1 (C2), 70.6 (C8), 171.2 (C7). Ratio of isomers A/B = 7/1.

The IR spectrum of [PdCl₂{(*S,S*)-*i*Bu₂eddl}] showed specific absorption bands ν (C=O) at 1735 cm⁻¹ (strong), (typical absorption for aliphatic esters), ν (C–O) at 1194 cm⁻¹ (strong), ν (–CH₃, –CH₂, –CH) at 2959 and 2873 cm⁻¹ (medium) (for comparison [(*S,S*)-H₂*i*Bu₂eddl]Cl₂: 1735, 1206, 2965 and 2871 cm⁻¹, respectively¹⁸). All of the mentioned bands including ν (C=O), were at similar positions to those in the spectrum of the free ligand, indicating that the oxygen atoms of the COOR moieties were not coordinated. As expected the ν (N–H) absorption bands were at 3130 cm⁻¹, (typical absorptions for secondary amino groups) and may indicate that coordination occurred *via* the nitrogen atoms.^{18–20} In the ¹H-NMR spectrum of **2**, the broad signal of hydrogen atoms belonging to secondary amino groups appeared in the range 5.8–6.8 ppm (compared with the ammonium groups of **1**: 9.9–10.4 ppm).^{18–20} The signals of the protons between the nitrogen atoms of **2** showed coordination-induced shifts in comparison with those in the spectrum of **1** and also, two signals. The situation was different in the spectrum of **1**, where only one signal was observed, which can also be confirmation of nitrogen coordination to the palladium atom. The signal for the hydrogen atom of the chiral carbon atom was observed at 4.13 ppm as a triplet for **1**, and at 4.14 ppm as a multiplet for **2**. The ¹³C-NMR spectra of **1** and **2** exhibited signals for the carbon atom of the COO moiety at similar positions, indicating that oxygen atoms were not coordinated.^{18–20} The chiral carbon atom showed a signal at 57.9 ppm for **1**, but two signals at 58.4 and 59.1 for **2**. Selected ¹H- and ¹³C-NMR data of **1** and **2** are compared in Table II.

TABLE II. Selected ¹H- and ¹³C-NMR data (δ / ppm, numbering as in Fig. 3 and analogous for [PdCl₂{(*S,S*)-*i*Bu₂eddl}]) of [(*S,S*)-H₂*i*Bu₂eddl]Cl₂, **1**, and [PdCl₂{(*S,S*)-*i*Bu₂eddl}], **2**

Compound	C5,6,10,11H ₃	C1H ₂	C2H	C10,11, C5,6	C1	C2	C7OO
1	0.90–1.00	3.42	4.13	18.9, 21.4	41.7	57.9	169.2
2 Isomer A	0.90–1.10	2.23 and 2.61	4.14	19.0, 21.9	47.0	58.4	170.1
Isomer B	0.90–1.10	2.40 and 2.85	4.14	19.0, 21.5	47.0	59.1	171.2

Crystal structure analysis of [(*S,S*)-H₂*i*Bu₂eddl]Cl₂, **1**

The compound [(*S,S*)-H₂*i*Bu₂eddl]Cl₂ (**1**) crystallized in the tetragonal crystal system in the chiral space group *P*4₂. The molecular structure is shown in Fig. 3. Selected bond lengths and angles are given in Table III.

The isolated crystals consisted of one dicationic species [(*S,S*)-H₂*i*Bu₂eddl]²⁺ and two Cl⁻. The most significant hydrogen bonds for the manner

of packing are N–H1N···Cl, 3.049(3) Å, 159(3)° and N–H2N···Cl, 3.100(3) Å, 164(3)° and these interactions form an infinite chain (Fig. 4). The compound has a C₂ symmetry. The axis passes through the C1–C1ⁱ bond vector and lies perpendicular to the plane N₂Cl₂.

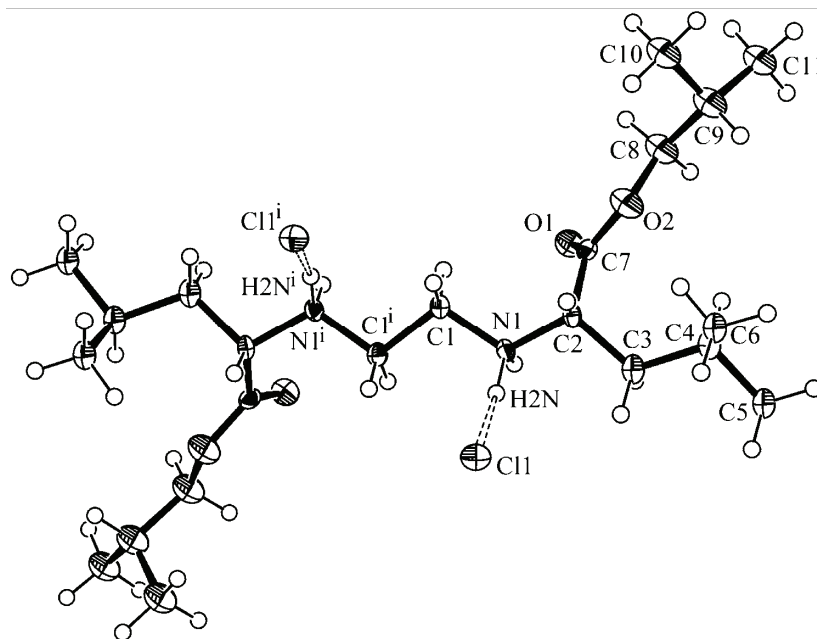


Fig. 3. ORTEP presentation of the molecular structure of **1** with the atom labeling scheme (H-bonds shown by dashed lines). The displacement ellipsoids are plotted at the 50 % probability level and the H atoms are shown as small spheres of arbitrary radii.

TABLE III. Selected bond lengths and angles for **1**

Bond	Length, Å	Bond	Angle, °
O1–C7	1.196(5)	N1–C2–C3	106.2(3)
O2–C7	1.334(5)	N1–C2–C7	110.8(3)
N1–H1N	0.99(2)	C3–C2–C7	109.9(3)
N1–H2N	0.99(2)	C7–O2–C8	115.9(4)
C3–C4	1.534(5)	C1–N1–C2	114.9(3)
C8–C9	1.507(7)	C1–N1–H1N	106(3)

Crystal structures of esters such as [(S,S)-H₂iPr₂eddip]Cl₂,¹⁸ (H₂Me₂eddip)Cl₂²⁸ and [(S,S)-H₂Cpe₂eddip]Cl₂²⁰ were previously determined. These structures are very similar to each other and to [(S,S)-H₂iBu₂edd1]Cl₂ having bond lengths and angles in the same ranges, however the space groups are quite different ([(S,S)-H₂iPr₂eddip]Cl₂, orthorhombic, P2₂1₂1; (H₂Me₂eddip)Cl₂, monoclinic, P2₁/c; [(S,S)-H₂Cpe₂eddip]Cl₂, orthorhombic, P2₁2₁2). The mentioned compounds

have a C_2 symmetry axis. All of these esters form layered structures *via* hydrogen bonding similar to that shown in Fig. 4.

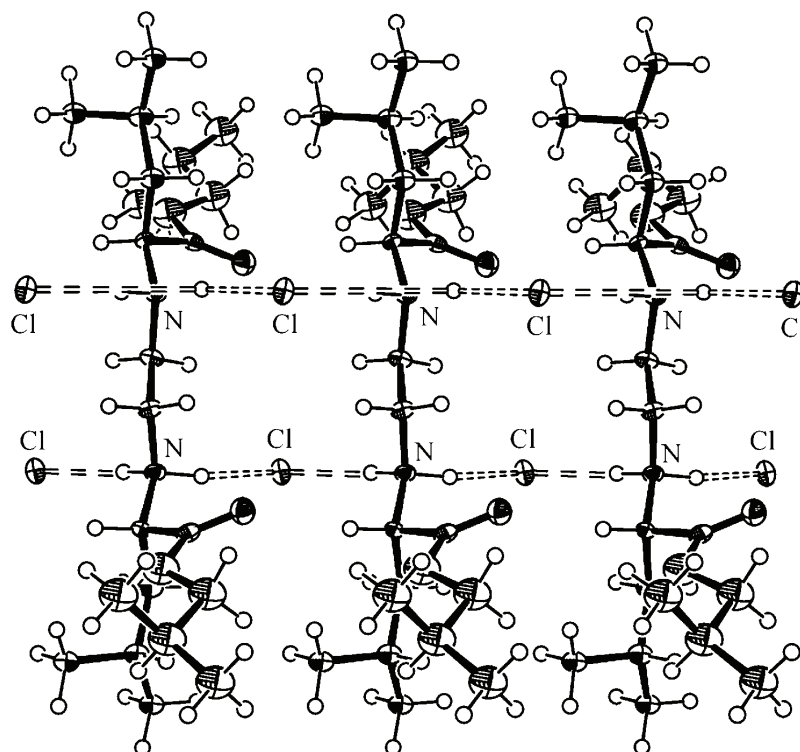


Fig. 4. ORTEP presentation of the packing *via* intermolecular hydrogen bonding of **1** viewed along the *b*-axis.

CONCLUSIONS

Two novel compounds, the R_2 edda-type ester [(*S,S*)- H_2iBu_2eddl] Cl_2 , and its palladium(II) complex [$PdCl_2\{(S,S)-iBu_2eddl\}$] were synthesized and characterized by IR, 1H -NMR and ^{13}C -NMR spectroscopy and elemental analysis. The crystal structure of [(*S,S*)- H_2iBu_2eddl] Cl_2 was determined by X-ray analysis. Two diastereoisomers formed in the reaction of potassium tetrachloropalladate(II) and [(*S,S*)- H_2iBu_2eddl] Cl_2 , as was deduced from the NMR spectra.

Acknowledgements. The authors are grateful to the Ministry of Science and Technological Development of the Republic of Serbia for financial support (Grant No. 142010).

ИЗВОД

КОМПЛЕКСИ ПАЛАДИЈУМА(II) СА ЛИГАНДИМА R₂edda ТИПА. ДЕО III.
ДИИЗОБУТИЛ-(S,S)-2,2'-(1,2-ЕТАНДИИЛДИИМИНО)-ДИ(4-МЕТИЛПЕНТАНОАТ)-
ДИХИДРОХЛОРИД И ЊЕГОВ КОМПЛЕКС СА ПАЛАДИЈУМОМ(II):
СИНТЕЗА И КАРАКТЕРИЗАЦИЈА

БОЈАНА Б. ЗМЕЈКОВСКИ¹, ГОРАН Н. КАЛУЂЕРОВИЋ¹, SANTIAGO GÓMEZ-RUIZ² И ТИБОР Ј. САБО³

¹Институт за хемију, технологију и металургију - Центар за хемију, Универзитет у Београду, Студентски
брг 12-16, 11000 Београд, ²Departamento de Química Inorgánica y Analítica, E.S.C.E.T., Universidad
Rey Juan Carlos, 28933 Móstoles, Madrid, Spain и ³Хемијски факултет,
Универзитет у Београду, б. бр. 158, 11001 Београд

Нови естар R₂edda-типа диизобутил-(S,S)-2,2'-(1,2-етандиилдиимино)-ди(4-метилпентаноат)-дихидрохлорид [(S,S)-H₂iBu₂eddl]Cl₂, **1**, и његов комплекс паладијума(II), дихлоридиизобутил-(S,S)-2,2'-(1,2-етандиилдиимино)-ди(4-метилпентаноат)-паладијум(II) [PdCl₂{(S,S)-iBu₂eddl}], **2**, синтетисани су и окарактерисани уз помоћ елементалне анализе, IR и NMR спектроскопије. Нађено је да је комплекс **2** добијен као смеша два дијастереоизомера, што је примећено у NMR спектрима. Кристална структура **1** је решена и описана. Изоловани кристали се састоје из једне дикатјонске врсте [(S,S)-H₂iBu₂eddl]²⁺ и два Cl⁻. Кристални систем је тетрагоналан са просторним групом P₄. Значајне водоничне везе за начин паковања су N-H1N...Cl, 3,049(3) Å, 159(3)° и N-H2N...Cl, 3,100(3) Å, 164(3)°. Тиме се формира бесконачан ланац и једнослојна структура, који су уобичајени за ове типове структура. Оса симетрије C₂ једињења пролази кроз C1-C1' вектор везе и лежи нормално на N₂Cl₂ раван.

(Примљено 3. априла, ревидирано 8. јуна 2009)

REFERENCES

1. G. N. Kaluđerović, H. Schmidt, D. Steinborn, T. J. Sabo, in *Inorganic Biochemistry: Research Progress* J. G. Hughes, A. J. Robinson, Eds., Nova Science Publishers, Hauppauge, NY, 2008, p. 305
2. G. N. Kaluđerović, H. Schmidt, S. Schwieger, C. Wagner, R. Paschke, A. Dietrich, T. Mueller, D. Steinborn, *Inorg. Chim. Acta* **361** (2008) 1395
3. T. J. Sabo, G. N. Kaluđerović, S. R. Grgurić-Šipka, F. W. Heinemann, S. R. Trifunović, *Inorg. Chem. Commun.* **7** (2004) 241
4. B. V. Zmejkovski, G. N. Kaluđerović, S. Gómez-Ruiz, T. J. Sabo, *Acta Crystallogr., Sect. E* **65** (2009) o656
5. T. J. Sabo, G. N. Kaluđerović, D. Poleti, Lj. Karanović, A. Boccarelli, F. Cannito, G. Natile, *J. Inorg. Biochem.* **98** (2004) 1378
6. S. Mijatović, D. Maksimović-Ivanić, J. Radović, D. Miljković, G. N. Kaluđerović, T. J. Sabo, V. Trajković, *Cell. Mol. Life Sci.* **62** (2005) 1275
7. G. N. Kaluđerović, H. Schmidt, C. Wagner, K. Merzweiler, D. Steinborn, *Collect. Czech. Chem. Commun.* **72** (2007) 560
8. G. N. Kaluđerović, F. W. Heinemann, N. Ž. Knežević, S. R. Trifunović, T. J. Sabo, *J. Chem. Crystallogr.* **34** (2004) 185
9. J. Ruiz, J. Lorenzo, L. Sanglas, N. Cutillas, C. Vicente, M. D. Villa, F. X. Avilés, G. López, V. Moreno, J. Pérez, D. Bautista, *Inorg. Chem.* **45** (2006) 6347
10. E. R. Jamieson, S. J. Lippard, *Chem. Rev.* **99** (1999) 2467

11. E. Budzisz, B. K. Keppler, G. Giester, M. Woźniczka, A. Kufelnicki, B. Nawrot, *Eur. J. Inorg. Chem.* (2004) 4412
12. E. Budzisz, U. Krajewska, M. Rozalski, *Pol. J. Pharmacol.* **56** (2004) 473
13. G. Zhao, H. Lin, P. Yu, H. Sun, S. Zhu, X. Su, Y. Chen, *J. Inorg. Biochem.* **73** (1999) 145
14. F. Huq, H. Tayyem, P. Beale, J. Q. Yu, *J. Inorg. Biochem.* **101** (2007) 30
15. L. Tušek-Božić, J. Matijašić, G. Bocelli, P. Sgarbotto, A. Furlani, V. Scarcia, A. Papaioannou, *Inorg. Chim. Acta* **185** (1991) 229
16. L. Tušek-Božić, J. Matijašić, G. Bocelli, G. Calestani, A. Furlani, V. Scarcia, A. Papaioannou, *J. Chem. Soc., Dalton Trans.* (1991) 195
17. T. A. K. Al-Allaf, L. J. Rasha, *Boll. Chim. Farm.* **140** (2001) 205
18. B. B. Krajčinović, G. N. Kaluđerović, D. Steinborn, H. Schmidt, C. Wagner, Ž. Žižak, Z. D. Juranić, S. R. Trifunović, T. J. Sabo, *J. Inorg. Biochem.* **102** (2008) 892
19. B. B. Krajčinović, G. N. Kaluđerović, D. Steinborn, Ch. Wagner, K. Merzweiler, S. R. Trifunović, T. J. Sabo, *J. Serb. Chem. Soc.* **74** (2009) 389
20. B. B. Zmejkovski, G. N. Kaluđerović, S. Gómez-Ruiz, Ž. Žižak, D. Steinborn, H. Schmidt, R. Paschke, Z. D. Juranić, T. J. Sabo, *Eur. J. Med. Chem.* **44** (2009) 3452
21. L. N. Schoenberg, D. W. Cooke, C. F. Liu, *Inorg. Chem.* **7** (1968) 2386
22. G. N. Kaluđerović, T. J. Sabo, *Polyhedron* **21** (2002) 2277
23. D. B. Haydock, T. P. C. Mulholland, *J. Chem. Soc. C* (1971) 2389
24. *SCALE3 ABSPACK: Empirical absorption correction*, CrysAlis – Software package, Oxford Diffraction Ltd., Oxford, 2006
25. G. M. Sheldrick, *SHELXS-97, Program for Crystal Structure Solution*, Göttingen, 1997
26. G. M. Sheldrick, *SHELXL-97, Program for the Refinement of Crystal Structures*, Göttingen, 1997
27. L. J. Farrugia, *ORTEP-3 for Windows, version 1.076*, *J. Appl. Crystallogr.* **30** (1997) 565
28. G. N. Kaluđerović, A. Paethamon, Ch. Wagner, T. J. Sabo, H. Schmidt, *Acta Crystallogr., Sect. E* **64** (2008) o1232.



J. Serb. Chem. Soc. 74 (11) 1259–1271 (2009)
JSCS–3916

Transition metal complexes with pyrazole-based ligands. Part 29. Reactions of zinc(II) and mercury(II) thiocyanate with 4-acetyl-3-amino-5-methylpyrazole

ŽELJKO K. JAĆIMOVIĆ¹, GORAN A. BOGDANOVIĆ², BERTA HOLLÓ^{3#},
VUKADIN M. LEOVAC^{3#} and KATALIN MÉSZÁROS SZÉCSÉNYI^{3*#}

¹Faculty of Metallurgy and Technology, Podgorica, Montenegro, ²“Vinča” Institute of Nuclear Sciences, Laboratory of Theoretical Physics and Condensed Matter Physics, Belgrade and ³Faculty of Sciences, Department of Chemistry, Novi Sad, Serbia

(Received 2 June, revised 4 October 2009)

Abstract: The work is concerned with the crystal and molecular structures of zinc(II) and mercury(II) complexes with 4-acetyl-3-amino-5-methylpyrazole (aamp) of the coordination formulae $[\text{Zn}(\text{NCS})_2(\text{aamp})_2]$ and $(\text{Haamp})_2[\text{Hg}(\text{SCN})_4]$. The zinc(II) complex was obtained by the reaction of a warm methanolic solution of aamp with a mixture of zinc(II) nitrate and ammonium thiocyanate, whereas the mercury(II) complex was prepared by the reaction of a warm ethanolic solution of aamp and a warm, slightly acidified aqueous solution of $[\text{Hg}(\text{SCN})_4]^{2-}$. Both complexes have a tetrahedral geometry, which in the case of zinc complex is formed by monodentate coordination of two aamp molecules and two isothiocyanate groups. The Zn(II) and Hg(II) atoms have significantly deformed coordination geometry. In both crystal structures the pyrazole derivative has a planar form, probably stabilized by an intramolecular N–H...O hydrogen bond. Apart from the X-ray structural analysis, the isolated complexes were characterized by elemental analysis, IR spectroscopy, conductometric measurements and thermal analysis.

Keywords: zinc(II) complex; mercury(II) complex; 4-acetyl-3-amino-5-methylpyrazole; crystal structure; thermal analysis.

INTRODUCTION

The focus of our research on transition metal complexes with pyrazole derivatives is due to the theoretical and practical significance of these compounds. A number of pyrazole derivatives show biological activity and, as a consequence, some are commercial products or compounds in the phase of activity evaluation. Their representatives show antipyretic,¹ antirheumatic² and antimicrobial³ be-

* Corresponding author. E-mail: mszk@uns.ac.rs

Serbian Chemical Society member.

doi: 10.2298/JSC0911259J

havior. Some of them are active ingredients of products with potential antitumor activity.^{4–6} In agriculture, they are in the use as pesticides.^{7–9} As pyrazoles readily form complexes, they are suitable agents for investigating the active sites of biomolecules¹⁰ and for modeling the biosystems of oxygen transfer.¹¹ In living organisms, metal ions are usually bonded to the imidazole part of histidine, which is a part of the proteins. In view of the similarity of pyrazole and imidazole,¹² they are suitable to mimic enzymatic reactions. From all the interesting pyrazole derivatives, our most intensive research is focused on the complexes of 4-acetyl-3-amino-5-methylpyrazole (aamp). This ligand exhibits outstanding complexing ability and, simultaneously, it displays considerable biological activity.¹³ The usual coordination mode of the aamp ligand is through its N2 (pyridine) nitrogen atom giving bis(aamp) complexes of the general formula $M(aamp)_2X_2$.¹⁴ In basic solutions, *via* the deprotonated N1 atom, it acts as a bidentate bridging ligand giving bi- or polynuclear complexes.¹⁵ In a previous publications, the synthesis and structure of tetrahedral Zn(II) and Hg(II) complexes with the formula $[Zn(NO_3)_2(aamp)_2]$ and $[HgCl_2(aamp)_2]$ were described.¹⁶ Herein, the synthesis, crystal and molecular structure, as well as physicochemical properties of the complexes with the same central atoms and aamp ligand of the formulae $[Zn(NCS)_2(aamp)_2]$ and $(Haamp)_2[Hg(SCN)_4]$ are presented.

EXPERIMENTAL

Synthesis

In a previous work,¹⁷ the synthesis of $[Zn(NCS)_2(aamp)_2]$ was described but the resulting crystals were not suitable for X-ray structural analysis. Crystals of the same compound appropriate for X-ray analysis were obtained from MeOH solutions according to the following procedure. A mixture of 0.50 mmol $Zn(NO_3)_2 \cdot 6H_2O$ and 1.2 mmol NH_4NCS was dissolved in 8.0 cm³ of MeOH. The ligand (1.0 mmol) was dissolved in 8.0 cm³ of warm MeOH. The two solutions were mixed together and left to crystallize at room temperature for seven days. The white prismatic crystals were filtered off, washed with MeOH and air-dried. Yield: 61 %. Anal. Calcd. for $ZnC_{14}H_{18}N_8O_2S_2$ (459.88 g mol⁻¹): C, 36.56; H, 3.95; N, 24.37; S, 13.94 %. Found: C, 36.52; H, 3.90; N, 24.38; S, 13.92 %.

$(Haamp)_2[Hg(SCN)_4]$ was obtained as follows: 0.20 mmol $Hg(SCN)_2$ and 0.50 mmol NH_4NCS were dissolved in 3 cm³ of water and one drop of *cc.* HCl was added. The ligand aamp (0.50 mmol) was dissolved in 3 cm³ of warm EtOH, and the warm solutions were mixed together. After two days standing at room temperature, the formed white, plate crystals were filtered off, washed with EtOH and air-dried at room temperature. Yield: 44 %. Anal. Calcd. for $HgC_{16}H_{20}N_{10}O_2S_4$ (713.26 g mol⁻¹): C, 26.94; H, 2.83; N, 19.64; S, 17.98 %. Found: C, 26.90; H, 2.80; N, 19.65; S, 18.00 %.

Elemental analysis data were obtained by standard methods.

FT-IR data were collected at room temperature as KBr pellets, in the range 4000–400 cm⁻¹ using a Thermo Nicolet (NEXUS 670 FT-IR) spectrophotometer.

Molar conductivities of freshly prepared 1.0 mmol dm⁻³ solutions were measured on a Jenway 4010 conductivity meter.

X-Ray experiments and crystal structure determination

Single-crystal X-ray diffraction data for $(\text{Haamp})_2[\text{Hg}(\text{SCN})_4]$ were collected on an Enraf-Nonius CAD-4 diffractometer¹⁸ using $\text{MoK}\alpha$ radiation ($\lambda = 0.71069 \text{ \AA}$) and $\omega/2\theta$ scans in the 2θ range from 1.67 to 29.96° . The cell constants and an orientation matrix for data collection, obtained from 24 centered reflections in the range 12.10 – 16.82° , corresponded to a monoclinic cell, the dimensions of which are given in Table I. The data were corrected for Lorentz and polarization effects.¹⁹ A Gaussian-type absorption correction^{20–22} based on the crystal morphology was applied ($T_{\min} = 0.217$; $T_{\max} = 0.354$).

TABLE I. Crystallographic data for the compounds $[\text{Zn}(\text{NCS})_2(\text{aamp})_2]$ and $(\text{Haamp})_2[\text{Hg}(\text{SCN})_4]$

Property	$[\text{Zn}(\text{NCS})_2(\text{aamp})_2]$	$(\text{Haamp})_2[\text{Hg}(\text{SCN})_4]$
Empirical formula	$\text{C}_{14}\text{H}_{18}\text{ZnN}_8\text{O}_2\text{S}_2$	$\text{C}_{16}\text{H}_{20}\text{HgN}_{10}\text{O}_2\text{S}_4$
Formula weight	459.85	713.26
Crystal size, mm^3	$0.28 \times 0.25 \times 0.10$	$0.18 \times 0.25 \times 0.35$
Crystal color/shape	White/plate	White/prism
Temperature, K	293(2)	293(2)
Wavelength, \AA	0.71069	0.71069
Crystal system	Triclinic	Monoclinic
Space group	<i>P1</i>	<i>C2/c</i>
Unit cell dimensions		
$a / \text{\AA}$	8.3466(4)	10.055(2)
$b / \text{\AA}$	10.8641(5)	10.379(3)
$c / \text{\AA}$	12.4718(5)	24.442(4)
$\alpha / ^\circ$	74.927(4)	90
$\beta / ^\circ$	88.563(4)	92.49(2)
$\gamma / ^\circ$	68.802(4)	90
$V / \text{\AA}^3$	1015.13(8)	2548.4(10)
Z	2	4
$D_{\text{calc}} / \text{g cm}^{-3}$	1.504	1.859
Absorption coefficient, mm^{-1}	1.442	6.402
Theta range for data collection ($^\circ$)	3.01–28.86	1.67–29.96
Index ranges	$-11 \rightarrow h \rightarrow 10$, $-13 \rightarrow k \rightarrow 14$, $-16 \rightarrow l \rightarrow 16$	$-14 \rightarrow h \rightarrow 14$, $0 \rightarrow k \rightarrow 14$, $0 \rightarrow l \rightarrow 34$
Reflections collected	10022	3785
Independent reflections	4638 ($R(\text{int}) = 0.017$)	3704 ($R(\text{int}) = 0.0237$)
Data/parameters	4638/248	3704/150
Goodness-of-fit on F^2	0.991	1.037
Final R indices [$I > 2\sigma(I)$]	$R_1 = 0.0307$, $wR_2 = 0.0752$	$R_1 = 0.0416$, $wR_2 = 0.1078$
Largest diff. peak and hole, e \AA^{-3}	0.368 and -0.410	0.703 and -0.813

A single white crystal of $[\text{Zn}(\text{NCS})_2(\text{aamp})_2]$ was selected and glued on glass fiber. X-Ray diffraction data were collected on an Oxford Diffraction Gemini S four-circle diffractometer equipped with a Sapphire CCD detector. The crystal to detector distance of 45.0 mm and graphite monochromated $\text{MoK}\alpha$ ($\lambda = 0.71073 \text{ \AA}$) were used. X-Radiation were employed

in the measurement. The data were reduced using the Oxford Diffraction program Crys-Alis^{Pro}.²³ A semi-empirical absorption correction based upon the intensities of equivalent reflections was applied, and the data were corrected for Lorentz, polarization, and background effects.²³ Crystallographic data are given in Table I.

Both structures were solved by heavy atom²⁴ and difference Fourier methods and refined on F^2 by the full-matrix least-squares method.²⁴ All H atoms were placed at the calculated positions and they were refined with isotropic displacement parameters set to 1.2 times (1.5 for methyl groups) the equivalent isotropic U value of the parent atom. The software used to prepare the material for publication: PARST²⁵ and WinGX.²¹ Molecular graphics: ORTEPIII.²⁶ Crystallographic details are given in Table I.

Thermal analysis

Thermal measurements were performed on a Q600 SDT TA Instruments thermal analyzer. Simultaneous TG–DTA curves were obtained using alumina crucibles with sample masses of about 2 mg with an empty crucible serving as the reference. The heating rate was 20 °C min⁻¹ in flowing nitrogen and air gas carriers. Flow rate: 100 cm³ min⁻¹.

RESULTS AND DISCUSSION

Synthesis and selected physicochemical properties of the compounds

Single crystals of the Zn(II) complex were obtained by the reaction of warm, dilute methanolic solutions of the aamp ligand and a mixture of Zn(NO₃)₂·6H₂O and NH₄NCS in a mole ratio of 1:0.5:1.2.

The Hg(II) complex resulted from the reaction of warm ethanolic solution of the ligand and a warm, slightly acidic aqueous solution of Hg(SCN)₂ and NH₄NCS in a mole ratio of 1:0.4:1; hence, it was in fact the reaction between [Hg(SCN)₄]²⁻ and aamp. In view of the high stability of [Hg(SCN)₄]²⁻, *i.e.*, the strong Hg–S bond, as well as the solution acidity, it is not surprising that it was possible to isolate [Hg(SCN)₄]²⁻ containing two Haamp⁺ as counter ions.

It should be mentioned that an attempt to prepare a mixed-ligand complex, *i.e.*, [Hg(SCN)₂(aamp)₂], in the same way as for the zinc(II) complex, was unsuccessful, as it resulted in the crystallization of the free ligand.

Both crystals were stable at room temperature. They were slightly soluble in water, EtOH and MeOH, but well soluble in DMF. The molar conductivity data of the colorless solutions of the Zn(II) and Hg(II) complexes, Λ_M , in DMF were 32 and 114 S cm² mol⁻¹, respectively. The value of the molar conductivity of [Zn(NCS)₂(aamp)₂] was somewhat larger than that for the non-electrolytes, which refers to the partial replacement of the NCS group with solvent molecules. The value of Λ_M of the (Haamp)₂[Hg(SCN)₄] complex is in agreement with its coordination formula and corresponds to a 2:1 electrolyte type.²⁷

In the IR spectra of the complexes, the thiocyanato group is identified by its very intensive bands, which appear at 2064 and 2082 cm⁻¹ (Zn–NCS) and 2099 and 2123 cm⁻¹ (Hg–SCN). The position of these bands agrees very well with the coordination mode of the corresponding group.²⁸

Molecular and crystal structures

Structure of $(\text{Haamp})_2[\text{Hg}(\text{SCN})_4]$. The structure of the $(\text{Haamp})_2[\text{Hg}(\text{SCN})_4]$ complex is presented in Fig. 1. In the unit cell, the Hg atom lies on a two-fold axis of symmetry (the second half of the complex anion and the other counter cation requires the symmetry operation $-x, y, -z + 1/2$). The two crystallographically different SCN groups have very similar bond distances (Table II). The nitrogen atoms from the two coordinated SCN groups participate in cyclic hydrogen bonds (Fig. 2) to the neighboring Haamp^+ ($\text{N1-H}\cdots\text{N4b}$ and $\text{N2-H}\cdots\text{N4a}$ hydrogen bonds in Table III). These hydrogen bonds influence the geometry of the complex anion and the mutual orientation of the SCN ligands with an $\text{N4a}\cdots\text{N4b}$ distance of only 3.31 Å. A search of the Cambridge Structural Database²⁹ for all crystal structures possessing an Hg atom with two or more bonded SCN ligands revealed that none of 72 Hg compounds had such a short $\text{N}\cdots\text{N}$ distance (less than 3.5 Å) for two coordinated SCN groups as exists in the complex studied herein. Another consequence of the observed cyclic H-bonds is that the C7b-S1b-Hg angle is bent to a value of $95.8(1)^\circ$, which is rather different from the expected, much higher value. It is noteworthy that such a low value of the C-S-Hg angle is also quite rare in the above mentioned 72 crystal structures found in the CSD database, although the Hg atom has four equivalent ligands. The S-Hg-S coordination angles are also very deformed and have the values over a rather wide range, from 102.3 to 114.8° (Table II). All this demonstrates the importance of intermolecular hydrogen bonds for the geometry of $[\text{Hg}(\text{SCN})_4]^{2-}$ and probably may be applied to similar tetrahedral molecules $[\text{ML}_4]$ that form intermolecular interactions through coordinated SCN groups. In other words, the mutual orientation of the ligands and the coordination angles could be significantly deformed due to intermolecular hydrogen bonds.

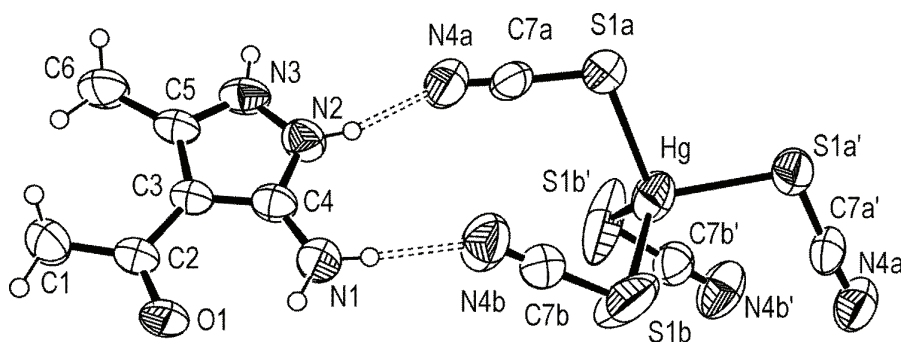


Fig. 1. The molecular geometry and atom labeling scheme of $(\text{Haamp})_2[\text{Hg}(\text{SCN})_4]$. The displacement ellipsoids are drawn at the 40 % probability level for non-H atoms. (The second half of the complex anion and the other counter cation requires the symmetry operation $-x, y, -z + 1/2$).

TABLE II. Selected Selected bond distances (Å) and angles (°) for [Zn(NCS)₂(aamp)₂] and (Haamp)₂[Hg(SCN)₄]. Symmetry code: (i) $-x, y, -z + 1/2$

[Zn(NCS) ₂ (aamp) ₂]			
Zn–N4a	1.9415(18)	N4a–Zn–N4b	114.10(9)
Zn–N4b	1.9537(19)	N4a–Zn–N2b	111.49(7)
Zn–N2b	2.0083(15)	N4b–Zn–N2b	109.04(7)
Zn–N2a	2.0124(16)	N4a–Zn–N2a	104.58(7)
S1a–C7a	1.603(2)	N4b–Zn–N2a	110.52(8)
N4a–C7a	1.152(3)	N2b–Zn–N2a	106.82(6)
S1b–C7b	1.608(2)		
N4b–C7b	1.143(3)		
(Haamp) ₂ [Hg(SCN) ₄]			
Hg–S1a	2.5386(15)	S1b ⁱ –Hg–S1b	114.8(2)
Hg–S1b	2.534(2)	S1b ⁱ –Hg–S1a ⁱ	108.00(7)
S1a–C7a	1.639(6)	S1b–Hg–S1a ⁱ	111.55(8)
N4a–C7a	1.150(7)	S1b ⁱ –Hg–S1a	111.55(8)
S1b–C7b	1.621(6)	S1b–Hg–S1a	108.00(7)
N4b–C7b	1.123(7)	S1a ⁱ –Hg–S1a	102.31(7)

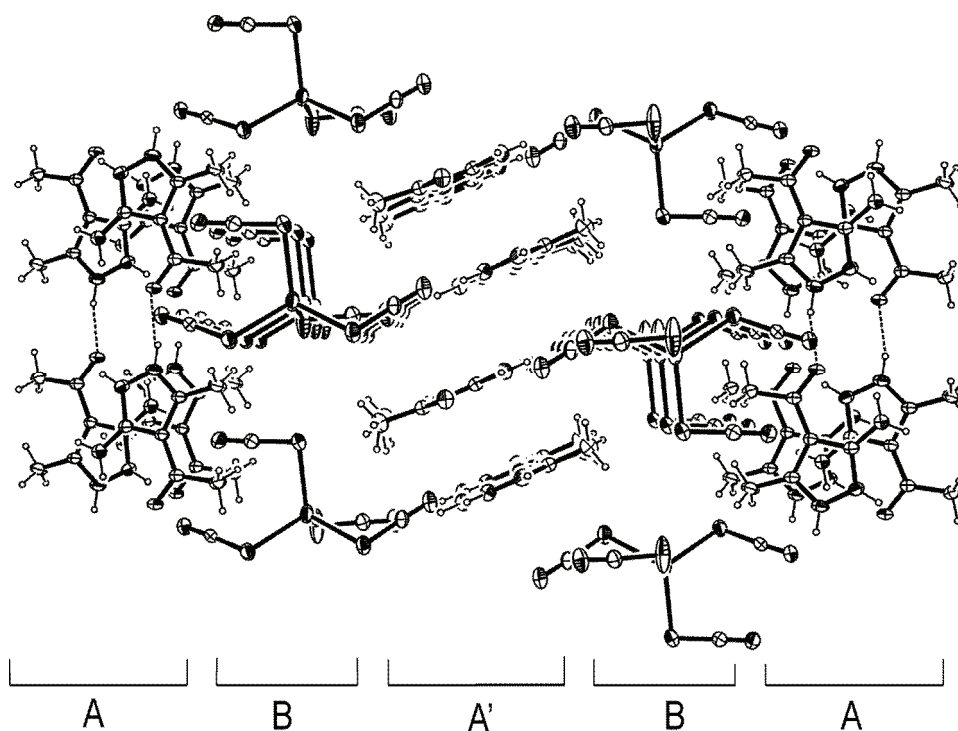
Fig. 2. The crystal lattice fragment of (Haamp)₂[Hg(SCN)₄] viewed down the $[-1, 1, 0]$ direction showing the mutual orientation of the complex anions and the pyrazolium cations.

TABLE III. The geometry of possible hydrogen bonds and selected intermolecular interactions for (Haamp)₂[Hg(SCN)₄]. Symmetry codes: (i) x, y, z ; (ii) $x-1/2, +y+1/2, +z$; (iii) $x+1/2, +y-1/2, +z$; (iv) $-x, -y, -z+1$

Bond	D–H (Å)	D···A (Å)	H···A (Å)	D–H···A (°)
N1–H1b···O1 ⁱ	0.86	2.787(5)	2.22	123
N1–H1a···N4b ⁱ	0.86	2.856(7)	2.00	175
N1–H1b···N4a ⁱⁱ	0.86	3.283(7)	2.56	142
N2–H2···N4a ⁱ	0.86	2.846(7)	2.03	159
N3–H3···O1 ⁱⁱⁱ	0.86	2.750(5)	1.92	164
C6–H6C···S1a ^{iv}	0.96	3.670(6)	2.81	149

All the non-hydrogen atoms in Haamp⁺ are approximately coplanar, which is probably due to the delocalization of the π -electrons within the pyrazole ring and the weak π -bonding between the C2 and C3 atoms (the C2–C3 bond has a partial double bond character). Another reason for this could be the existence of an intramolecular N1–H1b···O1 hydrogen bond (Table III), which favors the coplanar position of the C1–C2–O1 fragment to the rest of molecule. Quite similar molecular planarity, including the observed intramolecular N–H···O hydrogen bond, was observed in other crystal structures of metal(II) complexes with aamp.^{14–16,30}

The crystal packing, shown in Fig. 2, consists of two types of layers. Layer A is composed of Haamp⁺ arranged in parallel tapes with a mutual distance between the tapes (Haamp⁺ planes) of approximately 3.3 Å. Inside of the tapes, the cations are interconnected by strong N3–H3···O1 hydrogen bonds (Table III). Layers A and A' are of the same composition and mutual orientation of the protonated ligands, but have an orthogonal orientation to each other. Layer B consists of [Hg(SCN)₄]²⁻ which interconnect the neighboring Haamp⁺ from layers A and A' by strong N–H···N4 hydrogen bonds (Table III). Consequently, each complex anion (through its terminal nitrogen atoms) participates in four relatively strong hydrogen bonds. Additionally, N4a forms another (weak) hydrogen bond, while the S1a atom participates in a very weak C–H···S hydrogen bond, which deserves to be noted because of its relatively short H···S distance (Table III).

Crystal structure of [Zn(NCS)₂(aamp)₂]. A tetrahedral arrangement, most common in Zn(II) complexes, is established by the coordination of two NCS groups and two monodentate pyrazole ligands, which are, like in the majority of other structures, coordinated in the neutral form (Fig. 3). In contrast to the Hg(II) complex, where the thiocyanato groups are coordinated through the sulfur atom, the coordinating atoms in the Zn(II) complex are the nitrogens of the same group, which is in accordance with the Hard and Soft Acid and Base (HSAB) principle.^{31,32} However, the bond distances in the thiocyanato ligands are very similar in both complexes, with the S1–C7 bond being negligibly shorter in the Zn(II) complex than that in the Hg(II) complex. The N4–C7 bond lengths are practically the same in both compounds. Similarly to the Hg(II) complex, the coordination

angles are significantly deformed and vary in the 104.6–114.1° range (Table II). The widest angle, N4a–Zn–N4b, involve N atoms from the coordinated NCS groups.

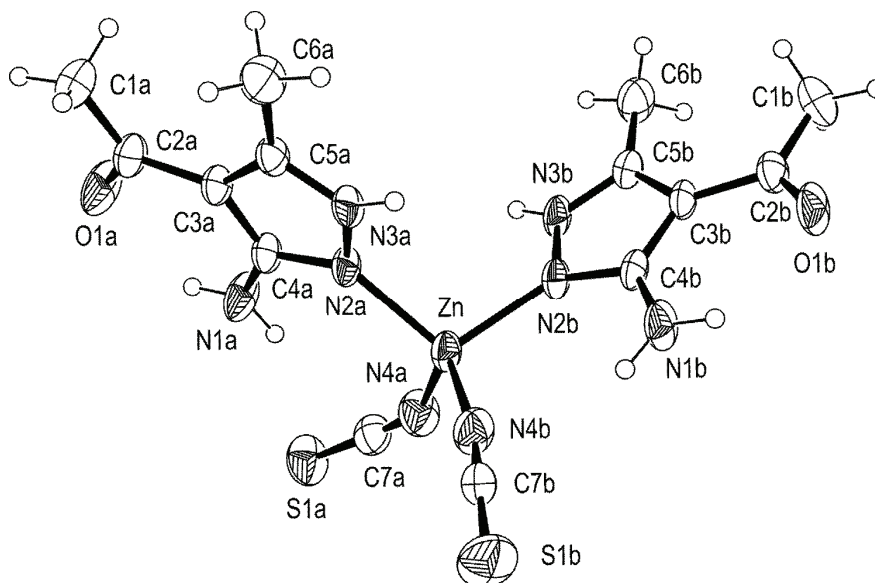


Fig. 3. The molecular geometry and atom labeling scheme of $[\text{Zn}(\text{NCS})_2(\text{aamp})_2]$. The displacement ellipsoids are drawn at the 40 % probability level for non-H atoms.

Despite the differences between the pyrazole derivatives in the two complexes, the analysis showed that the corresponding bond lengths are very similar (Table IV). The greatest deviation was observed in the N2–N3 bond length, which is shorter in the Hg(II) complex. The conformation of aamp is also very similar in both compounds. Namely, it has the same planar form, supported by possible N1–H···O1 intramolecular hydrogen bonds (Table V).

TABLE IV. A comparison of the bond distances (Å) in the pyrazole ligand for $[\text{Zn}(\text{NCS})_2(\text{aamp})_2]$ and $(\text{Haamp})_2[\text{Hg}(\text{SCN})_4]$

Bond	$[\text{Zn}(\text{NCS})_2(\text{aamp})_2]$		$(\text{Haamp})_2[\text{Hg}(\text{SCN})_4]$
	Ligand A	Ligand B	
O1–C2	1.233(2)	1.228(2)	1.233(5)
N1–C4	1.349(2)	1.339(2)	1.332(7)
N2–C4	1.334(2)	1.343(2)	1.339(6)
N2–N3	1.374(2)	1.379(2)	1.349(6)
N3–C5	1.313(2)	1.313(2)	1.324(6)
C2–C3	1.446(2)	1.438(2)	1.452(6)
C3–C4	1.403(2)	1.398(2)	1.405(7)
C3–C5	1.414(3)	1.420(3)	1.413(6)

TABLE V. The geometry of possible hydrogen bonds and selected intermolecular interactions for $[\text{Zn}(\text{NCS})_2(\text{aamp})_2]$. Symmetry codes: (i) x, y, z ; (ii) $-x+1, -y, -z+1, +z$; (iii) $-x+2, -y+1, -z, +z$; (iv) $-x+2, -y, -z+1$; (v) $-x+2, -y, -z$

Bond	D–H (Å)	D···A (Å)	H···A (Å)	D–H···A (°)
N1a–H1a2···O1a ⁱ	0.86	2.801(2)	2.23	124
N1a–H1a2···S1a ⁱⁱ	0.86	3.629(2)	2.83	154
N1a–H1a1···N4a ⁱ	0.86	3.128(2)	2.37	148
N1b–H1b2···O1a ⁱ	0.86	2.738(3)	2.16	125
N1b–H1b2···S1b ⁱ	0.86	3.638(2)	2.86	152
N1b–H1b1···N4b ⁱ	0.86	3.327(3)	2.57	147
N1a–H3a···O1b ⁱⁱⁱ	0.86	2.714(2)	1.86	174
N1b–H3b···O1a ^{iv}	0.86	2.769(2)	1.92	168
C1a–H1a5···S1b ^v	0.96	3.722(3)	2.87	148
C6a–H6a2···S1b ^v	0.96	3.684(3)	2.91	139

It is interesting to note that the oxygen atom of the pyrazole moiety forms the same H-bonds in both complexes. In addition to the already mentioned N1–H···O1 intramolecular H-bond, O1 participates in intermolecular N3–H···O1 H-bonds with very similar geometric parameters (Tables III and V). This is the strongest H-bond in the complexes, and it enables the chain formation, connecting the aamp molecules (Fig. 4). In the Zn(II) complex, the chains are additionally connected *via* weak C–H···S hydrogen bonds (Table V).

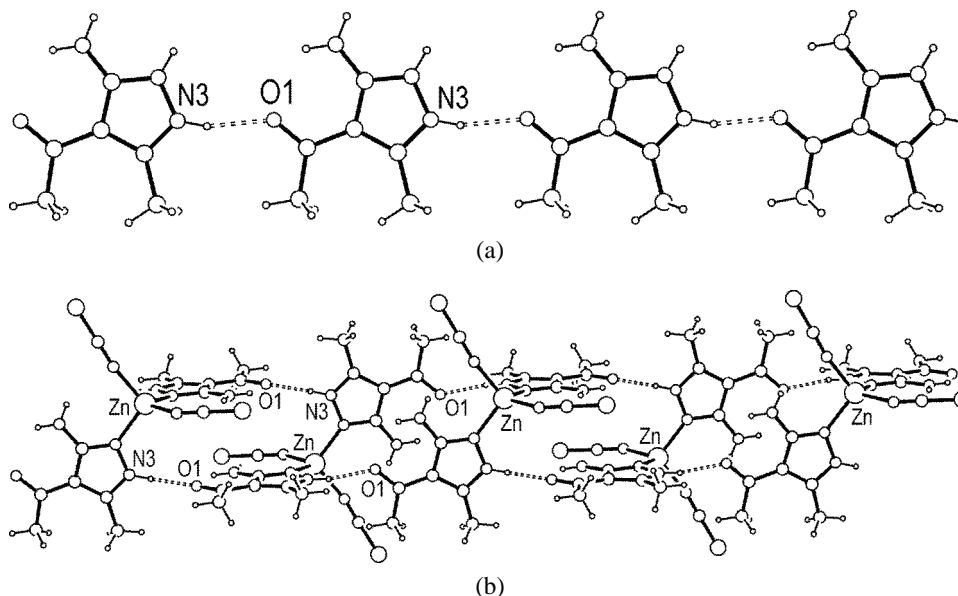


Fig. 4. In both crystal structures, the pyrazole derivatives form chains through the N3–H···O1 hydrogen bonds. The crystal lattice fragments for $(\text{Haamp})_2[\text{Hg}(\text{SCN})_4]$ and $[\text{Zn}(\text{NCS})_2(\text{aamp})_2]$ are illustrated in (a) and (b), respectively.

Thermal data

The thermal decomposition of $[\text{Zn}(\text{NCS})_2(\text{aamp})_2]$ has already been described.¹⁷ The repeated measurements have confirmed the former findings. According to the completely different crystal and molecular structure of the Hg(II) complex, its decomposition pattern is also different. The thermal stability of the Hg(II) compound is significantly lower compared to that of the zinc(II) complex (onset temperatures: 150 and 240 °C, respectively) and TG curve is continuous in the whole temperature range. As all four thiocyanato N4 atoms form relatively strong H-bonds with the neighboring Haamp⁺, it is reasonable to expect the departure of two HNCS molecules at the first decomposition step, which would be in accordance, within the experimental error, with the mass loss to the first minimum in DTG curve: 12.9 % (calcd. 16.57 %). Namely, according to the HSAB principle the interactions between the soft Hg(II) acid and the soft sulfur atom of the SCN⁻ base are remarkable. Therefore it is highly unlikely the loss of all four thiocyanato groups at the same time. With the loss of two HSCN molecule the Hg(II) analogue of the Zn(II) complex with a tentative composition of $\text{Hg}(\text{NCS})_2(\text{aamp})_2$ would be formed. The shape of the DTG curve may also support this proposition. However, it can be seen in Fig. 5 that the fragmentation of the organic part takes place simultaneously. The course of the decomposition is almost independent of the gas carrier up to 400 °C. Due to the high volatility of mercury, at higher temperatures, the oxidation of the organic fragments is ac-

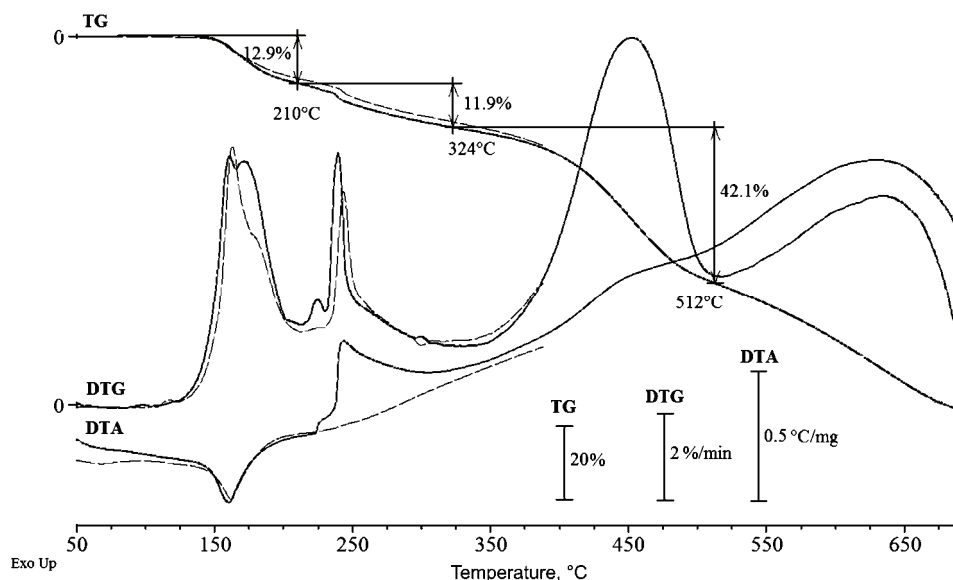


Fig. 5. TG, DTG and DTA curves of the decomposition of $(\text{Haamp})_2[\text{Hg}(\text{SCN})_4]$ in air (—) and in nitrogen (---).

accompanied by the evaporation of the mercury.³³ As there is no stable intermediate formation in the measured temperature range, the course of the decomposition, especially at higher temperatures cannot be explained without additional EGD data. At about 700 °C the decomposition of the compound is accomplished without residue.

The decomposition of Hg(II) complex begins with an endothermic peak in both gas carriers. An additional proof of the organic fragments evaporation is the different shape of DTA curves in air and nitrogen above 200 °C. In air, the DTA curve is asymmetric suggesting the occurrence of multiple processes and the decomposition is highly exothermic. The decomposition in nitrogen is accompanied with a very slightly endothermic process. Above 300 °C the decomposition in both atmospheres is exothermic in the measured range.

Crystallographic data for the structural analysis have been deposited with the Cambridge Crystallographic Data Centre, CCDC No. 736362 and CCDC No.736363 for compounds $[\text{Zn}(\text{NCS})_2(\text{aamp})_2]$ and $(\text{Haamp})_2[\text{Hg}(\text{SCN})_4]$, respectively. Copies of this information may be obtained free of charge from the Director, CCDC, 12 Union Road, Cambridge, CB2 1EZ, UK (fax: +44-1223-336033; e-mail: deposit@ccdc.cam.ac.uk or www: <http://www.ccdc.cam.ac.uk>).

Acknowledgements. The work was financed in part by the Ministry of Science and Technological Development of the Republic of Serbia (Grant No. 142028) and the Provincial Secretariat for Science and Technological Development of Vojvodina. The authors would like to thank Prof. Vladimir Divjaković (Department of Physics, University of Novi Sad, Republic of Serbia) for measuring the crystal data of $[\text{Zn}(\text{NCS})_2(\text{aamp})_2]$.

ИЗВОД

КОМПЛЕКСИ ПРЕЛАЗНИХ МЕТАЛА СА ДЕРИВАТИМА ПИРАЗОЛА.
ДЕО 29. РЕАКЦИЈЕ ЦИНКА(II) И ЖИВА(II) ТИОЦИЈАНАТА СА
4-АЦЕТИЛ-3-АМИНО-5-МЕТИЛПИРАЗОЛОМ

ЖЕЉКО К. ЈАЊИМОВИЋ¹, ГОРАН А. БОГДАНОВИЋ², BERTA HOLLÓ³, ВУКАДИН М. ЛЕОВАЦ³
и KATALIN MÉSZÁROS SZÉCSÉNYI³

¹*Metalurško-tehnološki fakultet, Podgorica, Crna Gora,* ²*Институт за нуклеарне науке "Винча",
Лабораторија за теоријску физику и физику кондензоване материје, Београд и*
³*Природно-математички факултет, Дејарман за хемију, Нови Сад*

Одређене су кристалне и молекулске структуре комплекса цинка(II) и живе(II) са 4-ацетил-3-амино-5-метилпиразолом (aamp) координационих формула $[\text{Zn}(\text{NCS})_2(\text{aamp})_2]$ и $(\text{Haamp})_2[\text{Hg}(\text{SCN})_4]$. Комплекс цинка(II) је добијен реакцијом топлих метанолних раствора смеше цинк(II)-нитрата и амонијум-тиоцијаната са aamp. Комплекс живе(II) настаје у реакцији топлог етанолног раствора aamp и топлог, слабо киселог воденог раствора $[\text{Hg}(\text{SCN})_4]^{2-}$. Оба комплекса имају тетраедарску геометрију, која се у случају комплекса цинка остварује монодентатном координацијом два молекула aamp и две изотиоцијанатне групе. Атоми Zn(II) и Hg(II) налазе се у знатно деформисаном координационом окружењу. У оба комплекса дериват пиразола има планарну форму која је вероватно стабилизована интрамолекулском N–H...O водоничном везом. Добијена једињења су, осим рендгенском структурном

анализом, окарактерисана елементалном анализом, IR-спектрометријом, кондуктометријским мерењима и термичком анализом.

(Примљено 2. јуна, ревидирано 4. октобра 2009)

REFERENCES

1. Y. A. Ivanenkov, K. V. Balakin, S. E. Tkachenko, *Drugs in R and D* **9** (2008) 397
2. M. J. Graneto, R. G. Kurumbail, M. L. Vazquez, Huey-Sheng Shieh, J. L. Pawlitz, J. M. Williams, W. C. Stallings, L. Geng, A. S. Naraian, F. J. Koszyk, M. A. Stealey, X. D. Xu, R. M. Weier, G. J. Hanson, R. J. Mourey, R. P. Compton, S. J. Mnich, G. D. Anderson, J. B. Monahan, R. Devraj, *J. Med. Chem.* **50** (2007) 5712
3. P. E. Almeida da Silva, D. F. Ramosa, H. G. Bonacorso, A. I. de la Iglesia, M. R. Oliveira, T. Coelho, J. Navarini, H. R. Morbidoni, N. Zanatta, M. A. P. Martins, *Int. J. Antimicrob. Agents* **32** (2008) 139
4. E. Reisner, V. B. Arion, B. K. Keppler, A. J. L. Pombeiro, *Inorg. Chim. Acta* **361** (2008) 1569
5. F. P. Pruchnik, P. Jakimowicz, Z. Ciunik, J. Zakrzewska-Czerwińska, A. Opolski, J. Wietrzyk, E. Wojdat, *Inorg. Chim. Acta* **334** (2002) 59
6. K. Sakai, Y. Tomita, T. Ue, K. Goshima, M. Ohminato, T. Tsubomura, K. Matsumoto, K. Ohmura, K. Kawakami, *Inorg. Chim. Acta* **297** (2000) 64
7. G. Lemaire, W. Mnif, J.-M. Pascussi, A. Pillon, F. Rabenoelina, H. Fenet, E. Gomez C. Casellas, J.-C. Nicolas, V. Cavaillès, M.-J. Duchesne, P. Balaguer, *Tox. Sci.* **91** (2006) 501
8. C. B. Vicentini, D. Mares, A. Tartari, M. Manfrini, G. Forlani, *J. Agric. Food Chem.* **52** (2004) 1898
9. N. Singh, N. K. Sangwan, K. S. Dhindsa, *Pest. Manag. Sci.* **56** (2000) 284
10. B. Barszcz, *Coord. Chem. Rev.* **249** (2005) 2259
11. J. Bol, *Ph.D. Thesis*, University Leiden, Leiden, Netherlands, 1997
12. N. E. Schore, *Study Guide and Solutions Manual for Organic Chemistry: Structure and Function*, 5th ed., W. H. Freeman and Company, 2007
13. V. M. Leovac, B. Holló, P. Bombicz, A. Kovács, K. Mészáros Szécsényi, Lj. S. Jovanović, G. Bogdanović, V. Kojić, M. D. Joksović, prepared for publication
14. V. M. Leovac, Z. D. Tomić, K. Mészáros Szécsényi, Lj. S. Jovanović, M. D. Joksović, *J. Serb. Chem. Soc.* **72** (2007) 1281
15. V. Yu. Kukushkin, E. A. Aleksandrova, V. M. Leovac, E. Z. Ivegeš, V. K. Belsky, V. M. Konovalov, *Polyhedron* **20** (1992) 2691
16. A. Hergold-Brundić, B. Kaitner, B. Kamenar, V. M. Leovac, E. Z. Ivegeš, N. Juranić, *Inorg. Chim. Acta* **188** (1991) 151
17. K. Mészáros Szécsényi, V. M. Leovac, Ž. K. Jaćimović, V. I. Češljević, A. Kovács, G. Pokol, S. Gál, *J. Therm. Anal. Cal.* **63** (2001) 723
18. *Enraf-Nonius CAD4 Software*, Version 5.0, Enraf-Nonius, Delft, The Netherlands, 1989
19. *CAD-4 Express Software*, Enraf-Nonius, Delft, The Netherlands, 1994
20. a) A. L. Spek, *Acta Crystallogr. A* **46** (1990) C34; b) A. L. Spek, *PLATON*, A. *Multi-purpose: Crystallographic Tool*, Utrecht University, Utrecht, The Netherlands, 1998
21. L. J. Farrugia, *J. Appl. Crystallogr.* **32** (1999) 837
22. A. L. Spek, *J. Appl. Cryst.* **36** (2003) 7
23. *Data collection and processing software*, Version 1, Oxford Diffraction Ltd., Oxford, 2006

24. G. M. Sheldrick, *Acta Crystallogr. A* **64** (2008) 112
25. M. Nardelli, *J. Appl. Crystallogr.* **28** (1995) 659
26. L. J. Farrugia, *J. Appl. Crystallogr.* **30** (1997) 565
27. W. J. Geary, *Coord. Chem. Rev.* **7** (1971) 81
28. K. Nakamoto, *Infrared and Raman Spectra of Inorganic and Coordination Compounds, Part B: Applications in Coordination, Organometallic, and Bioinorganic Chemistry*, 5th ed., Wiley, New York, 1997, p. 116
29. F. H. Allen, *Acta Crystallogr. B* **58** (2002) 380
30. Z. D. Tomić, Ž. K. Jaćimović, V. M. Leovac, V. I. Češljević, *Acta Crystallogr. C* **56** (2000) 777
31. R. G. Pearson, *J. Am. Chem. Soc.* **85** (1963) 3533
32. R. G. Pearson, *J. Chem. Educ.* **64** (1987) 561
33. G. R. Souza, I. A. Pastre, A. V. Benedetti, C. A. Ribeiro, F. L. Fertonani, *J. Therm. Anal. Cal.* **88** (2007) 127.



J. Serb. Chem. Soc. 74 (11) 1273–1282 (2009)
JSCS–3917

Journal of
the Serbian
Chemical Society

JSCS@tmf.bg.ac.rs • www.shd.org.rs/JSCS

UDC 547.652-304.4:546.562'742'472:
543.635.6

Original scientific paper

1-Naphthylazo derivatives of some 1,3-dicarbonyl compounds and their Cu(II), Ni(II) and Zn(II) complexes

K. KRISHNANKUTTY¹, MUHAMMED BASHEER UMMATHUR^{2*}
and PERUMPALLI UMMER¹

¹Department of Chemistry, University of Calicut, Kerala-673635 and ²Department of Chemistry, Unity Women's College, Manjeri, Kerala-676122, India

(Received 16. March, revised 12 July 2009)

Abstract: The coupling of diazotized 1-aminonaphthalene with 1,3-dicarbonyl compounds (acetylacetone, methylacetoacetate and acetoacetanilide) yielded a new series of bidentate ligand systems (HL). Analytical, IR, ¹H-NMR and mass spectral data indicate that the compounds exist in the intramolecularly hydrogen bonded keto-hydrazone form. With Ni(II), Cu(II) and Zn(II), these potential monobasic bidentate ligands formed [ML₂] type complexes. The IR, ¹H-NMR and mass spectral data of the complexes are consistent with the replacement of the chelated hydrazone proton of the ligand by a metal ion, thus leading to a stable six-membered chelate ring involving the hydrazone nitrogen and the hydrogen bonded carbonyl oxygen. The Ni(II) and Zn(II) chelates are diamagnetic, while the Cu(II) complexes are paramagnetic. In the metal complexes of the naphthylazo derivatives of acetylacetone and methylacetoacetate, the acetyl carbonyl is involved in coordination, whereas in the chelates of the naphthylazo derivative of acetoacetanilide, the anilide carbonyl is bonded with the metal ion.

Keywords: naphthylhydrazones; Cu(II), Ni(II) and Zn(II) complexes; IR, mass and NMR spectra.

INTRODUCTION

Coupling of 1,3-dicarbonyl compounds with the electrophile aryldiazonium ion provides the synthetic basis for a large number of technically important dye-stuffs.¹ These arylazo derivatives have gained considerable importance in recent years because of their application in the laboratory as acid-base, redox, metallochromic and other indicators,^{2–4} as stains for bacteriological and histological investigations,^{3–6} in the study of acid-base equilibrium and acidity constant values^{3,7} and in the preparation of a large number of biologically important hete-

* Corresponding author. E-mail: mbummathur@rediffmail.com

doi: 10.2298/JSC0911273K



rocyclic compounds.⁸ Many variations in the dicarbonyls as well as the diazonium salt have been studied in attempts to improve the colour, solubility and stability of the resulting dyes.⁹ The patent literature discloses seemingly endless combination of these arylazodicarbonyls and their metal complex dyestuffs. However, the structural aspect of many of these products and their metal derivatives has received only scant attention. In continuation of studies on arylazo derivatives of 1,3-dicarbonyl compounds and their metal complexes,^{10–15} the synthesis and characterization of 1-naphthylazo derivatives of three 1,3-dicarbonyl compounds: acetylacetone, methylacetoacetate and acetoacetanilide, is reported herein. Typical Cu(II), Ni(II) and Zn(II) complexes of these compounds were also synthesized and characterized.

EXPERIMENTAL

Methods, instruments and materials

The carbon, hydrogen and nitrogen contents were determined by microanalyses (Heraeus elemental analyzer from CDRI, Lucknow, India) and the metal contents of the complexes by AAS (Perkin Elmer 2380). The electronic spectra of the compounds in methanol (10^{-4} mol/L) were recorded on a 1601 Shimadzu UV–Vis spectrophotometer, the IR spectra (KBr discs) on an 8101 Shimadzu FTIR spectrophotometer, the $^1\text{H-NMR}$ spectra (CDCl_3 or $\text{DMSO-}d_6$) on a Varian 300 NMR spectrometer and the mass spectra on a Jeol/SX-102 mass spectrometer (FAB using Argon and *meta*-nitrobenzyl alcohol as the matrix). The molar conductance of the complexes was determined in DMF ($\approx 10^{-3}$ mol/L) at 28 ± 1 °C. The magnetic susceptibilities were determined at room temperature on a Guoy type magnetic balance. Corrections for diamagnetism of the constituents were realised using Pascal's constants.¹⁶

Acetylacetone, methylacetoacetate, acetoacetanilide, 1-aminonaphthalene, methanol, urea and metal acetates used were of Merck AR grade, Germany.

Synthesis of naphthylhydrazones, Hnaa, Hnma and Hnan

1-Aminonaphthalene was diazotized as reported.¹⁷ After destroying the excess nitrous acid with urea, the diazonium salt solution (0.010 mol) was added drop wise with stirring to an ice-cold methanolic solution of the required 1,3-dicarbonyl compound (0.010 mol, 50 mL). Concentrated sodium acetate solution was simultaneously added to maintain the pH of the solution at around 6. The formed precipitate was filtered, washed with cold deionized water and recrystallized from hot ethanol to obtain chromatographically pure material (TLC – silica gel, chloroform).

Synthesis of the Ni(II), Cu(II) and Zn(II) complexes

A solution of the metal salt (0.010 mol) in a minimum amount of water was added to a solution of the ligand in methanol (0.020 mol, 25 mL). The mixed solution was refluxed on a boiling water bath for ≈ 12 h. The pH of the solution was maintained around 8 by the addition of sodium acetate. The volume was reduced to half and the remaining solution cooled in an ice bath. The formed crystals were filtered, washed with water, recrystallized from hot ethanol and dried under vacuum.

RESULTS AND DISCUSSION

The elemental analytical data of the naphthylhydrazones (Table I) indicate that coupling between diazotized 1-aminonaphthalene and the 1,3-dicarbonyl compounds occurred in a 1:1 molar ratio. All the compounds were crystalline in nature and were soluble in common organic solvents. They formed stable complexes with Ni(II), Cu(II) and Zn(II) ions. Their analytical data (Table I) together with their non-electrolytic nature in DMF (specific conductance $< 10 \text{ S cm}^{-1}$; 10^{-3} M solution) suggest $[\text{ML}_2]$ stoichiometry of the complexes. The Ni(II) and Zn(II) chelates were diamagnetic, while Cu(II) complexes showed normal paramagnetic moments (μ_{eff} , 1.75–1.80 μ_{B}). The observed electronic, IR, $^1\text{H-NMR}$ and mass spectral data are in conformity with the structures of Hnaa and Hnma and of their complexes given in Figs. 1 and 2, respectively. The analytical and spectral data of Hnan and its complex are in agreement with the structure given Figs. 3 and 4, respectively. These data of the compounds are discussed separately.

TABLE I. Physical and analytical data of Hnaa, Hnma, Hnan and their metal complexes

Compound	Yield %	M.p. °C	Elemental analysis: Found (Calculated), %			
			C	H	N	M
Hnaa ^a , C ₁₅ H ₁₄ N ₂ O ₂	80	110	70.71 (70.87)	5.44 (5.51)	11.08 (11.02)	–
Hnma ^b , C ₁₅ H ₁₄ N ₂ O ₃	75	140	66.80 (66.67)	5.17 (5.19)	10.45 (10.37)	–
Hnan ^c , C ₂₀ H ₁₇ N ₃ O ₂	80	150	72.67 (72.51)	5.12 (5.14)	12.71 (12.69)	–
[Ni(naa ^d) ₂], C ₃₀ H ₂₆ N ₄ NiO ₄	70	270	63.59 (63.75)	4.62 (4.60)	9.84 (9.92)	10.34 (10.40)
[Ni(nma ^d) ₂], C ₃₀ H ₂₆ N ₄ NiO ₆	72	204	60.24 (60.33)	4.33 (4.36)	9.28 (9.38)	9.92 (9.83)
[Ni(nan ^d) ₂], C ₄₀ H ₃₂ N ₆ NiO ₄	75	210	66.91 (66.79)	4.42 (4.45)	11.54 (11.69)	8.12 (8.17)
[Cu(naa) ₂], C ₃₀ H ₂₆ CuN ₄ O ₄	65	190	63.30 (63.21)	4.51 (4.57)	9.64 (9.83)	11.25 (11.16)
[Cu(nma) ₂], C ₃₀ H ₂₆ CuN ₄ O ₆	70	180	59.72 (59.84)	4.32 (4.32)	9.26 (9.31)	10.48 (10.56)
[Cu(nan) ₂], C ₄₀ H ₃₂ CuN ₆ O ₄	75	200	66.52 (66.34)	4.36 (4.42)	11.54 (11.61)	8.60 (8.78)
[Zn(naa) ₂], C ₃₀ H ₂₆ N ₄ O ₄ Zn	68	182	63.10 (63.00)	4.53 (4.55)	9.70 (9.80)	11.50 (11.44)
[Zn(nma) ₂], C ₃₀ H ₂₆ N ₄ O ₆ Zn	70	160	59.54 (59.66)	4.32 (4.31)	9.19 (9.28)	10.78 (10.84)
[Zn(nan) ₂], C ₄₀ H ₃₂ N ₆ O ₄ Zn	65	180	66.32 (66.17)	4.44 (4.41)	11.50 (11.58)	9.02 (9.01)

^a1-naphthylazo(acetylacetone); ^b1-naphthylazo(methylacetoacetate); ^c1-naphthylazo(acetoacetanilide); ^dnaa, nma, nan = deprotonated ligands

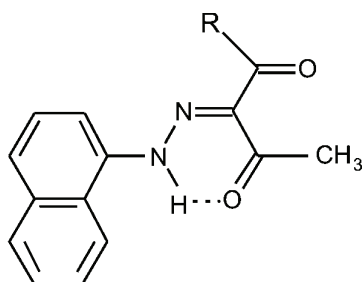


Fig. 1. Structure of Hnaa and Hnma; R = $-\text{CH}_3$ and $-\text{OCH}_3$ for Hnaa and Hnma, respectively.

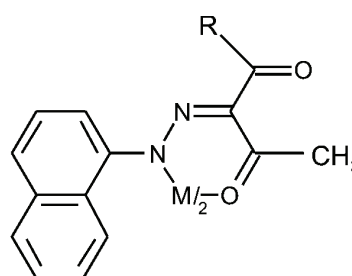


Fig. 2. Structure of the metal complexes of Hnaa and Hnma (M = Ni(II), Cu(II), Zn(II)).

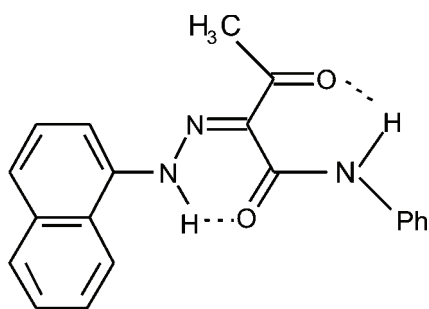


Fig. 3. Structure of Hnan.

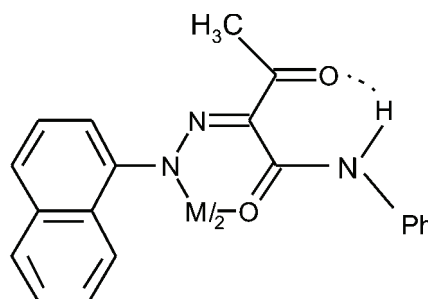


Fig. 4. Structure of the metal complexes of Hnan (M = Ni(II), Cu(II), Zn(II)).

Characterization of Hnaa, Hnma and their complexes

IR Spectra. The IR spectra of Hnaa and Hnma in the 1600–1800 cm^{-1} region both showed strong bands at 1678 and 1722 cm^{-1} due to the stretching of the free acetyl and ester carbonyls, respectively.^{13,14} The spectra also showed a strong band at $\approx 1630 \text{ cm}^{-1}$ and a medium intensity band at $\approx 1620 \text{ cm}^{-1}$, assignable to the stretching of intramolecularly hydrogen bonded acetyl carbonyl and C=N vibrations, respectively^{18,19} (Fig. 1). The broad band in the range 2500–3500 cm^{-1} indicates the existence of strong intramolecular hydrogen bonding in these compounds. In the spectra of all the complexes, the free carbonyl and C=N bands remained almost unaffected, suggesting that they were not involved in the coordination. However, the band due to the hydrogen bonded acetyl carbonyl at $\approx 1630 \text{ cm}^{-1}$ of the ligands disappeared and a new strong band assignable to the stretching of a metal bonded carbonyl group appeared at $\approx 1570 \text{ cm}^{-1}$. The spectra showed several medium intensity bands in the range 1580–1600 cm^{-1} due to various C=C vibrations. The broad band in the range 2500–3500 cm^{-1} of the ligands disappeared in the spectra of all the complexes and bands due to various $\nu(\text{C-H})$ vibrations appeared. This strongly supports the replacement of the chelated proton of the ligands by a metal ion, as shown in Fig. 2. The prominent band present at $\approx 1525 \text{ cm}^{-1}$ of the ligands, due to $\nu(\text{N-H})$ vibration, disappeared in the spectra of all the complexes as the consequence of the replacement of the hydrazone NH proton with a metal ion. The hydrazone nitrogen and the intramolecularly hydrogen bonded carbonyl oxygen participate in coordination, as evidenced by the two additional medium intensity bands at ≈ 420 and $\approx 550 \text{ cm}^{-1}$, assignable to $\nu(\text{M-O})$ and $\nu(\text{M-N})$ vibrations, respectively,²⁰ in the spectra of the complexes. Important bands in the IR spectra are given in Table II.

$^1\text{H-NMR}$ Spectra. The $^1\text{H-NMR}$ spectra of Hnaa and Hnma are both characterized by the presence of a low field, two proton signal at $\approx \delta 15 \text{ ppm}$ due to the N-H \cdots O=C group.^{21,22} The integrated intensities of all the signals agree well with the representation of the compounds given in Fig. 1. In the $^1\text{H-NMR}$ spectra of the diamagnetic Ni(II) and Zn(II) complexes, the low field signal due to the

TABLE II. Characteristic IR stretching bands (cm^{-1}) of Hnaa, Hnma, Hnan and their metal complexes (abbreviations as in Table I)

Compound	Free (C=O)	Chelated (C=O)	(C=N)	(M-N)	(M-O)
Hnaa	1678	1632	1618	–	–
[Ni(naa) ₂]	1675	1574	1612	562	428
[Cu(naa) ₂]	1672	1568	1614	548	428
[Zn(naa) ₂]	1670	1565	1615	550	425
Hnma	1722	1628	1615	–	–
[Ni(nma) ₂]	1718	1575	1617	545	432
[Cu(nma) ₂]	1718	1568	1618	534	420
[Zn(nma) ₂]	1720	1564	1616	530	420
Hnan	–	1645, 1635	1620	–	–
[Ni(nan) ₂]	–	1562, 1635	1618	560	426
[Cu(nan) ₂]	–	1568, 1635	1614	548	425
[Zn(nan) ₂]	–	1556, 1635	1616	558	420

chelated hydrogen disappeared, indicating the replacement of the hydrazone proton with a metal ion during coordination.²³ The positions of the methyl proton signals indicate that the acetyl carbonyl is involved in the coordination. The integrated intensities of all other protons are in agreement with the schematic view presented in Fig. 2 (Table III).

TABLE III. ¹H-NMR spectral data (δ / ppm) of Hnaa, Hnma, Hnan and their Ni(II) and Zn(II) complexes (abbreviations as in Table I)

Compound	CH ₃ CO	RCO	Naphthyl	NH
Hnaa	2.56 (3H, s)	2.44 (3H, s)	7.14–7.87 (7H, m)	15.82 (1H, s, br)
[Ni(naa) ₂]	2.86 (6H, s)	2.38 (6H, s)	7.10–7.82 (14H, m)	–
[Zn(naa) ₂]	2.90 (6H, s)	2.33 (6H, s)	6.98–7.77 (14H, m)	–
Hnma	2.48 (3H, s)	3.88 (3H, s)	7.12–7.95 (7H, m)	15.05 (1H, s, br)
[Ni(nma) ₂]	2.82 (6H, s)	3.84 (6H, s)	7.14–7.92 (14H, m)	–
[Zn(nma) ₂]	2.88 (6H, s)	3.82 (6H, s)	7.04–7.90 (14H, m)	–
Hnan	2.65 (3H, s)	7.05–8.12 ^a (m)		15.85 (1H, s, br), 11.78 (1H, s)
[Ni(nan) ₂]	2.67 (6H, s)	7.08–8.02 ^a (m)		11.62 (2H, s)
[Zn(nan) ₂]	2.62 (6H, s)	7.02–8.12 ^a (m)		11.66 (2H, s)

^aDue to anilide and naphthyl groups

Mass spectra. The formulation of the compounds as in Fig. 1 is clearly supported by the presence of an intense molecular ion peak in the mass spectra. Since peaks due to the elimination of ArN₂,^{24,25} a characteristic feature of the azo tautomer, were not observed in the mass spectra indicates the existence of the compounds in the hydrazone form. Other important peaks resulted from the elimination of CH₃CO, RCO, *etc.* from the molecular ion or subsequent fragments. The FAB mass spectra of the Cu(II) complexes showed molecular ion peaks of appreciable intensity corresponding to [CuL₂] stoichiometry. Peaks correspond-

ing to the elimination of CH_3CO , RCO , dicarbonyl moieties *etc.* from the molecular ion were also present in the spectra. The spectra of all the chelates possess a number of fragments containing copper in the natural 3:1 abundance of the ^{63}Cu and ^{65}Cu isotopes (Table IV).

TABLE IV. Mass spectral data of Hnaa, Hnma, Hnan and their Cu(II) complexes (abbreviations as in Table I)

Compound	<i>m/z</i>
Hnaa	254, 211, 168, 142, 127
Hnma	270, 227, 211, 168, 142, 127
Hnan	331, 288, 211, 168, 142, 127
[Cu(naa) ₂]	571, 569, 528, 526, 485, 483, 442, 440, 429, 427, 399, 397, 386, 384, 318, 316, 287, 285, 254, 244, 242, 211, 201, 199, 142
[Cu(nma) ₂]	603, 601, 560, 558, 517, 515, 544, 542, 485, 483, 461, 459, 442, 440, 402, 400, 399, 397, 343, 341, 334, 332, 319, 317, 270, 168, 142
[Cu(nan) ₂]	725, 723, 682, 680, 639, 637, 633, 631, 605, 603, 583, 581, 497, 495, 485, 483, 441, 439, 395, 393, 355, 353, 343, 341, 331, 288, 168, 127, 120

Electronic spectra. The UV spectra of Hnaa and Hnma show two absorption maxima at ≈ 380 nm and ≈ 250 nm due to various $n \rightarrow \pi^*$ and $\pi \rightarrow \pi^*$ transitions. In the spectra of the complexes, these absorption maxima were shifted to appreciably lower wave numbers. The Cu(II) complexes had a broad visible band with a maximum at ≈ 15000 cm^{-1} . This fact, together with the μ_{eff} values (1.75–1.80 μ_{B}) were ascribed to the square-planar geometry of the complexes. The observed diamagnetism and the broad medium-intensity band at ≈ 17600 cm^{-1} in the spectra of the Ni(II) chelates also suggested their square-planar geometry. Moreover, the spectra of the chelates in pyridine solution (10^{-3} mol/L) showed three bands corresponding to a configurational change to octahedral due to the association of pyridine.²⁶

Characterization of Hnan and its complexes

IR Spectra. The IR spectrum of Hnan in the 1650 – 1800 cm^{-1} region had no band assignable to free carbonyl groups. However, there were two strong bands at 1645 and 1635 cm^{-1} due to the stretching of intramolecularly hydrogen bonded anilide and acetyl carbonyl groups, respectively.^{13,14} There was also a medium intensity band at 1620 cm^{-1} , assignable to the C=N stretching vibration.^{18,19} The broad band in the range 2500 – 3200 cm^{-1} indicates the existence of strong intramolecular hydrogen bonding in the compound, as shown in Fig. 3. In the spectra of all the complexes, the acetyl carbonyl and C=N bands remained almost unaffected, indicating that they were not involved in the coordination. However, the band due to the hydrogen bonded anilide carbonyl at 1645 cm^{-1}

disappeared and instead a new strong band appeared at $\approx 1560\text{ cm}^{-1}$, assignable to the stretching of a metal bonded carbonyl group. The spectra showed several medium intensity bands in the range $1580\text{--}1600\text{ cm}^{-1}$ due to various C=C vibrations. As in the spectrum of the ligand, the complexes showed a band at 3380 cm^{-1} due to the NH group of the anilide moiety in their structure. A prominent band present at 1528 cm^{-1} in the spectrum of the ligand due to the hydrazone $\nu(\text{N-H})$ vibration was absent in the spectra of all the complexes. These indicate that the hydrazone NH proton had been replaced by the metal ion, while the anilide NH proton remained unchanged. It is evident that the hydrazone nitrogen and the intramolecularly hydrogen bonded carbonyl oxygen were involved in the complexation from the appearance of two additional medium intensity bands at ≈ 420 and $\approx 550\text{ cm}^{-1}$, assignable to $\nu(\text{M-O})$ and $\nu(\text{M-N})$ vibrations,²⁰ in the spectra of the complexes. Important bands found in the spectra are given in Table II.

¹H-NMR Spectra. The ¹H-NMR spectrum of Hnan is characterized by the presence of two low field signals corresponding to one proton at δ 15.85 and 11.78 ppm due to intramolecularly hydrogen bonded hydrazone and anilide NH protons.^{21,22} The integrated intensities of all the signals are in accordance with the compound presentation in Fig. 3. In the ¹H-NMR spectra of the diamagnetic Ni(II) and Zn(II) complexes, the low field signal due to the chelated hydrazone proton disappeared while the anilide proton remained unchanged, indicating the replacement of the hydrazone proton with a metal ion during coordination, whereas the anilide NH was excluded from the coordination.²³ The position of the methyl proton signals indicates that the acetyl carbonyl does not participate in coordination. The integrated intensities of all other protons are in agreement with the presentation in Fig. 4 (Table III).

Mass spectra. The structure of the compound shown in Fig. 3 is clearly supported by the presence of an intense molecular ion peak at m/z 331 in the mass spectrum. Since the peak due to the elimination of ArN_2 ,^{24,25} a characteristic feature of the azo tautomer, was not observed in the mass spectrum; thus the existence of the compound in the hydrazone form was assumed. The other important peaks found were due to the elimination of CH_3CO , $\text{C}_6\text{H}_5\text{NHCO}$, etc. from the molecular ion or subsequent fragments. The FAB mass spectrum of the Cu(II) complex showed the molecular ion peak of appreciable intensity corresponding to $[\text{CuL}_2]$ stoichiometry. Peaks corresponding to the elimination of CH_3CO , $\text{C}_6\text{H}_5\text{NHCO}$, dicarbonyl moieties, etc. from the molecular ion are also present in the spectrum. The spectrum of the chelate had a number of fragments containing copper in the 3:1 natural abundance of ⁶³Cu and ⁶⁵Cu isotopes (Table IV).

Electronic spectra. The UV spectrum of Hnan showed two absorption maxima at 370 and 260 nm due to the various $n\rightarrow\pi^*$ and $\pi\rightarrow\pi^*$ transitions. In the complexes, these maxima were shifted to appreciably lower wave numbers. The Cu(II) complex showed a broad visible band, with a maximum at 14850 cm^{-1} .

This, together with the μ_{eff} value (1.77 μ_B), suggests a square-planar geometry. The observed diamagnetism and broad medium-intensity band at 17,650 cm^{-1} in the spectrum of the Ni(II) chelate suggested square-planar geometry. In addition, the spectrum of the chelate in pyridine solution (10^{-3} mol/dm³) showed three bands, corresponding to a configurational change to octahedral due to the association of pyridine.²⁶ The three well-separated absorption maxima at 8230, 13570 and 24360 cm^{-1} corresponded to the transitions ${}^3A_{2g} \rightarrow {}^3T_{2g}$; ${}^3A_{2g} \rightarrow {}^3T_{1g}(\text{F})$ and ${}^3A_{2g} \rightarrow {}^3T_{1g}(\text{P})$, respectively.

CONCLUSIONS

A new series of bidentate ligands were prepared by the coupling of diazotized 1-aminonaphthalene with acetylacetone, methylacetoacetate and acetoacetanilide (HL). The analytical, IR, ¹H-NMR and mass spectral data revealed a 1:1 product in which one of the carbonyl group of the dicarbonyl compound was involved in intramolecular hydrogen bonding with the hydrazone hydrogen. The analytical, physical and spectral data of their [ML₂] complexes with Cu(II), Ni(II) and Zn(II) showed monobasic bidentate N,O coordination involving one of the hydrazone nitrogen atoms and the carbonyl oxygen. In the metal complexes of the naphthylazo derivatives of acetylacetone and methylacetoacetate, the acetyl carbonyl was involved in the coordination, whereas in the chelates of the naphthylazo derivative of acetoacetanilide, the anilide carbonyl was bonded with the metal ion.

ИЗВОД

1-НАФТИЛАЗО ДЕРИВАТИ НЕКИХ 1,3-ДИКАРБОНИЛНИХ ЈЕДИЊЕЊА И ЊИХОВИ Cu(II), Ni(II) И Zn(II) КОМПЛЕКСИ

K. KRISHNANKUTTY¹, MUHAMMED BASHEER UMMATHUR² и PERUMPALLI UMMER¹

¹Department of Chemistry, University of Calicut, Kerala-673635 и ²Department of Chemistry, Unity Women's College, Manjeri, Kerala-676122, India

Купловањем диазотованог 1-аминонафталена са 1,3-дикарбонилним једињењима (ацетилацетоном, метилацетоацетатом и ацетоацетанилидом) добијена је нова серија бидентатних лиганата (HL). Аналитички, IR, ¹H-NMR и масени спектрални подаци указују да једињења постоје у интрамолекуларски водонично-везаном кето-хидразонском облику. Ови потенцијално монобазни бидентатни лиганди са Ni(II), Cu(II) и Zn(II) граде [ML₂] тип комплекса. IR, ¹H-NMR и масени спектрални подаци комплекса су у складу са заменом хелатног хидразонског протона металним јоном, при чему настаје стабилан шесточлани хелатни прстен који укључује хидразонски азот и водонично везан карбонилни кисеоник. Хелати Ni(II) и Zn(II) су дијамагнетични, док су Cu(II) комплекси парамагнетични. У металним комплексима нафтилазо деривата ацетилацетона и метилацетоацетата, ацетил карбонил је укључен у координацију, док је у хелатима нафтилазо деривата ацетоацетанилида анилидни карбонил везан за метални јон.

(Примљено 16. марта, ревидирано 12. јула 2009)

REFERENCES

1. a) E. V. Shchegol'kov, Y. V. Burgart, V. I. Saloutin, *J. Fluor. Chem.* **128** (2007) 779; b) O. G. Khudina, Y. V. Burgart, V. I. Saloutin, O. N. Chupakhin, *J. Fluor. Chem.* **125** (2004) 401; c) O. G. Khudina, N. V. Murashova, Y. V. Burgart, V. Saloutin, *Mendeleev Commun.* **13** (2003) 228; d) E. V. Dontsova, V. V. Lukov, V. A. Kogan, L. D. Popov, *Russian J. Coord. Chem.* **29** (2003) 639; e) O. G. Khudina, Y. V. Burgart, N. V. Murashova, V. I. Saloutin, *Russian J. Org. Chem.* **39** (2003) 1421; f) W. H. Hegazy, *Monatsh. Chem.* **132** (2001) 639
2. C. S. Salazar, M. I. Toral, *J. Chilean Chem. Soc.* **49** (2004) 169
3. M. S. Masoud, G. B. Mohamed, Y. H. Abdul-Razek, A. E. Ali, F. N. Khairy, *J. Korean Chem. Soc.* **46** (2002) 99
4. J. J. Arias, F. Jiménez, A. I. Jiménez, F. G. Montelongo, *Anales de Química* **79** (1983) 248
5. F. G. Montelongo, V. G. Díaz, C. R. T. González, *Microchem. J.* **27** (1982) 194
6. M. I. Toral, P. Richter, N. Lara, M. T. Escudero, C. Soto, *Anal. Lett.* **33** (2000) 93
7. V. G. Díaz, C. R. T. González, F. G. Montelongo, *Anales de Química* **79** (1983) 83
8. I. V. Kravtsov, P. A. Belyakov, S. V. Baranin, V. A. Dorokhov, *Russ. Chem. Bull.* **56** (2007) 1561
9. E. Bishop, *Indicators, International Series of Monographs in Analytical Chemistry*, Vol. 51, Pergamon Press, Oxford, 1972
10. K. Krishnankutty, M. B. Ummathur, D. K. Babu, *Inorg. Chem., Indian J.* **4** (2009) 83
11. a) K. Krishnankutty, P. Sayudevi, M. B. Ummathur, *J. Indian Chem. Soc.* **85** (2008) 48; b) K. Krishnankutty, P. Sayudevi, M. B. Ummathur, *J. Indian Chem. Soc.* **84** (2007) 518; c) K. Krishnankutty, P. Sayudevi, M. B. Ummathur, *J. Indian Chem. Soc.* **84** (2007) 337; d) K. Krishnankutty, P. Sayudevi, M. B. Ummathur, *J. Serb. Chem. Soc.* **72** (2007) 1075
12. K. Krishnankutty, D. K. Babu, *J. Indian Chem. Soc.* **73** (1996) 379
13. K. Krishnankutty, V. T. Rema, *Synth. React. Inorg. Met.-Org. Chem.* **25** (1995) 243
14. a) K. Krishnankutty, J. Michael, *J. Indian Chem. Soc.* **70** (1993) 238; b) K. Krishnankutty, J. Michael, *J. Coord. Chem.* **28** (1993) 259; **22** (1990) 327
15. a) K. Krishnankutty, P. Ummer, *J. Indian Chem. Soc.* **66** (1989) 194; b) K. Krishnankutty, P. Ummer, *J. Indian Chem. Soc.* **65** (1988) 213
16. E. König, *Magnetic Properties of Coordination and Organometallic Transition Metal Compounds*, Springer-Verlag, Berlin, 1966
17. K. H. Saunders, R. L. M. Allen, *Aromatic Diazo Compounds*, 3rd ed., Edward Arnold, London, 1985
18. L. J. Bellamy, *The Infrared Spectra of Complex Molecules*, Chapman and Hall, London, 1980
19. C. N. R. Rao, *Chemical Applications of Infrared Spectroscopy*, Academic Press, London, 1963
20. N. Nakamoto, *Infrared Spectra and Raman Spectra of Inorganic and Coordination Compounds*, Wiley, New York, 1997
21. A. Mitchell, D. C. Nonhebel, *Tetrahedron* **35** (1979) 2013
22. A. Lycka, J. Jirman, A. Cee, *Magnetic Resonance Chem.* **28** (1990) 408
23. A. G. Evans, J. C. Evans, B. A. El-Shetary, C. C. Rowlands, P. H. Morgan, *J. Coord. Chem.* **9** (1979) 19

24. H. Budzikiewicz, C. Djerassi, D. H. Williams, *Mass Spectrometry of Organic Compounds*, Holden Day, San Francisco, 1967
25. a) K. Kobayashi, K. Kurishara, K. Hirose, *Bull. Chem. Soc. Jpn.* **45** (1972) 3551; b) D. Betteridge, D. John, *Talanta* **15** (1968) 1227; c) H. Nakata, A. Tatematsu, *Bull. Chem. Soc. Jpn.* **42** (1969) 1678
26. K. C. Joshi, V. N. Pathak, *Coord. Chem. Rev.* **22** (1977) 37.



J. Serb. Chem. Soc. 74 (11) 1283–1292 (2009)
JSCS–3918

T-2 toxin adsorption by hectorite

ALEKSANDRA DAKOVIĆ^{1*}, ŽIVKO SEKULIĆ¹, GEORGE E. ROTTINGHAUS²,
ANA STOJANOVIĆ¹, SONJA MILIČEVIĆ¹ and MILAN KRAGOVIĆ¹

¹Institute for Technology of Nuclear and Other Mineral Raw Materials, P.O. Box 390,
11000 Belgrade, Serbia and ²Veterinary Medical Diagnostic Laboratory, College
of Veterinary Medicine, University of Missouri, Columbia, MO 65211, USA

(Received 4 February 2009)

Abstract: The adsorption of T-2 toxin by the natural smectite mineral – hectorite at pH 3.0, 7.0 and 9.0 was investigated. The results of T-2 toxin adsorption on hectorite showed that the T-2 adsorption capacity decreased with increasing concentration of adsorbent in the suspension for all the investigated pH values. From the adsorption isotherms, an increase in T-2 toxin adsorption with increasing initial T-2 toxin concentration was observed for all the investigated pH values. The T-2 toxin adsorption by hectorite followed a non-linear (Langmuir) type of isotherm at pH 3.0, 7.0 and 9.0, with correlation coefficients (r^2) of 0.943 at pH 3.0, 0.919 at pH 7.0 and 0.939 at pH 9.0. The estimated maximum T-2 toxin adsorption by hectorite based on the Langmuir fit to the data (9.178 mg/g at pH 3.0, 9.930 mg/g at pH 7.0, and 19.341 mg/g at pH 9.0), indicated that the adsorption of T-2 toxin by hectorite is pH dependent. The obtained data suggest the existence of specific active sites in hectorite onto which the T-2 toxin is adsorbed.

Keywords: smectite; hectorite; mycotoxins; T-2 toxin; adsorption.

INTRODUCTION

The contamination of animal feed with mycotoxins represents a worldwide problem leading to economic losses in animal production. The most common naturally occurring mycotoxins are the aflatoxins, ochratoxins, fumonisins, trichothecenes, zearalenone and ergopeptine alkaloids. Trichothecenes constitute the largest group of *Fusarium* mycotoxins and are commonly found on cereals, such as wheat, barley, oats and corn. These cereals are commonly used in animal feed, thus, possibly, exposing livestock to relatively high levels of trichothecenes. Trichothecenes have a closely related sesquiterpenoid ring structure with a 12,13 epoxy ring and a number of hydroxyl, acetoxy or other substituents. T-2 toxin is one of the most acutely toxic trichothecenes and causes reduction in feed con-

* Corresponding author. E-mail: a.dakovic@itnms.ac.rs
doi: 10.2298/JSC0911283D

sumption and weight gain and severe oral lesions in broilers,^{1–3} The chemical structure of T-2 toxin is presented in Fig. 1.

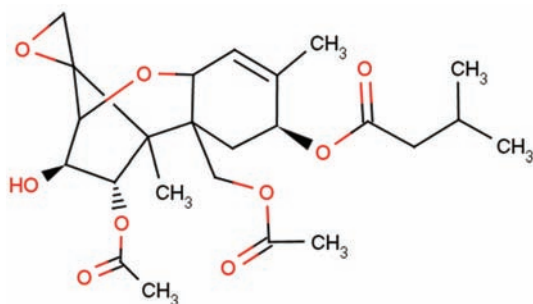


Fig. 1. Chemical structure of the T-2 toxin.

The most promising and economical approach for detoxifying mycotoxin contaminated feedstuffs is the addition of non-nutritive adsorbent materials to the diet, thus reducing gastrointestinal absorption of mycotoxins. Examples are activated carbon (AC), smectite minerals, zeolites and special polymers⁴ The efficiency of mycotoxin adsorbents differs considerably depending on the chemical structure of both the toxin and adsorbent. Thus, the binding efficacy of adsorbents is dependent on their crystal structures and physical properties (the total charge and charge distribution, the size of the pores, accessible surface area, *etc.*), as well as on the physico-chemical properties of the mycotoxins (polarity, solubility, shape, charge distribution, dissociation constants, *etc.*).⁵ It is well known that some of the extensively studied adsorbents such as smectite minerals – hydrated sodium calcium aluminosilicates (HSCAS) and zeolites – clinoptilolites are very effective in adsorbing aflatoxins, both *in vitro* and *in vivo*.^{6,7} However, their negatively-charged surfaces are not effective in preventing the toxic effects of *Fusarium* mycotoxins, such as fumonisins, trichothecenes or zearalenone. Avantiato *et al.*⁴ tested twenty-one adsorbent materials (AC, cholestyramine, Standard Q/FIS, Myco Ad A-Z, Mycofix Plus, Mycosorb, *etc.*) for the binding of fumonisin B1 (FB1), zearalenone (ZEA), and trichothecenes – deoxynivalenol (DON) and nivalenol (NIV) under *in vitro* conditions and found that AC showed the best binding activity, adsorbing 100 % of FB1 and ZEA, and a moderate amount of DON and NIV (>50 %). It is well known that chemical treatment of phyllosilicate clays and zeolites with long chain organic cations, *i.e.*, cetylpyridinium (CP), hexadecyltrimethylammonium (HDTMA) or octadecyldimethylbenzylammonium (ODMBA) ions results in an increased hydrophobicity of the mineral surface, providing a high affinity for hydrophobic organic molecules, such as the majority of the mycotoxins.^{8–10} In previous studies, it was shown that natural clinoptilolite and montmorillonite were effective in adsorbing aflatoxin B1,^{11,12} while surfactant modified zeolites had a high affinity for ZEA,¹³ ochratoxin A,¹⁴ and FB1.¹⁵

In addition to montmorillonite and zeolites, kaolinite and hectorite are commonly used industrial minerals.¹⁶ Hectorite is a 2:1 smectite clay, which is composed of units made up of two tetrahedral sheets with a central Mg octahedral sheet. It has permanent negative charges that arise due to the isomorphous substitution of Li⁺ for Mg²⁺. The negative charge is counterbalanced by the presence of inorganic cations.^{8,16,17} It is well known that hectorite has been used as an adsorbent for color removal of basic dyes and metal ions,¹⁸ while organically modified hectorites may be used as an adsorbent for the removal of anionic dyes, organic compounds and pesticides, *etc.*^{19,20} Recently, hectorite was considered as an adsorbent for ZEA detoxification, but high adsorption of this toxin was observed only when hectorite was used in combination with AC. Namely, the results of *in vitro* studies by Afriyie–Gyawu *et al.*²¹ showed that AC was the most efficient adsorbent for ZEA (adsorption index 99 %), followed by a combination of 2 parts of AC plus 3 parts of hectorite (HEC) (69 %), CP-exchanged low-pH montmorillonite (58 %), hexadecyltrimethylammonium-exchanged low-pH montmorillonite (54 %), and HEC alone (28 %). To the best of our knowledge, there are no data in the scientific literature on the efficacy of hectorite to bind trichothecenes mycotoxins.

The objective of the current study was to investigate the efficiency of the natural smectite mineral hectorite for *in vitro* adsorption of T-2 toxin at pH 3.0, 7.0 and 9.0.

EXPERIMENTAL

Hectorite (Hector, California) was obtained from the Mine-Engineering Com. (2286 E Carson St, #437 Long Beach, CA 90807, USA). The sample was dried at 60 °C and ground to yield particles smaller than 63 µm.

The cation exchange capacity (CEC) of the hectorite was measured with 1 M NH₄Cl.

The mineralogical composition of the starting sample was determined by X-ray powder diffraction analysis, XRPD, performed using a Philips PW-1710 diffractometer with monochromatic Cu-K α radiation, in the 2θ range 4–60°.

Investigations of the surface morphology of the hectorite were performed using a LINK AN 1000 EDS microanalyzer attached to a JEOL JSM – 6460 LV Scanning Electron Microscope (SEM). The accelerating potential was 15 kV, the beam current 3 nA, the surface electron beam measured 1 mm² and the counting time was 1250 s. ZAF-4/FLS software provided by LINK was used for corrections.

The hectorite was used without pretreatment for the T-2 toxin adsorption studies. A primary T-2 toxin stock solution (1000 ppm) was prepared in ethanol. The T-2 toxin test solutions for the adsorption studies were prepared by adding ethanol stock solution to 0.10 M phosphate buffer adjusted to pH 3.0, 7.0 and 9.0. Duplicate aliquots of 0.10 M phosphate buffer containing 10 ppm of T-2 toxin (10 mL) were added to 15 mL polypropylene Falcon tubes to which 100, 20, 10 or 5 mg of hectorite had been added. In order to eliminate exogenous peaks, controls were prepared by adding 10 mL of 0.10 M phosphate buffer plus 10 mg of hectorite to Falcon tubes. For investigations of the adsorption isotherms of T-2 toxin on hectorite, a 10 mL aliquot of T-2 toxin (4.0–10 mg L⁻¹) in buffer was added to 15 mL Falcon

tubes together with 10 mg of adsorbent. The adsorption isotherms for hectorite were examined at pH, 3.0, 7.0 and 9.0 with each sample being done in duplicate. The tubes were placed on a rotatory shaker for 30 min at room temperature (based on initial studies, data not shown). Each T-2 toxin test solution and control was centrifuged at 13000 rpm for 5 min and 2 mL of the aqueous supernatant was removed for HPLC analysis. An aliquot of the original buffered T-2 toxin test solution was used as the HPLC standard. HPLC analyses were performed on Hypersil C18-BDS column ((250×4.60) mm, 5 µm particle size) using a Hitachi L-7100 pump with a Hitachi L-7200 autosampler, and UV detection with a Hitachi L-7400 UV detector ($\lambda = 212$ nm). The mobile phase was acetonitrile:water (50:50) pumped at a flow rate of 1.0 mL min⁻¹. Data were recorded and processed using a Hitachi D-7000 data acquisition package with Concert Chrom software on a microcomputer. The percent bound T-2 toxin was calculated from the difference between the initial and final T-2 toxin concentration in the aqueous supernatant after equilibrium.

RESULTS AND DISCUSSION

The cation exchange capacity (CEC) of the hectorite was 0.892 meq g⁻¹, measured with 1.0 M NH₄Cl. Sodium was the dominant ion in the exchangeable positions (0.774 meq g⁻¹), while magnesium (0.094 meq g⁻¹), lithium (0.018 meq g⁻¹), and potassium (0.006 meq g⁻¹) were present at very low levels in the exchangeable positions of the hectorite. The chemical composition of the hectorite is presented in Table I.

TABLE I. Chemical composition of the employed hectorite

Content, mass %								
SiO ₂	Al ₂ O ₃	Fe ₂ O ₃	CaO	MgO	Na ₂ O	K ₂ O	Li ₂ O	I.L.
57.88	0.45	0.04	<0.10	23.62	2.22	0.04	1.46	15.00

The mineralogical composition of the starting sample was primarily hectorite, with smaller amounts of quartz, as measured by X-ray powder diffraction analysis. The X-ray diffraction pattern of the hectorite (Fig. 2) shows a symmetric (001) diffraction with $d_{001} = 12.49$ Å, a typical value for monovalent cation smectites with a monolayer of water molecules in the interlayer space. A similar basal spacing ($d_{001} = 12.61$ Å) for natural hectorite with a cation exchange capacity of 0.439 meq g⁻¹ was reported Baskaralingam *et al.*¹⁹

The surface morphology of the hectorite had a fluffy appearance with a fine platey structure, as can be seen from the SEM image of the hectorite presented in Fig. 3.

The T-2 toxin is a low polar organic molecule, slightly soluble in water.¹ In a preliminary study, the results obtained for T-2 toxin adsorption ($c_{0,T-2} = 10$ mg L⁻¹; $c_{\text{susp}} = 10$ g L⁻¹) by clinoptilolite (Vranje, Serbia), montmorillonite (Šipovo, Bosnia) and hectorite, at pH 3.0 showed that neither clinoptilolite nor montmorillonite were efficient in binding T-2 toxin under *in vitro* conditions (T-2 toxin adsorption indexes: clinoptilolite: 8 %; montmorillonite: 13 %). The properties of natural clinoptilolite and natural montmorillonite were given elsewhere.^{13–15}

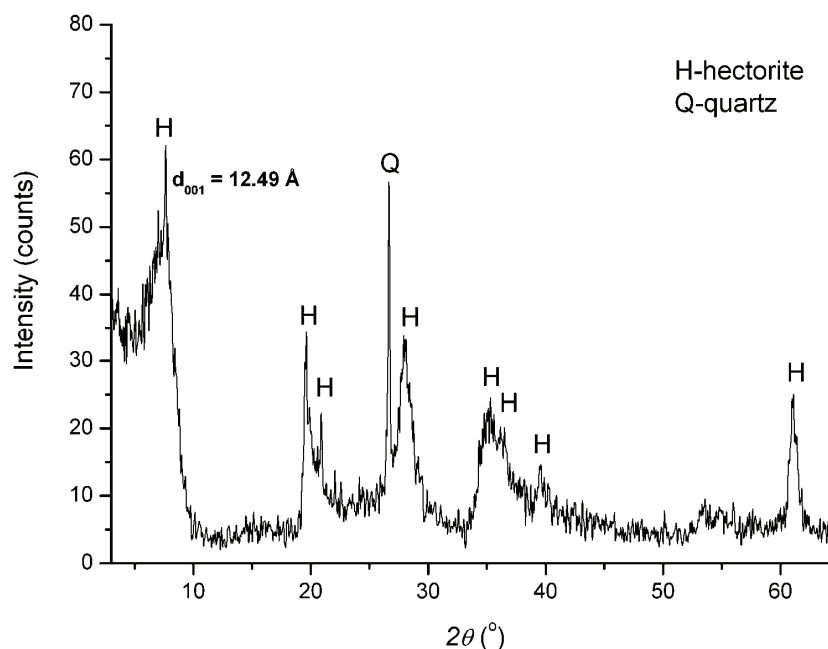


Fig. 2. XRPD Pattern of the employed hectorite.

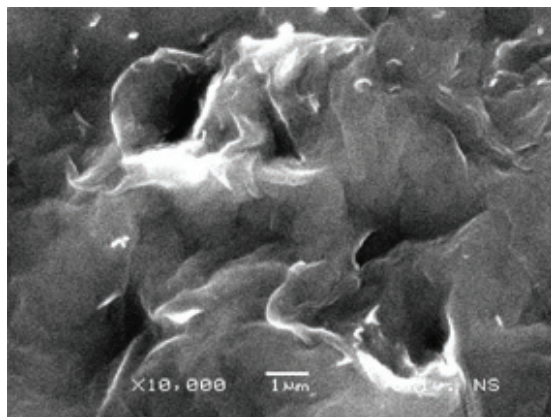


Fig. 3. SEM Image of the employed hectorite.

Compared to these minerals, the adsorption of T-2 toxin by the hectorite mineral was very high (adsorption index 95 %). The fact that montmorillonite, a di-octahedral smectite, does not adsorb T-2 toxin, while hectorite, a tri-octahedral magnesium smectite with some lithium substitution for magnesium in the octahedral layer, has a high affinity to adsorb this toxin indicates the presence of active sites in hectorite onto which this toxin may be adsorbed. Thus, to further investigate the adsorption of T-2 toxin by hectorite, experiments were performed

with different amounts of hectorite in the suspension, different initial T-2 toxin concentration and different pH values.

The effect of adsorbent mass on the amount of T-2 toxin adsorbed at pH 3.0, 7.0 and 9.0 is presented in Fig. 4.

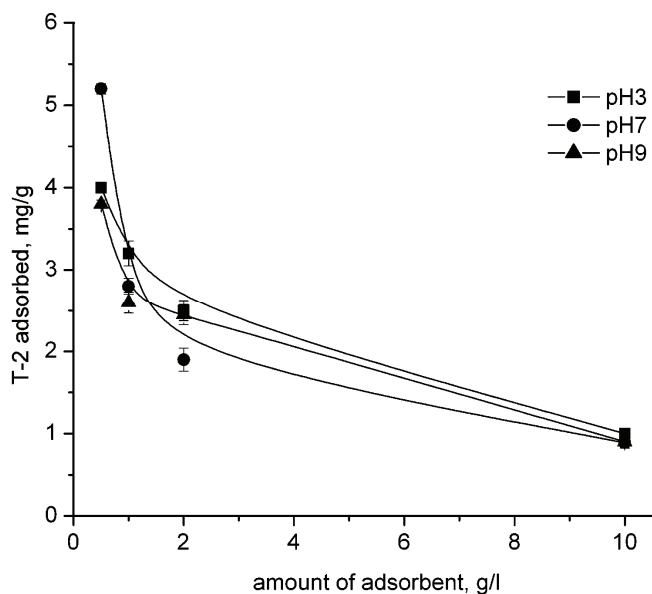


Fig. 4. T-2 toxin adsorption by hectorite vs. the amount of adsorbent in the suspension at different pH.

As can be seen from Fig. 4, a decrease in adsorption capacity with increasing adsorbent concentration was observed, at all investigated pH values. The decrease in adsorption capacity with increasing adsorbent concentration may be explained with the fact that adsorption sites remain unsaturated at higher adsorbent mass for the same initial toxin concentration solution.²⁰

The adsorption of T-2 toxin by hectorite was additionally investigated through the determination of the adsorption isotherms at pH 3.0, 7.0 and 9.0 (Figs. 5a–c). These isotherms were obtained by plotting the concentration of T-2 toxin in solution at equilibrium against the amount of T-2 toxin adsorbed per unit of weight of adsorbent.

There are only limited data in the scientific literature on the adsorption isotherms for the adsorption of mycotoxins by hectorite. Afriyie–Gyawu *et al.*²¹ reported a linear isotherm for ZEA adsorption by hectorite and suggested that hectorite appeared to sorb the low polar ZEA primarily *via* a partitioning phenomenon. Usually, it is assumed that the adsorption of low polar organic molecules to an organic-rich substrate through the partitioning mechanism obeys a linear adsorption isotherm.²² From Figs. 5a–c, T-2 toxin adsorption by hectorite followed non-linear types of isotherms at pH 3.0, 7.0 and 9.0. Additionally, an increase in

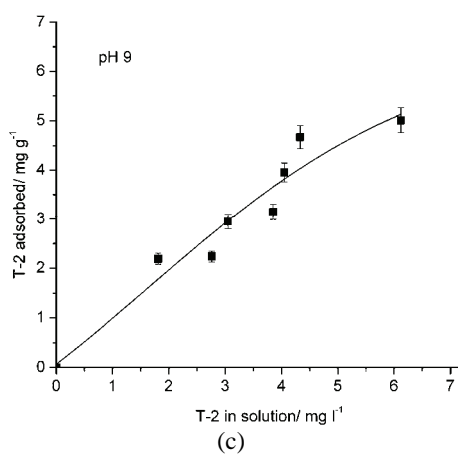
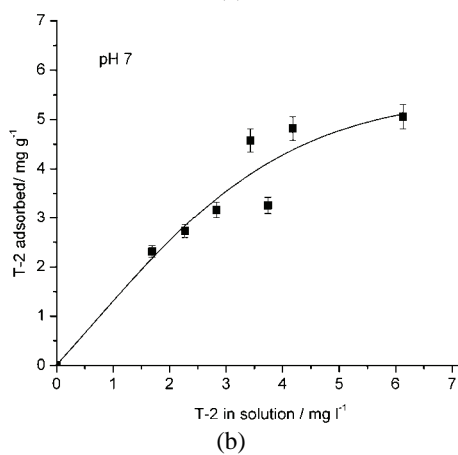
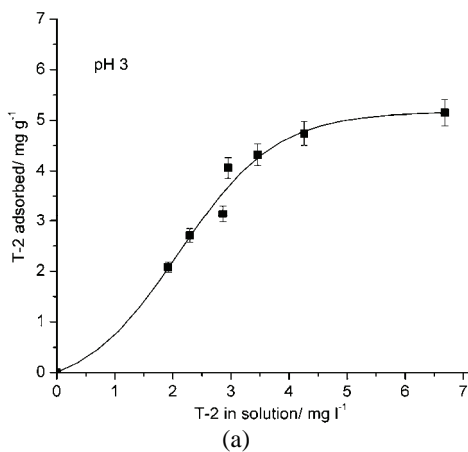


Fig. 5. T-2 toxin adsorption equilibrium data modeled by the Langmuir isotherm at pH 3.0 (a), 7.0 (b) and 9.0 (c).

T-2 toxin adsorption with increasing initial T-2 toxin concentration was observed at all investigated pH values. Non-linear (Langmuir) isotherms obtained for T-2 toxin adsorption by hectorite suggests that partition is not a relevant mechanism for its adsorption. The experimental data for T-2 toxin adsorption by hectorite at pH 3.0, 7.0 and 9.0 were accordingly fitted to the Langmuir isotherm equation:

$$c_{\text{ads}} = \frac{\alpha\beta c_{\text{eq}}}{1 + c_{\text{eq}}} \quad (1)$$

where c_{ads} and c_{eq} denote the equilibrium concentrations of T-2 toxin on the hectorite and in the aqueous phase, respectively, α is a constant related to the binding energy and β is the maximum amount of solute that can be adsorbed by the solid. It was proposed²³ that an adsorption conforms to the Langmuir model when the value of the correlation coefficient (r^2) is greater than 0.89. Thus, the calculated r^2 values of 0.943 at pH 3.0, 0.919 at pH 7.0 and 0.939 at pH 9.0 indicate that these isotherms are empirically consistent with the Langmuir model. Since a Langmuir isotherm is commonly associated with specific bonding,²⁴ the obtained results suggested the presence of specific active sites in hectorite onto which the T-2 toxin can be adsorbed. The estimated maximum T-2 toxin adsorption by hectorite, based on the Langmuir fit to the data, was 9.178, 9.930 and 19.341 mg g⁻¹ at pH 3.0, 7.0 and 9.0, respectively. This suggests that the adsorption of T-2 toxin by hectorite may depend on the solution pH. Since the T-2 toxin is non ionizable (Fig. 1), the increase in adsorption with increasing pH indicates some change at the hectorite surface that contributes to the adsorption. The fact that an increase of the solution pH increases the T-2 toxin adsorption suggests that additional interactions between the negative hectorite surface and T-2 toxin cause the greater adsorption. Based on the structure of the T-2 toxin and the obtained adsorption data, it is possible that more than one adsorption mechanism is involved in the adsorption of T-2 toxin by hectorite.

CONCLUSIONS

The effects of adsorbent mass, solution pH and the initial concentration of T-2 toxin in the solution on T-2 toxin adsorption by the natural mineral hectorite were investigated. It was found that adsorption capacity for the T-2 toxin decreased with increasing adsorbent concentration in the suspension, at all the investigated pH values. The adsorption of T-2 toxin by hectorite followed a non-linear (Langmuir) type of isotherm at pH 3.0, 7.0 and 9.0. The estimated maximum T-2 toxin adsorption by hectorite, based fitting the data to the Langmuir model, was 9.178 mg g⁻¹ at pH 3.0, 9.930 mg g⁻¹ at pH 7.0, and 19.341 mg g⁻¹ at pH 9.0, indicating that the adsorption of T-2 toxin by hectorite is pH dependent. The results presented in this paper show that hectorite possess a very high

capacity for T-2 toxin, over a wide pH range and may be suitable for potential practical applications.

Acknowledgements. Funding for this research was provided by the Ministry of Science and Technological Development of the Republic of Serbia under projects 142057 and 19022. The *in vitro* mycotoxin binding studies were performed at the Fusarium/Poultry Research Laboratory, Veterinary Medical Diagnostic Laboratory, University of Missouri, Columbia, Missouri, USA. We thank Drs. George Rottinghaus and David Ledoux for financial support of this research.

ИЗВОД

АДСОРПЦИЈА Т-2 ТОКСИНА НА ХЕКТОРИТУ

АЛЕКСАНДРА ДАКОВИЋ¹, ЖИВКО СЕКУЛИЋ¹, GEORGE E. ROTTINGHAUS², АНА СТОЈАНОВИЋ¹, СОЊА МИЛИЋЕВИЋ¹ и МИЛАН КРАГОВИЋ¹

¹Институт за технологију нуклеарних и других минералних сировина, п. бр. 390, 11000 Београд и

²Veterinary Medical Diagnostic Laboratory, College of Veterinary Medicine, University of Missouri, Columbia, MO 65211, USA

У овом раду су приказани резултати испитивања адсорпције Т-2 токсина на минералу из групе смектита – хекториту, на различитим рН вредностима (3,0; 7,0 и 9,0). Испитивања су показала да адсорбована количина Т-2 токсина на хекториту опада са порастом садржаја чврсте фазе у суспензији на свим испитиваним рН вредностима. Са адсорпционих изотерми се примећује да са повећањем почетне концентрације Т-2 токсина расте и адсорпција Т-2 токсина, на свим испитиваним рН вредностима. Адсорпција Т-2 токсина на хекториту се може описати нелинеарним (Ленгмир, *Langmuir*) типом изотерме на рН 3,0; 7,0 и 9,0, при чему фактор корелације (r^2) износи 0,943 на рН 3,0; 0,919 на рН 7,0 и 0,939 на рН 9,0. Максимална адсорбована количина Т-2 токсина на хекториту на основу Ленгмирове изотерме (9,178 mg g⁻¹ на рН 3,0; 9,930 mg g⁻¹ на рН 7,0 и 19,341 mg g⁻¹ на рН 9,0), указује да је адсорпција Т-2 токсина на хекториту зависна од рН. Добијени резултати указују на постојање специфичних активних центара на хекториту на којима се Т-2 токсин адорбује.

(Примљено 4. фебруара 2009)

REFERENCES

1. IARC Monographs on the Evaluation of Carcinogenic Risk to Humans. Some Naturally Occurring Substances: Food Items and Constituents, Heterocyclic Aromatic Amines and Mycotoxins, WHO International Agency for Research on Cancer, Lyon, France, 1993
2. C. Dall' Asta, S. Sfonza, G. Galaverna, A. Dossena, R. Marchelli, *J. Chromatogr. A* **1054** (2004) 389
3. T. V. Milanez, L. M. Valente-Soares, G. G. Baptista, *Food Control* **17** (2006) 293
4. G. Avantaggiato, M. Solfrizzo, A. Viscoti, *Food Addit. Contam.* **22** (2005) 379
5. D. Papaioannou, P. D. Katsoulos, N. Panousis, H. Karatzias, *Microporous Mesoporous Mater.* **84** (2005) 161
6. T. D. Phillips, A. B. Sarr, P. G. Grant, *Nat. Toxins* **3** (1995) 204
7. M. Tomašević-Čanović, M. Dumić, O. Vukićević, P. Radošević, I. Rajić, T. Palić, *Acta Vet.* **44** (1994) 309
8. R. W. Grimshaw, *The Chemistry and Physics of Clays and Applied Ceramic Materials*, 4th ed., Ernest Benn Ltd., London, 1971, p. 9

9. S. L. Lemke, P. G. Grant, T. D. Phillips, *J. Agric. Food Chem.* **46** (1998) 3789
10. M. Tomašević-Čanović, A. Daković, G. Rottinghaus, S. Matijašević, M. Đuričić, *Microporous Mesoporous Mater.* **61** (2003) 173
11. M. Tomašević-Čanović, A. Daković, V. Marković, D. Stojšić, *J. Serb. Chem. Soc.* **66** (2001) 555
12. A. Daković, S. Matijašević, G. E. Rottinghaus, D. R. Ledoux, P. Butkeraitis, Ž. Sekulić, *Colloids Surfaces B* **60** (2008) 20
13. A. Daković, S. Matijašević, G. E. Rottinghaus, V. Dondur, T. Pietrass, C. F. M. Clewett, *J. Colloid Interface Sci.* **311** (2007) 8
14. A. Daković, M. Tomašević-Čanović, G. Rottinghaus, V. Dondur, Z. Mašić, *Colloids Surfaces B* **30** (2003) 157
15. A. Daković, M. Tomašević-Čanović, G. E. Rottinghaus, S. Matijašević, Ž. Sekulić, *Microporous Mesoporous Mater.* **105** (2007) 285
16. J. Madejová, J. Bujdák, M. Janek, P. Komade, *Spectrochim. Acta A* **54** (1998) 1397
17. G. Borchardt, in *Minerals and Soil Environments*, J. B. Dixon, S. B. Weed Eds., Soil Science Society of America, Madison, WI, 1989, p. 675
18. M. G. Neumann, C. C. Schmitt, F. Gessner, *J. Colloid Interface Sci.* **177** (1996) 495
19. P. Baskaralingam, M. Pulikesi, V. Ramamuthi, S. Sivanesan, *J. Hazard Mater. B* **136** (2006) 989
20. P. Baskaralingam, M. Pulikesi, V. Ramamuthi, S. Sivanesan, *Applied Clay Sci.* **37** (2007) 207
21. E. Afriye-Gyawu, M. C. Wiles, H. J. Huebner, M. B. Richardson, C. Fickey, T. D. Phillips, *J. Toxicol. Environ. Health A* **68** (2005) 353
22. Z. Li, R. S. Bowman, *Environ. Sci. Technol.* **32** (1998) 2278
23. W. F. Jaynes, S. A. Boyd, *Clays Clay Miner.* **39** (1991) 428
24. L. Groisman, C. Rav-Acha, Z. Gerstl, U. Minelgrin, *Applied Clay Sci.* **24** (2004) 159.



J. Serb. Chem. Soc. 74 (11) 1293–1302 (2009)
JSCS–3919

Journal of
the Serbian
Chemical Society

JSCS@tmf.bg.ac.rs • www.shd.org.rs/JSCS

UDC 669.112.227+669.14.018.8:620.193

Original scientific paper

Effect of solution treatment conditions on the sensitization of austenitic stainless steel

XIAOFEI YU¹, SHENHAO CHEN^{1,2*} and LIANG WANG¹

¹Department of Chemistry, Shandong University, Jinan 250100 and ²State Key Laboratory for Corrosion and Protection, Shenyang 110016, PR China

(Received 5 February, revised 27 May 2009)

Abstract: In this study, the impact of the conditions of solution treatment on the degree of sensitization (DOS) of austenitic stainless steel (AISI 304) was investigated in detail. The results derived from the electrochemical potentiodynamic reactivation (EPR) test indicated that the DOS decreased as the solution treatment temperature and time increased. The reason for this was studied *via* the SEM morphologies and EDS results, which indicated that the grain size influenced the DOS. Furthermore, cellular automaton (CA) was utilized to simulate grain growth, the precipitation of Cr-rich carbides and the three dimensional distribution of the chromium concentration, which vividly illuminated the effect of the grain size on the DOS and was in accordance with the experiment results.

Keywords: intergranular corrosion; degree of sensitization; cellular automaton; austenitic stainless steel.

INTRODUCTION

Stainless steels have excellent corrosion resistance when properly heated and used in a low temperature environment. However, they are vulnerable to corrosion when exposed to temperatures between 450 and 900 °C.^{1–4} This is because the formation of Cr-rich carbides at the grain boundaries extracts chromium from the grain boundaries and neighboring matrix, leaving a Cr-depleted zone extending to both sides of the grain boundaries. The Cr-depleted zone is vulnerable to attack, leading to intergranular corrosion (IGC) or stress cracking corrosion.^{5–8} In order to correlate IGC with the grain boundary characteristics, many studies have been devoted to the quantitative evaluation of the depleted zones by empirical or analytical models.^{9–15}

Generally, these models are successful in calculating the chromium concentration profiles and their evolutions during aging. However, the chromium con-

* Corresponding author. E-mail: shchen@sdu.edu.cn
doi: 10.2298/JSC0911293Y



centration profiles can only reflect the distribution along a certain direction, rather than giving an overall view of the chromium distribution. Therefore, the intention of this work was to simulate the chromium distribution in a three dimensional manner. As an important algorithm, CA, that describes the discrete spatial and temporal microstructure evolution on a mesoscale, was applied to simulate recrystallization, grain coarsening, phase transformation and grain growth.^{16–25} However, hitherto, there has been no report about the employment of the CA to investigate IGC of austenitic stainless steel, except the simulation of general corrosion of a metal with defects.²⁶ Based on the above-mentioned, the CA was adopted to study the effect of solution treatment conditions on the degree of sensitization (DOS) of austenitic stainless steel (AISI 304), and the evolution of grain growth, the precipitation of Cr-rich carbides and the distribution of the chromium concentration are presented herein.

EXPERIMENTAL

Experiments

The steel (AISI 304) with a diameter of 3 mm investigated in this study contained of 0.055 % C, 1.00 % Mn, 8.48 % Ni, 0.600 % Si, 0.029 % P, 0.005 % S, 18.28 % Cr and Fe in balance. The samples were first solution treated at 900, 1000 and 1100 °C for 0, 15, 30 min, 1 h and 2 h and then sensitized at 650 °C for 12 h. After the pretreatment, the specimens were sealed with epoxy resin, with only the working area exposed. The electrodes were polished with emery paper to mirror-like brightness, rinsed with alcohol and Milli-Q ultrapure water before the electrochemical experiments.

The DOS of the samples was determined by the electrochemical potentiodynamic reactivation (EPR) test.² All the experiments were repeated several times and the average values represented the DOS. After the electrochemical experiments, the electrodes were cleaned in Milli-Q ultrapure water, immersed in alcohol and cleaned in an ultrasonic cleaner for 15 min, dried in air, and then EDS and SEM measurements were performed using a JSM-6700F field emission scanning electron microscope (Japan JEOL).

CA simulation model

The initial microstructure, used to simulate the precipitation of Cr-rich carbides and the distribution of the chromium concentration, resulted from grain growth at different temperatures. The detailed theory about grain growth can be found in the literature.^{19–25}

For the simulation of the precipitation of Cr-rich carbides, a nucleation model based on the classical nucleation theory was employed. This model can be described as follows:^{20–22}

$$I = K_1 D_\gamma (kT) \exp(-K_2/kT(\Delta G)^2), \quad (1)$$

where I is the nucleation density, K_1 is a constant related to the nucleation site density, K_2 is a constant related to all the interfaces involved in the nucleation, D_γ is the chromium diffusion coefficient, k is the Boltzmann constant and ΔG is the driving force.

Moreover, the growth of the carbides was assumed to be controlled by both the chromium diffusion and the interface mobility. As the interface moves during the precipitation, chromium atoms transfer from the matrix to the interface and then they precipitate to the carbides. Consequently, the growth of carbides can be described as a free boundary problem

for chromium diffusion in austenite and the dynamics of the interface. The chromium diffusion in austenite is described as follows:

$$dc/dt = \nabla(D\nabla c), \quad (2)$$

where c is the chromium concentration and D is the chromium diffusion coefficient.

Allowing for the characteristics of the precipitation of Cr-rich carbides, the mobility of interface is equal to the growth of carbides and the length that the interface covers can be expressed by:^{14,15}

$$l = \beta\sqrt{Dt}, \quad (3)$$

where t is the sensitization time, β is a constant and D is the chromium diffusion coefficient, which, being a thermally activated process, depends on the temperature. All of the key parameters are listed in Table I.

TABLE I. The key parameters used in the present model

$M_0 / \text{m}^4 \text{J}^{-1} \text{s}^{-1}$	$\gamma_m / \text{J m}^{-2}$	$\theta_m / ^\circ$	$a / \mu\text{m}$	β	$Q / \text{kJ mol}^{-1}$ (taken from ^{14,18})
1.56×10^{-11}	0.56	15 deg	1	0.137	245.7

RESULTS AND DISCUSSION

The effect of solution treatment temperature on the sensitization

The influence of the solution treatment temperature on the susceptibility to IGC was studied at 900, 1000 and 1100 °C while the other conditions were maintained constant. The DOS obtained from the EPR test is shown in Fig. 1, from which it can be seen that the DOS decreased gradually with increasing temperature irrespective of the treatment time. For example, when the samples were

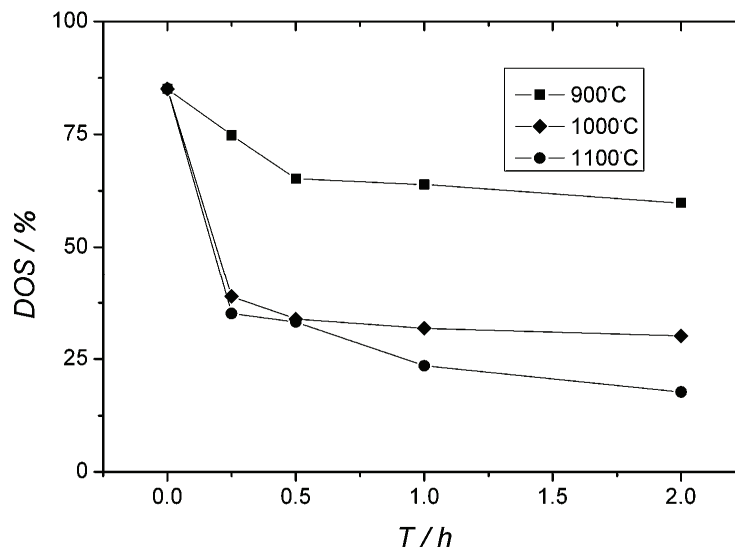


Fig. 1. The DOS obtained from the EPR test.

treated at 900, 1000 and 1100 °C for 1 h and then sensitized at 650 °C for 12 h, the DOS was 63.9, 31.8 and 23.5 % respectively. The changing trend of the DOS were the same when the solution treatment time was 15 min, 30 min and 2 h. The SEM morphologies shown in Fig. 2 were taken after the EPR test and revealed that IGC occurred at all three temperatures. However, the degree of IGC was reduced as the temperature increased.

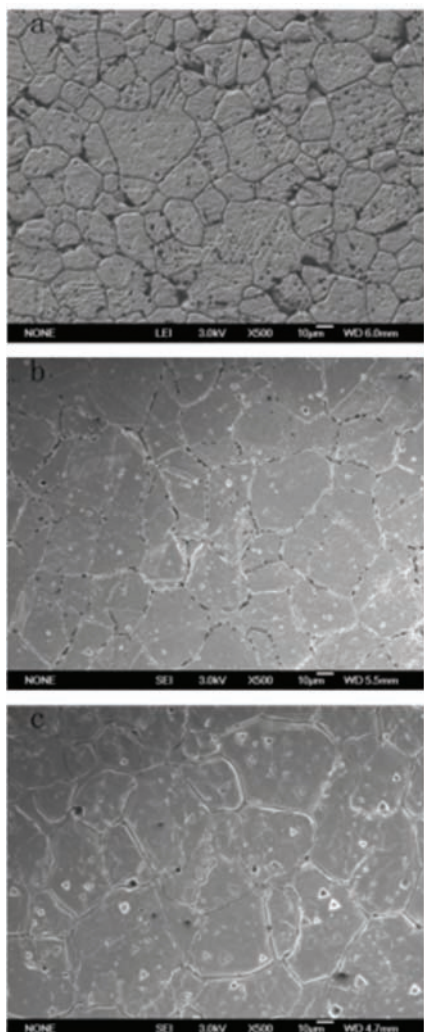


Fig. 2. SEM Morphologies of the samples heated at: a) 900, b) 1000 and c) 1100 °C for 0.5 h, and then sensitized at 650 °C for 12 h.

The effect of solution treatment time on the sensitization

Figure 1 not only shows the effect of solution treatment temperature on the DOS, but also indicates the impact of the treatment time on it. From the Figure, it

can be seen that the DOS for the sample without heat treatment was very high, but it decreased sharply for the samples subjected to heat treatment. When the samples were heated at 1100 °C for 15 min to 2 h, the DOS decreased from 35.1 to 17.7 %. At the other temperatures, the DOS also decreased as the time increased. The SEM morphologies of the samples heated at 1100 °C for 15 min, 30 min and 2 h and then sensitized at 650 °C for 12 h after the EPR test are shown in Fig. 3. The figure reveals that IGC occurred under all conditions, but it was reduced as the time was prolonged.

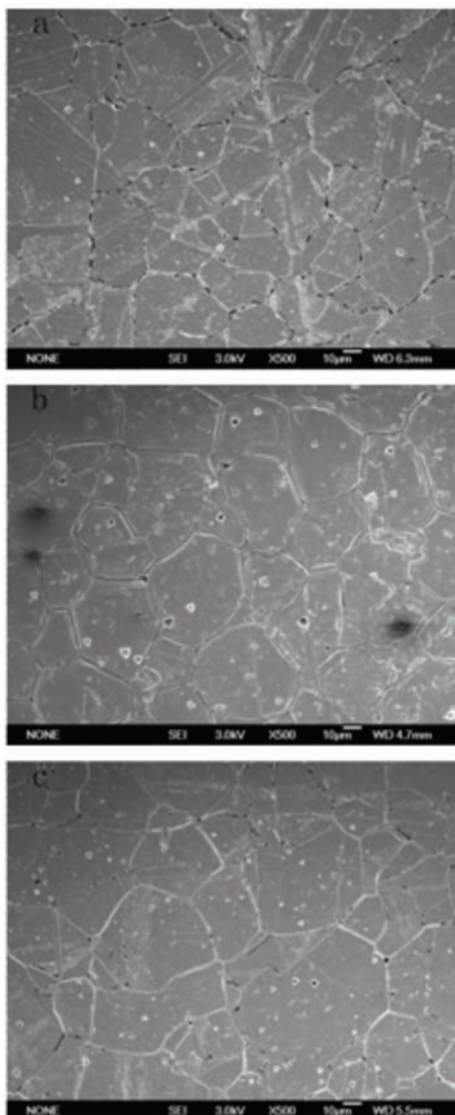


Fig. 3. SEM Morphologies of the samples heated at 1100 °C for: a) 15 min, b) 30 min and c) 2 h, and then sensitized at 650 °C for 12 h.

The effect of grain size on the sensitization

Grain size is one of the most important factors that can affect IGC and it mainly affects the time required to reach the state of complete sensitization.^{27,28} The relationship between the grain size and the time to attain the state of complete sensitization can be expressed as:

$$t_{\max,1} = (d_1/d_2)^{2/3}t_{\max,2} \quad (4)$$

where $t_{\max,1}$ and $t_{\max,2}$ are the times required to reach the state of complete sensitization, and d_1 and d_2 are the grain sizes.¹² The chromium concentration at the grain boundaries at any sensitization time during the sensitization stage is related to t_{\max} and is defined as:

$$c = c_0 \exp(-kt/t_{\max}), \quad (5)$$

where c is the chromium concentration at the grain boundaries at sensitization time t , c_0 is the initial concentration of chromium, t is the sensitization time, t_{\max} is the time required to reach the state of complete sensitization and k is a constant.¹⁵

From these two equations, it can be assumed that if t is shorter than t_{\max} and is kept the same for the different grain size samples, the chromium concentration at the grain boundaries of a large grain sample will be higher than that of a small grain one. This means the precipitation of a large grain sample will be less than that of a small grain one. As a result, the DOS of a large grain sample will be lower than that of a small grain one, which is determined by the volume of precipitation.

Although the grain boundary surface area became smaller as the grains grew larger, the precipitation of Cr-rich carbides per grain boundary surface area increased. The reason is that the samples were derived from the same material and the sensitization was performed at the same temperature. Hence, the precipitation volume was the same for the different grain size samples. However, as the grain size becomes larger, the chromium atoms must diffuse a longer distance to reach the grain boundaries and this is a time consuming procedure. Hence, if the sensitization time is very short, the DOS of the larger grain samples may be lower than that of the smaller grain samples. Through experiments, it was found that the DOS of the smallest grain sample was still increasing when the sensitization time was 192 h. Thus, the sensitization time of 12 h used in this study was shorter than the smallest t_{\max} . As a result, the DOS of the large grain sample was lower than that of the small grain sample.

From the SEM morphologies exhibited in Figs. 2 and 3, it can be observed that the grain size became larger as the temperature and time increased. The average grain sizes obtained from Fig. 2 were 19.5, 22.8 and 26.8 μm , respectively, while those obtained from Fig. 3 were 20.8, 23.6 and 37.8 μm , respectively. In

order to prove if it was the grain size that influenced the DOS, the chromium concentration at grain boundaries was determined by EDS. The measurement of the chromium concentration at the grain boundaries of each sample was repeated five times and the final concentration was the average value of the five determined values. According to Eqs. (1) and (2), $d^{2/3}$ should change linearly with $1/\ln(c)$. The relationship between the grain size and the chromium concentration is presented in Fig. 4. Allowing for experiment error, the results were in agreement with the theoretical calculation. This suggests that it was the grain size that had an impact on the DOS.

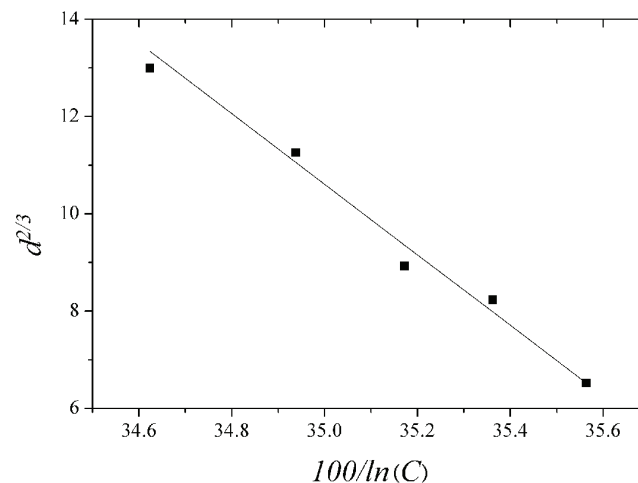


Fig. 4. The relationship between the grain size and the chromium concentration.

In order to show the effect of grain size on the DOS, the CA was utilized to simulate the precipitation of Cr-rich carbides and the distribution of the chromium concentration. The simulation was performed on a 100×100 square lattice and the distance between two neighboring cells was $1.0 \mu\text{m}$. The state of each lattice site was characterized by four state variables: the grain orientation variable representing the different grains; the phase state variable indicating whether it belonged to the carbides, the matrix, or the carbides/matrix interface; the fraction variable representing the fraction of carbides in an interface cell, and the chromium concentration. The Moore neighbor rule, which considers the first and the second nearest eight neighbors, was employed. The procedure and the transition rules were as follows: first, the initial variables for each cell were assigned, and then nucleation occurred randomly to those cells belonging to the preferential nucleation sites according to the nucleation model. In addition to nucleation, the carbides formed at the other steps would simultaneously grow into the matrix. When the fraction of the carbides in an interface cell was no less than one unit,

the phase state variable of this cell would change into the phase state variable of the carbides and the orientation variable was given randomly. At the same time, all its neighboring austenite cells changed their phase state variables into the phase state variable of the interface. In addition, the chromium concentration at each site was calculated according to Eq. (2). Lastly, the variables for each cell were updated and the simulation cycle was repeated until the simulation was completed.

The microstructures used to study the effect of grain size on the precipitation of Cr-rich carbides, which were obtained from grain growth at 900, 1000 and 1100 °C, are displayed in Fig. 5. The average grain sizes were 19.7, 22.5 and 26.5 μm , respectively, and were almost equal to the grain sizes of the material. The changes of the precipitation together with the grain size are shown in Fig. 6, from which it can be clearly seen that the volume of precipitate decreased with increasing grain size. The corresponding distribution of the chromium concentration, which clearly reflects the changes in the precipitation, is presented in Fig. 7. The concentration at the grain boundaries for the large grain sample was higher than that for the small grain one, which is in accordance with the experiment results. Hence, the simulation clearly showed the effect of the solution treatments on the DOS.

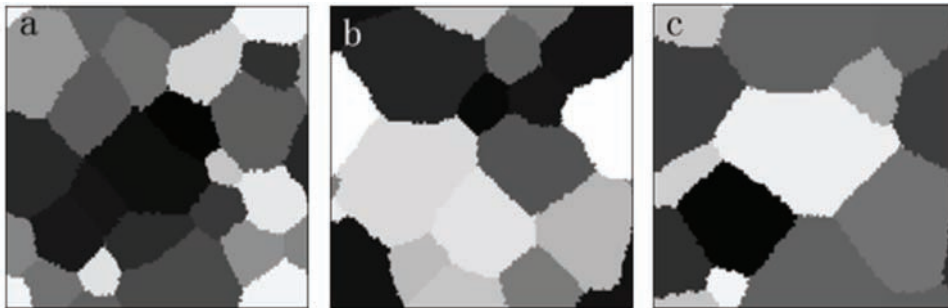


Fig. 5. The microstructure obtained from grain growth at different temperatures: a) 900, b) 1000 and c) 1100 °C.

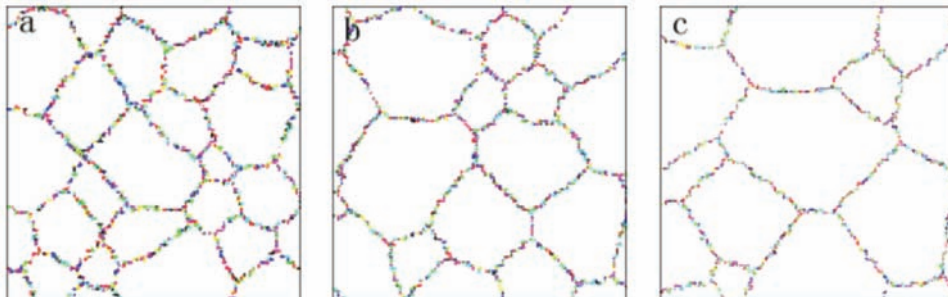


Fig. 6. Effect of grain size on the precipitation: a) 19.7, b) 22.5 and c) 26.5 μm .

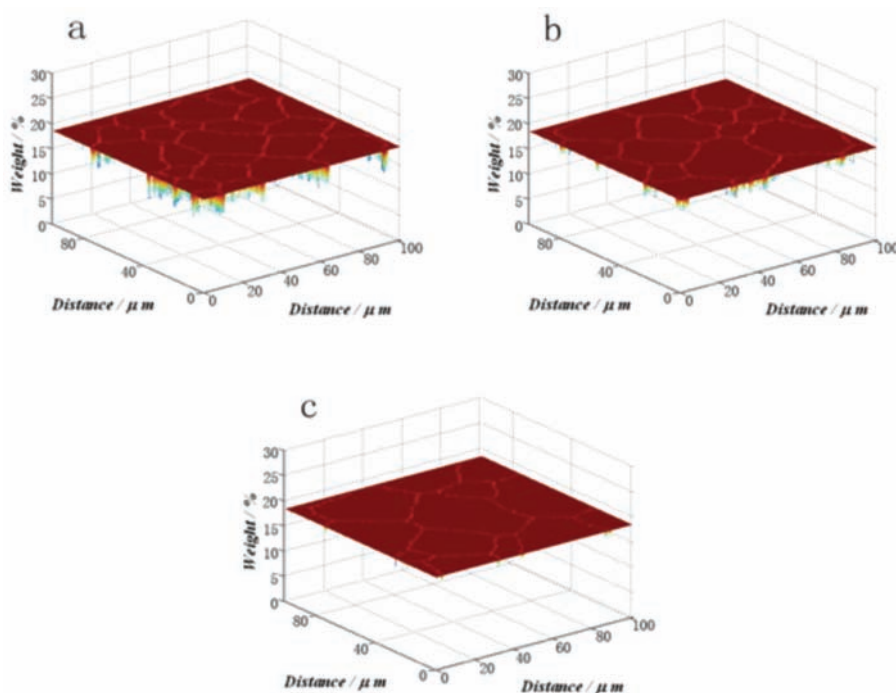


Fig. 7. The distribution of the chromium concentration corresponding to Fig. 6.

CONCLUSIONS

The effect of solution treatment conditions on the DOS of AISI 304 austenitic stainless steel was studied experimentally and by simulation methods. The experimental results showed that the DOS decreased as the temperature and time of the solution treatment increased. In order to understand the relationship between the DOS and the solution treatment temperature and time, a CA was used to simulate the grain growth, the precipitation and the three dimensional distribution of the chromium concentration, which perfectly explained the influence of temperature and time on the DOS.

Acknowledgements: The authors would like to thank the Special Funds for Major State Basic Research Projects (2006CB605004) for support of this research.

ИЗВОД

УТИЦАЈ УСЛОВА ТРЕТМАНА У РАСТВОРУ НА ПОВЕЋАЊЕ ОСЕТЉИВОСТИ АУСТЕНИТНОГ ЧЕЛИКА

XIAOFEI YU¹, SHENHAO CHEN^{1,2} и LIANG WANG¹

¹Department of Chemistry, Shandong University, Jinan 250100 и ²State Key Laboratory for Corrosion and Protection, Shenyang 110016, PR China

У раду је детаљно испитан утицај услова третмана у раствору на степен повећања осетљивости аустенитног челика (AISI 304). Резултати теста електрохемијске потенциостатске

реактивације указују да степен повећања осетљивости опада са повећањем температуре и времена третмана у раствору. Узроци таквог понашања су тражени у морфологији (која је одређена скенирајућом електронском микроскопијом, SEM) и резултатима енергетско-дисперзионе анализе X-зрацима (EDS). Показало се да величина зрна утиче на степен повећања осетљивости. Поред тога, моделом ћелијских аутомата су симулирани раст зрна, таложење карбида богатих хромом и тродимензиона расподела концентрације хрома, што је сликовито објаснило ефекат величине зрна на степен повећање осетљивости аустенитног челика који је експериментално утврђен.

(Примљено 5. фебруара, ревидирано 27. маја 2009)

REFERENCES

1. R. Singh, J. Mater. *Proc. Techol.* **206** (2008) 286
2. R. Singh, B. Ravikumar, A. Kumar, P. K. Dey, I. Chattoraj, *Metall. Mater. Trans. A* **34** (2003) 2441
3. G. Radenković, S. K. Zečević, Z. Cvijović, D. M. Dražić, *J. Serb. Chem. Soc.* **60** (1995) 53
4. H. Ma, S. Chen, C. Yang, J. Luo, *J. Serb. Chem. Soc.* **67** (2002) 425
5. Y. F. Cheng, L. Niu, *Electrochem. Commun.* **9** (2007) 558
6. R. Nishimura, A. Sulaiman, Y. Maeda, *Corros. Sci.* **45** (2003) 465
7. R. Nishimura, Y. Maeda, *Corros. Sci.* **45** (2003) 1847
8. G. H. Aydoğdu, M. K. Aydinol, *Corros. Sci.* **48** (2006) 3565
9. J. J. Kai, G. P. Yu, C. H. Tsai, M. N. Liu, S. C. Yao, *Metall. Trans. A* **20** (1989) 2057
10. C. Strawstrom, M. Hillert, *J. Iron Steel Inst.* **207** (1969) 77
11. G. S. Was, R. M. Kruger, *Acta Metall.* **33** (1985) 841
12. Y. F. Yin, R. G. Faulkner, *Corros. Sci.* **49** (2007) 2177
13. H. Sahlaoui, K. Makhlouf, H. Sidhom, J. Philibert, *Mater. Sci. Eng. A* **372** (2004) 98
14. W. E. Mayo, *Mater. Sci. Eng. A* **232** (1997) 129
15. H. Sahlaoui, H. Sidhom, J. Philibert, *Acta Mater.* **50** (2002) 1383
16. R. Ding, Z. X. Guo, *Acta Mater.* **49** (2001) 3163
17. G. Kugler, R. Turk, *Acta Mater.* **52** (2004) 4659
18. Y. J. Lan, D. Z. Li, Y. Y. Li, *Metall. Mater. Trans. B* **37** (2006) 119
19. J. Geiger, A. Roósz, P. Barkóczy, *Acta Mater.* **49** (2001) 623
20. Y. J. Lan, D. Z. Li, Y. Y. Li, *Acta Mater.* **52** (2004) 1721
21. S. Kundu, M. Dutta, S. Ganguly, S. Chandra, *Scripta Mater.* **50** (2004) 891
22. Y. J. Lan, N. M. Xiao, D. Z. Li, Y. Y. Li, *Acta Mater.* **53** (2005) 991
23. S. Raghavan, S. S. Sahay, *Mater. Sci. Eng. A* **445–446** (2007) 203
24. Y. Z. He, H. L. Ding, L. F. Liu, K. Shin, *Mater. Sci. Eng. A* **429** (2006) 236
25. H. L. Ding, Y. Z. He, L. F. Liu, W. J. Ding, *J. Cryst. Growth* **293** (2006) 489
26. A. Taleb, J. Stafiej, J. P. Badiali, *J. Phys. Chem. C* **111** (2007) 9086
27. R. Singh, S. G. Chowdhury, B. Ravikumar, S. K. Das, P. K. Dey, I. Chattoraj, *Scripta Mater.* **57** (2007) 185
28. R. Beltran, J. G. Maldonado, L. E. Murr, W. W. Fisher, *Acta Mater.* **45** (1997) 4351.



J. Serb. Chem. Soc. 74 (11) 1303–1318 (2009)
JSCS–3920

Journal of
the Serbian
Chemical Society

JSCS@tmf.bg.ac.rs • www.shd.org.rs/JSCS

UDC 547.263/.265+547.593:541.25:531.75

Original scientific paper

Densities and excess molar volumes of alcohol + cyclohexylamine mixtures

IVONA R. RADOVIĆ[#], MIRJANA LJ. KIJEVČANIN^{*#}, ALEKSANDAR Ž. TASIĆ,
BOJAN D. DJORDJEVIĆ[#] and SLOBODAN P. ŠERBANOVIĆ[#]

*Faculty of Technology and Metallurgy, University of Belgrade, Karnegijeva 4,
P. O. Box 35-03, 11120 Belgrade, Serbia*

(Received 2 April, revised 28 August 2009)

Abstract: Densities of binary mixtures of 1-propanol, or 2-butanol, or 1-pentanol + cyclohexylamine were measured at temperatures from 288.15 to 313.15 K and atmospheric pressure, while the densities for the system 2-methyl-2-propanol + cyclohexylamine were measured at temperatures from 303.15 to 323.15 K and atmospheric pressure. All measurements were performed using an Anton Paar DMA 5000 digital vibrating-tube densimeter. From the experimental densities, the excess molar volumes, V^E , were calculated.

Keywords: binary mixtures; densities; excess molar volumes; alcohols; cyclohexylamine.

INTRODUCTION

This study is a continuation of previous research dealing with the experimental determination or calculation of volumetric properties of binary and ternary mixtures containing different alcohols and aromatics, chlorinated aromatics or chlorinated alkanes.^{1–6} The intention of this study was to provide a set of volumetric data in order to assess the influence of temperature, as well as the structure of the alcohol molecule (position of the OH group and alcohol chain length) in mixtures with cyclohexylamine on the molecular interactions between them.

Mixtures of alcohols and primary amines are an interesting class of systems exhibiting very strong negative deviations from the Raoult law. From a theoretical viewpoint, the volumetric properties of these mixtures are an important source of information for the characterization of the interactions between the components and they are also useful for understanding the liquid state theory. In addition, alcohols and amines are widely used in a variety of industrial and consumer applications and hence, knowledge of their physical properties is also of

* Corresponding author. E-mail: mirjana@tmf.bg.ac.rs

[#] Serbian Chemical Society member.

doi: 10.2298/JSC0911303R



great importance from a practical point of view. Alcohols are in use as fuel, perfumes, cosmetics, paints, varnishes, drugs, explosives, fats, waxes, resins, plastics, rubber, detergents, *etc.*,¹⁻³ while cyclohexylamine is used in the production of pharmaceutical and other chemicals, including insecticides, pesticides, plasticizers, emulsifying agents, dyes, dry cleaning agents and corrosion inhibitors.⁷

In the present work, the densities, ρ , were measured for the following systems: 1-propanol, or 2-butanol, or 1-pentanol + cyclohexylamine at temperatures from 288.15 to 313.15 K and atmospheric pressure, and 2-methyl-2-propanol + cyclohexylamine at temperatures from 303.15 to 323.15 K and atmospheric pressure, since the melting point of 2-methyl-2-propanol is around 298 K. The excess molar volumes, V^E , of the investigated mixtures were calculated from the measured data.

Literature data of V^E values for the investigated systems cover a single temperature, 303.15 K.⁸ In the hitherto published articles, no values of V^E were found covering the entire temperature range of the mixtures studied here.

For a complete insight into the behavior of alcohol + cyclohexylamine mixtures, the 1-butanol + cyclohexylamine system⁹ was also included in the analysis.

EXPERIMENTAL

Materials

All products were of high purity (mass fraction purity > 0.99) and were used without further purification: 1-propanol > 0.995, 1-butanol > 0.995, 2-butanol > 0.99 and cyclohexylamine > 0.99 were supplied from Merck, while 2-methyl-2-propanol > 0.997 and 1-pentanol > 0.99 were products from Fluka. All organic liquids were stored in brown glass bottles under an inert nitrogen atmosphere. The pure components were degassed in an ultrasonic bath immediately before sample preparation. The densities of the pure components together with the corresponding literature values¹⁰⁻¹⁵ are listed in Table I.

TABLE I. Densities of the pure components

Substance	T / K	$\rho / \text{g} \cdot \text{cm}^{-3}$	
		Experimental	Literature
1-Propanol	298.15	0.799692	0.79969 ¹⁰ , 0.79960 ¹¹
2-Butanol	298.15	0.802528	0.8026 ¹¹ , 0.80254 ¹²
2-Methyl-2-propanol	303.15	0.775412	0.77541 ¹¹ , 0.77546 ¹³
1-Pentanol	298.15	0.810968	0.81090 ¹¹ , 0.81096 ¹⁴
Cyclohexylamine	303.15	0.857671	0.85777 ¹¹ , 0.85820 ¹⁵

Apparatus and procedure

The density measurements of the binaries (1-propanol, or 1-pentanol, or 2-butanol, or 2-methyl-2-propanol + cyclohexylamine) and the corresponding pure substances were realized using an Anton Paar DMA 5000 digital vibrating U-tube densimeter (with automatic viscosity correction) having an accuracy of $\pm 5 \times 10^{-6} \text{ g cm}^{-3}$. The temperature in the cell was controlled to $\pm 0.001 \text{ K}$ with a built-in solid-state thermostat. The temperature in the cell was measured by means of two integrated Pt 100 platinum thermometers and the temperature stability was

found to be better than ± 0.002 K. The apparatus was calibrated daily using ambient air and ultra pure water. To minimize the errors in composition, all mixtures were prepared by mass using the cell and the procedure described previously.^{16,17} A Mettler AG 204 balance with a precision of 1×10^{-4} g was used. The error in the calculation of the mole fraction was found to be less than $\pm 1 \times 10^{-4}$. The experimental uncertainty in the density was less than $\pm 1 \times 10^{-5}$ g cm⁻³, while the average error in the excess molar volume was estimated to be better than $\pm 3 \times 10^{-3}$ cm⁻³ mol⁻¹.

RESULTS AND DISCUSSION

The excess molar volumes, V^E , of binary mixtures were calculated from the density data by applying Eq. (1) (the values are given in Table II):

$$V^E = \frac{x_1 M_1 + x_2 M_2}{\rho} - \frac{x_1 M_1}{\rho_1} - \frac{x_2 M_2}{\rho_2} \quad (1)$$

where x_1 , x_2 , M_1 and M_2 are the mole fraction and molar mass of components 1 and 2, respectively, while ρ , ρ_1 and ρ_2 are the measured densities of the mixture and the pure components 1 and 2, respectively.

TABLE II. Experimental densities, ρ , and excess molar volumes, V^E , for the alkanol (1) + cyclohexylamine (2) binary mixtures at different temperatures 288.15–323.15 K and atmospheric pressure

x_1	$\rho / \text{g} \cdot \text{cm}^{-3}$	$V^E / \text{cm}^3 \text{mol}^{-1}$	x_1	$\rho / \text{g} \cdot \text{cm}^{-3}$	$V^E / \text{cm}^3 \text{mol}^{-1}$
1-Propanol (1) + cyclohexylamine (2)					
$T = 288.15 \text{ K}$					
0.0000	0.871290	0.0000	0.6002	0.852683	-1.3633
0.0509	0.870750	-0.2073	0.7000	0.844776	-1.2147
0.1017	0.870088	-0.4014	0.7997	0.834754	-0.9312
0.1486	0.869388	-0.5726	0.8500	0.828866	-0.7418
0.1992	0.868514	-0.7466	0.8998	0.822459	-0.5250
0.3007	0.866227	-1.0467	0.9502	0.815368	-0.2770
0.4009	0.863037	-1.2608	1.0000	0.807690	0.0000
0.4998	0.858771	-1.3819			
$T = 293.15 \text{ K}$					
0.0000	0.866747	0.0000	0.6002	0.848350	-1.3698
0.0509	0.866243	-0.2116	0.7000	0.840517	-1.2212
0.1017	0.865605	-0.4082	0.7997	0.830587	-0.9376
0.1486	0.864928	-0.5816	0.8500	0.824743	-0.7473
0.1992	0.864070	-0.7567	0.8998	0.818382	-0.5292
0.3007	0.861807	-1.0572	0.9502	0.811337	-0.2793
0.4009	0.858633	-1.2699	1.0000	0.803703	0.0000
0.4998	0.854393	-1.3896			
$T = 298.15 \text{ K}$					
0.0000	0.862207	0.0000	0.6002	0.843999	-1.3757
0.0509	0.861732	-0.2152	0.7000	0.836238	-1.2273
0.1017	0.861122	-0.4150	0.7997	0.826395	-0.9434
0.1486	0.860461	-0.5899	0.8500	0.820597	-0.7524

TABLE II. Continued

x_1	$\rho / \text{g cm}^{-3}$	$V^E / \text{cm}^3 \text{mol}^{-1}$	x_1	$\rho / \text{g cm}^{-3}$	$V^E / \text{cm}^3 \text{mol}^{-1}$
1-Propanol (1) + cyclohexylamine (2)					
$T = 298.15 \text{ K}$					
0.1992	0.859622	-0.7666	0.8998	0.814283	-0.5333
0.3007	0.857380	-1.0676	0.9502	0.807280	-0.2814
0.4009	0.854219	-1.2787	1.0000	0.799692	0.0000
0.4998	0.850004	-1.3959			
$T = 303.15 \text{ K}$					
0.0000	0.857671	0.0000	0.6002	0.839630	-1.3812
0.0509	0.857223	-0.2188	0.7000	0.831934	-1.2327
0.1017	0.856634	-0.4211	0.7997	0.822178	-0.9490
0.1486	0.855990	-0.5978	0.8500	0.816427	-0.7576
0.1992	0.855164	-0.7756	0.8998	0.810149	-0.5366
0.3007	0.852939	-1.0769	0.9502	0.803196	-0.2837
0.4009	0.849790	-1.2867	1.0000	0.795650	0.0000
0.4998	0.845594	-1.4023			
$T = 308.15 \text{ K}$					
0.0000	0.853138	0.0000	0.6002	0.835236	-1.3857
0.0509	0.852710	-0.2217	0.7000	0.827602	-1.2373
0.1017	0.852139	-0.4263	0.7997	0.817929	-0.9538
0.1486	0.851509	-0.6047	0.8500	0.812223	-0.7620
0.1992	0.850697	-0.7839	0.8998	0.805991	-0.5404
0.3007	0.848483	-1.0851	0.9502	0.799076	-0.2854
0.4009	0.845341	-1.2934	1.0000	0.791576	0.0000
0.4998	0.841161	-1.4076			
$T = 313.15 \text{ K}$					
0.0000	0.848607	0.0000	0.6002	0.830816	-1.3894
0.0509	0.848196	-0.2244	0.7000	0.823240	-1.2410
0.1017	0.847641	-0.4313	0.7997	0.813647	-0.9579
0.1486	0.847020	-0.6109	0.8500	0.807982	-0.7657
0.1992	0.846216	-0.7910	0.8998	0.801787	-0.5427
0.3007	0.844011	-1.0924	0.9502	0.794911	-0.2860
0.4009	0.840874	-1.2993	1.0000	0.787466	0.0000
0.4998	0.836705	-1.4118			
1-Pentanol (1) + cyclohexylamine (2)					
$T = 288.15 \text{ K}$					
0.0000	0.871290	0.0000	0.6003	0.848864	-1.1277
0.0506	0.870021	-0.1665	0.6998	0.842494	-0.9985
0.1001	0.868675	-0.3172	0.7962	0.835420	-0.7634
0.1500	0.867306	-0.4689	0.8500	0.831143	-0.5921
0.2002	0.865855	-0.6135	0.8995	0.827043	-0.4144
0.2997	0.862562	-0.8507	0.9501	0.822677	-0.2111
0.3995	0.858846	-1.0422	1.0000	0.818282	0.0000
0.5004	0.854296	-1.1412			

TABLE II. Continued

x_1	$\rho / \text{g cm}^{-3}$	$V^E / \text{cm}^3 \text{mol}^{-1}$	x_1	$\rho / \text{g cm}^{-3}$	$V^E / \text{cm}^3 \text{mol}^{-1}$
1-Pentanol (1) + cyclohexylamine (2)					
$T = 293.15 \text{ K}$					
0.0000	0.866747	0.0000	0.6003	0.844821	-1.1339
0.0506	0.865544	-0.1710	0.6998	0.838550	-1.0045
0.1001	0.864254	-0.3248	0.7962	0.831578	-0.7691
0.1500	0.862936	-0.4789	0.8500	0.827355	-0.5968
0.2002	0.861531	-0.6251	0.8995	0.823304	-0.4180
0.2997	0.858315	-0.8631	0.9501	0.818988	-0.2135
0.3995	0.854658	-1.0524	1.0000	0.814635	0.0000
0.5004	0.850173	-1.1489			
$T = 298.15 \text{ K}$					
0.0000	0.862207	0.0000	0.6003	0.840764	-1.1398
0.0506	0.861069	-0.1757	0.6998	0.834591	-1.0104
0.1001	0.859833	-0.3325	0.7962	0.827719	-0.7746
0.1500	0.858565	-0.4891	0.8500	0.823550	-0.6016
0.2002	0.857202	-0.6365	0.8995	0.819549	-0.4220
0.2997	0.854056	-0.8747	0.9501	0.815279	-0.2157
0.3995	0.850460	-1.0623	1.0000	0.810968	0.0000
0.5004	0.846039	-1.1565			
$T = 303.15 \text{ K}$					
0.0000	0.857671	0.0000	0.6003	0.836693	-1.1456
0.0506	0.856593	-0.1799	0.6998	0.830615	-1.0161
0.1001	0.855410	-0.3400	0.7962	0.823839	-0.7799
0.1500	0.854186	-0.4984	0.8500	0.819726	-0.6065
0.2002	0.852868	-0.6477	0.8995	0.815771	-0.4256
0.2997	0.849789	-0.8860	0.9501	0.811547	-0.2178
0.3995	0.846251	-1.0719	1.0000	0.807278	0.0000
0.5004	0.841893	-1.1638			
$T = 308.15 \text{ K}$					
0.0000	0.853138	0.0000	0.6003	0.832605	-1.1515
0.0506	0.852111	-0.1833	0.6998	0.826617	-1.0218
0.1001	0.850981	-0.3468	0.7962	0.819937	-0.7854
0.1500	0.849802	-0.5075	0.8500	0.815876	-0.6114
0.2002	0.848523	-0.6581	0.8995	0.811967	-0.4295
0.2997	0.845509	-0.8966	0.9501	0.807786	-0.2198
0.3995	0.842027	-1.0810	1.0000	0.803558	0.0000
0.5004	0.837730	-1.1709			
$T = 313.15 \text{ K}$					
0.0000	0.848607	0.0000	0.6003	0.828501	-1.1569
0.0506	0.847630	-0.1867	0.6998	0.822595	-1.0262
0.1001	0.846545	-0.3528	0.7962	0.816008	-0.7896
0.1500	0.845407	-0.5155	0.8500	0.811997	-0.6148
0.2002	0.844167	-0.6675	0.8995	0.808133	-0.4319
0.2997	0.841215	-0.9063	0.9501	0.803997	-0.2208
0.3995	0.837791	-1.0896	1.0000	0.799817	0.0000
0.5004	0.833551	-1.1773			

TABLE II. Continued

x_1	$\rho / \text{g cm}^{-3}$	$V^E / \text{cm}^3 \text{mol}^{-1}$	x_1	$\rho / \text{g cm}^{-3}$	$V^E / \text{cm}^3 \text{mol}^{-1}$
2-Butanol (1) + cyclohexylamine (2)					
$T = 288.15 \text{ K}$					
0.0000	0.871290	0.0000	0.5997	0.845367	-0.8520
0.0495	0.869943	-0.1407	0.7000	0.838111	-0.7422
0.1011	0.868364	-0.2692	0.7999	0.829857	-0.5521
0.1505	0.866768	-0.3858	0.8488	0.825461	-0.4333
0.1995	0.865069	-0.4914	0.8997	0.820714	-0.3012
0.3004	0.861240	-0.6829	0.9498	0.815822	-0.1579
0.3996	0.856833	-0.8145	1.0000	0.810689	0.0000
0.4974	0.851641	-0.8669			
$T = 293.15 \text{ K}$					
0.0000	0.866747	0.0000	0.5997	0.841061	-0.8560
0.0495	0.865431	-0.1436	0.7000	0.833870	-0.7465
0.1011	0.863878	-0.2674	0.7999	0.825685	-0.5562
0.1505	0.862303	-0.3917	0.8488	0.821326	-0.4373
0.1995	0.860621	-0.4977	0.8997	0.816614	-0.3046
0.3004	0.856824	-0.6894	0.9498	0.811753	-0.1599
0.3996	0.852442	-0.8198	1.0000	0.806646	0.0000
0.4974	0.847283	-0.8710			
$T = 298.15 \text{ K}$					
0.0000	0.862207	0.0000	0.5997	0.836727	-0.8617
0.0495	0.860918	-0.1464	0.7000	0.829591	-0.7524
0.1011	0.859388	-0.2722	0.7999	0.821468	-0.5619
0.1505	0.857832	-0.3978	0.8488	0.817137	-0.4423
0.1995	0.856164	-0.5044	0.8997	0.812454	-0.3087
0.3004	0.852393	-0.6966	0.9498	0.807614	-0.1621
0.3996	0.848033	-0.8261	1.0000	0.802528	0.0000
0.4974	0.842904	-0.8766			
$T = 303.15 \text{ K}$					
0.0000	0.857671	0.0000	0.5997	0.832362	-0.8693
0.0495	0.856405	-0.1492	0.7000	0.825272	-0.7602
0.1011	0.854895	-0.2771	0.7999	0.817199	-0.5692
0.1505	0.853354	-0.4041	0.8488	0.812891	-0.4489
0.1995	0.851700	-0.5118	0.8997	0.808227	-0.3138
0.3004	0.847947	-0.7044	0.9498	0.803402	-0.1651
0.3996	0.843604	-0.8336	1.0000	0.798326	0.0000
0.4974	0.838501	-0.8840			
$T = 308.15 \text{ K}$					
0.0000	0.853138	0.0000	0.5997	0.827960	-0.8790
0.0495	0.851889	-0.1518	0.7000	0.820909	-0.7704
0.1011	0.850393	-0.2816	0.7999	0.812872	-0.5785
0.1505	0.848866	-0.4106	0.8488	0.808580	-0.4572
0.1995	0.847222	-0.5194	0.8997	0.803926	-0.3201
0.3004	0.843483	-0.7132	0.9498	0.799109	-0.1690
0.3996	0.839155	-0.8429	1.0000	0.794030	0.0000
0.4974	0.834068	-0.8930			

TABLE II. Continued

x_1	$\rho / \text{g cm}^{-3}$	$V^E / \text{cm}^3 \text{mol}^{-1}$	x_1	$\rho / \text{g cm}^{-3}$	$V^E / \text{cm}^3 \text{mol}^{-1}$
2-Butanol (1) + cyclohexylamine (2)					
$T = 313.15 \text{ K}$					
0.0000	0.848607	0.0000	0.5997	0.823519	-0.8912
0.0495	0.847368	-0.1542	0.7000	0.816495	-0.7829
0.1011	0.845885	-0.2864	0.7999	0.808484	-0.5902
0.1505	0.844366	-0.4171	0.8488	0.804198	-0.4673
0.1995	0.842729	-0.5274	0.8997	0.799548	-0.3281
0.3004	0.838998	-0.7227	0.9498	0.794725	-0.1736
0.3996	0.834678	-0.8534	1.0000	0.789632	0.0000
0.4974	0.829603	-0.9040			
2-Methyl-2-propanol (1) + cyclohexylamine (2)					
$T = 303.15 \text{ K}$					
0.0000	0.857671	0.0000	0.5998	0.820236	-1.0212
0.0508	0.855457	-0.1703	0.6997	0.810864	-0.9197
0.1002	0.853151	-0.3215	0.7999	0.800285	-0.7173
0.1502	0.850673	-0.4619	0.8712	0.792153	-0.5281
0.2001	0.848023	-0.5854	0.8992	0.788654	-0.4232
0.3005	0.842301	-0.8051	0.9504	0.782167	-0.2309
0.3991	0.835940	-0.9560	1.0000	0.775412	0.0000
0.4996	0.828512	-1.0243			
$T = 308.15 \text{ K}$					
0.0000	0.853138	0.0000	0.5998	0.815570	-1.0686
0.0508	0.850919	-0.1761	0.6997	0.806147	-0.9683
0.1002	0.848606	-0.3324	0.7999	0.795480	-0.7610
0.1502	0.846119	-0.4776	0.8712	0.787246	-0.5629
0.2001	0.843460	-0.6058	0.8992	0.783692	-0.4522
0.3005	0.837714	-0.8337	0.9504	0.777091	-0.2476
0.3991	0.831325	-0.9915	1.0000	0.770193	0.0000
0.4996	0.823876	-1.0668			
$T = 313.15 \text{ K}$					
0.0000	0.848607	0.0000	0.5998	0.810845	-1.1164
0.0508	0.846376	-0.1816	0.6997	0.801362	-1.0173
0.1002	0.844050	-0.3430	0.7999	0.790593	-0.8046
0.1502	0.841553	-0.4936	0.8712	0.782252	-0.5976
0.2001	0.838878	-0.6262	0.8992	0.778642	-0.4811
0.3005	0.833102	-0.8630	0.9504	0.771925	-0.2642
0.3991	0.826681	-1.0284	1.0000	0.764884	0.0000
0.4996	0.819193	-1.1098			
$T = 318.15 \text{ K}$					
0.0000	0.844073	0.0000	0.5998	0.806063	-1.1649
0.0508	0.841824	-0.1869	0.6997	0.796506	-1.0665
0.1002	0.839485	-0.3541	0.7999	0.785624	-0.8479
0.1502	0.836970	-0.5096	0.8712	0.777167	-0.6313
0.2001	0.834276	-0.6469	0.8992	0.773501	-0.5092

TABLE II. Continued

x_1	$\rho / \text{g cm}^{-3}$	$V^E / \text{cm}^3 \text{mol}^{-1}$	x_1	$\rho / \text{g cm}^{-3}$	$V^E / \text{cm}^3 \text{mol}^{-1}$
2-Methyl-2-propanol (1) + cyclohexylamine (2)					
$T = 318.15 \text{ K}$					
0.3005	0.828457	-0.8922	0.9504	0.766665	-0.2799
0.3991	0.821996	-1.0656	1.0000	0.759488	0.0000
0.4996	0.814465	-1.1538			
$T = 323.15 \text{ K}$					
0.0000	0.839547	0.0000	0.5998	0.801219	-1.2122
0.0508	0.837268	-0.1913	0.6997	0.791580	-1.1145
0.1002	0.834906	-0.3635	0.7999	0.780572	-0.8893
0.1502	0.832370	-0.5243	0.8712	0.771995	-0.6632
0.2001	0.829655	-0.6667	0.8992	0.768268	-0.5351
0.3005	0.823784	-0.9207	0.9504	0.761320	-0.2944
0.3991	0.817275	-1.1023	1.0000	0.754015	0.0000
0.4996	0.809685	-1.1965			

The obtained V^E values were fitted to a modified Redlich–Kister (RK) polynomial,¹⁸ whereby the degree of polynomial expansion, m , was determined by means of the F -test:¹⁹

$$V^E = x_1 x_2 \sum_{p=0}^m B_p (x_1 - x_2)^p \quad (2)$$

where B_p denotes the temperature dependent parameter:

$$B_p = \sum_{q=0}^k B_{pq} T^q \quad (3)$$

where T is the absolute temperature. Additional analysis showed that the optimal number of parameters k was 3, because any further increase in the number of parameters did not result in an improvement of the fit quality.

The results were also fitted and explained using the reduced excess molar volume, $V^E/x_1(1-x_1)$, which has a better physical significance and is more sensitive than V^E to interactions which occur in dilute regions.²⁰

$$\frac{V^E}{x_1(1-x_1)} = \sum_{n=0}^1 A_n x_1^n = A_0 + A_1 x_1 + A_2 x_1^2 \quad (4)$$

where the optimal number of parameters A_n was 3.

The unique sets of adjustable parameters B_{pq} over whole temperature range and adjustable parameters A_n of Eq. (4) at each temperature for the investigated binary systems, and the corresponding root mean square deviations defined by the equation:

$$\sigma = \sqrt{\sum_{i=1}^N \frac{(Y_{\text{exp},i}^E - Y_{\text{cal},i}^E)^2}{N}} \quad (5)$$

are given in Table III and Table IV, respectively. In Eq. (5), Y stands for V^E and $V^E/x_1(1-x_1)$, while N denotes the number of experimental data points.

TABLE III. Fitting parameters, B_{pq} , of Eq. (3) and the root mean square deviation, $\sigma/\text{cm}^3 \text{mol}^{-1}$

1-Propanol (1) + cyclohexylamine (2)				
288.15–313.15 K	$B_{00} = 2.9470$	$B_{01} = -0.0515$	$B_{02} = 7.7 \times 10^{-5}$	$\sigma = 0.0030$
	$B_{10} = -4.9954$	$B_{11} = 0.0217$	$B_{12} = -2.8 \times 10^{-5}$	
	$B_{20} = 4.7076$	$B_{21} = -0.0184$	$B_{23} = 1.5 \times 10^{-5}$	
	$B_{30} = 1.9405$	$B_{31} = -0.0086$	$B_{32} = 1.0 \times 10^{-5}$	
1-Butanol(1) + cyclohexylamine (2)				
288.15–313.15 K	$B_{00} = -0.6285$	$B_{01} = -0.0244$	$B_{02} = 3.2 \times 10^{-5}$	$\sigma = 0.0050$
	$B_{10} = 2.5151$	$B_{11} = -0.0282$	$B_{12} = 5.6 \times 10^{-5}$	
	$B_{20} = 9.6774$	$B_{21} = -0.0518$	$B_{23} = 7.2 \times 10^{-5}$	
	$B_{30} = -17.7455$	$B_{31} = 0.1229$	$B_{32} = -2.1 \times 10^{-4}$	
1-Pentanol (1) + cyclohexylamine (2)				
288.15–313.15 K	$B_{00} = -2.9435$	$B_{01} = -0.0051$	$B_{02} = -0.2 \times 10^{-5}$	$\sigma = 0.0025$
	$B_{10} = -6.7427$	$B_{11} = 0.0322$	$B_{12} = -4.2 \times 10^{-5}$	
	$B_{20} = 19.1794$	$B_{21} = -0.1133$	$B_{23} = 1.7 \times 10^{-4}$	
	$B_{30} = 3.6921$	$B_{31} = -0.0184$	$B_{32} = 2.5 \times 10^{-5}$	
2-Butanol (1) + cyclohexylamine (2)				
288.15–313.15 K	$B_{00} = -12.2075$	$B_{01} = 0.0638$	$B_{02} = -1.2 \times 10^{-4}$	$\sigma = 0.0033$
	$B_{10} = -10.2348$	$B_{11} = 0.0656$	$B_{12} = -1.1 \times 10^{-4}$	
	$B_{20} = -6.7604$	$B_{21} = 0.0558$	$B_{23} = -1.1 \times 10^{-4}$	
	$B_{30} = -0.0725$	$B_{31} = 0.0039$	$B_{32} = -1.0 \times 10^{-5}$	
2-Methyl-2-propanol (1) + cyclohexylamine (2)				
288.15–313.15 K	$B_{00} = 2.8491$	$B_{01} = -0.0119$	$B_{02} = -3.6 \times 10^{-5}$	$\sigma = 0.0042$
	$B_{10} = 8.1933$	$B_{11} = -0.0350$	$B_{12} = 1.9 \times 10^{-5}$	
	$B_{20} = 31.3276$	$B_{21} = -0.1879$	$B_{23} = 2.8 \times 10^{-4}$	
	$B_{30} = 10.4360$	$B_{31} = -0.0654$	$B_{32} = 1.0 \times 10^{-4}$	

The results of ρ and V^E for the investigated binaries, in the investigated temperature range and over the entire concentration range, are summarized in Table II, while Fig. 1 shows the dependence $V^E - x_1$ for all systems measured in this work and for 1-butanol + cyclohexylamine⁹ at the temperature 303.15 K. The symbols in Fig. 1 present the experimental V^E values, while the solid lines refer to the values calculated from the modified Redlich–Kister equation using the B_{pq} parameters given in Table III.

The ρ and V^E data taken from literature for the systems studied cover only 303.15 K.⁸ For the 1-pentanol + cyclohexylamine binary system, the agreement between the presented and the literature values is very good, while the experimental points of Dharmaraju *et al.*⁸ obtained at 303.15 K for the systems con-

taining 1-propanol, or 2-butanol, or 2-methyl-2-propanol and cyclohexylamine are somewhat higher. In minimum region, at equimolar composition, the discrepancy between the present determined and the literature values is about 10 % for 1-propanol, or 2-methyl-2-propanol + cyclohexylamine, and 15 % for the 2-butanol + cyclohexylamine system.

TABLE IV. Fitting parameters, A_n , of Eq. (4) and root mean square deviation, σ

T / K	A_0	A_1	A_2	$\sigma / \text{cm}^3 \text{mol}^{-1}$
1-Propanol (1) + cyclohexylamine (2)				
288.15	-4.0167	-4.0083	2.1905	0.0394
293.15	-4.1111	-3.8102	2.0319	0.0384
298.15	-4.2023	-3.6064	1.8660	0.0350
303.15	-4.2896	-3.4024	1.6961	0.0334
308.15	-4.3637	-3.2313	1.5528	0.0302
313.15	-4.4289	-3.0968	1.4569	0.0285
1-Butanol(1) + cyclohexylamine (2) ^a				
288.15	-3.6363	-3.7635	2.2793	0.0744
293.15	-3.7373	-3.5188	2.0767	0.0745
298.15	-3.8246	-3.3350	1.9444	0.0717
303.15	-3.9118	-3.1409	1.7990	0.0703
308.15	-3.9889	-2.9728	1.6721	0.0678
313.15	-4.0544	-2.8346	1.5640	0.0654
1-Pentanol (1) + cyclohexylamine (2)				
288.15	-3.1369	-4.2954	2.9793	0.0593
293.15	-3.2460	-4.0521	2.7925	0.0566
298.15	-3.3586	-3.7894	2.5880	0.0554
303.15	-3.4627	-3.5553	2.4074	0.0534
308.15	-3.5537	3.3630	2.2572	0.0502
313.15	-3.6354	-3.2083	2.1564	0.0498
2-Butanol (1) + cyclohexylamine (2)				
288.15	-2.7800	-2.2347	1.7603	0.0488
293.15	-2.8223	-2.1408	1.6646	0.0513
298.15	-2.8903	-1.9786	1.5148	0.0508
303.15	-2.9587	-1.8253	1.3591	0.0501
308.15	-3.0222	-1.7012	1.2114	0.0491
313.15	-3.0831	-1.5993	1.0655	0.0472
2-Methyl-2-propanol (1) + cyclohexylamine (2)				
303.15	-3.4535	-1.1049	-0.3463	0.0396
308.15	-3.5752	-1.0557	-0.6481	0.0411
313.15	-3.6922	-1.0383	-0.9189	0.0431
308.15	-3.8057	-1.0598	-1.1377	0.0432
323.15	-3.9089	-1.1000	-1.3263	0.0427

^aParameters obtained for the experimental data already presented in the literature⁹

The experimental $V^E/x_1(1 - x_1)$ values and those calculated by Eq. (4) at 303.15 K are plotted in Fig. 2 as a function of the mole fraction of an alcohol.

The non-linear curves obtained for all investigated systems clearly show their non-ideal behavior.

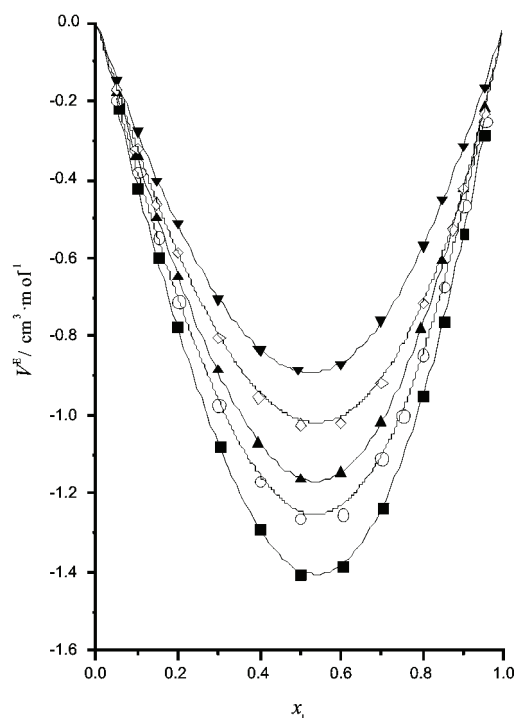


Fig. 1. Experimental values of V^E at 303.15 K for the systems: (■) 1-propanol (1) + cyclohexylamine (2); (○) 1-butanol (1) + cyclohexylamine (2);⁹ (▲) 1-pentanol (1) + cyclohexylamine (2); (▼) 2-butanol (1) + cyclohexylamine (2); (◇) 2-methyl-2-propanol (1) + cyclohexylamine (2). The symbols refer to the experimental points, while the lines present the results calculated using Eq. (2) with the parameters presented in Table III.

The magnitude and the sign of V^E can arise from two opposing factors:²¹ (i) the positive contribution is a consequence of the disruption of the hydrogen bonds in the self-associated alcohol and the dipole–dipole interactions between alcohol monomer and multimer. The self-association of the amine molecules is rather small; (ii) negative contributions arise from strong intermolecular interactions attributed to charge-transfer, dipole–dipole interactions and hydrogen bonding between unlike molecules. Hence, the negative V^E values of the investigated systems assume that heteroassociates forming cross complexes in the alcohol + amine mixtures have stronger O–H···N bonds than O–H···O and N–H···N bonds. This can be explained qualitatively by the fact that the free electron pair around the N atoms with less *s* and more *p* character has a higher polarizability and acts as a good proton acceptor for the donor –OH groups of the alcohols, which are more efficient than the –OH group itself. The negative sign of V^E indicates a net packing effect contributed to by structural changes arising from interstitial accommodation. As can be seen from Fig. 1, the negative V^E values are larger in the mixture with 1-propanol and decrease as the chain length of the 1-alkanol increases. This trend indicates that the strength of the intermolecu-

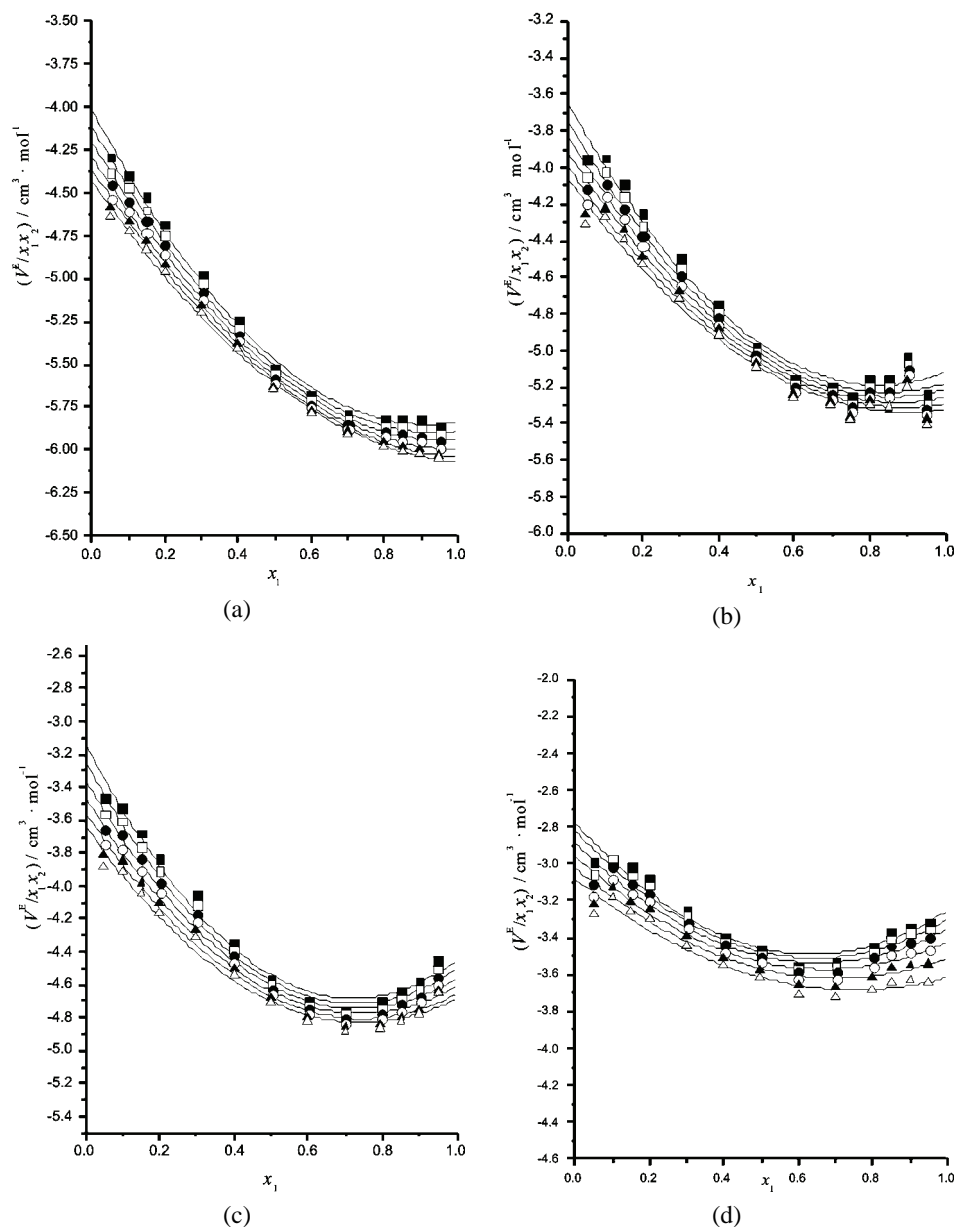


Fig. 2. Values of $V^E/x_1(1-x_1)$ data at (■) 288.15, (□) 293.15 K, (●) 298.15 K, (○) 303.15 K, (▲) 308.15 K, (△) 313.15 K, (◆) 318.15 K and (◇) 323.15 K for the systems: (a) 1-propanol (1) + cyclohexylamine (2); (b) 1-butanol (1) + cyclohexylamine (2);⁹ (c) 1-pentanol (1) + cyclohexylamine (2); (d) 2-butanol (1) + cyclohexylamine (2). The symbols refer to the experimental points, while the lines present the results calculated using Eq. (4) with the parameters presented in Table IV.

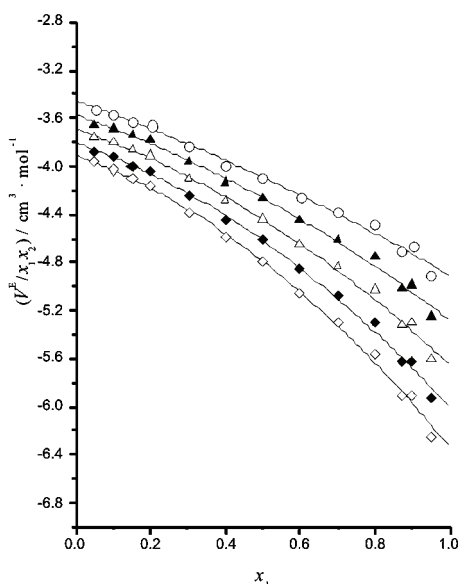


Fig. 2e. Values of $V^E/x_1(1-x_1)$ data at (■) 288.15, (□) 293.15 K, (●) 298.15 K, (○) 303.15 K, (▲) 308.15 K, (△) 313.15 K, (◆) 318.15 K and (◇) 323.15 K for the system 2-methyl-2-propanol (1) + cyclohexylamine (2). The symbols refer to the experimental points, while the lines present the results calculated using Eq. (4) with the parameters presented in Table IV.

lar hydrogen bonding of cyclohexylamine with 1-propanol is much stronger than with the other higher 1-alcohols in the following order: 1-propanol > 1-butanol > 1-pentanol. These strengths of the interaction $\text{OH}\cdots\text{NH}_2$ bonds suggest that the proton donating ability of 1-alcohols is of the same order. Namely, longer 1-alcohols would increase the basicity of the oxygen and make the hydroxyl proton less available for H bonding. In addition, it means that the most efficient packing can be attributed to the lower alcohol, which decreases with increasing chain length of 1-alcohol, where the packing effects are the result of their lower self-association (higher breaking of their H bonds) and the fact that the crowded molecules of amine, as a consequence of steric hindrance, are better packed in the more open structure of the longer alcohols. Also, the effect of increasing chain length of the 1-alcohol for a given amine can be considered using the effective dipole moment. Bearing in mind the discussions given in previous works referring to 1-alcohols and various amines, it can be concluded that in the present systems the following behavior could be expected. In the systems of 1-alcohols with cyclohexylamine, the absolute value of the V^E decreases with decreasing effective dipole moment of the alcohol.

The trend in the negative values of V^E for mixtures of cyclohexylamine with branched alcohols (2-butanol, 2-methyl-2-propanol) (Table II) compared to 1-butanol⁹ is in the order: 1-butanol > 2-methyl-2-propanol > 2-butanol, suggesting that the interactions between tertiary alcohol and cyclohexylamine are stronger than between the secondary alcohol with cyclohexylamine, which in turn are stronger than the interactions between the primary alcohol and the amine.⁸ The

results shown in Fig. 1 indicate that V^E of the mixture with 2-methyl-2-propanol are more negative than those with 2-butanol. Qualitatively, this could be explained by the fact that the oxygen atom of 2-methyl-2-propanol should be regarded as a better acceptor towards the NH proton of the amine than the oxygen atoms of the 2-butanol. Also, the system with 2-methyl-2-propanol suggests that the steric hindrance of the *tert*-butyl group tends to hamper the complex less than with 2-butanol. This is a consequence of a predominating electrometric effect (+I effect) over steric effect in 2-methyl-2-propanol.^{8,22}

The influence of temperature on the V^E for the systems containing 1-propanol, or 1-butanol,⁹ or 1-pentanol, or 2-butanol is almost negligible and the V^E values become only slightly more negative with increasing temperature. Only in the case of 2-methyl-2-propanol system was the influence of temperature more expressed. These facts can possibly be explained as a balance of two opposing effects caused by an increase in the kinetic energy of the different molecules: (i) the association constants of mixed complexes decrease with increasing temperature and the OH–N interactions decrease, (ii) the number of species increases after breakage of the complexes and (iii) the interstitial accommodation of one molecule into the other is facilitated. Thus, the effects (i) give an increase of V^E , while the effects (ii) and (iii) cause a decrease of V^E .

CONCLUSIONS

The densities of the binary mixtures (1-propanol, or 1-pentanol, or 2-butanol, or 2-methyl-2-propanol + cyclohexylamine) were measured in the temperature range 288.15–323.15 K at atmospheric pressure and the excess molar volumes V^E were calculated.

For all the investigated binary systems and the system with 1-butanol,⁹ the negative values of V^E for the mixtures of cyclohexylamine with 1-alcohols lie in the order 1-propanol > 1-butanol > 1-pentanol. The value of V^E absolutely decreases when the chain length of the 1-alcohol molecules increases. The negative values of V^E in the mixtures of the same amine with branched alcohols compared to 1-butanol⁹ are in the order: 1-butanol > 2-methyl-2-propanol > 2-butanol, suggesting that the interactions of tertiary alcohols are stronger than those of secondary alcohols in mixtures with cyclohexylamine. It is clear that the magnitude of V^E depends on the chain length of the alcohol and position of hydroxyl group in the alcohol molecule.

Acknowledgement. The authors gratefully acknowledge the financial support received from the research fund of the Ministry of Science and Technological Development of the Republic of Serbia and the Faculty of Technology and Metallurgy, University of Belgrade (project No 142064).

ИЗВОД
 ГУСТИНЕ И ДОПУНСКЕ МОЛАРНЕ ЗАПРЕМИНЕ СМЕША
 АЛКОХОЛ + ЦИКЛОХЕКСИЛАМИН

ИВОНА Р. РАДОВИЋ, МИРЈАНА Љ. КИЈЕВЧАНИН, АЛЕКСАНДАР Ж. ТАСИЋ,
 БОЈАН Д. ЂОРЂЕВИЋ И СЛОБОДАН П. ШЕРБАНОВИЋ

Технолошко-медицалуршки факултет, Универзитет у Београду, Карнегијева 4, 11120 Београд

Густине бинарних смеша (1-пропанол или 2-бутанол или 1-пентанол + циклохексил-амин) су мерене у температурном интервалу 288,15–313,15 К и на атмосферском притиску, а густине система 2-метил-2-пропанол + циклохексиламин су мерене у температурном интервалу 303,15–323,15 К и на атмосферском притиску. Сва мерења су извршена на Anton Paar DMA 5000 дигиталном густиномеру. Из експерименталних вредности густина израчунате су допунске моларне запремине наведених смеша.

(Примљено 2. априла, ревидирано 28. августа 2009)

REFERENCES

1. S. P. Šerbanović, M. Lj. Kijevčanin, I. R. Radović, B. D. Djordjević, *Fluid Phase Equilib.* **239** (2006) 69
2. M. Lj. Kijevčanin, S. P. Šerbanović, I. R. Radović, B. D. Djordjević, A. Ž. Tasić, *Fluid Phase Equilib.* **251** (2007) 78
3. I. R. Radović, M. Lj. Kijevčanin, E. M. Djordjević, B. D. Djordjević, S. P. Šerbanović, *Fluid Phase Equilib.* **263** (2008) 205
4. M. Lj. Kijevčanin, M. M. Djuriš, I. R. Radović, B. D. Djordjević, S. P. Šerbanović, *J. Chem. Eng. Data* **52** (2007) 1136
5. M. Lj. Kijevčanin, I. M. Purić, I. R. Radović, B. D. Djordjević, S. P. Šerbanović, *J. Chem. Eng. Data* **52** (2007) 2067
6. B. D. Djordjević, S. P. Šerbanović, I. R. Radović, A. Z. Tasić, M. Lj. Kijevčanin, *J. Serb. Chem. Soc.* **72** (2007) 1437
7. L. I. N. Tomé, M. T. S. Rosado, M. E. S. Eusébio, J. S. Redinha, *J. Mol. Struct. THEOCHEM* **804** (2007) 65
8. G. Dharmaraju, G. Narayanaswamy, G. K Raman, *J. Chem. Thermodyn.* **13** (1981) 249
9. M. Lj. Kijevčanin, I. R. Radović, S. P. Šerbanović, A. Ž. Tasić, B. D. Djordjević, *Thermochim. Acta* (2009), accepted for publication
10. A. J. Treszczanowicz, G. C. Benson, *J. Chem. Thermodyn.* **10** (1978) 967
11. J. A. Riddick, W. B. Bunger, T. K. Sakano, *Physical Properties and Methods of Purification, Vol. II, Organic Solvents*, John Wiley & Sons, New York, 1986
12. H. Iloukhani, B. Samiey, M. A. Moghaddasi, *J. Chem. Thermodyn.* **38** (2006) 190
13. A. Sacco, A. K. Rakshit, *J. Chem. Thermodyn.* **7** (1975) 257
14. J. M. Resa, C. González, J. M. Goenaga, M. Iglesias, *J. Chem. Eng. Data* **49** (2004) 804
15. A. Grenner, M. Klauck, M. Kramer, J. Schmelzer, *J. Chem. Eng. Data* **51** (2006) 176
16. N. Radojković, A. Tasić, B. Djordjević, D. Grozdanić, *J. Chem. Thermodyn.* **8** (1976) 1111
17. A. Ž. Tasić, D. K. Grozdanić, B. D. Djordjević, S. P. Šerbanović, N. Radojković, *J. Chem. Eng. Data* **40** (1995) 586
18. O. Redlich, A. Kister, *Ind. Eng. Chem.* **40** (1948) 345

19. P. R. Bevington, D. K. Robinson, *Data Reduction and Error Analysis for the Physical Sciences*, McGraw-Hill, Singapore, 1994
20. J. E. Desnoyers, G. J. Perron, *J. Solution Chem.* **26** (1997) 749
21. B. D. Djordjević, I. R. Radović, M. Lj. Kijevčanin, A. Ž. Tasić, S. P. Šerbanović, *J. Serb. Chem. Soc.* **74** (2009) 477
22. L. Pikkarainen, *J. Chem. Thermodyn.* **14** (1982) 503.



J. Serb. Chem. Soc. 74 (11) 1319–1333 (2009)
JSCS–3921

Journal of
the Serbian
Chemical Society

JSCS@tmf.bg.ac.rs • www.shd.org.rs/JSCS

UDC 504.3.054:614.78:614.71(497.11)

Original scientific paper

Physical and chemical characterization of the particulate matter suspended in aerosols from the urban area of Belgrade

JASMINKA D. JOKSIĆ^{1*}, MILENA JOVAŠEVIĆ-STOJANOVIĆ¹, ALENA BARTONOVA², MIRJANA B. RADENKOVIĆ¹, KARL-ESPEN YTTTRI², SNEŽANA MATIĆ-BESARABIĆ³ and LJUBIŠA IGNJATOVIĆ⁴

¹Vinča Institute of Nuclear Sciences, P.O. Box 522, 11001 Belgrade, Serbia ²NILU, Norwegian Institute for Air Research, P.O. Box 100, 2027 Kjeller, Norway, ³Public Health Institute, Bul. Despota Stefana 54, 11000 Belgrade and ⁴Faculty of Physical Chemistry, Studentski trg 12–16, 11000 Belgrade, Serbia

(Received 2 March, revised 7 April 2009)

Abstract: Within this study, attempts were made to characterize the coarse and fine particulate aerosol fractions in urban area of Belgrade and define the inorganic chemical composition of the aerosol fractions. For this purpose, daily deposits of PM₁₀, PM_{2.5} and PM₁ aerosol fractions were collected during spring and autumn sampling periods in 2007 and analyzed for the PM mass concentrations, trace elements and secondary ions. The results obtained in the two campaigns showed average daily mass concentrations of 37 and 44 µg/m³ for PM₁₀, 22 and 23 µg/m³ for PM_{2.5} and 15 and 17 µg/m³ for the finest particulate matter fraction PM₁ with the maximums exceeding the limit values set by the EU air quality regulations. A correlation with the gas-phase ambient air pollutants SO₂, NO₂ and O₃ was found and is discussed. The concentrations of trace elements (Mg, Al, K, V, Cr, Mn, Fe, Co, Ni, Cu, Zn, As, Se, Mo, Cd, Sb, Ba, Tl, Pb and Th) and secondary ions (NO₃⁻, SO₄²⁻, NH₄⁺, K⁺, Ca²⁺ and Na⁺) determined in the PM₁₀, PM_{2.5} and PM₁ aerosol fractions showed levels and distributions indicating soil and traffic-related sources as the main pollution sources. This study was conducted as the first step of PM assessment in order to point out main air pollution sources and suggest a remedy strategy specific for this region.

Keywords: aerosols; particulate matter; characterization; trace elements; secondary ions.

INTRODUCTION

Particulate matter is an air pollution component directly emitted into the atmosphere through man-made and natural processes, including combustion from car-engines, households, industrial activities, road erosions, *etc.*, or formed as se-

* Corresponding author. E-mail: jasnaj@vinca.rs
doi: 10.2298/JSC0911319J



condary aerosols due to chemical transformations of gases mainly emitted by traffic or industry. It is a complex mixture of particles that may be solid, liquid or both, suspended in the air and consisting of organic and inorganic substances.¹ The coarse fraction (PM₁₀), consisting of particles with an aerodynamic diameter of up to 10 µm, usually spends no more than a few hours suspended after emission before being removed from the atmosphere by sedimentation or precipitation processes, whereas the fine particles, of 2.5 µm diameter (PM_{2.5}) or less (PM₁), may remain in the atmosphere for days or even weeks and, consequently, be transported over long distances. Comprehensive toxicological and epidemiological studies conducted over the last decades have implicated that human exposure to such small airborne particles (PM₁₀ and less) have adverse health effects and may be a cause of a number of respiratory and cardiovascular inflammations.² During inhalation, the coarse particulate fraction usually remains in the upper part of the airways and lung but the fine particles penetrate deeper and reach the alveolar region. The chemical composition of air particulate matter fractions thus becomes very important and engrosses both scientific and public auditory.^{3,4} The main adverse health effects were evident during episodes of extremely high levels of air pollution so that extensive air pollution control was initiated by authorities contributing to establishment and adoption of regulations for air quality improvement.⁵ Regulations on the EU level have set objectives and limit values for ambient concentrations of PM with significant results (WHO, 2002). Their implementation in Serbia is, however, not completed so far and a new methodology for sampling and analysis is to be adopted and established within the existing air quality monitoring network.⁶

Since 2002, the suspended particles PM₁₀ and PM_{2.5} in aerosols and their physical and chemical characterization were the subject of a few research projects dealing with air quality assessment in the Belgrade urban area.⁷⁻⁹ The first air quality assessment resulted in valuable conclusions on air pollution in this area and some attempts were made to specify the emission sources using statistical methods and modeling. The main pollution sources were identified to be traffic and local heating units. These evaluations had, however, limitations due to non-referenced sampling facilities and incomplete chemical characterization of the aerosol fractions. Recently, a comprehensive study on PM₁₀, M_{2.5} and PM₁ in aerosols of the urban area of Belgrade have started within the frame of the WeBIOPATR project.¹⁰ The main goal of the project is to introduce and establish standard operating procedures and quality assurance procedures in all stages of aerosol management and analysis, to use advanced analytical techniques for PM chemical characterization and finalize the research with source apportionment analysis.¹¹ The very first results of this study concerning mass concentrations measurements, elemental analyses and secondary ions determination in PM₁₀, PM_{2.5} and PM₁ aerosol fractions, collected during two sampling cam-

paigns (spring/autumn) in the urban residential area of Belgrade, will be presented and discussed in this paper. The obtained results should define mass concentration ranges of different aerosol fractions, trace elements and ions concentrations as a set of complementary data on the inorganic part of the chemical composition of PM. These data are compared with previously obtained data from the monitoring network and give some insight into the present situation in the residential area of New Belgrade concerning the particulate matter composition related to different air pollution sources.

EXPERIMENTAL

Aerosol sampling

The sampling campaigns were performed at the urban background residential site (Fig. 1) in Omladinskih Brigada Street (OBS), a fast developing New Belgrade area of the Serbian capital city (44°49'7" N, 20°28'5" E, 116 A) during two periods: from April 26th to May 2nd 2007 and from September 15th to September 19th 2007.

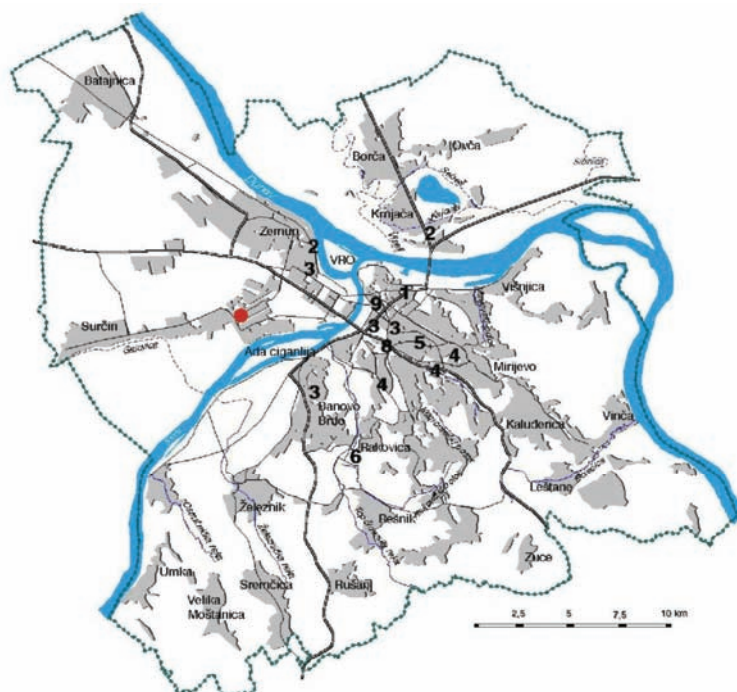


Fig. 1. Schematic position of the urban background residential sampling site OBS in Belgrade, labeled with the red point.

The aerosol sampling was conducted using three separate European reference low-volume samplers (Sven/Leckel LVS3) with inlets for collecting PM₁₀, PM_{2.5} and PM₁ fractions; all with flow rates 2.3 m³ h⁻¹. During the first campaign, the sampling devices were placed 1 m above the ground at 3 m distance to the building, with the PM heads next to each other. Their

position was changed in the next campaign, when the samplers were mounted on the 15 m high roof of the building and the inlets were pointed 2 m away from each other to allow independent aerosol collection. This position should be representative enough to enable further source apportionment analysis. The suspended particles were collected onto 47 mm Whatman QM-A double-sided quartz fiber filters, taken from the same batch and handled with special care, according to the standard operating procedure.¹² The PM₁₀, PM_{2.5} and PM₁ aerosol fractions were sampled on a daily basis (24 h, beginning at 7 a.m.) with one "field blank" per week, according to the sampling reference method defined by the EU Directive 1999/30/EC.¹³

An automatic air monitoring station with Horiba monitors: APSA-360, APNA-360, APOA-360 for SO₂, NO₂ and O₃ measurements, respectively, and an Eberline FH-62I/R air particulate monitor for PM₁₀ mass concentration measurements was placed 1 m above the ground in front of the building at the OBS site, within the Belgrade municipal monitoring network. The corresponding hourly readings of SO₂, NO₂, O₃ and PM₁₀ concentrations were recalculated into average daily values and were used for comparison as considerable additional data from the same location in the same time periods.

Gravimetric measurements

Before exposure, the quartz fiber filters were pre-fired at 900 °C for 3 h to remove organic impurities¹⁴ and the preconditioning procedure of both non-exposed and loaded filters was applied prior to gravimetric measurements.¹⁵

During the first (spring) sampling campaign, pre-fired quartz filters were placed in opened Petri dishes into a dessicator for 48 h in a Class 100 clean room with controlled temperature and relative humidity (20±2 °C, 50±5 %). The mass concentrations were determined as the average of two gravimetric measurements using a Sartorius 160P semi-micro balance with a minimum 0.01 mg mass resolution. Quality assurance was provided by the simultaneous measurement of a set of three blank filters that were interspersed within the pre- and post-weighing sessions of each set of sample filters and the mean change in the weight of the blank filter mass between the weighing sessions was used to correct the sample filter mass changes. This procedure was applied to both unexposed and exposed filters.

During the second (autumn) sampling campaign, the gravimetric procedure was conducted under improved conditions, according to EN 12341 for PM₁₀.¹² The filters were exposed in opened Petri-slides for 48 h at 20±1 °C temperature and 50±5 % relative humidity in a Class 100 clean room with automatic temperature and pressure regulation. After preconditioning, the filters were weighed twice using a Precisa XR 125 SB micro-balance with 0.01 mg mass resolution and the mass concentrations were calculated as average values. Two pre-fired blank quartz filters were exposed in the conditioning room all the time and their mass checked after each series of eight sample measurements. Before and after each weighing session, certified test weights of 100 and 200 mg were used for accuracy control of the micro-balance. Following the gravimetric measurements, the loaded filters were stored in a cool room at 4 °C until analysis.

Chemical analysis

Once the gravimetric measurements were realized, loaded filters with PM₁₀, PM_{2.5} and PM₁ aerosol fractions were punched and areas of 6 and 3 cm² of each filter were used for trace elements analysis and secondary ions analysis, respectively. The CEN/TC 264 N779 procedure¹⁶ was applied for extraction of the trace elements. The loaded quartz filters were treated with acidic mixture: HNO₃ (c)/30 % H₂O₂/H₂O (3/2/5) using analytical grade reagents (Merck) and distilled/deionized water (MiliQ, 18.2 MΩ). The filters were digested in closed

100 ml Teflon vessels in a Mars 5 microwave accelerated reaction system with a two-stage programmed temperature progress up to 200 °C. The concentrations of 20 elements: Mg, Al, K, V, Cr, Mn, Fe, Co, Ni, Cu, Zn, As, Se, Mo, Cd, Sb, Ba, Tl, Pb and Th were determined by inductively coupled plasma–mass spectrometry (ICP–MS) using an Agilent 7500 device with an Octopole Reaction System.

Quality control and verification of the applied procedures for microwave digestion and multi-elemental trace analysis using ICP MS was realized by the analysis of 2783 NIST (National Institute of Standard and Technology, MD, USA) standard reference material containing a $PM_{2.5}$ fraction of urban dust from a mixed industrial urban area of Vienna, collected on a polycarbonate membrane filter.

Before secondary ions analysis, the samples underwent a nano-pure water extraction for 24 h.¹⁷ The aqueous extracts were further analyzed by standard ion chromatography using a Dionex DX-500 IC system to determine: NO_3^- , SO_4^{2-} , NH_4^+ , K^+ , Ca^{2+} and Na^+ according to SOP MDL 064.¹⁸

RESULTS AND DISCUSSION

Mass concentrations of PM_{10} , $PM_{2.5}$ and PM_1 fractions

The results of the PM_{10} , $PM_{2.5}$ and PM_1 mass concentrations measurements in 24-hour aerosol deposits on quartz fiber filters collected in the spring and autumn sampling periods are shown in Fig. 2.

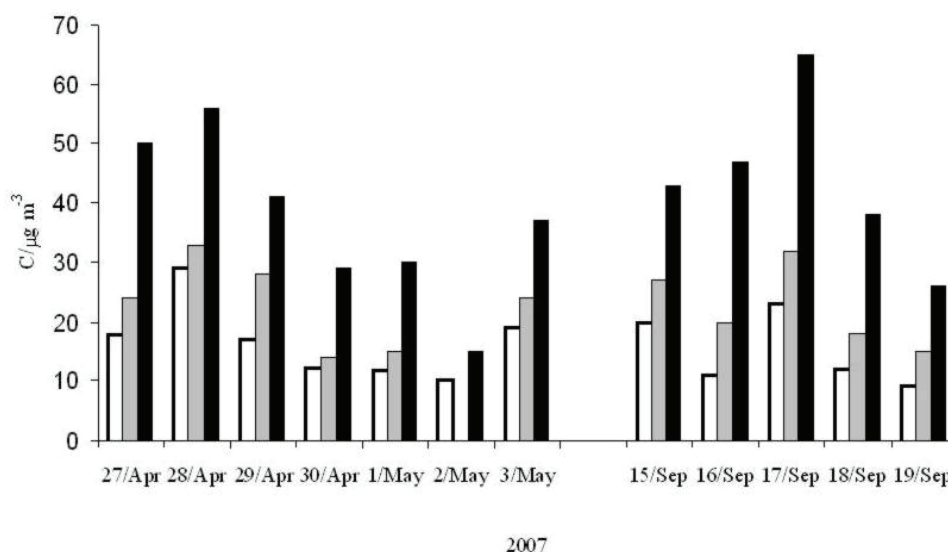


Fig. 2. Mass concentrations of the PM_{10} , $PM_{2.5}$ and PM_1 fractions in ambient aerosol deposits collected during the spring and autumn sampling periods at the OBS sampling site.

In the graph PM_{10} , $PM_{2.5}$ and PM_1 are presented by the black, gray and white bars, respectively.

It may be seen that all fractions follow the same trend, with noticeable working day/holiday differences. The spring sampling campaign was performed du-

ring non-working days, since the weekend was linked with holidays, except the first and last days of the sampling period. Consequently, on the 27th and 28th Apr, when the traffic frequency was very high, the PM₁₀ mass concentrations had maximum values of 50 and 56 µg/m³ and the maximum mass concentrations of PM_{2.5} and PM₁ were 33 and 29 µg/m³, respectively. During the autumn campaign, the PM₁₀ mass concentration had the maximum value of 65 µg/m³ on Monday, 17th Sep, the first working day of the week. The corresponding PM_{2.5} and PM₁ mass concentrations were also the highest in the period, with values of 32 and 23 µg/m³, respectively.

European air quality regulations stipulated that the average daily PM₁₀ mass concentrations should not exceed 50 µg/m³ more than 35 times a year by 2005 and 7 times by 2010, with average annual limit values of 40 and 20 µg/m³, respectively. Monitoring of the fine particulate fraction is still not obligatory in EU,¹⁹ although a recently published Directive²⁰ for PM_{2.5} proposes 20 µg/m³ as the annual average daily limit value and 35 µg/m³ not to be exceeded more than 35 times a year. According to WHO, the PM₁₀ average annual mass concentrations vary widely, from 16 µg/m³ in Finland and Ireland, to 50–52 µg/m³ in Bulgaria and Romania in 2004, and the levels were higher during 2006 by at least 5 µg/m³ in Austria, Hungary, Norway and Poland, and lower by at least 5 µg/m³ in Bulgaria, Greece, Slovenia and Serbia.²¹ These values mostly came from the air quality monitoring programs of the countries, in which 566 cities were assessed, with different QA/QC applied. If the mass concentrations values obtained within a few regional research projects are evaluated, there are observable but no remarkable differences. In urban areas from neighboring countries, the mean values of PM₁₀ mass concentrations were reported as: 75 µg/m³ for Athens, Greece;²² 72 µg/m³ for Sophia, Bulgaria;²³ 51 µg/m³ for Genoa, Italy;²⁴ 2001, 75 µg/m³ for Bucharest, Romania.²³ Within earlier studies on air quality in Belgrade urban area, the mean biannual PM₁₀ and PM_{2.5} concentration values were 68 and 61.4 µg/m³ respectively.²⁵ Comparing these data, the mass concentrations values of both the coarse and fine particulate fractions obtained for Belgrade were within expectable levels for the region, with reserve concerning the considerable differences in data assessment periods and methodologies.

Concerning the particles size distribution in the mass concentrations, in the spring campaign, PM₁ on average counted for about 78 % of PM_{2.5} and 47 % of PM₁₀, while PM_{2.5} counted 56 % of PM₁₀. In the autumn campaign, the average PM₁ counted for about 66 % of PM_{2.5} and 34 % of PM₁₀, while PM_{2.5} counted for 50 % of PM₁₀. In general, a regular pattern of the distribution of the coarse and fine fractions in air particulate matter does not exist for urban background sites in Europe, in spite of a number of projects. Again, comparing to previous results for Belgrade urban areas,²⁵ there is a discrepancy in the ratios of the

fractions. Obviously, a better differentiation between two size fractions was achieved due to use of separate reference air-samplers with different inlets.

Seasonal variations of the PM₁₀, PM_{2.5} and PM₁ mass concentrations values as well as their ratios are slightly noticeable since both campaigns were performed in non-heating periods and in similar weather conditions. During the sampling periods, the mean values of temperature, relative humidity and wind speed were: 17.4 °C, 40 % and 0.8 m s⁻¹, respectively, in the spring and 19.4 °C, 59 % and 0.2 m s⁻¹, respectively, in the autumn campaign. There was no measurable precipitation level during both sampling periods, except for 0.1 dm³ m⁻² on September 18th.

In general, the present results on the PM mass concentrations in the residential urban area may be reputed as a reliable indicator of still high air pollution in Belgrade City, as in previous periods of assessment, indicating the necessity of further studies and remediation.

Correlations of the mass concentrations with other parameters

During the sampling campaigns, the concentrations of SO₂, NO₂ and O₃, as well as the *PM₁₀ mass concentration were simultaneously recorded by the automatic monitoring station situated at the OBS site within the Belgrade monitoring network. Hourly readings obtained at this station were recalculated into average daily values, which are given in Table I.

TABLE I. Average daily concentrations of SO₂, NO₂, O₃ and *PM₁₀ obtained during the spring (26th Apr.–2nd May) and autumn (15th Sep–19th Sep) sampling campaigns at the automatic monitoring station at the OBS site

Date	$c(\text{SO}_2) / \mu\text{g m}^{-3}$	$c(\text{NO}_2) / \mu\text{g m}^{-3}$	$c(\text{O}_3) / \mu\text{g m}^{-3}$	$c(\text{PM}_{10}) / \mu\text{g m}^{-3}$
26 Apr. 2007	16.9	57.5	69	38
27. Apr. 2007	16.9	48	67.6	48
28 Apr. 2007	7.6	19.6	106.2	38
29 Apr. 2007	6.3	17.7	88.4	29
30 Apr. 2007	3.6	10.4	86.6	20
1 May 2007	4.6	18.6	86.7	21
2 May 2007	24.3	49.6	74.9	24
15 Sep. 2007	15	37	58	30
16 Sep. 2007	17	64	52	40
17 Sep. 2007	45	89	44	65
18 Sep. 2007	22	54	55	44
19 Sep. 2007	12	27	39	18

The concentrations of the ambient air gas-phase pollutants $c(\text{SO}_2)$, and $c(\text{NO}_2)$, and the mass concentration $c(*\text{PM}_{10})$ obtained at the automatic air-monitoring station are shown in Fig. 3, together with the mass concentration $c(\text{PM}_{10})$ obtained using the separate sampling device with a PM₁₀ inlet, for both the spring and autumn sampling periods.

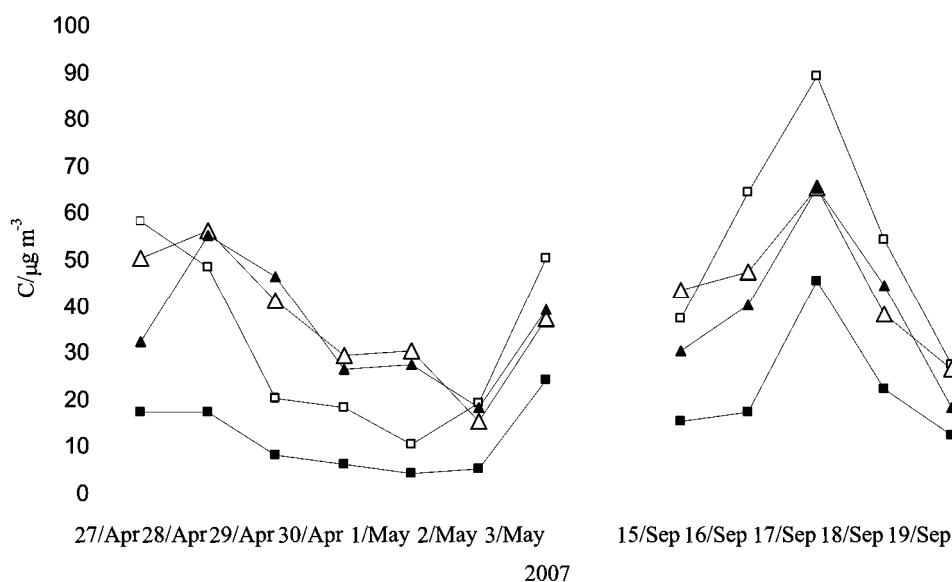


Fig. 3. Correlations between the daily concentration values of $C(\text{PM}_{10})$ determined in this work and the $c(\text{SO}_2)$, $c(\text{NO}_2)$ and $c(*\text{PM}_{10})$ values obtained at the automatic air-monitoring station (presented with the symbols \blacktriangle , \blacksquare , \square and \triangle , respectively) during the spring and autumn campaigns at the OBS sampling site.

It may be concluded that the same trends of data exist between the parameters presented in Fig. 3. Quantitatively, the correlations obtained after linear statistical analysis applied on the PM_{10} daily mass concentrations $C(\text{PM}_{10})$ and the average daily concentrations $c(\text{SO}_2)$, $c(\text{NO}_2)$, $c(\text{O}_3)$ and $c(*\text{PM}_{10})$ are listed in Table I. The corresponding Pearson's coefficients of regression R^2 for $c(\text{SO}_2)$, $c(\text{NO}_2)$ and $c(*\text{PM}_{10})$ with respect to $c(\text{PM}_{10})$, were: 0.38; 0.52 and 0.76 in the spring and 0.75, 0.85 and 0.83 in the autumn sampling period, respectively. No significant correlation between the O_3 and PM_{10} concentration values was obtained. In the autumn period, it was $R^2 < 0.01$ and in the spring period, the correlation was negative with $R^2 = 0.23$. However, these conclusions may be taken only as indicative due to the considerable lack of data.

Trace elements and ion contents in the PM fractions

The chemical characterization of the PM_{10} , $\text{PM}_{2.5}$ and PM_1 aerosol fractions comprised the determination of the elemental concentrations of Mg, Al, K, V, Cr, Mn, Fe, Co, Ni, Cu, Zn, As, Se, Mo, Cd, Sb, Ba, Tl, Pb and Th and the concentrations of the secondary ions NO_3^- , SO_4^{2-} , NH_3^+ , Na^+ , Ca^+ and K^+ .

Prior to trace elements determination, the microwave acid extraction described in the previous section was applied to the aerosol deposits and the obtained extracts were further analyzed using the ICP MS technique. The utilized analyti-

cal procedure was validated by the analysis of the NIST 2783 standard reference urban dust material containing a PM_{2.5} aerosol fraction, collected on a polycarbonate membrane filter. The results of this analysis are listed in Table II.

TABLE II. Results of the ICP–MS analysis of the NIST 2783 standard reference urban dust material containing a PM_{2.5} fraction deposited on a polycarbonate membrane filter

Element	Certified value, ng	Observed value, ng	Recovery, %	LLD / ng
Al	23210±530	17124	74	0.1
As	11.8±1.2	6.9	58	0.03
Ba	335±50	350	104	0.034
Ca	13200±1700	9575	73	60
Co	7.7±1.2	7.6	98	1
Cr	135±25	143	106	0.04
Cu	404±42	357	88	0.025
Fe	26500±1600	25769	97	4
K	5280±520	5475	104	2.3
Mg	8620±520	7386	86	2.7
Mn	320±12	319	100	0.03
Na	1860±100	3689	198	40
Ni	68±12	44	64	0.02
Pb	317±54	346	109	0.03
Sb	71.8±2.6	3.5	5	0.025
V	48.5±6	45	93	0.03
Zn	1790±130	1574	88	0.13

The obtained recoveries in two runs were within $\pm 15\%$ of the certified values for most of the elements. Some lower recoveries were attained for As, Ni and the crystal originating elements Cr, Al and Ca, which was already observed by other authors and usually explained by incomplete dissolution during the microwave digestion.^{26–28} An exceptionally high recovery (198 %) was obtained for Na and an extremely low recovery (5 %) for Sb, consequently, these elements will not be further rendered. No reliable explanation for these results can be given, except that Na contamination might have occurred during the performance of the analysis. The lack of data on Na and Ca concentrations from ICP–MS analysis may partly be rectified by IC analysis of Na⁺ and Ca⁺. In spite of outliers, the results of the elemental analysis NIST 2783 were satisfactory for the majority of the elements and the method may be considered as approved.

After this verification, the described analytical procedure of microwave acid extraction followed by ICP–MS analysis was applied to the aerosol samples. The mean and maximum concentration values of the trace elements determined in the PM₁₀, PM_{2.5} and PM₁ aerosol fractions from the spring and autumn periods are summarized in Table III.

TABLE III. The mean and maximum concentrations of trace elements in the PM₁₀, PM_{2.5} and PM₁ aerosol fractions in the spring and autumn sampling periods

Element	<i>c</i> / ng m ⁻³														
	PM ₁			PM _{2.5}			PM ₁₀			Spring			Autumn		
	Mean	Max	Autumn	Mean	Max	Autumn	Mean	Max	Autumn	Mean	Max	Spring	Mean	Max	Autumn
Mg	36	56.1	56	20.33	22.9	46.6	122	150.8	232	268.4	621	—	803.4	1606	
Al	53.42	126.3	92	53.75	78.3	164.4	207	—	—	—	—	—	—	—	
K	99.12	156.6	83	76.94	124.5	162.2	361	280	366	315.6	572	—	—	—	
V	3.31	10.7	1.44	3.29	9.9	1.9	2.2	5.6	14.5	3.56	5.3	—	—	—	
Cr	0.65	1.5	2.52	0.73	2.2	4.55	8.9	4.02	8.2	5.76	13.5	—	—	—	
Mn	3.21	8.7	5.8	4.12	12	12.04	24.9	18.9	39.8	12.04	24.9	—	—	—	
Fe	104.01	294	58.4	161.7	492	147	319	924.4	2187	1167	2013	—	—	—	
Co	0.13	0.42	0.05	0.08	0.14	0.07	0.11	0.27	0.35	0.392	0.75	—	—	—	
Ni	12.48	23	1.68	13.42	16.6	1.94	3.6	29.92	54.4	3.48	5.1	—	—	—	
Cu	1.88	4.6	—	3.16	8.4	2.88	4.11	15.53	34.5	9.03	23.12	—	—	—	
Zn	7.05	13.7	14.4	9.9	18.5	53.2	173	22.53	44.4	53.2	173	—	—	—	
As	0.15	0.26	0.3	0.18	0.28	0.472	0.68	0.45	0.84	1.026	2.17	—	—	—	
Se	0.15	0.24	0.32	0.16	0.26	0.438	0.63	0.24	0.35	0.556	0.99	—	—	—	
Mo	1.58	3.35	3.76	3.49	5	4.54	6.3	2.01	3.5	4.56	10.7	—	—	—	
Cd	0.17	0.28	0.24	0.21	0.33	0.298	0.42	0.29	0.48	0.326	0.51	—	—	—	
Sb	0.07	0.18	0.04	0.06	0.1	0.085	0.13	0.21	0.44	0.248	0.52	—	—	—	
Ba	0.61	1.86	3.74	1.43	4	5.2	7.8	13.85	27.7	17.46	31.7	—	—	—	
Tl	0.02	0.04	0.032	0.03	0.05	0.03	0.057	0.04	0.07	0.04	0.051	—	—	—	
Pb	23.42	62.6	35.2	30.05	80	57	161	42.88	86	74.8	212	—	—	—	
Th	0.01	0.026	0.085	—	—	0.044	0.115	0.1	0.12	0.159	0.331	—	—	—	

Additionally, the contents of NO_3^- , SO_4^{2-} , NH_3^+ , Na^+ , Ca^{2+} and K^+ in the PM_{10} , $\text{PM}_{2.5}$ and PM_1 aerosol fractions, determined by the ion-chromatography (IC) technique described in the previous section, are given in Table IV.

TABLE IV. The mean and maximum concentrations of secondary ions in the PM_{10} , $\text{PM}_{2.5}$ and PM_1 aerosol fractions in the spring and autumn sampling periods

Ion	$c / \mu\text{g m}^{-3}$											
	PM_1				$\text{PM}_{2.5}$				PM_{10}			
	Spring		Autumn		Spring		Autumn		Spring		Autumn	
	Mean	Max	Mean	Max	Mean	Max	Mean	Max	Mean	Max	Mean	Max
NO_3^-	0.52	0.42	0.77	1.48	0.67	0.67	1.11	2.09	1.00	1.18	1.88	2.87
SO_4^{2-}	4.03	6.46	4.59	7.36	4.16	8.10	5.20	6.61	3.98	6.00	5.20	8.03
NH_3^+	1.22	1.68	0.54	0.92	0.83	1.36	0.71	1.20	1.21	1.82	0.63	1.18
Na^+	0.61	1.77	1.22	1.79	0.90	1.88	1.09	1.56	0.33	0.42	1.03	1.67
Ca^+	1.21	1.40	0.20	0.22	1.64	1.89	0.21	0.24	1.23	2.11	1.69	3.67
K^+	0.51	1.66	0.11	0.17	0.80	1.77	0.15	0.21	0.23	0.32	0.20	0.28

Although the chemical composition of the aerosol fractions may not be accomplished by the data presented in Tables III and IV, these data indicated the main characteristics of the air pollution in this area. The crystal, soil-related elements, Fe, Mg, Al and K, had mean concentration values much higher than those of the other elements in both the coarse and fine aerosol fractions, especially in the autumn season, when resuspension processes are significant. In the total K concentration, there is usually a contribution from biomass combustion.²⁹ The anthropogenic originating elements Zn, Ni, As, Se, Mo, Cd, Ba and Pb present in the coarse aerosol fraction were higher in the autumn than in the spring, while the concentrations of V and Cu were higher in the spring season. The Zn concentrations determined in PM_{10} and $\text{PM}_{2.5}$ were observable but not much higher than the concentrations of other trace elements, as was the case in recent assessments of the Belgrade air quality.⁷⁻⁹ However, the concentrations of Pb, Ni and Zn were the highest among the trace elements in PM_1 , that is the very fine aerosol fraction and, consequently, the most vulnerable for lungs. These elements originated mainly from traffic; Zn usually reported as a tracer for unleaded fuel and diesel powered motor vehicle emissions and Ni and Pb as lead gasoline exhaust emission products.³⁰ The EU Directive defines the Pb limit concentration value as 500 ng/m^3 in PM_{10} and target values: 6, 5 and 20 ng/m^3 in the PM_{10} aerosol fraction for As, Cd and Ni, respectively. Both mean and maximum concentrations of Pb, As and Cd observed in this work were below these values, except for the Ni mean 29.9 ng/m^3 and maximum 54.4 ng/m^3 concentrations determined in the spring period. In addition to heavy oil combustions and mechanical abrasion of metallic surfaces,³¹ enhanced values of Ni may be caused by industrial activities.

The results showed significant concentrations of sulfates that may be associated with ammonia in the fine particles and preferably with nitrates in the PM₁₀ fraction. Sulfates, nitrates and ammonia are primarily associated with anthropogenic activities, referring to pollution from fuel or wood combustion. Moreover, nitrates usually present a coarse mode as a consequence of the reaction of HNO₃ with soil particles containing calcium carbonate.^{32,33}

In general, as a result of the applied acidic and water extraction procedures and the highly sensitive measurements, the concentration values of a number of particulate matter constituents were determined with high precision and accuracy. Low-level concentrations of trace elements were easily detected in the finest particles fraction (PM₁) due to the low detection limits of the employed measurement techniques. Although the obtained results may not be used to define the aerosol particulate matter composition as a whole, the results indicate that, in addition to natural sources, particulate matter from traffic might be an important source of air pollution in non-heating seasons.

CONCLUSIONS

A review of selected methods and means of monitoring and physical and chemical characterization of aerosol particulate matter in the urban area of Belgrade, followed by results obtained in spring and autumn sampling periods within the Project WeBIOPATR, are presented in this paper. A few conclusions may be drawn.

The mass concentration values of the PM₁₀ and PM_{2.5} aerosol fractions obtained here are in accordance with previous results on the air quality in the Belgrade urban area and with other results in the region, showing the enhanced pollution levels in comparison with the limit values permitted by EU recommendations. Results for the finest fraction PM₁ were obtained for the first time in the urban area of Belgrade and they showed the same characteristics as the coarser fractions.

Correlations of the PM₁₀ mass concentrations with the concentrations of gas-phase ambient air pollutants $c(\text{SO}_2)$, $c(\text{NO}_2)$ and $c(\text{O}_3)$ and the mass concentration $c(*\text{PM}_{10})$ obtained by the automatic air-monitoring station the same trend of concentrations during the campaigns, except for $c(\text{O}_3)$.

The air particulate composition concerning the elements: Mg, Al, K, V, Cr, Mn, Fe, Co, Ni, Cu, Zn, As, Se, Mo, Cd, Sb, Ba, Tl, Pb and Th and the contents of secondary ions: NO₃⁻, SO₄²⁻, NH₃⁺, Na⁺, Ca⁺ and K⁺ determined in the aerosol fractions PM₁₀, PM_{2.5} and PM₁ indicated soil and traffic related sources of pollution as dominant in the residential Belgrade urban area (OBS) in non-heating seasons.

Considering the limited numbers of aerosol samples taken into consideration, the presented results are just indicative but, from the aspect of data

quality, this evaluation enclosed all relevant internationally recommended standards and procedures.

Acknowledgements. This research was conducted within the WeBIOPATR project (2006–2009) funded by the Research Council of Norway through Programme of Research and High Education of Norway and Western Balkan Countries. The gravimetric room was established and funded in 2007 by the Institute of Public Health of Belgrade. Thanks go to Slobodan Tošović, Radomir Nikodinović, Sežana Vukčević and Ljiljana Adanski, from the Institute of Public Health of Belgrade for help in the experimental part of work concerning the gravimetric, ICP–MS and IC analyses.

ИЗВОД

ФИЗИЧКО-ХЕМИЈСКА КАРАКТЕРИЗАЦИЈА ЧЕСТИЦА СУСПЕНДОВАНИХ У
ВАЗДУХУ УРБАНОГ ПОДРУЧЈА БЕОГРАДА

ЈАСМИНКА Д. ЈОКСИЋ¹, МИЛЕНА ЈОВАШЕВИЋ-СТОЈАНОВИЋ¹, АЛЕНА ВАРТОНОВА², МИРЈАНА Б.
РАДЕНКОВИЋ¹, KARL-ESPEN YTTRI², СНЕЖАНА МАТИЋ-БЕСАРАБИЋ³ и ЉУБИША ИГЊАТОВИЋ⁴

¹Институт за нуклеарне науке Винча, б. бр. 522, 11001 Београд, ²NILU, Norwegian Institute for Air Research, P.O. Box 100, 2027 Kjeller, Norway, ³Институт за јавно здравље, Бул. Деспоина Стефана 54, 11000 Београд и ⁴Факултет за физичку хемију, Студентски брз 12–16, 11000 Београд

У оквиру овог истраживања урађена је карактеризација различитих фракција ваздуха урбане средине Београда и одређен је неограничен удео у фракцијама аеросола. У ту сврху, узорковани су и анализирани дневни депозити PM₁₀, PM_{2,5} и PM₁ фракција аеросола током пролећног и јесењег периода 2007. године да би се одредиле масене концентрације и садржаји одабраних елемената и секундарних јона. Резултати добијени током ових кампања узорковања показују да су средње дневне масене концентрације: 37 и 44 µg/m³ за фракцију PM₁₀, 22 и 23 µg/m³ за PM_{2,5} и 15 и 17 µg/m³ за најфинију фракцију PM₁, са максималним вредностима које превазилазе граничне нивое постављене прописима ЕУ за квалитет ваздуха. Приказана је и дискутована веза ових концентрација са гасовитим загађивачима, CO₂, NO₂ и O₃. Концентрације елемената (Mg, Al, K, V, Cr, Mn, Fe, Co, Ni, Cu, Zn, As, Se, Mo, Cd, Sb, Ba, Tl, Pb и Th) и јона (NO₃⁻, SO₄²⁻, NH₄⁺, K⁺, Ca²⁺ и Na⁺) одређених у PM₁₀, PM_{2,5} и PM₁ аеросолним фракцијама имају вредности које указују на природне изворе и саобраћај као главне изворе емитовања честица. Ова мерења су урађена као први корак при одређивању и карактеризацији честица аеросола да би се указало на главне изворе загађења и предложили одговарајући поступци ремедијације, специфични за овај регион.

(Примљено 2. марта, ревидирано 7. априла 2009)

REFERENCES

1. WHO, *Fact sheet EURO/04/05*, Berlin, Copenhagen, Rome
2. M. R. Gwinn, V. Vallyathan, *Environ. Health Perspec.* **14** (2006) 1818
3. M. R. Heal, L. R. Hibbs, R. M. Agius, I. J. Beverland, *Atmos. Environ.* **39** (2005) 1417
4. R. Reiss, E. L. Anderson, E. C. Cross, G. Hidy, D. Hoel, R. McClellan, S. Moolgavkar, *Inhal. Toxicol.* **19** (2007) 419
5. C. Buzea, I. P. Blandino, K. Robbie, *Biointerph.* **2** (2007) 17
6. M. Jovašević-Stojanović, S. Matić-Besarabić, in *Proceedings of the First International Webiopatr Workshop*, Book of extended abstracts, (2007), Belgrade, Serbia, 2007, p. 71
7. M. Tasić, S. Rajšić, V. Novaković, Z. Mijić, *Facta Universitatis* **4** (2006) 83

8. S. Rajšić, Z. Mijić, M. Tasić, M. Radenkovic, J. Joksic, *Environ. Chem. Lett.* **6** (2008) 95
9. M. Tasić, S. Rajšić, M. Tomašević, Z. Mijić, M. Aničić, V. Novaković, D. M. Marković, D. A. Marković, L. Lazić, M. Radenković, J. Joksić, *Environmental Technologies, New Developments*, E. Burcu Ozkaraova Gungor, (Ed.), I-Tech Education and Publishing, Vienna, 2008, p. 209
10. M.Jovašević, A.Bartonova, in *Proceedings of the First International Webiopatir Workshop*, Book of extended abstracts, (2007) Belgrade, Serbia, 2007, p. 10
11. C. W. Lewis, G. A. Norris, T. L. Conner, R. C. Henry, *J. Air Waste Manag. Assoc.* **53** (2003) 325
12. CEN 1998, *Air Quality. Determination of PM₁₀ Fraction of Suspended Particulate Matter. Reference Method and Field Test Particulate to Demonstrate Reference Equivalence of Measurement Methods (EN 12341)*, Brussels, 1998
13. EEC (1999), European Council Directive 1999/30/EC, *Official Journal L* **163** (1999) 41
14. *EMEP manual for sampling and chemical analysis*, Norwegian Institute for Air Research, Kjeller, 2001
15. *SOP MLD055: Standard operating procedure for the determination of PM_{2.5} mass in ambient air by gravimetric analyses*, Northern Laboratory Branch, Monitoring and Laboratory Division, Air Resources Board, California Environmental Protection Agency, Washington D.C., 2003
16. *CEN/TC 264 N799: Ambient Air Quality – Standard method for the measurement of Pb, Cd, As and Ni in PM₁₀ fraction of suspended particulate matter*, European Committee for Standardization, Brussels, 2006
17. C. Lin, S. Chen, K. Huang, W. Lee, W. Lin, C. Liao, H. Chaung, C. Chiu, *Environ. Pollut.* **145** (2007) 562
18. *SOP MLD064: Standard operating procedure for the analysis of anions and cations in PM 2.5 speciation by ion chromatography*, Northern Laboratory Branch, Monitoring and Laboratory Division, Air Resources Board, California Environmental Protection Agency, Washington D.C., 2002
19. CEN, EN 14907, *Ambient Air Quality – Standard Gravimetric Measurement Method for the Determination of the PM_{2.5} Mass Fraction of Suspended Particulate Matter*, European Committee for Standardization, Brussels, 2005
20. EC (European Commission), *Council Directive 2008/50/EC of the European Parliament and of the Council of 21 May 2008 on ambient air quality and cleaner air for Europe*, Official Journal European, 2008
21. *Exposure of children to air pollution (particulate matter) in outdoor air*, http://www.enhis.org/object_document/o4741n27382.html (October 2008)
22. A. Valavanidis, K. Fiotakis, T. Vlahogianni, E. B. Bakeas, S. Triantafillaki, V. Paraskevopoulou, M. Dassenakis, *Chemosphere* **65** (2006) 760
23. D. Houthuijs, O. Breugelmans, G. Hoek, E. Vaskovi, E. Mihalikova, J. S. Pastuszka, V. Jirik, S. Sachelarescu, D. Lolova, K. Meliefste, E. Uzunova, C. Marinescu, J. Volf, F. Leeuw, H. Wiel, T. Fletcher, E. Lebre, B. Brunekreef, *Atmos. Environ.* **35** (2001) 2757
24. V. Ariola, A. D. Alessandro, F. Lucarelli, G. Marazzan, F. Mazzei, S. Nava, I. Garcia-Orellana, P. Prati, G. Valli, R. Vecchi, A. Zucchiatti, *Chemosphere* **62** (2006) 226
25. M. Tasić, S. Rajšić, V. Novaković, Z. Mijić, *J. Phys. Conf. Series* **71** (2007) 012016
26. C. Hueglin, R. Gehrig, U. Baltensperger, M. Gysel, C. Monn, H. Vonmont, *Atmos. Environ.* **39** (2005) 637
27. N. J. Pekney, C. I. Davidson, *Anal. Chim. Acta* **540** (2005) 269
28. S. Karthikeyan, U. M. Joshi, R. Balasubramanian, *Anal. Chim. Acta* **576** (2006) 23

29. E. S. Lindgren, D. Henriksson, M. Lundin, P. Therning, J. Laursen, N. Pind, *X-Ray Spectrom.* **35** (2006) 19
30. J. M. Pacyna, E. G. Pacyna, *Environ. Rev.* **9** (2001) 269
31. T. Okuda, S. Naoko, M. Katsuno, S. Tanaka, *Atmos. Environ.* **41** (2007) 7642
32. N. Galindo, J. F. Nikolas, E. Yubero, S. Caballero, C. Pastor, J. Crespo, *Atmos. Res.* **88** (2008) 305
33. M. Viana, X. Querol, A. Alastuey, *Chemosphere* **62** (2006) 947.